5-2013

Earthquake Petrology: Linking Fault-Related Deformation to the Earthquake Cycle

Mitchell R. Prante
Utah State University

EARTHQUAKE PETROLOGY: LINKING FAULT-RELATED DEFORMATION

TO THE EARTHQUAKE CYCLE

by

Mitchell R. Prante

A dissertation submitted in partial fulfillment
of the requirements for the degree

of

DOCTOR OF PHILOSOPHY

in

Geology

Approved:

_____   _____
Dr. James P. Evans, Ph.D.   Dr. Mary S. Hubbard, Ph.D.
Major Professor   Committee Member

_____   _____
Dr. Susanne U. Janecke, Ph.D.   Dr. Alvar Braathen, Ph.D.
Committee Member   Committee Member

_____   _____
Dr. Anthony R. Lowry, Ph.D.   Dr. Mark McLellan, Ph.D.
Committee Member   Vice President for Research and
                                                   Dean of the School of Graduate Studies

UTAH STATE UNIVERSITY
Logan, Utah

2013

ABSTRACT

Earthquake Petrology: Linking Fault-Related Deformation to the Earthquake Cycle

by

Mitchell Ryan Prante, Doctor of Philosophy

Utah State University, 2013

Major Professor: Dr. James P. Evans
Department: Geology

Despite the relationship between faults and seismicity, few fault-related rocks have been identified in natural fault zones that are diagnostic of seismic slip. Despite focused research the only unequivocal evidence for ancient seismicity in exhumed fault zones is pseudotachylyte (rapidly-quenched frictional melt). Thermodynamic calculations indicate that the generation of frictional heat at seismic slip rates is expected to exceed the melting point of common rock-forming minerals. There is, however, a disconnect between the large number of modern earthquakes and rare reports of pseudotachylyte. The first three chapters of this dissertation focus on the discussion of fault-zone conditions during seismicity and the documentation of fault-related deformation that is the result of ancient seismicity. The conclusions from this work include: 1) some hydrothermal alteration in fault-zones is driven by the production of frictional heat, 2) grain size, shape, and nearest neighbor analysis of fault-related rocks can be used to

distinguish between a frictional melt and cataclastic origin of fault-related rocks, 3) iridescent-metallic highly-polished slip surfaces are the result of flash heating during ancient seismicity and the result of slip at seismic rates, 4) roughness analysis of highly-polished slip surfaces indicates that these surfaces are anomalously smooth from the nm- to cm-scales, and 5) the anomalously smooth nature of highly-polished slip surfaces may result from refinement during seismic slip.

This work also presents evidence for ancient seismicity along a low-angle normal fault (LANF) in the form of voluminous pseudotachylyte. The documentation of pseudotachylyte and therefore ancient seismicity along LANFs is uncommon and has significant implications for fault mechanics and the slip behavior of LANFs. We also present a synthesis of other reported LANF pseudotachylyte, which suggests that LANF seismicity was common during LANF evolution. The association of pseudotachylyte and LANFs restricts the models for LANF formation to those that incorporate periodic seismicity.

A new method for collecting 3D data in geology is also presented. The Windows Kinect™ has been employed in surface metrology studies as an inexpensive and accurate 3D range camera. We expand the use of the Kinect™ to several applications including geomorphology, paleontology, and structural geology.

(239 pages)

PUBLIC ABSTRACT

Earthquake Petrology: Linking Fault-Related Deformation to the Earthquake Cycle

Mitchell R. Prante

Faults have a controlling influence on a variety of geologic processes including fluid flow, the mechanical behavior of the crust, and seismicity. The geologic sciences have long recognized that faults generate earthquakes; however, few indicators of ancient earthquakes exist in fault-zones. This dissertation documents several indicators for the preservation of ancient earthquakes in fault-zones including frictional melt (pseudotachylyte), highly-polished fault slip surfaces, and hydrothermal alteration. These deformation products result from rapid generation of frictional heat during earthquakes.

This dissertation also focuses on the seismic potential of continental low-angle normal faults (LANF). We document the preservation of voluminous pseudotachylyte along a LANF suggesting that the fault repeatedly nucleated large earthquakes. Additionally, a synthesis of reported occurrences of LANF pseudotachylyte indicates that LANF seismicity is common during extension. This has important implication for the mechanics and evolution of LANFs and for the assessment of seismic hazards.

We also present a little used, high resolution, and low-cost 3D range camera for use in geolgy. The Kinect™ is a 3D infrared range camera that can be used to collect high-resolution ($\pm$ 1 mm), 3D data in both field and laboratory settings. We describe the use of the Kinect™ in geologic appications and recommend more widespread use.

ACKNOWLEDGMENTS

CONTENTS

LIST OF TABLES

LIST OF FIGURES

CHAPTER 1

EARTHQUAKE PETROLOGY: LINKING FAULT-RELATED DEFORMATION

TO THE EARTHQUAKE CYCLE

Abstract

Faults have a controlling influence on a wide range of crustal-scale processes including fluid flow, the mechanical behavior and tectonic processes of the crust, and seismicity. Despite the long-recognized relationship between faults and seismicity few features have been identified in naturally formed fault zones that are diagnostic of seismic slip along exhumed faults. Calculations of the total energy budget of earthquakes suggest that up to 80 % of the energy released during an earthquake is consumed by processes in and around the fault zone. This energy may be consumed by fracture formation, refinement of slip surfaces, grain-size reduction, generation of frictional heat, overcoming gravity, and/or driving chemical changes. Basic thermodynamics indicate that the generation of frictional heat during seismic slip is expected to exceed the melting point of common rock-forming minerals (> 1000 ˚C). Rapidly quenched frictional melt rocks are preserved as pseudotachylyte and is the only unequivocal evidence for ancient seismicity in exhumed fault zones. Despite the prediction that frictional melt and therefore pseudotachylyte should commonly be generated at seismic slip rates, pseudotachylyte remains rarely reported from exhumed fault zones. Part of this study examines the conditions of faulting during the generation and preservation of pseudotachylyte along several exhumed fault zones and associated fault-related rocks.

The documentation of fault-related rocks and deformation products that are diagnostic of seismic slip in exhumed faults has important implications for the total energy budget of earthquakes, stress-drop during seismicity, strong ground motion prediction, and fault zone properties. This study uses a variety of compositional and structural analyses to describe pseudotachylyte, cataclasites, and highly polished slip surfaces from strike-slip, normal faults, and a low-angle normal fault in the western United States in order to better characterize fault-zone conditions during seismicity and characterizes seismogenisis along a low-angle normal fault.

This study documents pseudotachylyte from the shallow-crust (< 10 km depths) in the central Sierra Nevada, CA, in association with cataclastic fault-related rocks and hydrothermal alteration. The association of pseudotachylyte with hydrothermal fluid flow suggests that the conditions for pseudotachylyte formation are broader than previously estimated. We also suggest that this hydrothermal alteration may be driven by co-seismic heating in the fault zone. The hypothesis that some hydrothermal alteration in faults zones is related to seismicity helps to quantify the total energy budget of earthquakes, and is consistent with the results from other studies. This study also presents detailed textural analysis of fault-related rocks from seismogenic depths in an effort to connect textural analysis to deformation. The connection between cataclasite and pseudotachylyte clast shape and deformation mechanisms has been studied by numerous workers. This work contributes to this discussion by adding additional data and interpretation as well as documenting a new analysis to fault-rock textural analysis. We use nearest neighbor

analysis of fault-related rock clast distributions to confirm a frictional melt origin for pseudotachylyte. The use of nearest neighbor analysis is a new and useful tool for distinguishing a frictional melt origin for fault-related rocks. We also document and interpret the presence of pseudotachylyte along the West Salton detachment fault, a low-angle normal fault in southern California.

Pseudotachylyte is uncommon along low-angle normal faults and confirms the seismic potential of low-angle normal faults worldwide. This study presents convincing evidence for a frictional melt and repeated seismicity along the West Salton detachment fault a low-angle normal fault in Southern California. The thick accumulations (> 1 m) and lateral extent (> 2 km along strike) of pseudotachylyte associated with the West Salton detachment fault suggest that seismicity was common during the evolution of the detachment. Additionally, this work also presents a new synthesis of confirmed and plausible occurrences of voluminous pseudotachylyte from low-angle normal faults suggesting that seismicity is common during the evolution of some low-angle normal faults.

This study also presents evidence for a previously undocumented fault-related deformation product and deformation mechanisms. Fault-related highly polished slip surfaces (HPSS) have long been recognized in the geologic record and may be related to seismicity. However, it is difficult to provide an unequivocal link between seismicity and HPSS. This study examines unique iridescent-metallic HPSS that are exposed in the damage zone of the Wasatch fault, Utah. Textural and compositional analyses of the

iridescent-metallic HPSS were conducted using a variety of traditional and little-used methods in the geosciences. Using these methods this study investigates the nano-scale topography, composition, and crystallinity of the iridescent-metallic highly polished slip surfaces. Using these data we draw a link between the observed hematite-rich HPSS and elevated temperature conditions (300 ˚C < T < 800 ˚C). These elevated temperatures can only reasonably be explained by heating during seismogenesis, perhaps at asperities. Therefore we argue that the iridescent-metallic highly polished slip surfaces is the result of ancient seismicity.

Finally we also present a very useful new tool for geologic research. The Windows Kinect™ is a three-dimensional (3D) infrared range camera that is capable of capturing high-resolution topographic data from cm to mm resolution. The use of the Kinect for geologic studies is uncommon; however, applications in the earth sciences are abundant. We present a method for the acquisition and processing of 3D point cloud data with the Kinect. We also provide several example data sets and propose the use of the Kinect in structural geology, neo-tectonics, paleontology, and geosciences education.

Introduction

Faults in the brittle-crust are the most conspicuous evidence for elastic deformation of earth materials at the surface. Though faults comprise a small volume of the crust, they influence the mechanical and fluid flow properties of the crust, and are mechanisms for accommodating most of the elastic strain in the crust through a variety of slip-behaviors (Ward, 1998; Lockner and Beeler, 2002; Kanamori and Brodsky, 2004;

Scholz, 2010; Faulkner et al., 2010; Marone and Richardson, 2010; Peng and Gomberg, 2010). Fault zones are typically composed of a damage zone, fault core, and one or more slip surfaces (Chester and Logan, 1986; Faulkner et al., 2010) (Fig. 1-1). Fault damage zones contain small faults, fractures and/or veins associated with the principal trace of the fault, and typically exhibit increasing fracture density approaching the fault core (Anders and Wiltschko, 1994; Schulz and Evans, 2000; Faulkner et al., 2010; Mitchell et al., 2011). Fault cores are comprised of intensely-deformed and/or altered fault-related rocks depending on the tectonic setting, pressure and temperature conditions during faulting, fluid flow, and protolith (Sibson, 1977; Evans and Chester, 1995; Sibson, 2003; Fagereng and Toy, 2011) (Fig. 1-1). Principal slip surfaces are pervasive slip surfaces that accommodate the majority of slip across the fault zone, and may be < 5 cm-thick and in some cases mm's wide (Chester and Logan, 1986; Chester et al., 1993; Evans and Chester, 1995; Caine et al., 1996; Sibson, 2003; Sagy and Brodsky, 2009; Caine et al., 2010; Faulkner et al., 2010). Because faults are the principal structures that accommodate strain during seismicity in the brittle portion of the crust, are long-lived, preserve a clear elastic deformation history, and earthquakes are common, it is reasonable to conclude that exhumed fault zones preserve evidence for ancient seismicity (Sibson, 1975, 2003; Spray, 1987; Cowan, 1999; Marone and Richardson, 2010).
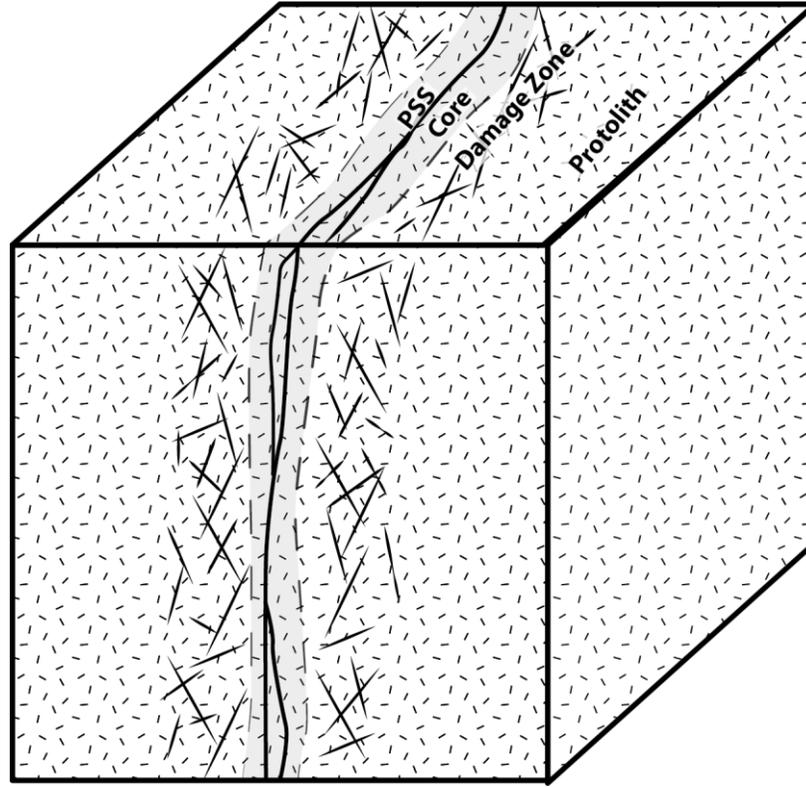
Figure 1-1: Typical fault zone structure with single high-strain fault core and discrete

principal slip surface (PSS) surrounded by a damage zone and unaltered protolith

(Modified from Chester and Logan, 1986; Faulkner et al., 2010).

The work done during seismic slip can be defined by:

$$W_f = Q + E_s + U_s + W_g \tag{1}$$

where W_f is the work done in faulting including: heat (Q), seismic waves (E_s), gouge

formation and surface refinement (U_s), and work against gravity (W_g) (Sibson and Toy,

2006; Jacobs et al., 2006; Shipton et al., 2006). In most analyses, E_s is considered to be

between 5 and 20% of the total energy released during an earthquake (McGarr, 1999; Kanamori and Brodsky, 2004; Di Toro et al., 2005; Kanamori and Riveiro, 2006). The value W_g depends on the depth of nucleation and fault orientation (Di Toro et al., 2005). Therefore, up to 80 and 95 % of the energy released during an earthquake results in creation of new fractures (U_s), generation of frictional heat (Q) and other dissipative processes (Di Toro et al., 2005; Jacobs et al., 2006; Shipton et al., 2006).

The change in temperature during frictional slip can be approximated by:

$$\Delta T = \frac{\tau_f \cdot u}{c_p \cdot \rho \cdot t_s} \qquad (2)$$

where ΔT is the change in temperature, τ_f=shear resistance during slip, u=distance of slip increment, c_p=specific heat of fault-related rocks, ρ=density of fault-related rocks, and ts=thickness of the slip surface (Sibson, 2003). Using typical values for c_p, ρ, and t_s for rocks and faults in the brittle-crust, representative seismic slip rates between 0.5-1.0 m/sec, $10 < \tau_f < 100$ MPa, and u of approximately 1 m, ΔT of up to 1000°C is expected (Sibson, 2003). Given average geothermal gradients between 20-30 °C/km, the depths where large earthquakes nucleate (~6-14 km), and the melting point of rock-forming minerals (Fig. 1-2), frictional melt is expected to be common in exhumed fault zones (McKenzie and Brune, 1972; Sibson, 1975; Spray, 1992, 2010; Bjørnerud and Magloughlin, 2004; Kirkpatrick et al., 2009; Kirkpatrick and Rowe, 2013). Rapidly quenched frictional melt is preserved in the form of tectonic pseudotachylyte from a variety of tectonic environments, formation depths, and rock types (Sibson, 1975; Magloughlin, 1989, 2011; Magloughlin and Spray, 1992; Cowan, 1999; Wenk et al.,

2000; Boullier et al., 2001; Plattner et al., 2003; Allen, 2005; Di Toro et al., 2005; Sibson and Toy, 2006; Lin, 2008; Kirkpatrick and Shipton, 2009; Bestmann et al., 2011; and many others). Published reports of tectonic pseudotachylyte however, are uncommon given the abundance of earthquakes and the large number of fault zones studied (Sibson, 2003; Sibson and Toy, 2006; Lin, 2008; Kirkpatrick et al., 2009; Kirkpatrick and Rowe, 2013). The apparent rareness of tectonic pseudotachylyte can be explained by: 1) uncommon pseudotachylyte formation during seismicity, 2) uncommon preservation of pseudotachylyte during post-seismic deformation, exhumation and alteration or 3) a lack of identification and reporting of pseudotachylyte in the geologic literature (Sibson, 1975, 2003; Spray, 1992; Lin, 2008; Kirkpatrick et al., 2009; Bjørnerud, 2010; Kirkpatrick and Rowe, 2013).

In this study we examine tectonic pseudotachylyte and associated fault-related rocks from strike-slip faults in the Sierra Nevada, CA, and a low-angle normal fault in the Salton trough, CA (Fig. 1-3). This study also describes highly polished slip surfaces from the Wasatch fault zone in the eastern Basin and Range, UT (Fig. 1-3). This study employs traditional and novel methods to investigate the structure, composition, and alteration of fault-related rocks from these fault zones. These methods include field mapping, structural analysis, micro-structural analysis, scanning electron microscopy (SEM), energy-dispersive x-ray spectroscopy (EDS), x-ray diffraction (XRD), x-ray florescence (XRF), white-light interferometry, and infrared range camera techniques.
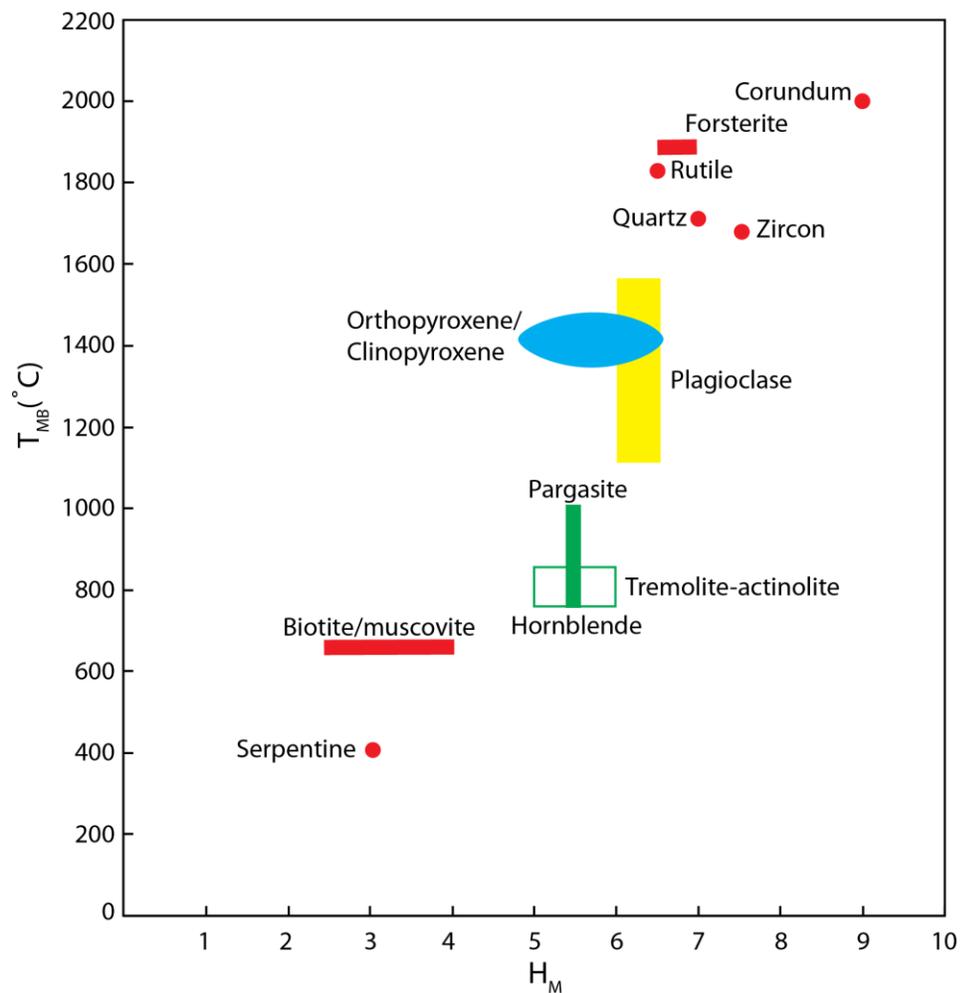
Figure 1-2: Approximate melting or breakdown temperature (T_{MB}) vs. Mohs hardness (H_M) for a range of common rock-forming minerals. Note the strong correlation between melting point and Mohs hardness.Modified from Spray (2010).
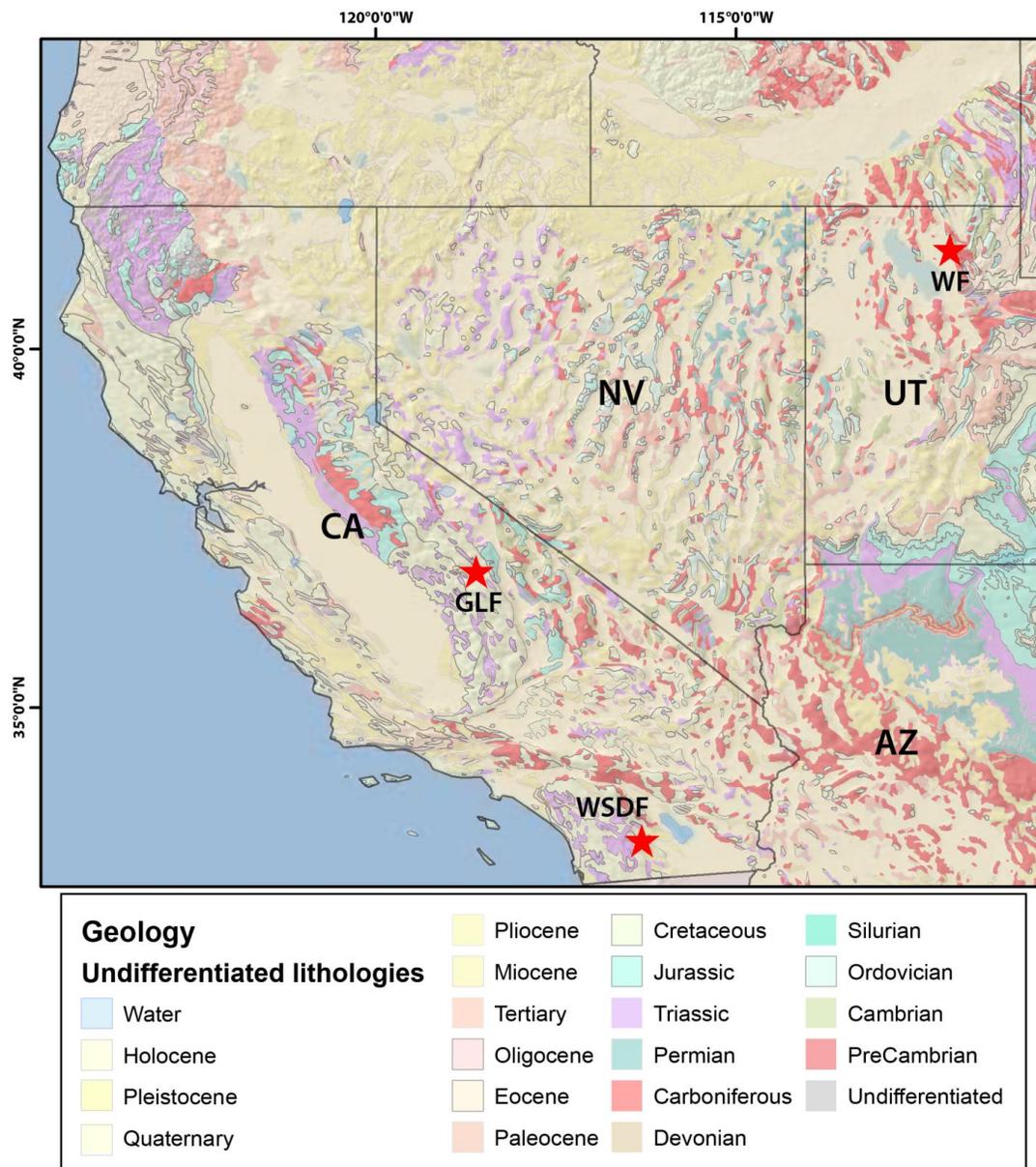
Figure 1-3: Simplified geologic map of the western U.S. (King and Beikman, 1974), with locations of field areas in this study (red stars), West Salton detachment fault (WSDF), Glacier Lakes fault (GLF), and the Wasatch fault (WF).

Earthquake Geology (Chapters 2 & 3)

Chapters 2 and 3 of this dissertation are focused on fault-related deformation that is diagnostic of seismic slip and can be used to constrain the total energy budget of earthquakes (Chapter 2, 3; Prante and Evans, in review; Prante et al., in prep). Several fault-related deformation products have been proposed to be diagnostic of seismic slip in addition to tectonic pseudotachylyte (Table 1-1). Despite this focused research some of these deformation products and fault-related rocks remain controversial (Smith et al., 2008; Meneghini et al., 2010), subject to multiple interpretations (Power and Tullis, 1989; Eichhubl and Boles, 2000; Rowe et al., 2012), lack sufficient evidence for seismic slip (Eichhubl and Boles, 2000; Boutareaud et al., 2010), or remain little studied (Evans and Langrock, 1994; Wenk et al., 2011; Levi et al., 2011; Bestmann et al., 2012; Siman-Tov et al., 2013; Smith et al., 2013). To unequivocally demonstrate a seismic origin for fault-related deformation products a connection must be made between the observed deformation and strain rate ($\dot{e}$), temperature (T), and or pressure (P) and show that these $\dot{e}$, T, and P are in disequilibrium with the geologic context of the fault zone (Cowan, 1999; Marone and Richardson, 2010). In this study we examine and discuss tectonic pseduotachylyte and other fault-related deformation from the Glacier Lakes fault (CA, USA), and the West Salton detachment fault (CA, USA), (Fig. 1-3). We also examine fault-related rocks and highly polished slip surfaces from the Wasatch fault, UT (Fig. 1-3). This study examines the meso- to microscale structure, composition, crystallinity, microstructure, and fluid-rock interactions associated with fault zones that preserve

evidence for seismic activity and are exhumed from seismogenic depths (Fig. 1-4). This study seeks to describe the geologic context, deformation mechanisms, and composition of several fault-related rock types including: pseudotachylyte, cataclasite, and highly polished slip surfaces. The overarching goal of this study is to identify fault-products that are diagnostic of seismic slip and better quantify the total energy budget of earthquakes.

Table 1-1: Proposed Indicators of Ancient Seismogenesis

Evidence for seismogenesis	Deformation mechanisms	References
fault breccia and cataclastic rocks	elevated fluid pressure and soft sediment deformation	(Sibson, 1985; Cashman et al., 2007; Smith et al., 2008)
fluidized fault gouge and clastic dikes forming injection structures	elevated fluid pressure	(Lin, 1996, 2008, 2011; Monzawa and Otsuki, 2003; Ujiie et al., 2007; Sagy et al., 2007; Levi et al., 2011; Rowe et al., 2012)
crystal-plastic deformation	Elevate temperatures and pressures	(Wenk et al., 2011; Bestmann et al., 2012)
clast-cortex grains	Fluidization of confined layer	(Boutareaud et al., 2010; Smith et al., 2011)
cyclic fibrous slickenside growth	Periodic fluid flow	(Eichhubl and Boles, 2000; Fagereng et al., 2011)
highly polished slip surfaces	Melt and dynamic recrystallization	(Engelder, 1974; Spray, 1989; Power and Tullis, 1989, 1992; Evans and Langrock, 1994; Han et al., 2007; Caine et al., 2010; Siman-Tov et al., 2013; Smith et al., 2013)
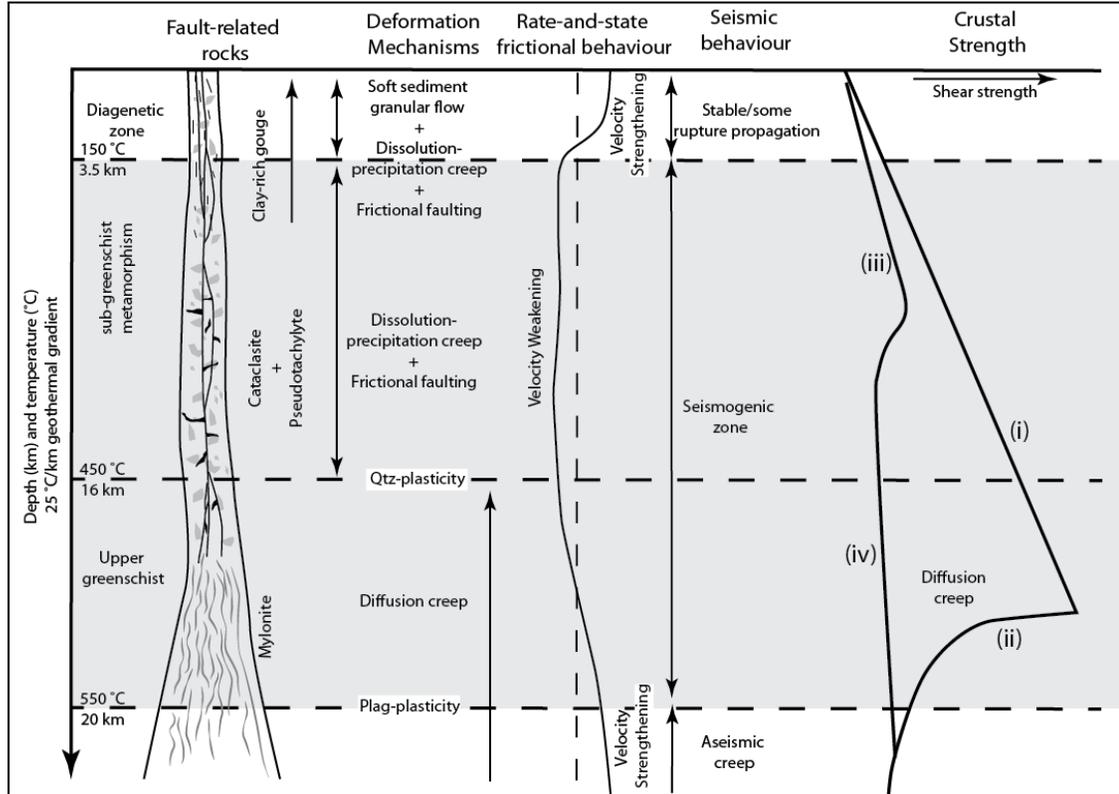
Figure 1-4: Conceptual model of seismogenic strike-slip fault-zone with depth. Modified from Sibson (1983), Janecke and Evans (1988), Scholz (1988, 2002), Fagereng and Toy (2011).

Pseudotachylyte and Cataclasite

Tectonic pseudotachylyte (referred to here as pseudotachylyte) is the only unambiguous product of ancient seismicity along exhumed faults (Philpotts, 1964; Sibson, 1975; Maddock, 1983; Spray, 1987, 1992, 2010; Cowan, 1999; Sibson and Toy, 2006; Fagereng and Toy, 2011; Kirkpatrick and Rowe, 2013). Many studies have focused

on: 1) descriptions of pseudotachlyte from exhumed faults (Philpotts, 1964; Sibson, 1975, 1983; Allen, 1979; Maddock, 1983; Bossière, 1991; Magloughlin, 1992; O'Hara, 1992; Lin, 1994, 1999; Boullier et al., 2001; Di Toro and Pennacchioni, 2004; Allen, 2005; Barker, 2005; Sibson and Toy, 2006; Kirkpatrick and Shipton, 2009; Bjørnerud, 2010; Toy et al., 2011); 2) generated artificial frictional melt in the laboratory to describe conditions during seismicity (Friedman et al., 1974; Killick, 1990; Spray, 1987, 1988; Tsutsumi and Shimamoto, 1997; Lin and Shimamoto, 1998; Tsutsumi, 1999; Hirose and Shimamoto, 2005; Lin, 2008; Nielsen et al., 2008; Di Toro et al., 2010; Niemeijer et al., 2011; Togo and Shimamoto, 2012); and 3) considered the energy requirements and conditions necessary for the generation of frictional melt (Philpotts, 1964; McKenzie and Brune, 1972; Sibson, 1975, 2003; Scholz, 1980; Maddock, 1983; Spray, 1992, 2010; Bjørnerud and Magloughlin, 2004; Di Toro et al., 2005; Rice, 2006; Rempel and Rice, 2006; Barker et al., 2010; Bjørnerud, 2010; Kirkpatrick et al., 2009; White, 2012; Kirkpatrick and Rowe, 2013). Notwithstanding the wealth of research focused on understanding the formation and preservation conditions of frictional melt and many studies focused on fault zones in general, pseudotachylyte remains rarely reported (e.g. Sibson and Toy, 2006; Kirkpatrick et al., 2009; Kirkpatrick and Rowe, 2013) relative to most other fault-related rocks found in nature.

Several workers have focused on identifying characteristics of cataclastic rocks that are diagnostic of seismic slip (Lin, 1996; Rowe et al., 2005; Heilbronner and Keulen, 2006; Sagy and Brodsky, 2009; Stünitz et al., 2010; Lin et al., 2012; Rowe et al., 2012).

These characteristics include injection vein morphology (Lin, 1996, 2011; Monzawa and Otsuki, 2003; Otsuki et al., 2005; Rowe et al., 2005, 2012; Lin et al., 2012), clast shape and size distribution (Lin and Shimamoto, 1998; Lin, 1999; Ray, 1999, 2004; Han et al., 2007; Smith et al., 2011), and other textures that are indicative of rapid increase in pore-fluid pressure (Sibson, 1985; Smith et al., 2008; Caine et al., 2010).

In chapter 2 we describe pseudotachylyte and associated fault-related rocks from the central Sierra Nevada, CA (Prante and Evans, in review) (Fig. 1-3). Pseudotachylyte from the Glacier Lakes fault is mixed with cataclastic rocks in the fault-core and has complex cross-cutting relationships with hydrothermal alteration (Kirkpatrick et al., 2008; Kirkpatrick and Shipton, 2009). These complex relationships suggest that the co-seismic energy was distributed over several deformation products (Kirkpatrick and Shipton, 2009). In this study we explore the possibility of multiple deformation mechanisms operating coevally in the fault-zone.

Highly Polished Slip Surfaces

Highly polished slip surfaces (HPSS) are a common fault-related rock texture and are found in a variety of rock types and tectonic settings (Gilbert, 1928; Power et al., 1987; Will and Wilson, 1989; Power and Tullis, 1989; Evans and Langrock, 1994; Candela et al., 2009, 2011; Sagy and Brodsky, 2009; Caine et al., 2010; Siman-Tov et al., 2013; Smith et al., 2013). Despite the pervasiveness of highly polished slip surfaces in the rock record, their characteristics and formation mechanisms have been little studied (Power and Tullis, 1989; Will and Wilson, 1989; Spray, 1989; Han et al., 2007; Sagy and

Brodsky, 2009; Caine et al., 2010; Mouslopoulou et al., 2011; Siman-Tov et al., 2013; Smith et al., 2013). Highly polished slip surfaces have been attributed to frictional grinding by ultrafine-grained material (Engelder, 1974, 1978; Siman-Tov et al., 2013), the development of thin mineralized and sheared surfaces (Will, 1987; Means, 1993), melting (Friedman et al., 1974; Spray, 1989), preferred orientation of grains by rotation during slip (Power and Tullis, 1989; Caine et al., 2010), preferred alignment of phyllosilicates during slip (Will and Wilson, 1989), and dynamic recystallization (Smith et al., 2013). It is important to note that not all of the hypotheses for HPSS formation are mutually exclusive, and are likely highly dependent on the deformation history, tectonic setting, and protolith of the host fault zone. We also enphasisze that polished surfaces do not represent fast slip (i.e. glacially polished surfaces) and therefore alayses of the slip surfaces is critical.

This dissertation tests the hypothesis that some highly polished slip surfaces are the result of seismicity (Chapter 3) (Power and Tullis, 1989, 1992; Siman-Tov et al., 2013; Smith et al., 2013), this study focuses on linking the structure, composition, crystallinity, and roughness of highly polished slip surfaces and the generation of co-seismic heat from the Wasatch fault zone, central Utah (Fig. 1-3). I used a variety of techniques including field descriptions, petrographic analysis, x-ray diffraction, scanning electron microscopy, white light interferometry, bench top laser profilometry, infrared range cameras, and x-ray photoelectron spectroscopy toquantify the structure and composition of highly polished slip surfaces from the nm- to cm-scales. Linking highly

polished slip surfaces from the Wasatch fault zone to the seisimic cycle is consistent with

the conclusion from other workers that much of the energy released during seismicity is

consumed by processes in the fault zone (McGarr, 1999; Sibson and Toy, 2006;

Kanamori and Riveiro, 2006; Jacobs et al., 2006; Shipton et al., 2006).

Low-angle normal fault seismicity (Chapter 4)

This work also documents and describes anomalously voluminous accumulations

of tectonic pseduotachylyte from a low-angle normal fault in southern California (Prante

et al., in press) (Fig. 1-3). The documentation of ancient seismicity along low-angle

normal faults is rare and this study contributes additional data sets that help to explain the

low-angle normal fault paradox (John, 1987; Wang, 1997; Goodwin, 1999; Kairouz et al.,

2003; Collettini, 2009; Magloughlin, 2011). Low-angle normal faults (detachment faults)

are normal faults with gentle dips, large aerial extent, large displacements ($\geq$ 5-15 km),

that may exhume mid to lower continental crust in their footwalls (Davis and Lister,

1988). Debate has focused on whether low-angle normal faults formed and/or slipped at

low-angles in the brittle crust (<30°), based on predictions made by Andersonian fault

mechanics (Anderson, 1951) that low-angle normal fault are unfavorably oriented for

slip, and that seismic activity on low-angle normal faults is rare (Jackson, 1987; Jackson

and White, 1989; Thatcher and Hill, 1991; Abers et al., 1997; Abers, 2001, 2009; Axen,

2004; Collettini and Sibson, 2001; Collettini, 2011). However, a growing body of

research worldwide shows that low-angle normal faults have nucleated moderate to large

earthquakes, localized seismicity on coordinate normal faults in their hanging walls, and

slipped seismically when earthquakes propagate onto them (Abers, 1991, 2001; Rietbrock et al., 1996; Axen, 1999; Sorel, 2000; Boncio et al., 2000; Collettini, 2011). The relative paucity of seismicity associated with low-angle normal faults contrasts with compelling geologic evidence that some low-angle normal faults were active in the brittle-crust and has significant implications for fault mechanics and the evolution of highly extended terranes.

In this study we document convincing evidence for ancient seismicity along a low-angle normal (West Salton detachment fault, CA) from relatively shallow depths (< 5 km) and dry co-seismic conditions (Fig. 1-3). The documentation of tectonic pseudotachylyte along the West Salton detachment fault and other examples of low-angle normal fault pseudotachylyte provides convincing evidence that at least some low-angle normal faults generate earthquakes. Furthermore, the highly atypical thickness (up to 1.5 m) and lateral extent of pseudotachylyte in the West Salton detachment fault-zone and similar exposures of pseudotachylyte from other low-angle normal faults suggest conditions that were particularly amenable to generation of frictional melt. This has important implications for the seismic potential of low-angle normal faults and constrains the models of low-angle normal fault formation.

A new technique for collecting and analyzing 3D data sets for the

Earth sciences (Chapter 5)

We also present a new method for collecting three-dimensional (3D) point cloud data at the cm to mm scale in the geological sciences. Three-dimensional data collection

and interpretation has become increasingly common in many fields of Earth science at the outcrop scale (Bellian et al., 2005; Renard et al., 2006; Sagy et al., 2007; Buckley et al., 2008, 2010; McCaffrey et al., 2008; Armesto et al., 2009; Enge et al., 2010; Pearce et al., 2011; and many others). Terrestrial light detection and ranging (LiDAR) is a commonly used technique to measure geologic features at a high resolution and has been used in a variety of applications (Bellian et al., 2005; Sagy et al., 2007; Bates et al., 2008; Buckley et al., 2008; McCaffrey et al., 2008; Armesto et al., 2009; Enge et al., 2010; Brodsky et al., 2011; Pearce et al., 2011; Nelson et al., 2011; Stoinski, 2011; Candela and Renard, 2012; Jessop et al., 2012). While terrestrial LiDAR is a very robust tool for collecting high-resolution (mm-scale) point cloud data over large areas its cost and portability is limiting for many studies. Here we present the use of a low-cost ($300), high resolution (mm-scale), and easy to use 3D range camera for indoor and outdoor applications. The Windows Kinect™ utilizes triangulation of a projected infrared array and electronic speckle pattern interferometry to produce 3D images, and is rarely used in the geological sciences (Mankoff and Russo, 2012; Khoshelham and Elberink, 2012; Gonzalez-Jorge et al., 2013; Smisek et al., 2013). We present several pilot data sets and applications for the Kinect™ in the Earth sciences.

Conclusions

The documentation of fault-related deformation that can be linked to ancient seismicity is of great interest to structural geology and seismology (Kanamori and Riveiro, 2006; Jacobs et al., 2006; Fagereng and Toy, 2011). Earthquake geology is

focused on documenting and quantifying the processes that consume energy released during earthquakes (e.g. Kanamori and Riveiro, 2006; Fagereng and Toy, 2011). This study documents well-established and novel deformation products that are diagnostic of ancient seismicity. Detailed analyses focuses on the texture, composition, and deformation of pseudotachylyte from two fault zones provides new insight in to fault melting processes, slip localization, and co-seismic deformation of frictional melt. We also present analyses of other fault-related rocks and deformation products including: cataclasite and ultracataclasite, highly-polished slip surfaces, and hydrothermal alteration. The focus of these analyses is to better quantify the total energy budget of earthquakes. This study also tests the seismicity of low-angle normal faults and presents a new technique for collecting 3D data sets in field and laboratory studies.

References

Abers, G.A., 1991, Possible seismogenic shallow-dipping normal faults in the Woodlark-D'Entrecasteaux extensional province, Papua New Guinea: Geology, v. 19, p. 1205–1208, doi: 10.1130/0091-7613(1991)019<1205:PSSDNF>2.3.CO;2.

Abers, G.A., 2001, Evidence for seismogenic normal faults at shallow dips in continental rifts: Geological Society, London, Special Publications, v. 187, p. 305–318, doi: 10.1144/GSL.SP.2001.187.01.15.

Abers, G.A., 2009, Slip on shallow-dipping normal faults: Geology, v. 37, p. 767–768, doi: 10.1130/focus082009.1.

Abers, G.A., Mutter, C.Z., and Fang, J., 1997, Shallow dips of normal faults during rapid extension: Earthquakes in the Woodlark-D'Entrecasteaux rift system, Papua New Guinea: Journal of Geophysical Research: Solid Earth, v. 102, p. 15301–15317, doi: 10.1029/97JB00787.

Allen, A.R., 1979, Mechanism of frictional fusion in fault zones: Journal of Structural Geology, v. 1, p. 231–243, doi: 10.1016/0191-8141(79)90042-7.

Allen, J.L., 2005, A multi-kilometer pseudotachylyte system as an exhumed record of earthquake rupture geometry at hypocentral depths (Colorado, USA): Tectonophysics, v. 402, p. 37–54, doi: 10.1016/j.tecto.2004.10.017.

Anders, M.H., and Wiltschko, D.V., 1994, Microfracturing, paleostress and the growth of faults: Journal of Structural Geology, v. 16, p. 795–815, doi: 10.1016/0191-8141(94)90146-5.

Anderson, E.M., 1951, The Dynamics of Faulting: Oliver and Boyd, Edinburgh.

Armesto, J., Ordóñez, C., Alejano, L., and Arias, P., 2009, Terrestrial laser scanning used to determine the geometry of a granite boulder for stability analysis purposes: Geomorphology, v. 106, p. 271–277, doi: 10.1016/j.geomorph.2008.11.005.

Axen, G.J., 1999, Low-angle normal fault earthquakes and triggering: Geophysical Research Letters, v. 26, p. 3693–3696, doi: 10.1029/1999GL005405.

Axen, G.J., 2004, Mechanics of low-angle normal faults, *in* Karner, G., Taylor, B., Driscoll, N.W., and Kohlstedt, D.L. eds., Rheology and deformation in the lithosphere at continental margins, Columbia University Press, New York, p. 46–91.

Barker, S.L.L., 2005, Pseudotachylyte-generating faults in Central Otago, New Zealand: Tectonophysics, v. 397, p. 211–223, doi: 10.1016/j.tecto.2004.12.005.

Barker, S.L., Sibson, R.H., Palin, J.M., FitzGerald, J.D., Reddy, S., Warr, L.N., and van der Pluijm, B.A., 2010, Cretaceous age, composition, and microstructure of pseudotachylyte in the Otago Schist, New Zealand: New Zealand Journal of Geology and Geophysics, v. 53, p. 15–29, doi: 10.1080/00288301003631764.

Bates, K.T., Rarity, F., Manning, P.L., Hodgetts, D., Vila, B., Oms, O., Galobart, À., and Gawthorpe, R.L., 2008, High-resolution LiDAR and photogrammetric survey of the Fumanya dinosaur tracksites (Catalonia): implications for the conservation and interpretation of geological heritage sites: Journal of the Geological Society, v. 165, p. 115–127, doi: 10.1144/0016-76492007-033.

Bellian, J.A., Kerans, C., and Jennette, D.C., 2005, Digital outcrop models: Applications of terrestrial scanning lidar technology in stratigraphic modeling: Journal of Sedimentary Research, v. 75, p. 166–176, doi: 10.2110/jsr.2005.013.

Bestmann, M., Pennacchioni, G., Frank, G., Göken, M., and de Wall, H., 2011, Pseudotachylyte in muscovite-bearing quartzite: Coseismic friction-induced melting and plastic deformation of quartz: Journal of Structural Geology, v. 33, p. 169–186, doi: 10.1016/j.jsg.2010.10.009.

Bestmann, M., Pennacchioni, G., Nielsen, S., Göken, M., and de Wall, H., 2012, Deformation and ultrafine dynamic recrystallization of quartz in pseudotachylyte-bearing brittle faults: A matter of a few seconds: Journal of Structural Geology, v. 38, p. 21–38, doi: 10.1016/j.jsg.2011.10.001.

Bjørnerud, M., 2010, Rethinking conditions necessary for pseudotachylyte formation: Observations from the Otago schists, South Island, New Zealand: Tectonophysics, v. 490, p. 69–80, doi: 10.1016/j.tecto.2010.04.028.

Bjørnerud, M., and Magloughlin, J.F., 2004, Pressure-related feedback processes in the generation of pseudotachylytes: Journal of Structural Geology, v. 26, p. 2317–2323, doi: 10.1016/j.jsg.2002.08.001.

Boncio, P., Brozzetti, F., and Lavecchia, G., 2000, Architecture and seismotectonics of a regional low-angle normal fault zone in central Italy: Tectonics, v. 19, p. 1038–1055, doi: 10.1029/2000TC900023.

Bossière, G., 1991, Petrology of pseudotachylytes from the Alpine Fault of New Zealand: Tectonophysics, v. 196, p. 173–193, doi: 10.1016/0040-1951(91)90295-4.

Boullier, A.-M., Ohtani, T., Fujimoto, K., Ito, H., and Dubois, M., 2001, Fluid inclusions in pseudotachylytes from the Nojima fault, Japan: Journal of Geophysical Research: Solid Earth, v. 106, p. 21965–21977, doi: 10.1029/2000JB000043.

Boutareaud, S., Boullier, A.-M., Andréani, M., Calugaru, D.-G., Beck, P., Song, S.-R., and Shimamoto, T., 2010, Clay clast aggregates in gouges: New textural evidence for seismic faulting: Journal of Geophysical Research, v. 115, doi: 10.1029/2008JB006254.

Brodsky, E.E., Gilchrist, J.J., Sagy, A., and Collettini, C., 2011, Faults smooth gradually as a function of slip: Earth and Planetary Science Letters, v. 302, p. 185–193, doi: 10.1016/j.epsl.2010.12.010.

Buckley, S.J., Enge, H.D., Carlsson, C., and Howell, J.A., 2010, Terrestrial laser scanning for use in virtual outcrop geology: The Photogrammetric Record, v. 25, p. 225–239, doi: 10.1111/j.1477-9730.2010.00585.x.

Buckley, S.J., Howell, J.A., Enge, H.D., and Kurz, T.H., 2008, Terrestrial laser scanning in geology: data acquisition, processing and accuracy considerations: Journal of the Geological Society, v. 165, p. 625–638, doi: 10.1144/0016-76492007-100.

Caine, J.S., Bruhn, R.L., and Forster, C.B., 2010, Internal structure, fault rocks, and inferences regarding deformation, fluid flow, and mineralization in the seismogenic Stillwater normal fault, Dixie Valley, Nevada: Journal of Structural Geology, v. 32, p. 1576–1589, doi: 10.1016/j.jsg.2010.03.004.

Caine, J.S., Evans, J.P., and Forster, C.B., 1996, Fault zone architecture and permeability structure: Geology, v. 24, p. 1025–1028, doi: 10.1130/0091-7613(1996)024<1025:FZAAPS>2.3.CO;2.

Candela, T., and Renard, F., 2012, Segment linkage process at the origin of slip surface roughness: Evidence from the Dixie Valley fault: Journal of Structural Geology, v. 45, p. 87–100, doi: 10.1016/j.jsg.2012.06.003.

Candela, T., Renard, F., Bouchon, M., Brouste, A., Marsan, D., Schmittbuhl, J., and Voisin, C., 2009, Characterization of Fault Roughness at Various Scales: Implications of Three-Dimensional High Resolution Topography Measurements: Pure and Applied Geophysics, v. 166, p. 1817–1851, doi: 10.1007/s00024-009-0521-2.

Candela, T., Renard, F., Schmittbuhl, J., Bouchon, M., and Brodsky, E.E., 2011, Fault slip distribution and fault roughness: Geophysical Journal International, v. 187, p. 959–968, doi: 10.1111/j.1365-246X.2011.05189.x.

Cashman, S.M., Baldwin, J.N., Cashman, K.V., Swanson, K., and Crawford, R., 2007, Microstructures developed by coseismic and aseismic faulting in near-surface sediments, San Andreas fault, California: Geology, v. 35, p. 611, doi: 10.1130/G23545A.1.

Chester, F.M., Evans, J.P., and Biegel, R.L., 1993, Internal structure and weakening mechanisms of the San Andreas Fault: Journal of Geophysical Research: Solid Earth, v. 98, p. 771–786, doi: 10.1029/92JB01866.

Chester, F.M., and Logan, J.M., 1986, Implications for mechanical properties of brittle faults from observations of the Punchbowl fault zone, California: pure and applied geophysics, v. 124, p. 79–106, doi: 10.1007/BF00875720.

Collettini, C., 2009, Hypothesis for the mechanics and seismic behaviour of low-angle normal faults: the example of the Altotiberina fault Northern Apennines: Annals of Geophysics, v. 45.

Collettini, C., 2011, The mechanical paradox of low-angle normal faults: Current understanding and open questions: Tectonophysics, v. 510, p. 253–268, doi: 10.1016/j.tecto.2011.07.015.

Collettini, C., and Sibson, R.H., 2001, Normal faults, normal friction?: Geology, v. 29, p. 927–930, doi: 10.1130/0091-7613(2001)029<0927:NFNF>2.0.CO;2.

Cowan, D.S., 1999, Do faults preserve a record of seismic slip? A field geologist's opinion: Journal of Structural Geology, v. 21, p. 995–1001, doi: 10.1016/S0191-8141(99)00046-2.

Davis, G.A., and Lister, G.S., 1988, Detachment faulting in continental extension; Perspectives from the Southwestern U.S. Cordillera: Geological Society of America Special Papers, v. 218, p. 133–160, doi: 10.1130/SPE218-p133.

Di Toro, G., Nielsen, S., and Pennacchioni, G., 2005, Earthquake rupture dynamics frozen in exhumed ancient faults: Nature, v. 436, p. 1009–1012, doi: 10.1038/nature03910.

Di Toro, G., Niemeijer, A., Tripoli, A., Nielsen, S., Di Felice, F., Scarlato, P., Spada, G., Alessandroni, R., Romeo, G., Di Stefano, G., Smith, S., Spagnuolo, E., and Mariano, S., 2010, From field geology to earthquake simulation: A new state-of-the-art tool to investigate rock friction during the seismic cycle (SHIVA): Rendiconti Lincei, v. 21, p. 95–114, doi: 10.1007/s12210-010-0097-x.

Di Toro, G., and Pennacchioni, G., 2004, Superheated friction-induced melts in zoned pseudotachylytes within the Adamello tonalites (Italian Southern Alps): Journal of Structural Geology, v. 26, p. 1783–1801, doi: 10.1016/j.jsg.2004.03.001.

Eichhubl, P., and Boles, J., 2000, Rates of fluid flow in fault systems-evidence from episodic rapid fluid flow in Miocene Monterey Formation, coastal California: American Journal of Science, v. 300, p. 571–600.

Enge, H.D., Howell, J.A., and Buckley, S.J., 2010, The Geometry and Internal Architecture of Stream Mouth Bars in the Panther Tongue and the Ferron Sandstone Members, Utah, U.S.A.: Journal of Sedimentary Research, v. 80, p. 1018–1031, doi: 10.2110/jsr.2010.088.

Engelder, J.T., 1974, Microscopic wear grooves on slickensides: Indicators of paleoseismicity: Journal of Geophysical Research, v. 79, p. 4387–4392, doi: 10.1029/JB079i029p04387.

Engelder, T., 1978, Aspects of asperity-surface interaction and surface damage of rocks during experimental frictional sliding: pure and applied geophysics, v. 116, p. 705–716, doi: 10.1007/BF00876533.

Evans, J.P., and Chester, F.M., 1995, Fluid-rock interaction in faults of the San Andreas system: Inferences from San Gabriel fault rock geochemistry and microstructures: Journal of Geophysical Research: Solid Earth, v. 100, p. 13007–13020, doi: 10.1029/94JB02625.

Evans, J.P., and Langrock, H., 1994, Structural analysis of the Brigham City-Weber segment boundary zone, Wasatch normal fault, Utah: Implications for fault growth and structure: Pageoph, v. 142, p. 663–685.

Fagereng, Å., Remitti, F., and Sibson, R.H., 2011, Incrementally developed slickenfibers — Geological record of repeating low stress-drop seismic events?: Tectonophysics, v. 510, p. 381–386, doi: 10.1016/j.tecto.2011.08.015.

Fagereng, A., and Toy, V.G., 2011, Geology of the earthquake source: an introduction: Geological Society, London, Special Publications, v. 359, p. 1–16, doi: 10.1144/SP359.1.

Faulkner, D.R., Jackson, C.A.L., Lunn, R.J., Schlische, R.W., Shipton, Z.K., Wibberley, C.A.J., and Withjack, M.O., 2010, A review of recent developments concerning the structure, mechanics and fluid flow properties of fault zones: Journal of Structural Geology, v. 32, p. 1557–1575, doi: 10.1016/j.jsg.2010.06.009.

Friedman, M., Logan, J.M., and Rigert, J.A., 1974, Glass-Indurated Quartz Gouge in Sliding-Friction Experiments on Sandstone: Geological Society of America Bulletin, v. 85, p. 937–942, doi: 10.1130/0016-7606(1974)85<937:GQGISE>2.0.CO;2.

Gilbert, G.K., 1928, Studies of Basin-Range structure: U.S. Geological Survey Professional Paper 153, 146 p.

Gonzalez-Jorge, H., Riveiro, B., Vazquez-Fernandez, E., Martínez-Sánchez, J., and Arias, P., 2013, Metrological evaluation of Microsoft Kinect and Asus Xtion sensors: Measurement, v. 46, p. 1800–1806, doi: 10.1016/j.measurement.2013.01.011.

Goodwin, L.B., 1999, Controls on pseudotachylyte formation during tectonic exhumation in the South Mountains metamorphic core complex, Arizona: Geological Society, London, Special Publications, v. 154, p. 325–342, doi: 10.1144/GSL.SP.1999.154.01.15.

Han, R., Shimamoto, T., Ando, J., and Ree, J.-H., 2007, Seismic slip record in carbonate-bearing fault zones: An insight from high-velocity friction experiments on siderite gouge: Geology, v. 35, p. 1131, doi: 10.1130/G24106A.1.

Heilbronner, R., and Keulen, N., 2006, Grain size and grain shape analysis of fault rocks: Tectonophysics, v. 427, p. 199–216, doi: 10.1016/j.tecto.2006.05.020.

Hirose, T., and Shimamoto, T., 2005, Growth of molten zone as a mechanism of slip weakening of simulated faults in gabbro during frictional melting: Journal of Geophysical Research: Solid Earth, v. 110, doi: 10.1029/2004JB003207.

Jackson, J.A., 1987, Active normal faulting and crustal extension: Geological Society, London, Special Publications, v. 28, p. 3–17, doi: 10.1144/GSL.SP.1987.028.01.02.

Jackson, J.A., and White, N.J., 1989, Normal faulting in the upper continental crust: observations from regions of active extension: Journal of Structural Geology, v. 11, p. 15–36, doi: 10.1016/0191-8141(89)90033-3.

Jacobs, J.R., Evans, J.P., and Kolesar, P.T., 2006, Energetics of chemical alteration in fault zones and its relationship to the seismic cycle, *in* Abercrombie, R., McGarr, A., Kanamori, H., and Di Toro, G. eds., Geophysical Monograph Series, American Geophysical Union, Washington, D. C., p. 181–191.

Janecke, S.U., and Evans, J.P., 1988, Feldspar-influenced rock rheologies: Geology, v. 16, p. 1064–1067, doi: 10.1130/0091-7613(1988)016<1064:FIRR>2.3.CO;2.

Jessop, D.E., Kelfoun, K., Labazuy, P., Mangeney, A., Roche, O., Tillier, J.-L., Trouillet, M., and Thibault, G., 2012, LiDAR derived morphology of the 1993 Lascar pyroclastic flow deposits, and implication for flow dynamics and rheology: Journal of Volcanology and Geothermal Research, v. 245–246, p. 81–97, doi: 10.1016/j.jvolgeores.2012.06.030.

John, B.E., 1987, Geometry and evolution of a mid-crustal extensional fault system: Chemehuevi Mountains, southeastern California: Geological Society, London, Special Publications, v. 28, p. 313–335, doi: 10.1144/GSL.SP.1987.028.01.20.

Kairouz, M.E., Axen, G.J., Grove, M., Lovera, O., and Stockli, D.F., 2003, Late Cenozoic 40Ar/39Ar ages of fault rocks formed along the West Salton detachment system, southern California: Geological Society of America Abstracts with Programs, v. 35, p. 629.

Kanamori, H., and Brodsky, E.E., 2004, The physics of earthquakes: Reports on Progress in Physics, v. 67, p. 1429, doi: 10.1088/0034-4885/67/8/R03.

Kanamori, H., and Riveiro, L., 2006, Energy partitioning during an earthquake, *in* Abercrombie, R., McGarr, A., and Kanamori, H. eds., Earthquakes: Radiated Energy and the Physics of Faulting, Geopysical Monograph Series 170, American Geophysical Union, Washington, D. C., p. 3–13.

Khoshelham, K., and Elberink, S.O., 2012, Accuracy and Resolution of Kinect Depth Data for Indoor Mapping Applications: Sensors, v. 12, p. 1437–1454, doi: 10.3390/s120201437.

Killick, A.M., 1990, Pseudotachylite generated as a result of a drilling "burn-in:" Tectonophysics, v. 171, p. 221–227, doi: 10.1016/0040-1951(90)90100-M.

King, P.B., and Beikman, H.M., 1974, Geologic map of the United States: United States Geological Survey.

Kirkpatrick, J.D., and Rowe, C.D., 2013, Disappearing ink: How pseudotachylytes are lost from the rock record: Journal of Structural Geology, v. (in press), doi: 10.1016/j.jsg.2013.03.003.

Kirkpatrick, J.D., and Shipton, Z.K., 2009, Geologic evidence for multiple slip weakening mechanisms during seismic slip in crystalline rock: Journal of Geophysical Research: Solid Earth, v. 114, doi: 10.1029/2008JB006037.

Kirkpatrick, J.D., Shipton, Z.K., Evans, J.P., Micklethwaite, S., Lim, S.J., and McKillop, P., 2008, Strike-slip fault terminations at seismogenic depths: The structure and kinematics of the Glacier Lakes fault, Sierra Nevada United States: Journal of Geophysical Research: Solid Earth, v. 113, doi: 10.1029/2007JB005311.

Kirkpatrick, J.D., Shipton, Z.K., and Persano, C., 2009, Pseudotachylytes: Rarely Generated, Rarely Preserved, or Rarely Reported?: Bulletin of the Seismological Society of America, v. 99, p. 382–388, doi: 10.1785/0120080114.

Levi, T., Weinberger, R., and Eyal, Y., 2011, A coupled fluid-fracture approach to propagation of clastic dikes during earthquakes: Tectonophysics, v. 498, p. 35–44, doi: 10.1016/j.tecto.2010.11.012.

Lin, A., 1994, Glassy pseudotachylyte veins from the Fuyun fault zone, northwest China: Journal of Structural Geology, v. 16, p. 71–83, doi: 10.1016/0191-8141(94)90019-1.

Lin, A., 1996, Injection veins of crushing-originated pseudotachylyte and fault gouge formed during seismic faulting: Engineering Geology, v. 43, p. 213–224, doi: 10.1016/0013-7952(96)00062-2.

Lin, A., 1999, Roundness of clasts in pseudotachylytes and cataclastic rocks as an indicator of frictional melting: Journal of Structural Geology, v. 21, p. 473–478, doi: 10.1016/S0191-8141(99)00030-9.

Lin, A., 2008, Fossil Earthquakes: the formation and preservation of pseudotachylytes: Springer, New York, 348 p.

Lin, A., 2011, Seismic slip recorded by fluidized ultracataclastic veins formed in a coseismic shear zone during the 2008 Mw 7.9 Wenchuan earthquake: Geology, v. 39, p. 547–550, doi: 10.1130/G32065.1.

Lin, A., and Shimamoto, T., 1998, Selective melting processes as inferred from experimentally generated pseudotachylytes: Journal of Asian Earth Sciences, v. 16, p. 533–545, doi: 10.1016/S0743-9547(98)00040-3.

Lin, A., Shin, and Kano, K., 2012, Fluidized Cataclastic Veins along the Itoigawa-Shizuoka Tectonic Line Active Fault System, Central Japan, and Its Seismotectonic Implications: The Journal of Geology, v. 120, p. 453–465, doi: 10.1086/665795.

Lockner, D.A., and Beeler, N.M., 2002, Rock failure and earthquakes, *in* William H.K. Lee, H.K. ed., International Geophysics, Academic Press, p. 505–537.

Maddock, R.H., 1983, Melt origin of fault-generated pseudotachylytes demonstrated by textures: Geology, v. 11, p. 105–108, doi: 10.1130/0091-7613(1983)11<105:MOOFPD>2.0.CO;2.

Magloughlin, J.F., 1989, The nature and significance of pseudotachylite from the Nason terrane, North Cascade Mountains, Washington: Journal of Structural Geology, v. 11, p. 907–917, doi: 10.1016/0191-8141(89)90107-7.

Magloughlin, J.F., 1992, Microstructural and chemical changes associated with cataclasis and frictional melting at shallow crustal levels: the cataclasite-pseudotachylyte connection: Tectonophysics, v. 204, p. 243–260, doi: 10.1016/0040-1951(92)90310-3.

Magloughlin, J.F., 2011, Bubble Collapse Structure: A Microstructural Record of Fluids, Bubble Formation and Collapse, and Mineralization in Pseudotachylyte: The Journal of Geology, v. 119, p. 351–371, doi: 10.1086/659143.

Magloughlin, J.F., and Spray, J.G., 1992, Frictional melting processes and products in geological materials: introduction and discussion: Tectonophysics, v. 204, p. 197–204, doi: 10.1016/0040-1951(92)90307-R.

Mankoff, K.D., and Russo, T.A., 2012, The Kinect: a low-cost, high-resolution, short-range 3D camera: Earth Surface Processes and Landforms, doi: 10.1002/esp.3332.

Marone, C., and Richardson, E., 2010, Learning to read fault-slip behavior from fault-zone structure: Geology, v. 38, p. 767–768, doi: 10.1130/focus082010.1.

McCaffrey, K.J.W., Feely, M., Hennessy, R., and Thompson, J., 2008, Visualization of folding in marble outcrops, Connemara, western Ireland: An application of virtual outcrop technology: Geosphere, v. 4, p. 588–599, doi: 10.1130/GES00147.1.

McGarr, A., 1999, On relating apparent stress to the stress causing earthquake fault slip: Journal of Geophysical Research: Solid Earth, v. 104, p. 3003–3011, doi: 10.1029/1998JB900083.

McKenzie, D., and Brune, J.N., 1972, Melting on Fault Planes During Large Earthquakes: Geophysical Journal International, v. 29, p. 65–78, doi: 10.1111/j.1365-246X.1972.tb06152.x.

Means, W.D., 1993, Elementary geometry of deformation processes: Journal of Structural Geology, v. 15, p. 343–349, doi: 10.1016/0191-8141(93)90131-S.

Meneghini, F., Toro, G.D., Rowe, C.D., Moore, J.C., Tsutsumi, A., and Yamaguchi, A., 2010, Record of mega-earthquakes in subduction thrusts: The black fault rocks of Pasagshak Point (Kodiak Island, Alaska): Geological Society of America Bulletin, v. 122, p. 1280–1297, doi: 10.1130/B30049.1.

Mitchell, T.M., Ben-Zion, Y., and Shimamoto, T., 2011, Pulverized fault rocks and damage asymmetry along the Arima-Takatsuki Tectonic Line, Japan: Earth and Planetary Science Letters, v. 308, p. 284–297, doi: 10.1016/j.epsl.2011.04.023.

Monzawa, N., and Otsuki, K., 2003, Comminution and fluidization of granular fault materials: implications for fault slip behavior: Tectonophysics, v. 367, p. 127–143, doi: 10.1016/S0040-1951(03)00133-1.

Mouslopoulou, V., Moraetis, D., and Fassoulas, C., 2011, Identifying past earthquakes on carbonate faults: Advances and limitations of the "Rare Earth Element" method based on analysis of the Spili Fault, Crete, Greece: Earth and Planetary Science Letters, v. 309, p. 45–55, doi: 10.1016/j.epsl.2011.06.015.

Nelson, C.E., Jerram, D.A., Hobbs, R.W., Terrington, R., and Kessler, H., 2011, Reconstructing flood basalt lava flows in three dimensions using terrestrial laser scanning: Geosphere, v. 7, p. 87–96, doi: 10.1130/GES00582.1.

Nielsen, S., Di Toro, G., Hirose, T., and Shimamoto, T., 2008, Frictional melt and seismic slip: Journal of Geophysical Research: Solid Earth, v. 113, doi: 10.1029/2007JB005122.

Niemeijer, A., Di Toro, G., Nielsen, S., and Di Felice, F., 2011, Frictional melting of gabbro under extreme experimental conditions of normal stress, acceleration, and sliding velocity: Journal of Geophysical Research: Solid Earth, v. 116, p. n/a–n/a, doi: 10.1029/2010JB008181.

O'Hara, K., 1992, Major- and trace-element constraints on the petrogenesis of a fault-related pseudotachylyte, western Blue Ridge province, North Carolina: Tectonophysics, v. 204, p. 279–288, doi: 10.1016/0040-1951(92)90312-T.

Otsuki, K., Uduki, T., Monzawa, N., and Tanaka, H., 2005, Clayey injection veins and pseudotachylyte from two boreholes penetrating the Chelungpu Fault, Taiwan: Their implications for the contrastive seismic slip behaviors during the 1999 Chi-Chi earthquake: Island Arc, v. 14, p. 22–36, doi: 10.1111/j.1440-1738.2004.00455.x.

Pearce, M.A., Jones, R.R., Smith, S.A.F., and McCaffrey, K.J.W., 2011, Quantification of fold curvature and fracturing using terrestrial laser scanning: American Association of Petroleum Geologists Bulletin, v. 95, p. 771–794, doi: 10.1306/11051010026.

Peng, Z., and Gomberg, J., 2010, An integrated perspective of the continuum between earthquakes and slow-slip phenomena: Nature Geoscience, v. 3, p. 599–607, doi: 10.1038/ngeo940.

Philpotts, A.R., 1964, Origin of pseudotachylites: American Journal of Science, v. 262, p. 1008–1035, doi: 10.2475/ajs.262.8.1008.

Plattner, U., Markl, G., and Sherlock, S., 2003, Chemical heterogeneities of Caledonian (?) pseudotachylites in the Eidsfjord Anorthosite, north Norway: Contributions to Mineralogy and Petrology, v. 145, p. 316–338, doi: 10.1007/s00410-003-0455-0.

Power, W.L., and Tullis, T.E., 1989, The relationship between slickenside surfaces in fine-grained quartz and the seismic cycle: Journal of Structural Geology, v. 11, p. 879–893.

Power, W.L., and Tullis, T.E., 1992, The contact between opposing fault surfaces at Dixie Valley, Nevada, and implications for fault mechanics: Journal of Geophysical Research: Solid Earth, v. 97, p. 15425–15435, doi: 10.1029/92JB01059.

Power, W.L., Tullis, T.E., Brown, S.R., Boitnott, G.N., and Scholz, C.H., 1987, Roughness of natural fault surfaces: Geophysical Research Letters, v. 14, p. 29–32, doi: 10.1029/GL014i001p00029.

Ray, S.K., 1999, Transformation of cataclastically deformed rocks to pseudotachylyte by pervasion of frictional melt: inferences from clast-size analysis: Tectonophysics, v. 301, p. 283–304, doi: 10.1016/S0040-1951(98)00229-7.

Ray, S.K., 2004, Melt–clast interaction and power-law size distribution of clasts in pseudotachylytes: Journal of Structural Geology, v. 26, p. 1831–1843, doi: 10.1016/j.jsg.2004.02.009.

Rempel, A.W., and Rice, J.R., 2006, Thermal pressurization and onset of melting in fault zones: Journal of Geophysical Research, v. 111, doi: 10.1029/2006JB004314.

Renard, F., Voisin, C., Marsan, D., and Schmittbuhl, J., 2006, High resolution 3D laser scanner measurements of a strike-slip fault quantify its morphological anisotropy at all scales: Geophysical Research Letters, v. 33, doi: 10.1029/2005GL025038.

Rice, J.R., 2006, Heating and weakening of faults during earthquake slip: Journal of Geophysical Research, v. 111, doi: 10.1029/2005JB004006.

Rietbrock, A., Tiberi, C., Scherbaum, F., and Lyon-Caen, H., 1996, Seismic slip on a low angle normal fault in the Gulf of Corinth: Evidence from high-resolution cluster analysis of microearthquakes: Geophysical Research Letters, v. 23, p. 1817–1820, doi: 10.1029/96GL01257.

Rowe, C.D., Kirkpatrick, J.D., and Brodsky, E.E., 2012, Fault rock injections record paleo-earthquakes: Earth and Planetary Science Letters, v. 335–336, p. 154–166, doi: 10.1016/j.epsl.2012.04.015.

Rowe, C.D., Moore, J.C., Meneghini, F., and McKeirnan, A.W., 2005, Large-scale pseudotachylytes and fluidized cataclasites from an ancient subduction thrust fault: Geology, v. 33, p. 937–940, doi: 10.1130/G21856.1.

Sagy, A., and Brodsky, E.E., 2009, Geometric and rheological asperities in an exposed fault zone: Journal of Geophysical Research: Solid Earth, v. 114, doi: 10.1029/2008JB005701.

Sagy, A., Brodsky, E.E., and Axen, G.J., 2007, Evolution of fault-surface roughness with slip: Geology, v. 35, p. 283–286, doi: 10.1130/G23235A.1.

Scholz, C.H., 1980, Shear heating and the state of stress on faults: Journal of Geophysical Research: Solid Earth, v. 85, p. 6174–6184, doi: 10.1029/JB085iB11p06174.

Scholz, C.H., 1988, The critical slip distance for seismic faulting: Nature, v. 336, p. 761–763, doi: 10.1038/336761a0.

Scholz, C.H., 2002, The Mechanics of Earthquakes and Faulting: Cambridge University Press, 508 p.

Scholz, C.H., 2010, Large Earthquake Triggering, Clustering, and the Synchronization of Faults: Bulletin of the Seismological Society of America, v. 100, p. 901–909, doi: 10.1785/0120090309.

Schulz, S.E., and Evans, J.P., 2000, Mesoscopic structure of the Punchbowl Fault, Southern California and the geologic and geophysical structure of active strike-slip faults: Journal of Structural Geology, v. 22, p. 913–930, doi: 10.1016/S0191-8141(00)00019-5.

Shipton, Z.K., Evans, J.P., Abercrombie, R.E., and Brodsky, E.E., 2006, The missing sinks: Slip localization in faults, damage zones, and the seismic energy budget, *in* Abercrombie, R., McGarr, A., Kanamori, H., and Di Toro, G. eds., Geophysical

Monograph Series, American Geophysical Union, Washington, D. C., p. 217–222.

Sibson, R.H., 1975, Generation of Pseudotachylyte by Ancient Seismic Faulting: Geophysical Journal of the Royal Astronomical Society, v. 43, p. 775–794, doi: 10.1111/j.1365-246X.1975.tb06195.x.

Sibson, R.H., 1977, Fault rocks and fault mechanisms: Journal of the Geological Society, v. 133, p. 191–213, doi: 10.1144/gsjgs.133.3.0191.

Sibson, R.H., 1983, Continental fault structure and the shallow earthquake source: Journal of the Geological Society, v. 140, p. 741–767, doi: 10.1144/gsjgs.140.5.0741.

Sibson, R.H., 1985, Stopping of earthquake ruptures at dilational fault jogs: Nature, v. 316, p. 248–251, doi: 10.1038/316248a0.

Sibson, R.H., 2003, Thickness of the Seismic Slip Zone: Bulletin of the Seismological Society of America, v. 93, p. 1169–1178, doi: 10.1785/0120020061.

Sibson, R.H., and Toy, V.G., 2006, The habitat of fault-generated pseudotachylyte: Presence vs. absence of friction-melt: Geophysical Monograph Series, v. 170, p. 153–166, doi: 10.1029/170GM16.

Siman-Tov, S., Aharonov, E., Sagy, A., and Emmanuel, S., 2013, Nanograins form carbonate fault mirrors: Geology, v. 41, p. 703–706, doi: 10.1130/G34087.1.

Smisek, J., Jancosek, M., and Pajdla, T., 2013, 3D with Kinect, *in* Fossati, A., Gall, J., Grabner, H., Ren, X., and Konolige, K. eds., Consumer depth cameras for computer vision, advances in computer vision and pattern recognition, Springer London, p. 3–25.

Smith, S.A.F., Billi, A., Toro, G.D., and Spiess, R., 2011, Principal Slip Zones in Limestone: Microstructural Characterization and Implications for the Seismic Cycle (Tre Monti Fault, Central Apennines, Italy): Pure and Applied Geophysics, v. 168, p. 2365–2393, doi: 10.1007/s00024-011-0267-5.

Smith, S.A.F., Collettini, C., and Holdsworth, R.E., 2008, Recognizing the seismic cycle along ancient faults: CO_2-induced fluidization of breccias in the footwall of a sealing low-angle normal fault: Journal of Structural Geology, v. 30, p. 1034–1046, doi: 10.1016/j.jsg.2008.04.010.

Smith, S. A. F., Toro, G.D., Kim, S., Ree, J.-H., Nielsen, S., Billi, A., and Spiess, R., 2013, Coseismic recrystallization during shallow earthquake slip: Geology, v. 41, p. 63–66, doi: 10.1130/G33588.1.

Sorel, D., 2000, A Pleistocene and still-active detachment fault and the origin of the Corinth-Patras rift, Greece: Geology, v. 28, p. 83–86, doi: 10.1130/0091-7613(2000)28<83:APASDF>2.0.CO;2.

Spray, J.G., 1987, Artificial generation of pseudotachylyte using friction welding apparatus: simulation of melting on a fault plane: Journal of Structural Geology, v. 9, p. 49–60, doi: 10.1016/0191-8141(87)90043-5.

Spray, J.G., 1988, Generation and crystallization of an amphibolite shear melt: an investigation using radial friction welding apparatus: Contributions to Mineralogy and Petrology, v. 99, p. 464–475, doi: 10.1007/BF00371937.

Spray, J.G., 1989, Slickenside formation by surface melting during the mechanical excavation of rock: Journal of structural geology, v. 11, p. 895–905.

Spray, J.G., 1992, A physical basis for the frictional melting of some rock-forming minerals: Tectonophysics, v. 204, p. 205–221, doi: 10.1016/0040-1951(92)90308-S.

Spray, J.G., 2010, Frictional Melting Processes in Planetary Materials: From Hypervelocity Impact to Earthquakes: Annual Review of Earth and Planetary Sciences, v. 38, p. 221–254, doi: 10.1146/annurev.earth.031208.100045.

Stoinski, S., 2011, From a Skeleton to a 3D Dinosaur, *in* Elewa, A.M.T. ed., Computational Paleontology, Springer, Berlin Heidelberg, p. 147–164.

Stünitz, H., Keulen, N., Hirose, T., and Heilbronner, R., 2010, Grain size distribution and microstructures of experimentally sheared granitoid gouge at coseismic slip rates – Criteria to distinguish seismic and aseismic faults?: Journal of Structural Geology, v. 32, p. 59–69, doi: 10.1016/j.jsg.2009.08.002.

Thatcher, W., and Hill, D.P., 1991, Fault orientations in extensional and conjugate strike-slip environments and their implications: Geology, v. 19, p. 1116–1120, doi: 10.1130/0091-7613(1991)019<1116:FOIEAC>2.3.CO;2.

Togo, T., and Shimamoto, T., 2012, Energy partition for grain crushing in quartz gouge during subseismic to seismic fault motion: An experimental study: Journal of Structural Geology, v. 38, p. 139–155, doi: 10.1016/j.jsg.2011.12.014.

Toy, V.G., Ritchie, S., and Sibson, R.H., 2011, Diverse habitats of pseudotachylytes in the Alpine Fault Zone and relationships to current seismicity: Geological Society, London, Special Publications, v. 359, p. 115–133, doi: 10.1144/SP359.7.

Tsutsumi, A., 1999, Size distribution of clasts in experimentally produced pseudotachylytes: Journal of Structural Geology, v. 21, p. 305–312, doi: 10.1016/S0191-8141(98)00113-8.

Tsutsumi, A., and Shimamoto, T., 1997, High-velocity frictional properties of gabbro: Geophysical Research Letters, v. 24, p. 699–702, doi: 10.1029/97GL00503.

Ujiie, K., Yamaguchi, A., Kimura, G., and Toh, S., 2007, Fluidization of granular material in a subduction thrust at seismogenic depths: Earth and Planetary Science Letters, v. 259, p. 307–318, doi: 10.1016/j.epsl.2007.04.049.

Wang, C., 1997, A microstructural study on pseudotachylytes and microbreccias from the Whipple low-angle normal fault: Geological Society of America Abstracts with Programs, v. 29, p. 72–73.

Ward, S.N., 1998, On the consistency of earthquake moment release and space geodetic strain rates: Europe: Geophysical Journal International, v. 135, p. 1011–1018, doi: 10.1046/j.1365-246X.1998.t01-2-00658.x.

Wenk, H.-R., Janssen, C., Kenkmann, T., and Dresen, G., 2011, Mechanical twinning in quartz: Shock experiments, impact, pseudotachylites and fault breccias: Tectonophysics, v. 510, p. 69–79, doi: 10.1016/j.tecto.2011.06.016.

Wenk, H.-R., Johnson, L.R., and Ratschbacher, L., 2000, Pseudotachylites in the Eastern Peninsular Ranges of California: Tectonophysics, v. 321, p. 253–277, doi: 10.1016/S0040-1951(00)00064-0.

White, J.C., 2012, Paradoxical pseudotachylyte – Fault melt outside the seismogenic zone: Journal of Structural Geology, v. 38, p. 11–20, doi: 10.1016/j.jsg.2011.11.016.

Will, T.M., 1987, Structural investigations on experimental and naturally produced slickensides [M.S. thesis]: State University of New York at Albany.

Will, T.M., and Wilson, C.J., 1989, Experimentally produced slickenside lineations in pyrophyllitic clay: Journal of Structural Geology, v. 11, p. 657–667, doi: 10.1016/0191-8141(89)90002-3.

CHAPTER 2

PSEUDOTACHYLYTE AND FLUID ALTERATION AT SEISMOGENIC DEPTHS

(GLACIER LAKES AND GRANITE PASS FAULTS, CENTRAL SIERRA

NEVADA USA)

Abstract

We present evidence for ancient seismicity in the form of tectonic

pseudotachylyte and coeval or cyclic hydrothermal alteration and cataclasis along fault

zones exhumed from 2.4-6.0 km in the central Sierra Nevada, CA. The Glacier Lakes

fault (GLF) and Granite Pass fault (GPF) are left-lateral to left-lateral oblique, strike-slip

faults with up to 125 m of left-lateral separation exposed in Mesozoic granite and

granodiorite plutons. Precipitation of epidote anlong fault slip-surfaces, chloritization of

biotite, saussurite and sericite alteration of plagioclase, and quartz and calcite filled veins

are present in the GLF and GPF zones. Cross-cutting hydrothermal alteration and calcite

deformation-twins constrain the temperature conditions in the fault zone to between 170-

320 °C during pseudotachylyte formation. Based on previous thermochronologic studies

the temperature conditions of the country rock during faulting were between 110-160 °C,

10-210 °C less than the temperatures in the fault zone. The elevated temperatures in the

fault zone can be explained by: 1) infiltration of hydrothermal fluids into the fault zone,

or 2) elevated temperatures as a result of frictional heating in the fault zone during

seismic slip. Distinguished between these two hypotheses is difficult and a unique

conclusion is not suggested here. However, the documentation of hydrothermal alteration that was driven by co-seismic frictional heat helps to explain the lack of significant heat flow anomalies associated with large strike-slip faults.

One difficulty encountered by studies in exhumed fault zones is providing convincing evidence for a frictional melt origin of pseudotachylyte. Rocks in the field may preserve convincing evidence for frictional melt (i.e. aphanitic, dark, injection structures) that are later shown to be related to cataclasis or injection of hydrothermal fluids. Another challenge results from the low preservation potential of several of the microscopic features that are convincing of a frictional melt origin (microlites, amygdules, and glassy matrix). Here we test the usefullness of grain shape and nearest neighbor distribution analysis of pseudotachylyte and cataclasites from the GLF and GPF to discriminate between these fault rocks and to determine a frictional melt origin for pseudotachylyte. Pseudotachylytes have more circular clasts and a more random nearest neighbor clast distribution than cataclasites. With increased comminution and melting the mean clast circularity increases and the nearest neighbor distances approach a random distribution. We conclude that this observed pattern can be applied to other fault zones as an indicator of a frictional melt origin for fault-related rocks.

The documentation of hydrothermal alteration associated with pseudotachylyte formation that we document here suggests that the conditions at which pseudotachylyte formed are broader than previously estimated and that the generation of frictional melt is possible under hydrothermal conditions.

1. Introduction

Studies of exhumed fault zones from meso- to microscales provide significant insights into deformation associated with earthquake rupture and the total energy budget of the seismic cycle (Chester et al., 1993; Ben-Zion and Sammis, 2003; Wibberley and Shimamoto, 2003; Di Toro and Pennacchioni, 2005; Kirkpatrick and Shipton, 2009; Mittempergher et al., 2009; Nielsen et al., 2010; Meneghini et al., 2010), and this work has contributed significantly to our understanding of earthquake processes at depths between 0-12 km. There is, however, a disconnect between the rate of seismic activity and definitive evidence for seismic slip on exposed faults (Sibson and Toy, 2006; Kirkpatrick and Shipton, 2009; Kirkpatrick and Rowe, 2013), and a relative paucity of data to constrain models for rupture nucleation and propagation at depths where large crustal earthquakes typically nucleate (~6-12 km) (Fig. 2-1). Critical observations for determining the deformational processes active on faults include the dimensions of fault components, relationships between structures, and compositional variation across the fault zone (Chester et al., 1993; Cowan, 1999; Schulz and Evans, 2000; Wibberley and Shimamoto, 2003; Jacobs et al., 2006; Shipton et al., 2006). Further characterization of the distribution of damage in fault zones at and below the seismogenic zone are needed for constraining models of rupture nucleation and propagation, fluid pressure generation, frictional heat generation and dissipation, and off-fault damage (Schulz and Evans, 2000). Description and identification of fault-related deformation products that are diagnostic of seismic slip have been topics of recent geologic research, and these products have

implications for the energy budget of earthquakes, fault strength, and fault-rock

assemblage (Cowan, 1999; Austrheim et al., 1996; Di Toro and Pennacchioni, 2005;

Jacobs et al., 2006; Shipton et al., 2006; Smith et al., 2008, 2013; Beggan and Hamilton,

2010; Stünitz et al., 2010; Rowe et al., 2012; Griffith et al., 2012).
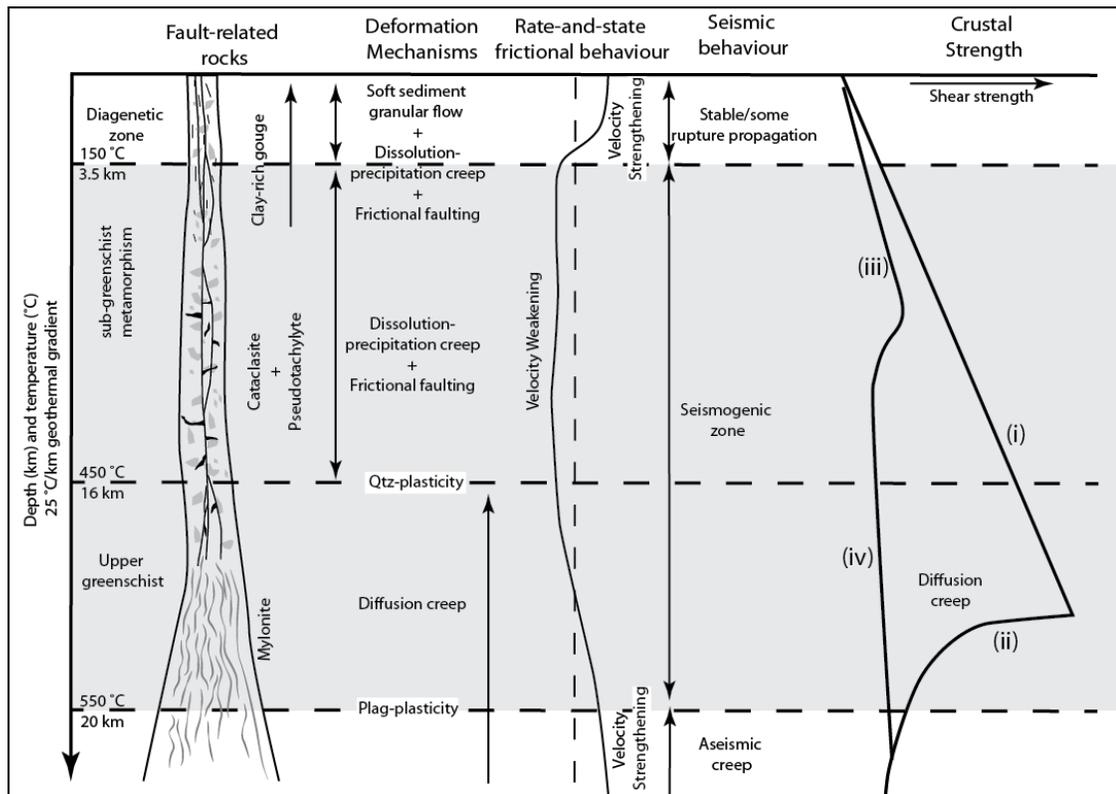
Figure 2-1: Conceptual model of seismogenic strike-slip fault-zone with depth and

schematic strength profiles in quartzofelspathic (i, ii) and phyllosilicate-bearing rocks (iii,

iv). (Modified from Sibson, 1983; Janecke and Evans, 1988; Blanpied et al., 1991, 1995;

Scholz, 2002; Imber et al., 2001; Fagereng and Toy, 2011).

The work done during seismic slip can be defined by:

$$W_f = Q + E_s + U_s + W_g \qquad (1)$$

where W_f is the work done in faulting including: heat (Q), seismic waves (E_s), gouge formation and surface refinement (U_s), and work against gravity (W_g) (Kanamori and Riveira, 2006; Sibson and Toy, 2006; Jacobs et al., 2006; Shipton et al., 2006). In most analyses, E_s is considered to be between 5 and 20% of the total energy released during an earthquake (Lockner and Okubo, 1983; McGarr, 1999; Di Toro et al., 2005; Tanaka et al., 2006; Kanamori and Riveira, 2006). W_g depends on the depth of nucleation and fault orientation (Di Toro et al., 2005). Therefore, up to 80 and 95 % of the energy released during an earthquake results in creation of new fractures (U_s), frictional heat (Q) and other dissipative processes in fault-related rocks (Lockner and Okubo, 1983; Di Toro et al., 2005; Jacobs et al., 2006; Shipton et al., 2006; Pittarello et al., 2008).

With the exception of fault-related pseudotachylyte, few if any fault-related deformation products provide unequivocal evidence for paleoseismicity along exhumed faults (Tullis, 1994; Cowan, 1999; Marone and Richardson, 2010). Tectonic pseudotachylytes have been reported from a variety of tectonic environments, depths, and rock types (Sibson, 1975; Magloughlin, 1989; Magloughlin, 2011; Magloughlin and Spray, 1992; Cowan, 1999; Wenk et al., 2000; Boullier et al., 2001; Plattner et al., 2003; Allen, 2005; Di Toro et al., 2005; Sibson and Toy, 2006; Lin, 2008; Kirkpatrick and Shipton, 2009; Bestmann et al., 2011; and many others). High temperatures required to generate pseudotachylyte (650-1700 °C at 1 atm) (Lin, 2008; Spray, 2010; Nielsen et al.,

2010), can only reasonably be explained by frictional heating at seismic slip rates (0.1-1.0 m/sec^{-1}) (McKenzie and Brune, 1972; Sibson, 1975; Cowan, 1999; Lin, 2008; Spray, 2010; Di Toro et al., 2010). We present evidence for meso- to microscale structures, fault-rock composition, and fluid-rock interactions associated with fault zones that preserve evidence for seismic activity in fault-related rocks at depth. We describe the geologic context, deformation mechanisms, and composition of several fault-related rock types including: pseudotachylyte, ultracataclasite, and highly polished slip surfaces, as well as evidence for fluid-alteration.

The documentation of pseudotachylyte here and by previous studies (Table 2-1) (Kirkpatrick et al., 2008, 2012; Kirkpatrick and Shipton, 2009), and the detailed analyses of the chemical and microstructural processes presented here allow us to test hypotheses regarding the nature of slip at seismogenic depths and constrain our understanding of the total energy budget of earthquakes. The exceptional preservation of pseudotachylyte along the GLF and GPF enable us to link evidence for ancient seismicity with microscopic processes, and the interplay of melt-production and hydrothermal processes. We also explore the coseismic strain of pseudotachylyte veins using amygdules (filled vesicles) as a strain marker.

Table 2-1: Observations of GLF and GPF fault-related rocks that are consistent with a frictional melt origin for pseudotachylyte (Magloughlin and Spray, 1992; Lin, 2008; Kirkpatrick et al., 2009; Kirkpatrick and Rowe, 2013)

Feature	Quality of evidence*	Outcrop	Optical Microscopy	SEM
Microlites	e.		x	x
Amygdules	e.		x	x
Glassy Silicate Matrix	e.		x	x
Flow Structures	v.g.		x	x
Quartz and Feldspar clasts	g.		x	x
Rounded/embayed clasts	g.		x	x
Random clast distribution	g.		x	
Injection vein morphology	g.	x	x	x
Aphanitic matrix	g.	x	x	x
* Quality of evidence assessments: good (g.), very good (v.g.), and excellent (e.) are ranked on qualitative usefulness of a feature as an indicator of rapidly quenched melt.				

1.1 Study Area

The Volcanic lakes area of Sequoia and Kings Canyon National Park, California, in the central portion of the Sierra Nevada batholith, consist of a series of plutons emplaced from 102 to 88 Ma along the western margin of North America (Fig. 2-2) (Stern et al., 1981; Chen and Moore, 1982; Bateman, 1992). Left-lateral strike-slip faults in the study area strike northeast-southwest and are up to 8 km in trace length (Fig. 2-2) (Kirkpatrick and Shipton, 2009; Kirkpatrick et al., 2008). These faults include the Glacier Lakes (GLF) and Granite Pass (GPF) faults. The GLF and GPF are the principal faults of interest in this study due to excellent exposure and a body of recent work focused on understanding the geometry, textural relationships, temperature, and timing of faulting

(Segall et al., 1990; Pachell and Evans, 2002; Pachell et al., 2003; Kirkpatrick et al., 2008, 2012; Kirkpatrick and Shipton, 2009). When placed into a thermochronologic framework for the plutonic host rock, ^{40}Ar/^{39}Ar dates of tectonic pseudotachylyte (76.6 ± 0.3 Ma) have been used to infer that pseudotachylyte formed at depths between 2.4-6.0 km with ambient temperatures between 110-160 °C (Kirkpatrick et al., 2012). The GLF is an E-W to NE-SW striking, steeply-dipping, left-lateral strike-slip fault with a maximum observed displacement of 125 m (Kirkpatrick et al., 2008). The western termination of the GLF is comprised by a series of NE-SW striking, steeply-dipping, left-lateral strike-slip faults that splay from the GLF to the southwest (Kirkpatrick et al., 2008). These splay faults have a highly asymmetric displacement gradient, with the greatest displacement close to the GLF and decreasing to zero to the southwest (Fig. 2-3; Table 2-2) (Kirkpatrick et al., 2008). The E-W striking, steeply-dipping, left-lateral strike-slip GPF is cross-cut by the GLF splays and preserves more pervasive crystal-plastic deformation (Kirkpatrick et al., 2008).
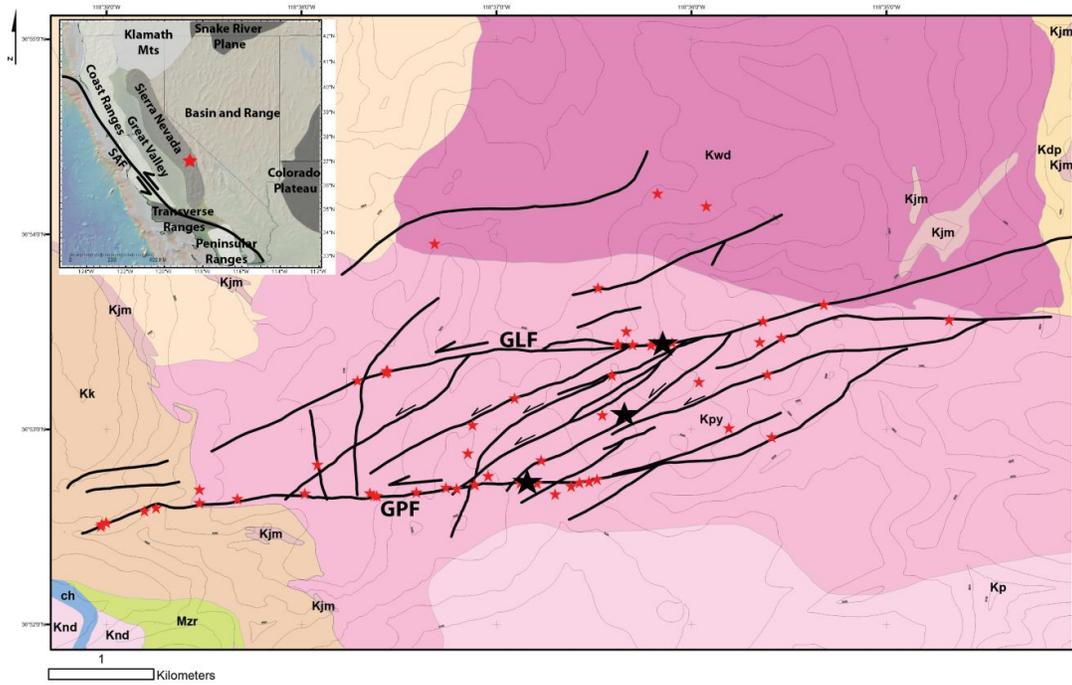
Figure 2-2: Geologic map (modified from Moore, 1978) of northern Kings Canyon National Park, central Sierra Nevada, California, and inset map with location of field area (red star) and physiographic provinces. Seventy seven (77) samples have been collected throughout the field area (red stars) and pseduotachylyte samples (black stars), focused on fault related rocks. This is Pyramid pluton (Kpy), mafic plutonic rock (Kjm), Granite of Kennedy lakes (Kk), Paradise pluton (Kp), Granodiorite of White divide (Kwd), Granite of Tehipite Dome (Kt).
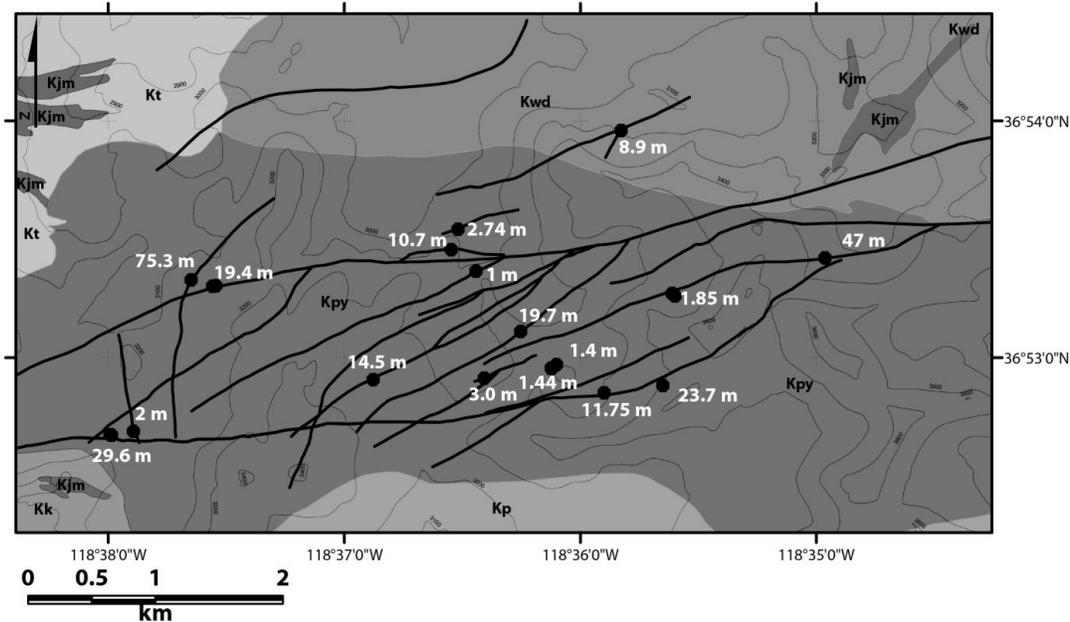
Figure 2-3: Geologic map (modified from Moore, 1978), and offset measurements along the GLF, GLF-splays, and GPF.

2. Methods

Sample characterization includes optical petrographic microscopy, scanning electron microscopy, and x-ray diffraction (XRD) analyses focused on microstructural and mineralogical characterization of the GLF and GPF zones. Petrographic analyses were conducted using transmitted light microscopy, grain-size analyses and measurements were conducted using NIH Image J, and Geological Imaging Analysis Software (GIAS) image processing software (Beggan and Hamilton, 2010; http://rsbweb.nih.gov/ij/). Standard scanning electron microscopy, back-scattered electron images (SEM-BSE) and energy-dispersive x-ray spectroscopy (EDS) analyses were

conducted using a FEI Quanta 200 equipped with an EDAX EDS system at operating

voltages between 15-20 kV at Weber State University. The XRD analyses were

conducted using an X Pert Pro Diffractometer system (45kV/40 MA) at Utah State

University.

3. Structural Geology

Cretaceous plutons in the field area are cross-cut by the Glacier Lakes fault

(GLF), the Granite Pass fault (GPF), ~ 10-15 km long, left lateral strike-slip fault zones

as well as smaller sub-parallel faults (Fig. 2-2) (Kirkpatrick et al., 2008). Geologic

mapping and aerial photo interpretation was used to describe the structure of the Glacier

Lakes and Granite Pass faults (Fig. 2-2; Fig. 2-3) (Supplemental data). Offset aplite dikes

and slickensides were used to determine total displacement along strike (Fig. 2-3; Table

2-2). These data are used to generate a structural framework for detailed microstructural

analyses of fault-related rocks.

3.1 Granite Pass fault

The Granite Pass fault is a moderately- to steeply-dipping (40-90°), E-W

to NE-SW striking, left-lateral strike-slip fault zone (Fig. 2-4 C). Slickenlines from the

Granite Pass fault zone have rakes that range from 00° to 47° to the E and W (Fig. 2-4 C).

The Granite Pass fault zone is up to 10 m wide, composed of several anastamosing fault

cores, and principal slip surfaces (Fig. 2-5). Fault cores are composed of a principal slip

surface, fault-breccia, cataclasite, and ultracataclasite on the eastern side of the area (Fig.

2-5 A). The fault zone is more heterogeneous on the western side of the area than to the

east with a variety of fault-related rocks and alteration, including mylonites, cataclasite

and ultracataclasite, and hydrothermal alteration (Fig. 2-5 A, C, D).

Table 2-2: Displacement data from GLF and GPF localities (Loc.), left lateral (LL) and

some right-lateral (RL) offsets were observed.

Loc.	Type	Long.	Lat.	offset
1	LL	-118.583	36.890	47 m
2	LL	-118.609	36.891	10.7 m
6	LL	-118.604	36.885	19.7 m
8	LL	-118.602	36.883	1.4 m
9	LL	-118.602	36.883	1.44 m
13	LL	-118.598	36.881	11.75 m
15	RL	-118.597	36.899	8.9 m
16	LL	-118.626	36.888	19.4 m
19	LL	-118.627	36.889	75.3 m
21	LL	-118.607	36.882	3 m
22	LL	-118.593	36.888	1.85 m
25	LL	-118.594	36.881	23.7 m
27	LL	-118.633	36.878	2 m
26	LL	-118.633	36.878	29.6 m
28	RL	-118.632	36.878	3.31 m
30	LL	-118.615	36.882	14.5 m
31	LL	-118.607	36.889	1 m
32	LL	-118.609	36.892	2.74 m
Location data in WGS 1984				

3.2 Glacier Lakes fault

The Glacier Lakes fault is an E-W to NE-SW striking, steeply dipping (40-90°), left-lateral strike-slip fault, with a maximum observed offset of 125 m (Kirkpatrick et al., 2008) (Fig. 2-2). Slickensides from the Glacier Lakes fault zone have rakes that range from 02° to 45° to the E and W (Fig. 2-4A). The Glacier Lakes fault zone is up to 60 m wide, with two to three fault cores and principal slip surfaces (Kirkpatrick et al., 2008). Fault cores are composed of a principal slip surface with distinct slickensides, chlorite and epidote fault-breccia (Fig. 2-5 A), cataclasite and ultracataclasite, and pseudotachylyte (Kirkpatrick et al., 2008). Offset data from the Glacier Lakes fault shows a highly asymmetric displacement gradient from the central portion of the fault, to the western termination (Fig. 8 of Kirkpatrick et al., 2008). The western termination of the Glacier Lakes fault is characterized by a series of smaller displacement, NE-SW striking, left-lateral oblique strike-slip faults (Fig. 2-2, 2-4 B). These splays (or "horse-tail" structure) have similar fault-related rocks and displacement gradients as the main fault zone (Fig. 8 of Kirkpatrick et al., 2008). These fault splays also contain evidence for ancient seismicity in the form of pseudotachylyte, suggesting that seismicity that initiated along the principal trace of the fault continued on to the splay faults (Fig. 2-4) (Kirkpatrick et al., 2008).
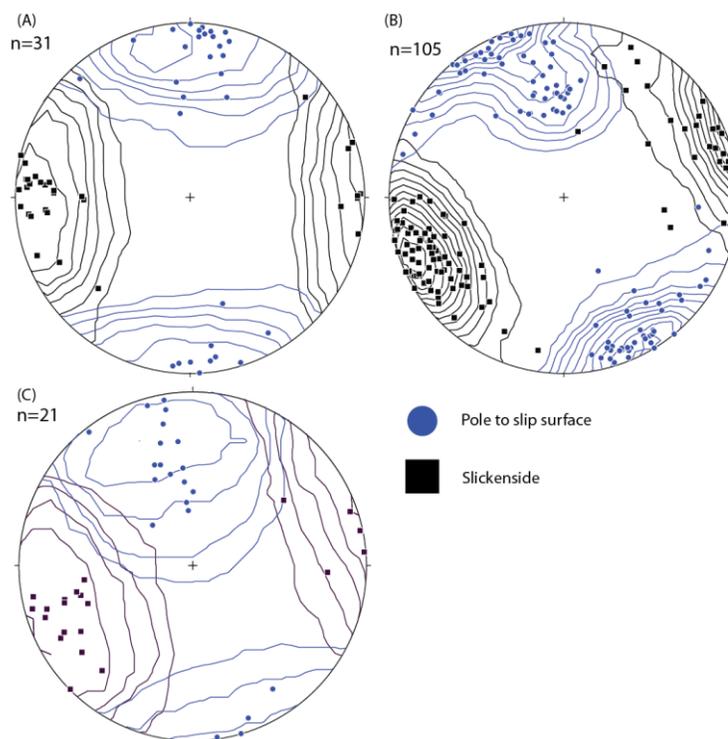
Figure 2-4: Structural data from the Volcanic Lakes area. A) Glacier Lakes fault orientation and slickenside data, B) Glacier Lakes fault "horse-tail" structure fault orientations and slickenside data, C) Granite Pass fault orientation and slickenside data.

4. Crystal-plastic deformation

Crystal-plastic deformation is present throughout the GLF and GPF zones and is most pervasive along the western termination of the GPF (Kirkpatrick et al., 2008).

Evidence for crystal-plastic deformation associated with the GPF and GPF zones includes undulose extinction, grain boundary bulging, deformation lamellae, subgrain formation and rotation in quartz, and kinking and folding, deformation twin development in plagioclase (Fig. 2-6 A-F). These textures are the result of deformation mechanisms
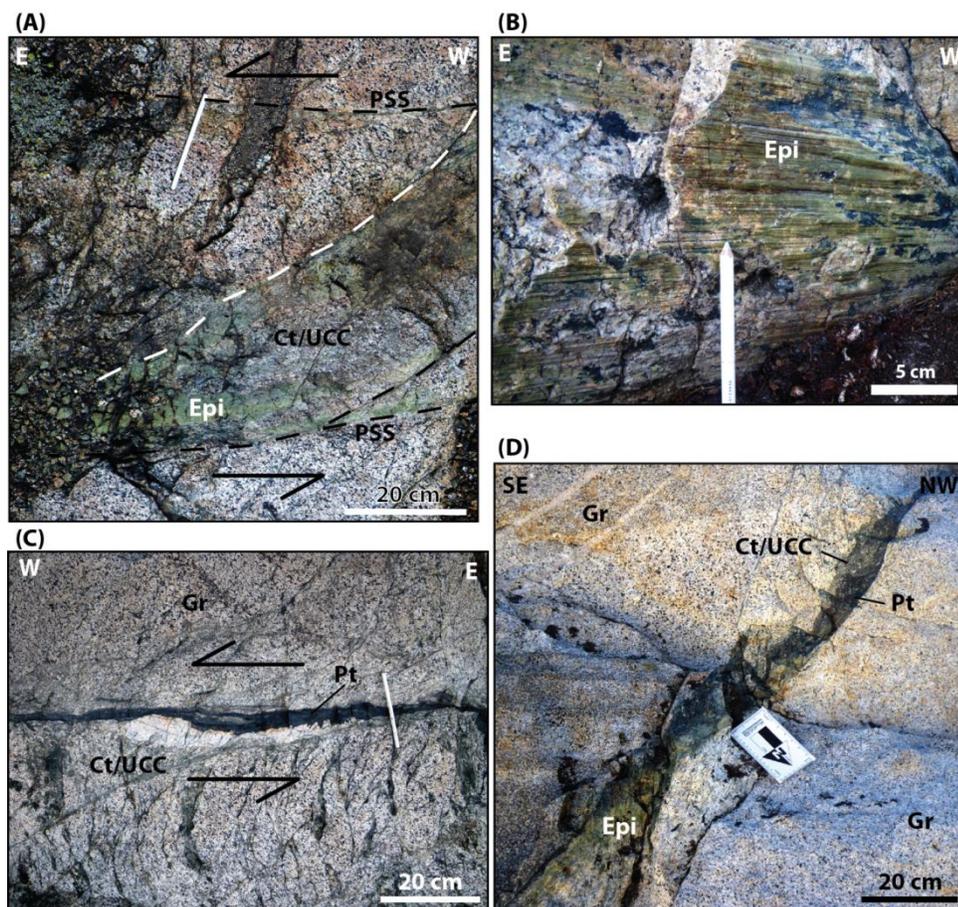
Figure 2-5: Field photographs of fault-related rocks from the GLF and GPF zones. A) GLF core with sub-parallel principal slip-surfaces (PSS) and numerous fractures, cataclasite (Ct) and ultracataclasite, and epidote (Epi) in the fault core, -118.5922, 36.8884. B) Epidote (Epi) rich fault slip-surface, associated with GLF, slickenlines used as indicator of direction of slip, -118.6028, 36.9035. C) GPF slip-surface and fault core with ~1 m damage zone composed of fractured and altered granitic rock (Gr), fault core composed of cataclasite (CT), ultracataclasite (UCC), and pseudotachylyte (Pt), -118.6268, 36.8777. D) GPF core with epidote (Epi) mineralization, and cross-cutting cataclasite (Ct), ultracataclasite (UCC), and pseudotachylyte (Pt), -118.6457, 36.8766.

consistent with deformation temperatures between 300-500 °C (Passchier and Trouw, 2005). This plastic deformation is overprinted by brittle deformation and plastically-deformed clasts are present in cataclasite and fault-breccia (Fig. 2-6 E, F). This cross-cutting relationship confirms that plastic-deformation occurred prior to brittle-deformation.

5. Fault-related rocks

5.1 Cataclastic rocks

Cataclastic fault-rocks preserved in the GLF and GPF include fault-breccia, cataclasite, and ultracataclasite (Fig. 2-5 A, C, D; Fig. 2-7). Fault-breccia from the GLF and GPF is present in the damage zone and core of the fault zones, composed of angular to sub-rounded clasts of quartzofeldspathic, granitic protolith, and matrix composed of highly comminuted silicate minerals (Fig. 2-7 C). Some fault-breccia matrix is also composed of hydrothermal epidote and chlorite that support angular to sub-rounded clasts (Fig. 2-7 A).

5.2 Pseudotachylyte

5.2.1 Field and outcrop description

Tectonic pseudotachylyte occurs in the core and damage zone of the GLF and GPF as injection veins and fault veins (Fig. 2-5 C, D) . Dark-gray to black pseudotachylyte veins are typically less than 5 cm thick, less than 50 cm long, and have aphanitic matrix, with very fine-grained clasts (Fig. 2-5 C, D; Fig. 2-7 C).

(A) xpl — Chess Board SG — 200 μm

(B) xpl — Plag — 1 mm

(C) xpl — SG — Qtz — 200 μm

(D) xpl — Plag — 100 μm

(E) Slip Surface — ppl — UCC — Ct — Qtz — Epi — 1 mm

(F) xpl — Plag — SG — Epi — 1 mm
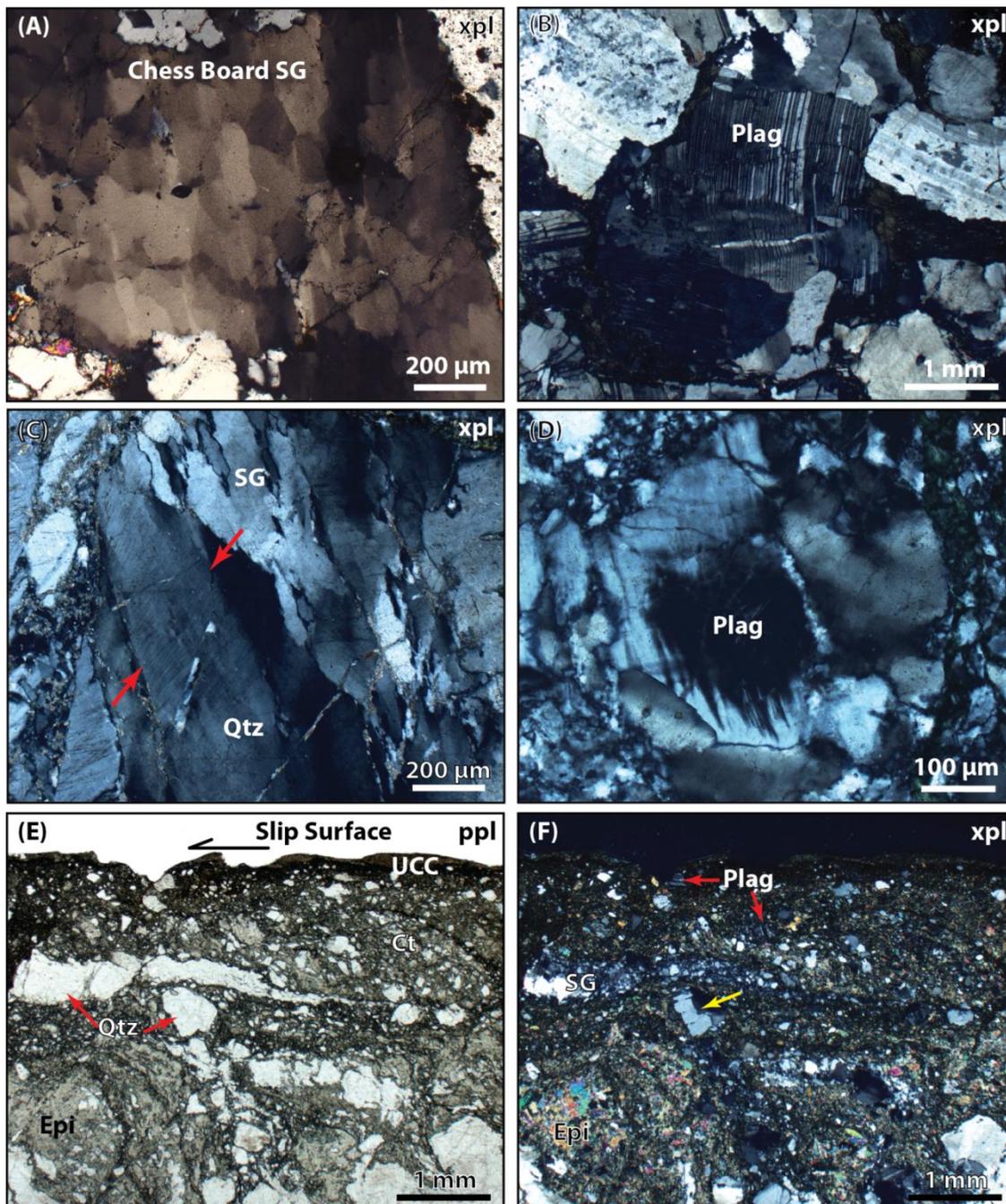
Pseudotachylyte veins cross-cut cataclasite, ultracataclasite, epidote fault-breccia, and undeformed granitic rocks in the fault zones (Fig. 2-5 C, D; Fig. 2-7 C). Cross-cutting pseudotachylyte veins tend to be well preserved with few fractures present, or incorporation as clasts in later cataclasite. Preservation of pseudotachylyte and lack of subsequent overprinting indicates frictional melt formation in the late stages of faulting. Identification of pseudotachylyte in the field remains difficult because of the similarity between pseudotachylyte and very fine-grained, epidote-filled injection veins (Fig. 2-7 B). Localities with convincing evidence for melt-related pseudotchylyte are located along the main strands of the GLF and GPF as well as the NE-SW-striking GLF-splay faults (Fig. 2-2).

5.3 Pseudotachylyte microstructures

5.3.1 Microlites and spherulites

The pseudotachylyte matrix is a very fine-grained amorphous, opaque, to light-green-gray material that consists of, silicate material, titanite, chlorite, and microlites. Microlites are very fine-grained crystals that form during the rapid cooling of a frictional melt (Sibson, 1975; Lin, 1994, 2008). Microlites with variable composition and shape have been documented in numerous studes of pseudotachylyte and are considered convincing evidence for a frictional melt origin (Sibson, 1975; Magloughlin and Spray, 1992; Fabbri et al., 2000; Di Toro and Pennacchioni, 2004; Kirkpatrick et al., 2009; Lin, 2008; Toy et al., 2011; Kirkpatric and Rowe, 2013). Four types of microlites have been

identified from pseudotachylyte from the GLF and GPF at the microscale using optical and scanning electron microscopy: 1) isolated-tabular, 2) spherulites radiating from central point, 3) spherulites radiating from a clast, and 4) bow-tie (Fig. 2-8 F). The SEM-EDS analyses indicate that the microlites are composed of plagioclase, and K-feldspar, and are typically less than 100 μm-long and 10 μm-wide (Fig. 2-9). The morphology, size, and composition of microlites are consistent with previous descriptions of microlite from pseudotachylyte (Sibson, 1975; Magloughlin and Spray, 1992; Di Toro and Pennacchioni, 2004; Kirkpatrick et al., 2009; Toy et al., 2011).
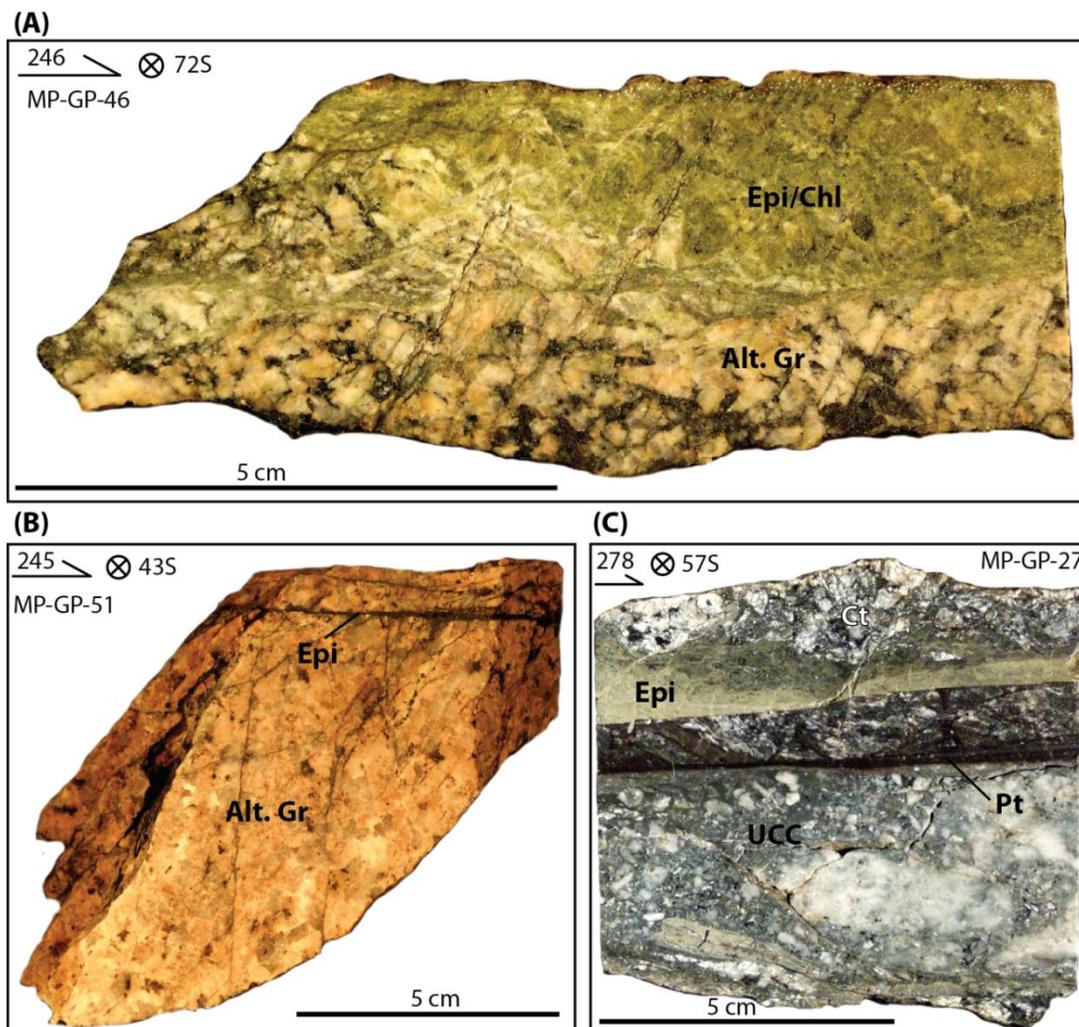
Figure 2-7: Hand sample photos of fault-related rocks from the GLF and GPF zones. A) Epidote (Epi) and chlorite (Chl), fault breccia and cataclasite slip-surface and altered granitic protolith (Alt. Gr) from the GLF. B) Altered granitic protolith (Alt. Gr) and cross-cutting dark-grey to black epidote veins (Epi), interpreted to be a product of hydrothermal alteration. C) Fault core sample for GLF splay, with epidote (Epi) rich cataclasite, cataclasite (Ct), ultracataclasite (UCC), and cross-cutting pseudotachylyte (Pt).

5.3.2 Flow structures (folds and flow streaks)

A very fine-grained (< 5 μm), opaque to light-green pseudotachylyte matrix form alternating bands that are deformed in streaks and folds (Fig. 2-8 A,C,D). These folds and streaks have been interpreted to represent flow structures that formed when the pseudotachylyte was molten and viscous (Lin, 2008; Craddock and Magloughlin, 2005). Quartz and feldspar clasts are entrained in these flow structures and often define the fabric in the pseudotachylyte vein (Fig. 2-8 D). Flow streaks and fold axes are parallel to vein margins (Fig. 2-8 A, C).

5.3.3 Amygdules (filled vesicles)

Preserved vesicles (amygdules) are present in most pseudotachylyte samples from the GLF and GPF. Amygdules are filled with quartz and are sometimes surrounded by white (quartz rich) reaction rims (Fig. 2-8 A, B, E). Fine-grained (15-70 μm), circular to elliptical monocrystalline quartz is surrounded by a very fine-grained (< 5 μm) matrix composed of chlorite, titanite, and other silicate material (Fig. 2-8 B, E). The interpretation that these features represent filled vesicles rather than survivor clasts is supported by the high circularity and small-constant grain size of the amygdules (Fig. 2-8 B, E). Filled vesicles are typically less than 100 μm in diameter (Supplemental data); this size range is consistent with previously documented pseudotachylyte amygdules (Lin, 1994a, 2008; Craddock and Magloughlin, 2005; Magloughlin, 2011).

57

(A)

(B)
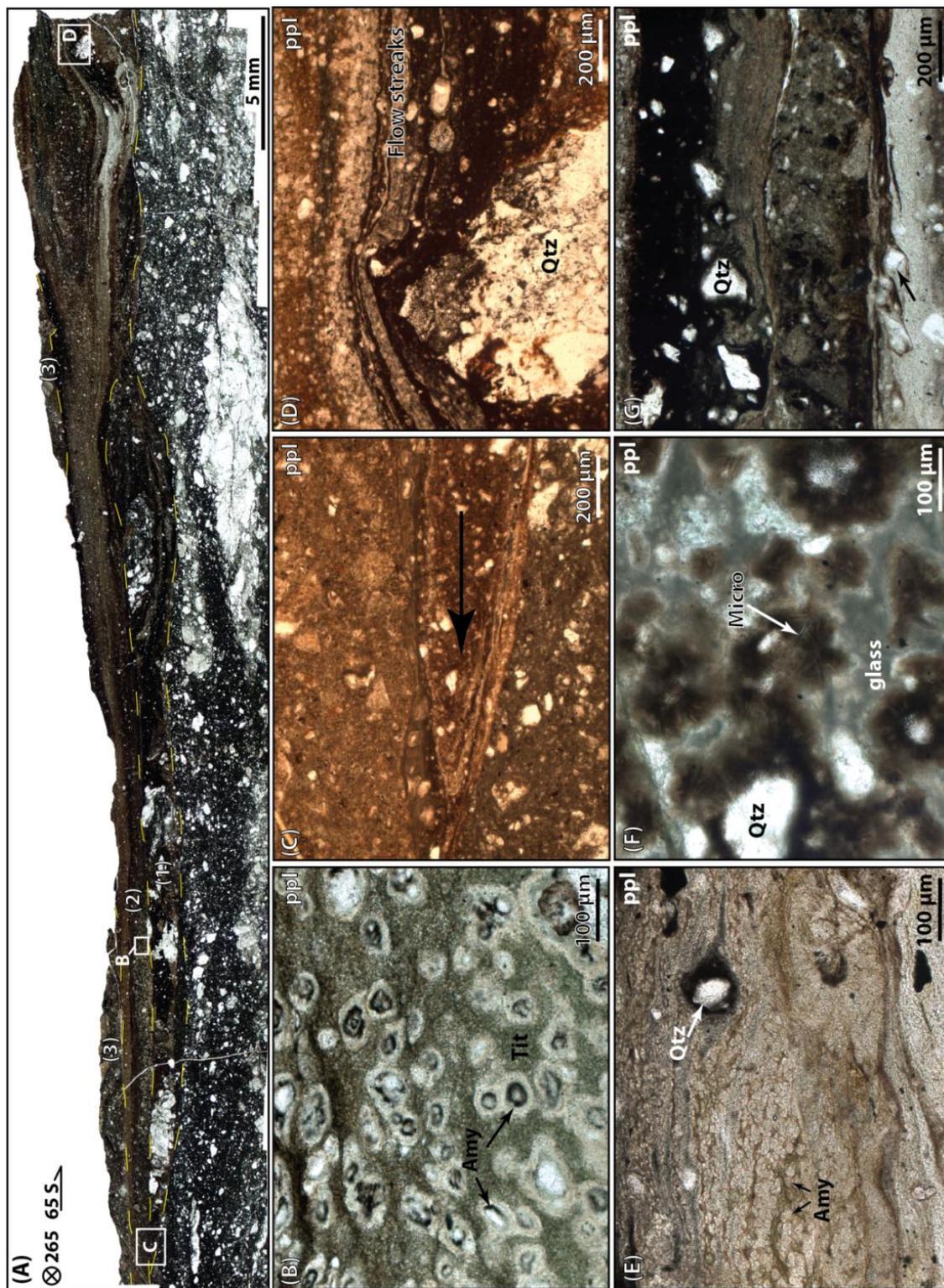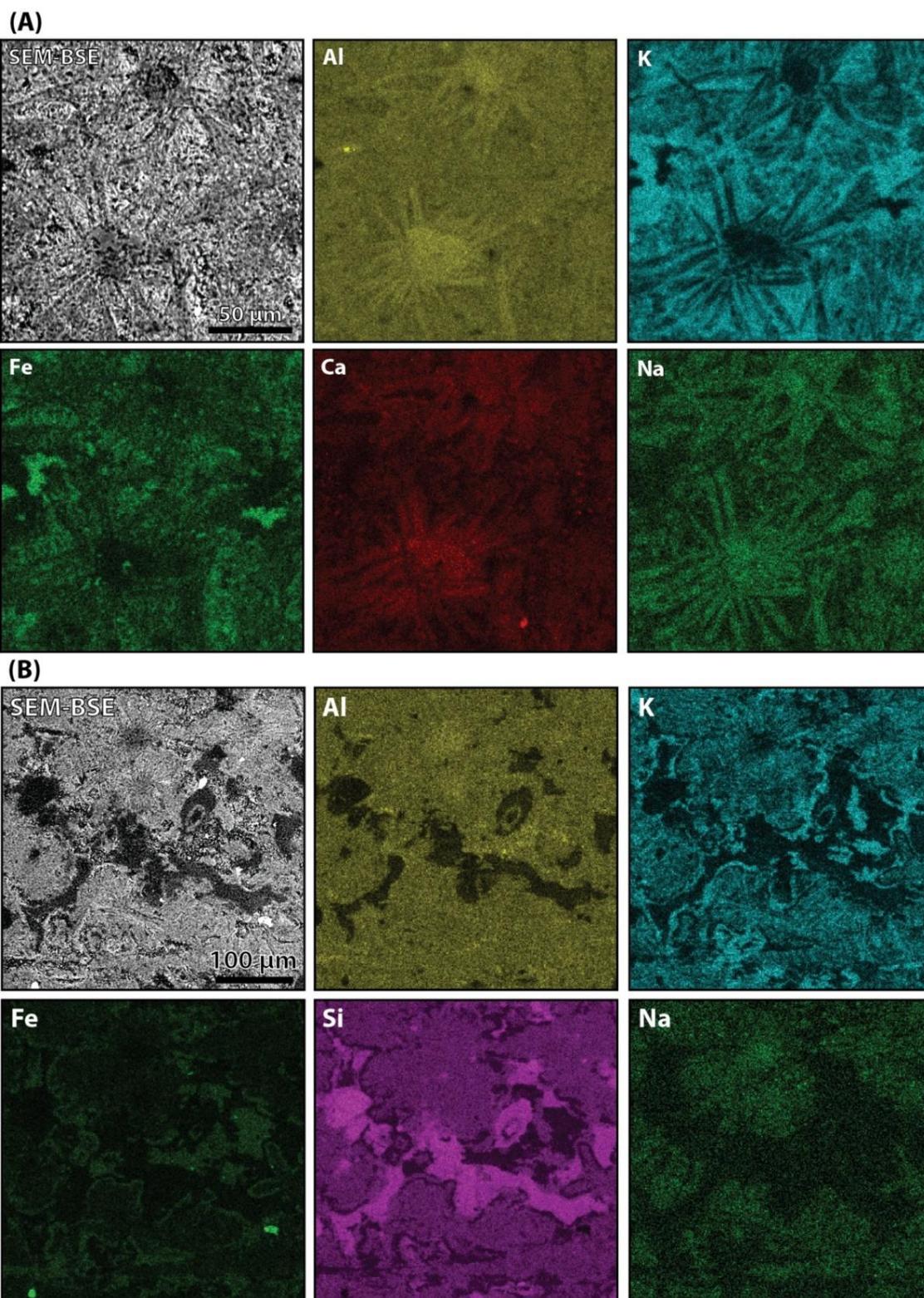
5.3.4 Preserved High temp clasts

Survivor clasts in the pseudotachylyte are composed primarily of quartz and feldspar and range in size from <10 μm to > 1 mm in diameter (Fig. 2-8 F, G; Fig. 2-10 A). Numerous quartz and minor feldspar clasts are consistent with a frictional melt origin for the pseudotachylyte (Fig. 2-8 A, F, G; Fig. 2-10 A) (Spray, 1987; Magloughlin and Spray, 1992; Barker et al., 2010; Nielsen et al., 2010; Toy et al., 2011). Experimentally produced pseudotachylyte typically contain numerous quartz and less commonly plagioclase clasts; this has been attributed to mechanical breakdown processes of weaker minerals (e.g. biotite, hornblende, epidote) which precedes melting and the lower melting point of hydrous mineral phases (biotite melts at 650 °C and quartz at 1700 °C at 1-atm) (Spray, 1987, 1992; Nielsen et al., 2010; Spray, 2010).

5.3.5 Isotropic glassy matrix

In some samples of pseudotachylyte, the very fine-grained (< 1 μm) matrix is isotropic, and enriched in silica relative to the ground mass of the pseudotachylyte (Fig. 2-9 B). This isotropic matrix forms amoeboid shaped bodies surrounded by a rim enriched in iron, magnesium, and potassium (Fig. 2-9 B). This isotropic silica is interpreted to represent rapidly quenched silicate melt (glass) (Lin, 2008). Reports of preserved glass are rare in pseudotachylyte due to the low preservation potential of glass in the subsurface (Lin, 1994a, 2008; Warr and van der Pluijm, 2005; Kirkpatrick and Rowe, 2013). The morphology and composition of the isotropic matrix however, is

consistent with expected crystallization of a pseudotachylyte (Warr and van der Pluijm, 2005).

5.4 Textural analyses of fault-related rocks

Pseudotachylyte and cataclasite microstructures and clasts from the GLF and GPF zones were analyzed using NIH Image-J and GIAS image analysis software (Beggan and Hamilton, 2010; http://rsb.info.nih.gov/ij/). Transmitted light photomicrographs were used at multiple scales to describe clast size, distribution, aspect ratio, orientation, and circularity (Supplemental data). Clast size, shape, and nearest neighbor distribution data were collected and analyzed using methods from Jerram et al. (2007) and Beggan and Hamilton (2010) to quantify the distribution and shape of survivor clasts in pseudotachylyte and cataclastic rocks from the GLF and GPF zones. Nearest neighbor distribution analysis has not previously been applied to the analysis of pseudotachylyte. Using these data we test the utility of grain-shape and grain-size distribution as an indicator of a frictional melt origin for pseudotachylyte. Several workers have described the roundness and grain-size distributions of pseudotachylyte survivor clasts and compared these results to clast shape data from cataclastic rocks with the aim of correlating the shape and size distribution of survivor clasts with a melt-origin (Lin, 1999, 2008; Heilbronner and Keulen, 2006; Ozawa and Takizawa, 2007; Kirkpatrick and Rowe, 2013). The distribution of clasts in pseudotachylyte veins is expected to follow a Poissonian-random nearest neighbor distribution if clasts are suspended in a viscous fluid (Fig. 2-11). In contrast one expects clasts in a cataclasite or ultracataclasite to have a
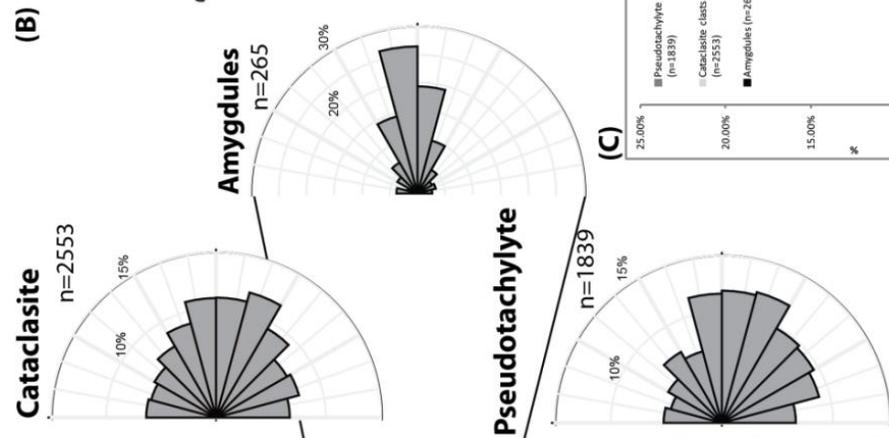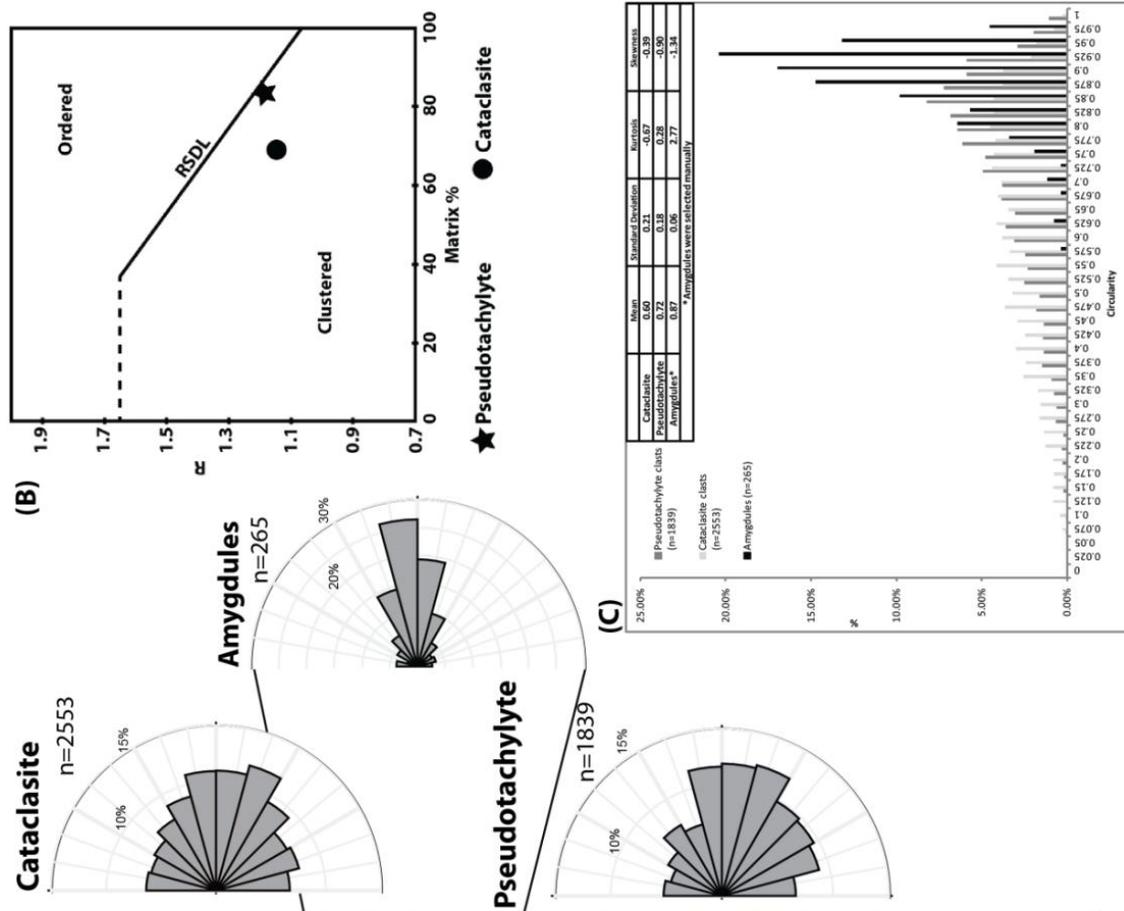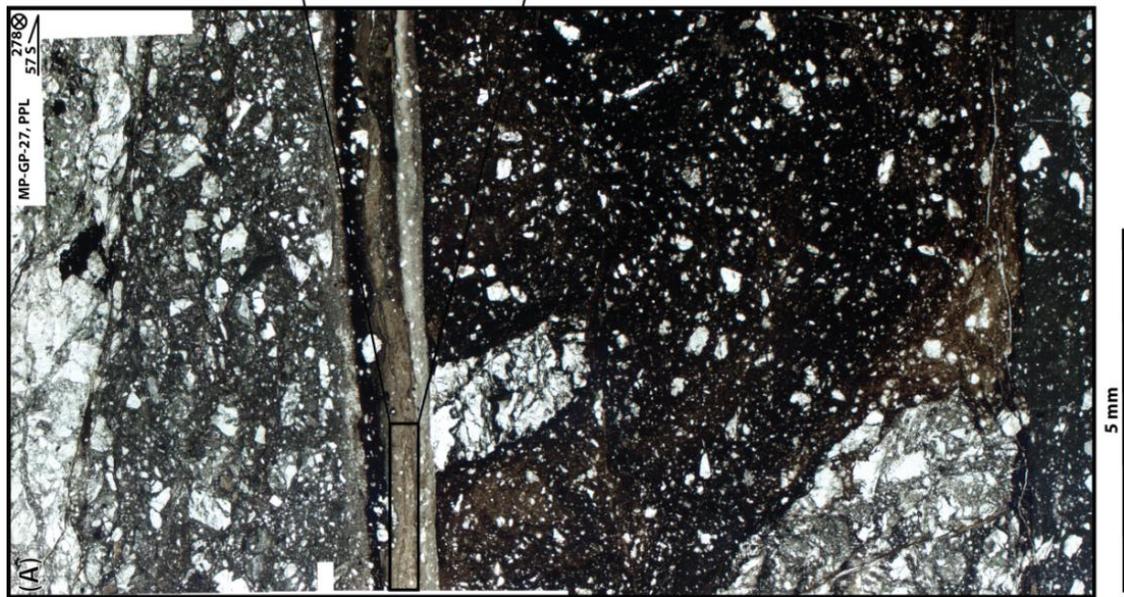
clustered nearest neighbor distribution if they are produced via comminution of coarse-grained granitic rocks (Fig. 2-11). The nearest neighbor distribution of clasts approaches a random distribution with increasing comminution and matrix to clast ratio approaching fault slip surfaces (Fig. 2-12). Additionally, the circularity of clasts increases approaching the melt layer and slip surface (Fig. 2-13 A). The distribution of clasts also changes approaching slip surfaces and pseudotachylyte with the number of large (> 1 mm) clasts decreasing (Fig. 2-13 B).
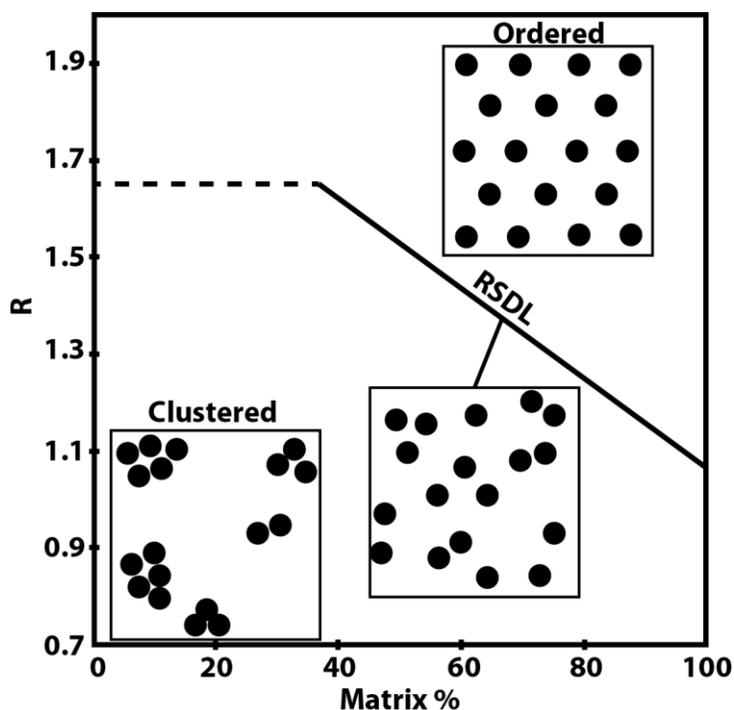
Figure 2-11: Matrix % (% melt) vs R plot with Random Sphere Distribution Line (RSDL). R values above and below the RSDL have a mean nearest neighbor distance greater than and less than randomly distributed spheres respectively.

(A) MP-GP-25b

Course grained Ct. (n=2885)

Medium grained Ct. (n=4132)

Fine grained Ct. (n=2227)

Pseudotachylyte (n=1375)

	Mean	Standard Deviation	Kurtosis	Skewness
Course Grained Ct.	0.54	0.21	-0.85	-0.23
Medium Grained Ct.	0.59	0.21	-0.73	-0.44
Fine Grained Ct.	0.59	0.22	-0.83	-0.45
Pseudotachylyte Clasts	0.71	0.23	0.11	-1.08
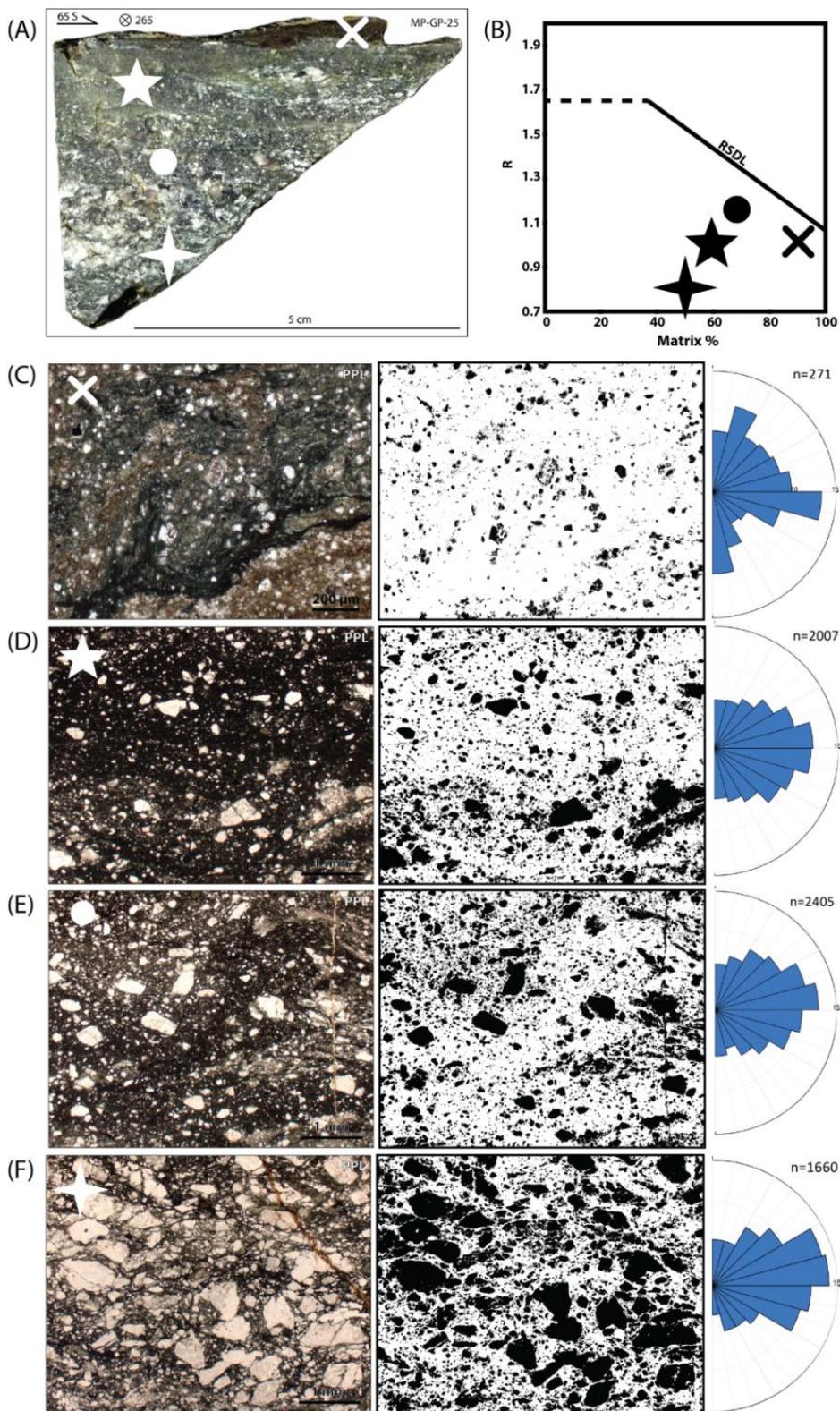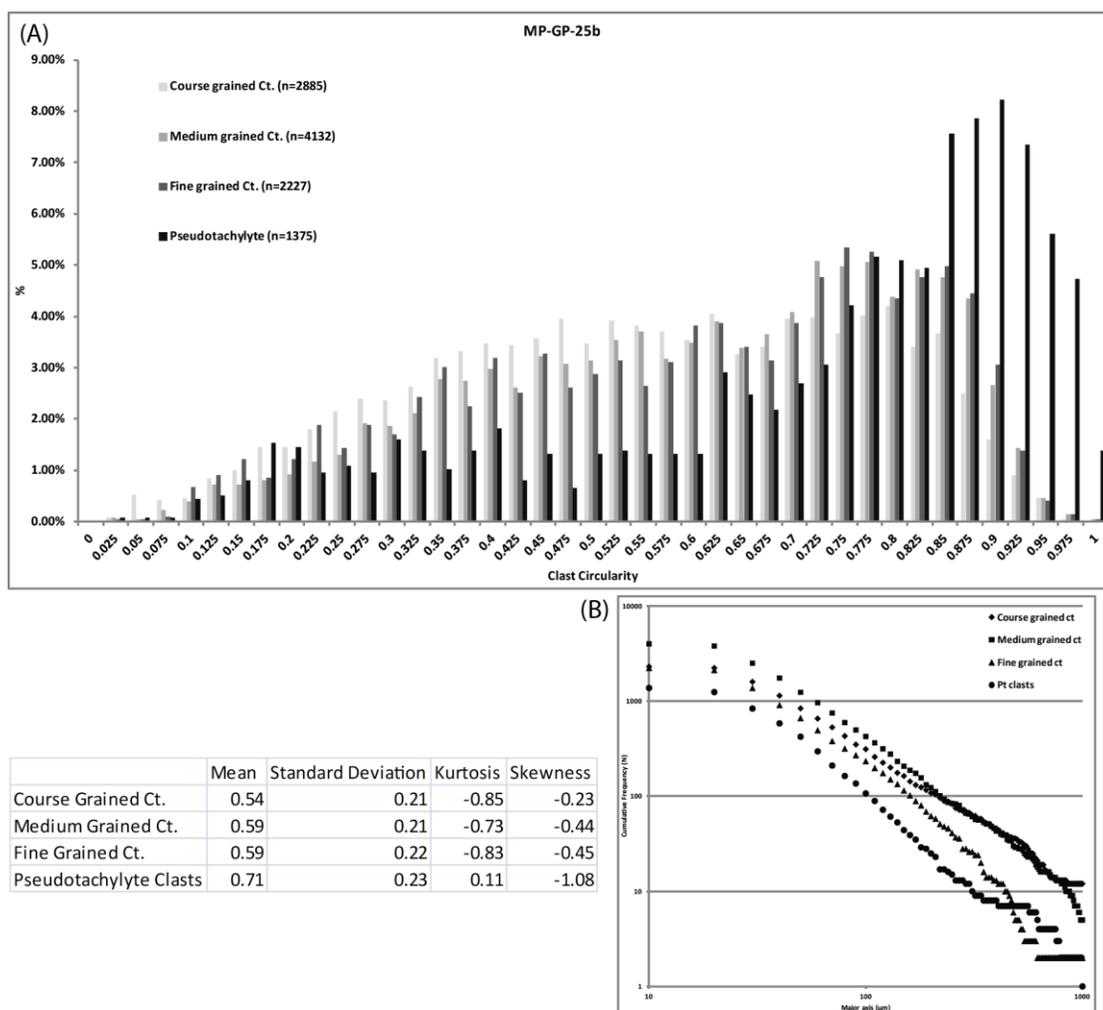
Figure 2-13: A) Histogram of clast circularity data from Glacier Lakes fault, with course, medium, and fine-grained cataclasite (Ct.) and pseudotachylyte, note the increasing circularity approaching the pseudotachylyte. B) Log-Log plot of clast size (major axis) vs. cumulative number, N=cumulative number of clasts whose major axis (A) is longer than A.

The pseudotachylyte from the GLF and GPF zones contain numerous well-rounded quartz and minor feldspar survivor clasts (Fig. 2-8). Clasts are randomly distributed in the very fine-grained matrix of the pseudotachylyte injection and faults veins, with a preferred orientation of the long-axes of clasts sub-parallel to the margin of the veins (Fig. 2-10A; Fig. 2-12; Fig. 2-13 A). Pseudotachylyte clasts are also more circular than cataclasite clasts from the same samples (Fig. 2-10 C; Fig. 2-13). The increased circularity of pseudotachylyte clasts has been interpreted to represent partial melting of angular clast corners in a frictional melt (Sibson, 1975; Lin, 2008). The greater surface area to volume ratio at clast corners results in preferential heating and melting of clast corners (Sibson, 1975). Other workers have noted increased clast roundness associated with pseudotachylyte fault and injection veins (Lin, 1999, 2008; Heilbronner and Keulen, 2006; Ozawa and Takizawa, 2007). We therefore consider the increased circularity of pseudotachylyte clasts to be a good indicator of frictional melt. We interpret the preferred orientation of clasts in the pseudotachylyte matrix to be caused by the alignment of the long axes of clasts parallel to flow during injection and/or shear.

6. X-ray diffraction analyses

X-ray diffraction analyses were conducted to evaluate the mineralogic changes associated with faulting and hydrothermal alteration in the GLF and GPF zones. Relatively undeformed granitic rocks from the GLF and GPF are composed primarily of albite, quartz, orthoclase, and minor amounts of biotite, and hornblende. Fault-related rocks contain clinochlore (chlorite), epidote, and phlogopite (biotite) (Fig. 2-14). This

fault-related mineral assemblage and textures described below suggest that hydrothermal

alteration occurred in the fault zone.
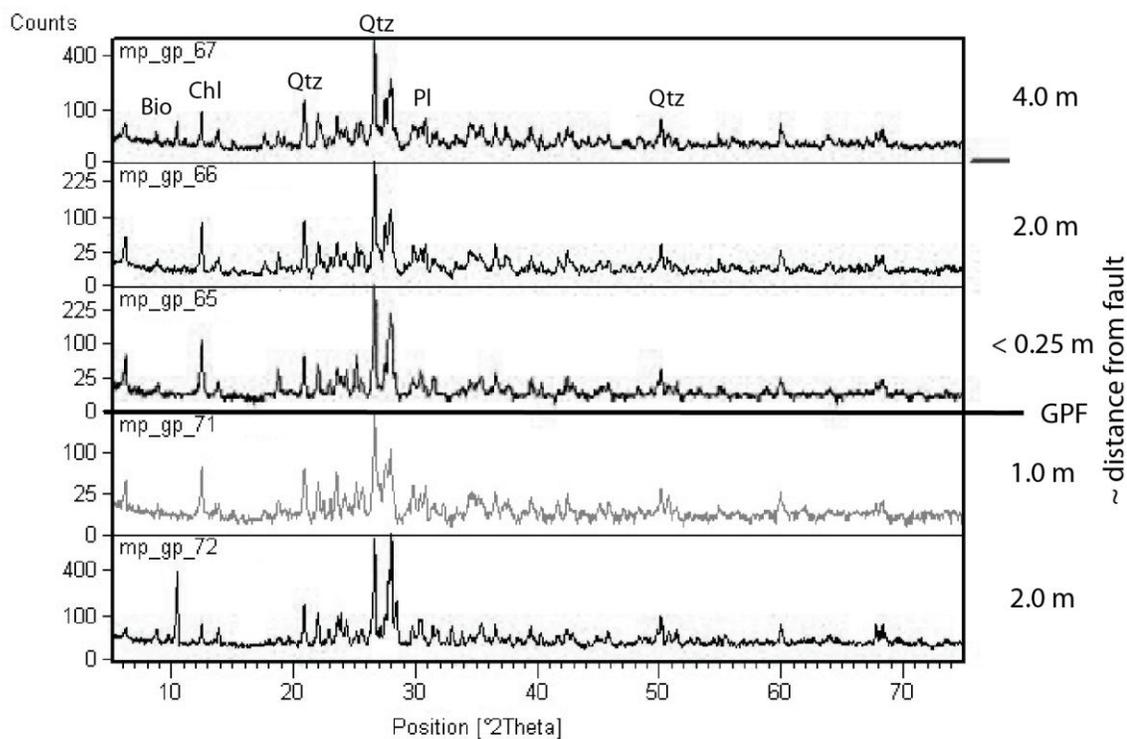
Figure 2-14: X-ray diffraction spectra from sample traverse across the Granite Pass fault

(GPF), note relative homogeneity of major-mineral composition across the fault zone.

Major phases identified include: quartz (Qtz), Plagioclase (Pl), Biotite (Bio), and chlorite

(Chl).

7. Microstructural evidence for fluid alteration and migration

The GPF and GLF fault zones contain abundant evidence for fluid flow and hydrothermal alteration during faulting. Thin (< 1mm thick) epidote-coated fault slickenside surfaces and fault breccia to were deposited by hydrothermal fluids which moved into the fault zone (Fig. 2-5 A, B, D; Fig. 2-7). Very fine- to medium-grained, equant epidote in fault breccia, veins, and slip-surfaces is cross-cut by (and cross-cuts) cataclasite and pseudotachylyte (Fig. 2-5 A, B, D; Fig. 2-7). Abundant sericite alteration of plagioclase is present in the fault core and damage zones of the GLF and GPF (Fig. 2-15A. C). Chlorite pseudomorphs after biotite and fine-grained fracture fill are also present in cataclasite from the fault core of the GLF and GPF (Fig. 2-7; Fig. 2-15 B). Quartz and calcite filled veins cross-cut fault-related rocks in the core and damage zone of the GLF and GPF (Fig. 2-15 F). Calcite vein fill is typically medium to fine grained, equant grains, with thick (> 10 μm) polysynthetic twins (Fig. 2-15 F). Chloritization of biotite during hydrothermal alteration has been documented to approximately occur between 200-320 °C and thick mechanical twins in calcite form between 170-200 °C (Parry and Downey, 1982; Fiebig and Hoefs, 2002; Ferrill et al., 2004). The thermochronologic data presented by Kirkpatrick et al. (2012) indicate that the ambient temperature conditions during faulting were between 110-160 ˚C. These data suggest that the GLF and GPF zones experienced temperatures 10 to 210 ˚C greater than ambient temperatures during faulting (Kirkpatrick et al., 2012). Kirkpatrick et al. (2012) conclude that high temperature hydrothermal fluids preferentially infiltrated fractures and faults

resulting in the observed mineral assemblage. Alternatively, the hydrothermal alteration

in the GLF and GPF zones may be the result of frictional heat generated during

seismicity (Kanamori and Brodsky, 2004; Kanamori and Riveiro, 2006; Jacobs et al.,

2006; Shipton et al., 2006). This hypothesis suggests that the expulsion of fluids in the

fault zone was driven by thermal pressurization during flash heating (Rice, 2006; Rempel

and Weaver, 2008).

8. Strain analysis of amygdules

Because pseudotachylyte amygdules are filled vesicles it is reasonable to infer

that their original shape approximated a sphere (Maddock et al., 1987; Lin, 1994a, 1994b;

Bjørnerud and Magloughlin, 2004; Magloughlin, 2005; Lin, 2008; Magloughlin, 2011;

Lavallée et al., 2012). Other workers have noted the presence of elliptical amygdules in

pseudotachylyte and the existence of a preferred alignment parallel to flow banding and

the margins of pseudotachylyte veins, suggesting shear of vesicles in a viscous melt

(Maddock et al., 1987; Lin, 1994a; Bjørnerud and Magloughlin, 2004; Magloughlin,

2005; Lin, 2008). The constrained timing of amygdule formation (post melt and pre-

solidification) and deformation (pre-solidification), and the assumed original spherical

geometry, allows for the use of these amygdules as a minimum strain marker within the

pseudotachylyte when the melt is viscous (Fig. 2-16). This method assumes that the

volume and therefore cross-sectional area of amygdules remains constant; this is a

reasonable assumption given the formation conditions of amygdules (Maddock et al.,

1987; Lin, 1994a; Magloughlin, 2005). To calculate the strain of individual amygdules
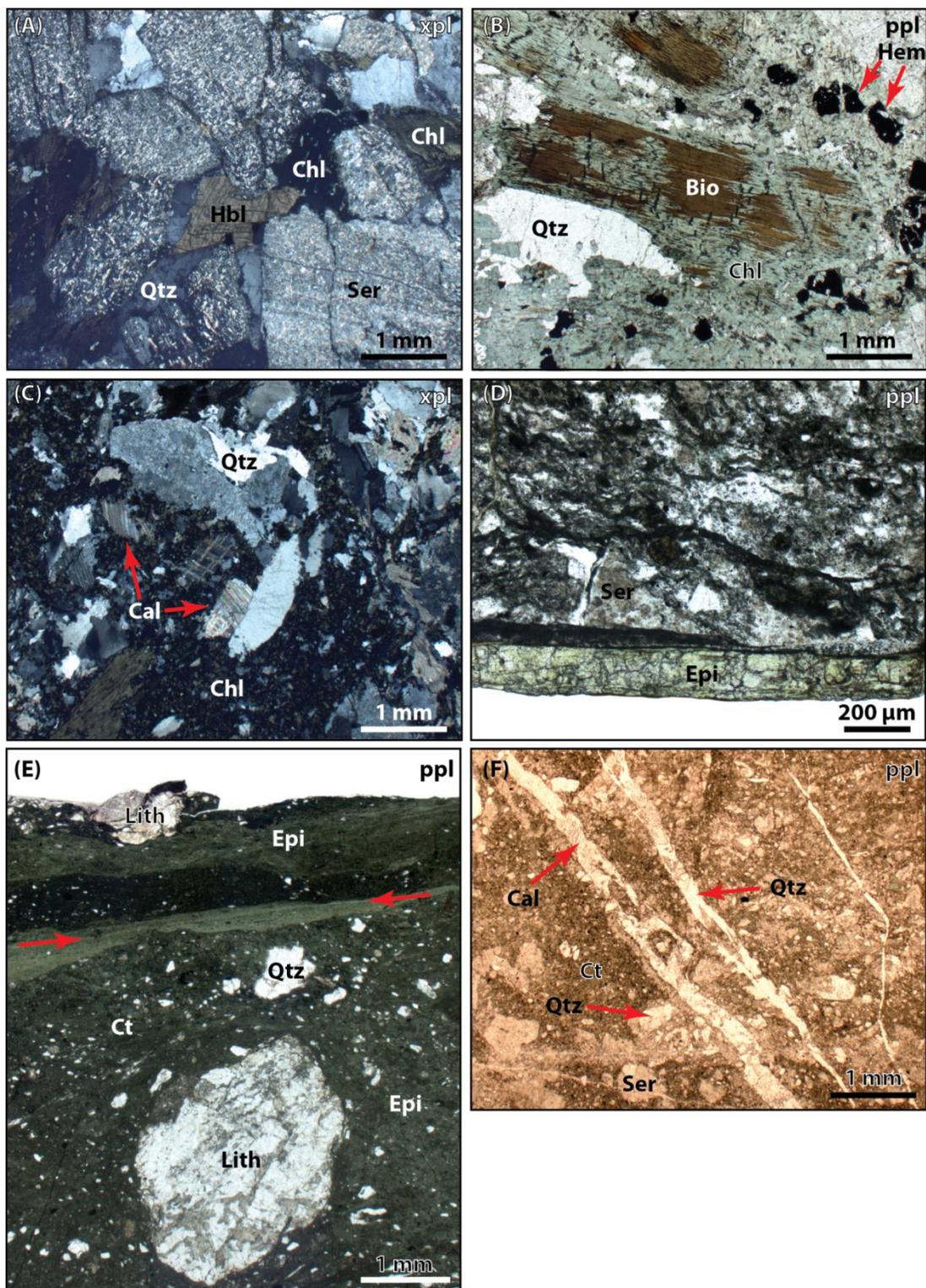
first the radius (*r*) of equal area circles was determined, then using the deformed major

and minor axes of the elliptical, deformed amygdule stain is calculated (Fig. 2-16 E)

(Equation 2-2) (Table 2-3).

$$e = \frac{l_{amy} - r}{r} \qquad \qquad (2\text{-}2)$$

where l_{amy} is the length of major (*M*) and minor (*m*) axes of the deformed amygdule and *r*

is the radius the equal area circle (Fig. 2-16). The long axis extension of individual

amygdules range from 0.0 to 0.85, with a mean of 0.22 (Fig. 2-16 F) (Table 2-3). This

wide range in strain can be used to calculate the post-seismic stress that drives injection

of pseudotachylyte.

9. Discussion

9.1 Timing of faulting

Crystal-plastic deformation of quartz, feldspar, and biotite has been documented

along the GLF and GPF zones (Kirkpatrick et al., 2008). The most extensive plastic

deformation is along the western termination of the GPF where protomylonite crops out

along the fault zone (Fig. 2-2) (Kirkpatrick et al., 2008). This crystal-plastic deformation

includes undulose extinction, grain-boundary bulging, deformation lamellae, subgrain

formation and rotation in quartz, as well as kinking and folding, and deformation twin

development in plagioclase, suggesting deformation temperatures between 300-500 °C
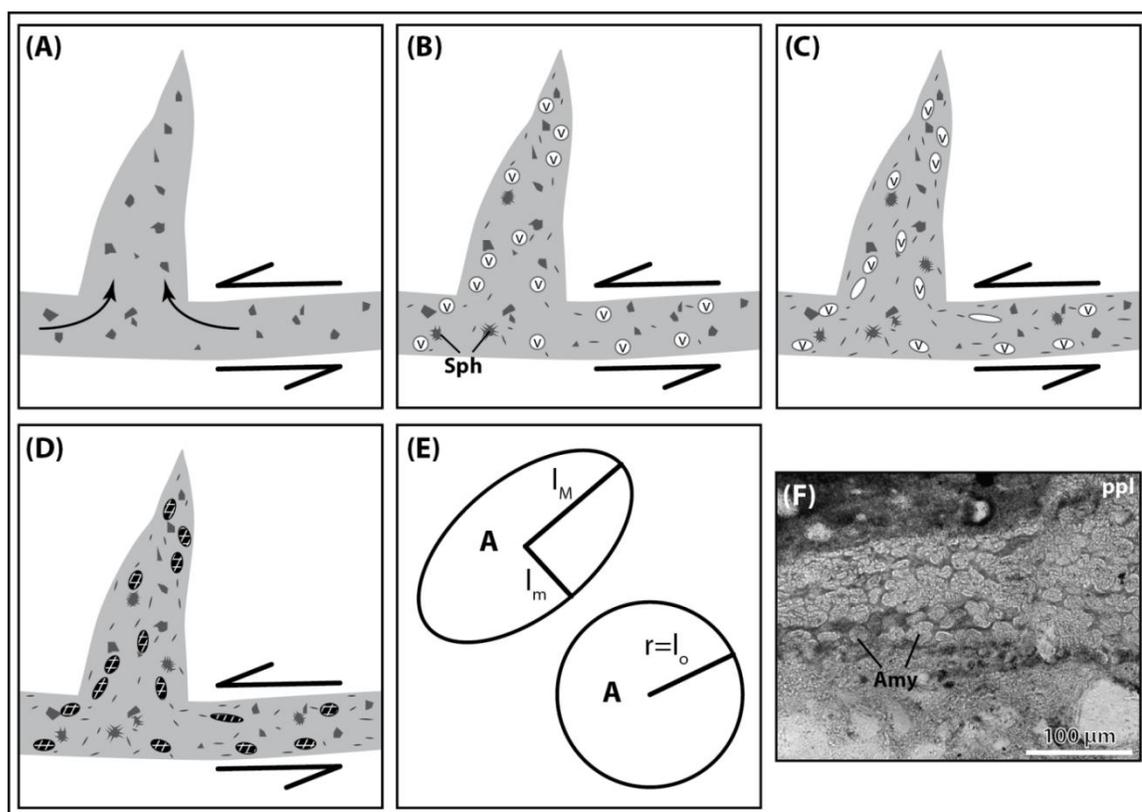
Figure 2-16: Model illustrating the evolution of pseudotachylyte fault and injection veins and amydgules through the earthquakes cycle and alteration illustrating the brief strain history preserved in deformed amygdules. A) Initial generation and injection of melt with survivor clasts and aphanitic matrix. B) spherical vesicle (V) and spherulite (Sph) formation, immediately following melt generation. C) deformation of vesicles and parallel alignment of microlites to the direction of flow while melt is still viscous. D) vesicles fill with quartz during alteration of pseudotachylyte preserving deformed shape of amygdule. E) illustration of final elliptical amygdule with long and short axes (l_M and l_m) and assumed original circular geometry of equal area (A). F) pseudotachylyte vein with elliptical amygdules.

Table 2-3: Summary of amygdule shape and strain analyses from samples MP-GP-25 and

27 (Supplemental Data). Amygdule area, perimeter (Perim.), major axis (Major), Minor

axis (Minor), Circularity (Circ.) equivalent circle radius, and major (eM), and minor (em)

axis strain.

	Area (μm^2)	Perim. (μm)	Major (μm)	Minor (μm)	Circ.	equivalent cir. Radius (μm)	eM	em
Mean	365.16	67.43	24.29	16.44	0.86	9.93	0.22	-0.17
Standard Deviation	347.31	28.70	10.58	7.30	0.07	4.20	0.14	0.09
Kurtosis	6.19	1.51	1.71	2.19	2.11	1.79	1.48	-0.20
Skewness	2.34	1.32	1.34	1.47	-1.28	1.39	1.09	-0.46
Minimum	31.26	20.91	7.27	5.48	0.53	3.15	0.00	-0.46
Maximum	2273.00	182.60	70.38	49.14	0.97	26.90	0.85	0.00
Confidence Level (95.0%)	30.64	2.53	0.93	0.64	0.01	0.37	0.01	0.01

(Fig. 2-6) (Passchier and Trouw, 2005). Plastically deformed fault-related rocks have

been incorporated as clasts in cataclastically deformed rocks in the GLF and GPF zones

and cross-cut by later brittle deformation (Fig. 2-6 E, F). This cross-cutting relationship

suggest that faulting in the Glacier lakes area initiated in the ductile-regime shortly after

pluton emplacement and faulting continued as the Pyramid pluton cooled and exhumed in

to the brittle-regime (Kirkpatrick et al., 2008, 2012). This timing is consistent with the

geochronology and thermobarometry which constrains the timing and temperature

conditions of faulting and similar fault-pluton cooling relationships in the north-central

Sierra Nevada (McNulty, 1995; Pachell and Evans, 2002; Pachell et al., 2003;

Kirkpatrick et al., 2008, 2012).

9.2 Hydrothermal alteration driven by frictional heat

Complex cross-cutting relationships between fault-related rocks suggest that

multiple deformation mechanisms operated simultaneously or cyclically during the

seismic cycle along the GPF and GLF. Tectonic pseudotachylyte is present in the fault

core of the GLF and GPF zones in the form of injection- and fault-veins (Fig. 2-5; Fig. 2-

7). Pseudotachylyte cross-cuts and is cross-cut by cataclasites and hydrothermal

alteration products (Fig. 2-5 C, D; Fig. 2-7 C; Fig. 2-8A). The coeval or cyclic

relationship between hydrothermal alteration and pseudotachylyte allow for the use of

temperature estimates that constrain the hydrothermal alteration to constrain the fault-

zone temperature conditions during seismicity to between 170 and 320 °C (Parry and

Downey, 1982; Fiebig and Hoefs, 2002; Ferrill et al., 2004). Kirkpatrick et al. (2012)

however, note that the temperatures inferred from hydrothermal alteration are 10 to 210

°C greater than the ambient temperatures during faulting from thermochronology of the

host rocks in the area (110-160 °C) (Kirkpatrick et al., 2012). The majority of energy

released during seismicity is consumed by processes in the fault zone and much of this

energy is converted to heat (Lockner and Okubo, 1983; Di Toro et al., 2005; Rice, 2006;

Sibson and Toy, 2006; Jacobs et al., 2006; Tanaka et al., 2006). Despite the prediction for

heat flow anomalies associated with large fault zones due to the frictional work done,

active fault zones tend not to generate significant surface heat flow anomalies

(Lachenbruch and Sass, 1980; Mount and Suppe, 1987; Chester et al., 1993; Tanaka et al., 2006; Fulton and Saffer, 2009). The lack of a heat flow anomaly and a general lack of widespread evidence for weak faults suggest that much of the heat generated during seismicity is consumed in the fault zone, refracted by basement topography, or advected away via pulses of ground water (Tanaka et al., 2006; Jacobs et al., 2006; Fulton and Saffer, 2009). The GLF and GPF preserve evidence for high coseismic temperatures in the form of pseudotachylyte (Table 2-1). In addition to the presence of pseudotachylyte, coeval or cyclic hydrothermal alteration is also pervasive in the GLF and GPF. The inferred temperature conditions of the hydrothermal alteration are greater than the background temperature conditions during faulting (Kirkpatrick et al., 2012). The elevated temperature conditions during faulting, and restricted nature of hydrothermal alterations to the fault-zones can be explained in several ways: 1) the increased fracture porosity and permeability related to the GLF and GPF acted as conduits for hydrothermal fluids, or 2) the majority of the heat consumed by hydrothermal alteration was sourced from the fault zone during seismicity. The second hypothesis is supported by modeling of the dissipation of heat generated during seismicity (Bestmann et al., 2012). Bestmann et al. (2012) find that the damage zone of a fault may experience temperature conditions up to 250 ˚C above ambient for over an hour following the generation of frictional melt.

9.3 Textural analyses of fault-related rocks

The observation of multiple generations of pseudotachylyte and reworked pseudotachylyte clasts in cataclasite from the GLF and GPF zones is consistent with

multiple earthquakes nucleating along the same thin slip surface (Fig. 2-8 A). The recognition that thin (< 5 mm thick) pseudotachylyte fault-veins contain up to three cross-cutting generations of pseudotachylyte suggests that using field and hand sample data for pseudotachylyte vein thickness and length data may be misleading when calculating the volume of frictional melt generated during seismicity (Wenk et al., 2000; Di Toro and Pennacchioni, 2005; Griffith et al., 2008; Pittarello et al., 2008; Rowe et al., 2012). This is also important when considering calculations based on estimates of pseudotachylyte vein thickness, length, or volume, i.e. dynamic shear stress resistance (Sibson, 1975; Wenk et al., 2000), the coefficient of friction and slip-weakening distance during earthquakes (Hirose and Shimamoto, 2003, 2005), co-seismic overpressure in fault zones (Lin, 2011; Rowe et al., 2012; Griffith et al., 2012), and the energy budget of earthquakes (Di Toro and Pennacchioni, 2005; Pittarello et al., 2008; Lin, 2008).

The textural analysis of fault-related rocks from the GLF and GPF zone shows a clear relationship between rock type, clast shape, and preferred orientation (Fig. 2-10). Pseudotachylyte from the fault zones contain fewer, more circular clasts compared to cataclasite from the fault zone (Fig. 2-11). Nearest neighbor analysis of clast distribution in cataclasite and pseudotachylyte are consistent with the interpretation that cataclasites form via fracture and comminution and pseudotachylyte represents a rapidly quenched frictional melt (Fig. 2-10: Fig. 2-11; Fig. 2-12). During comminution one expects clasts to be closely spaced or clustered together as larger grains are fractured and rotated during shear (Spray, 2010). In contrast survivor clasts in a melt are expected to be randomly

distributed in a viscous matrix (Jerram and Higgins, 2007). Clasts in the cataclasite and pseudotachylyte have a preferred orientation with the long axes of clasts sub-parallel to the inferred direction of offset of the fault and the margin of the pseudotachylyte vein (Fig. 2-11; Fig. 2-12). The results from nearest neighbor and clast shape distribution analyses suggest that the roundness and average nearest neighbor distance are reliable indicators of a frictional melt origin for some pseudotachylytes (Fig. 2-12).

9.4 Amygdule strain analysis

The preservation of amygdules in pseudotachylyte from the GLF and GPF allows for the use of these amygdules as minimum strain markers assuming an original spherical morphology and constant volume during deformation (Fig. 2-11) (Table 2-3).

Using the equation for shear stress for a Newtonian fluid we calculate the shear stress during pseudotachylyte injection and shear, where the shear stress (σ_τ) is a function of the viscosity of the melt (η_m), and the strain rate ($\dot{e}$) (Equation 2-3).

$$\sigma_\tau = \eta_m \dot{e} \qquad (3)$$

Given rapid pseudotachylyte cooling rates (1-100 s) (Ujiie et al., 2007; Bestmann et al., 2012; Kirkpatrick and Rowe, 2013), and the strain values obtained from amygdule analyses (0.22 σ=0.13) we use a strain rate of 0.22 s^{-1}, this value assumes that the amygdules only preserve a portion of the vein cooling history. The viscosity of silicate melts is highly dependent on composition, temperature, volatile content, and clast content and shape (Shaw, 1972; Spray, 1993; Ujiie et al., 2007; Kirkpatrick et al., 2012). A range

of viscosity values spanning several orders of magnitude is obtained for a single melt composition depending on temperature (Spray, 1993; Webb and Knoche, 1996; Sipp and Richet, 2002; Ujiie et al., 2007). Because of the inherent difficulty in estimating pseudotachylyte temperature and therefore viscosity we use a wide range of previously calculated viscosities (10^2-10^4 Pa s) in our estimation of shear stress (Spray, 1993; Ujiie et al., 2007; Rowe et al., 2012). We also assume that silicate melts behave as a Newtonian fluid; however, given the variable clast content of pseudotachylyte, presence of vesicles (amygdules), and the continuous pathway from the melt to glass states of frictional melt, it may be unreasonable to assume Newtonian behavior (e.g. Mysen and Richet, 2005). Using these values for viscosity and strain rate we calculate shear stress values between 22-2.2x10^4 Pa. If we assume that the driving force of pseudotachylyte injection is the thermal expansion of the melt, coseismic pressure increases of 10^7 Pa are expected (Rowe et al., 2012). These values are much greater than the calculated values values using deformed amygdules. An alternative driving force of pseudotachylyte injection could be a pressure gradient resulting from dilatational strain in the fault zone during seismicity (Sibson, 1975; Bjørnerud and Magloughlin, 2004; Griffith et al., 2012; Rowe et al., 2012). Several examples of pseudotachylyte 'source zones' or 'implosion breccias' have been noted by other workers (Sibson, 1975; Swanson, 1992; Bjørnerud and Magloughlin, 2004; Sibson and Toy, 2006). The change in pressure (ΔP) can be calculated using equation 2-4, which is dependent on the change in volume (ΔV) and the bulk modulus (K) of the rock.

$$\Delta P = \left(\frac{\Delta V}{V}\right) K \tag{4}$$

using a bulk modulus (K) of 50 GPa and small dilatation (ΔV) of 2 %, ΔP is on the order

of 1 GPa (Bjørnerud and Magloughlin, 2004). This value is well above the shear stress

calculated from the amygdule strain analysis (22-2.2x10^4 Pa). This however, is consistent

with the conclusion that the amygdules only preserve a small portion of the

pseudotachylyte vein history during the final stages of cooling.

10. Conclusions

The conclusion that single, thin (< 1 cm thick) pseudotachylyte veins preserve up

to three generations of pseudotachylyte and therefore three earthquake-cycles is

consistent with previous work that shows that strike-slip fault slip surfaces are long lived

and accommodate the majority of slip in fault zones (Chester et al., 1993; Evans and

Chester, 1995; Caine et al., 1996; Chester and Chester, 1998). Furthermore, this

conclusion suggests that assuming pseudotachylyte veins reflect single earthquakes may

be misleading when calculating the volume of melt produced in single earthquakes

(Bjørnerud and Magloughlin, 2004; Sibson and Toy, 2006; Rowe et al., 2012; Lin, 2011;

Lin et al., 2013).

Detailed textural and grain-shape analysis of pseudotachylyte and cataclasite from

the GLF and GPF show that clast shape and average nearest neighbor distribution is

altered during increased comminution and frictional melting (Fig. 2-12). These results

build on previously published conclusions that clast shape is modified during frictional

melt (Sibson, 1975; Lin and Shimamoto, 1998; Lin, 1999, 2008; Kirkpatrick and Rowe, 2013). We also use nearest neighbor analysis to describe the distribution of clasts in cataclasites and pseudotachylyte. We find that clasts in cataclastically deformed rocks have a clustered nearest neighbor distribution and pseudotachylyte have a near-random distribution (Fig. 2-12; Fig. 2-13). The random nearest neighbor distribution is an expected result if clasts in pseudotachylyte are mixed during injection. In contrast it is reasonable to conclude that during shear and comminution for cataclastic rocks to have clustered nearest neighbor clast relationships. We suggest that the clast shape and nearest neighbor distribution is a reasonable criteria for distinguishing a frictional melt origin for fault related rocks.

Cross-cutting relationships indicate that hydrothermal alteration and seismicity in the fault zone were coeval or cyclic. Additionally, the elevated temperature conditions (10-210 ˚C > ambient conditions) of hydrothermal alteration suggest that additional heat was added to the system during faulting (Kirkpatrick et al., 2012). The isolated hydrothermal alteration and elevated temperatures in the fault zone can be explained by two hypotheses: 1) deeply sourced hydrothermal fluids infiltrated the fault zone during the seismic cycle, or 2) heat produced during seismicity locally elevated temperature conditions in the fault zone resulting in hydrothermal alteration. Distinguishing between these hypotheses is difficult and beyond the scope of this study. It is however, possible that the hydrothermal alteration observed in the GLF and GPF consumed some of the energy released during seismicity.

We also evaluate an novel strain marker in pseudotachylyte from the GLF in the form of deformed amygdules (Fig. 2-16). This analysis yields a minimum value for syn-injection strain of pseudotachylyte of approximately 0.22 (Table 2-3). This approximation represents a minimum because pseudotachylyte only represents a small portion of the seismic cycle (Fig. 2-16; Fig. 2-17). However, because the viscosity of frictional melt is difficult to constrain, and is likely to change by several orders of magnitude during injection it is difficult to quantify the driving force of pseudotachylyte based on these results (Spray, 1993; Kirkpatrick et al., 2012; Rowe et al., 2012; Lavallée et al., 2012).
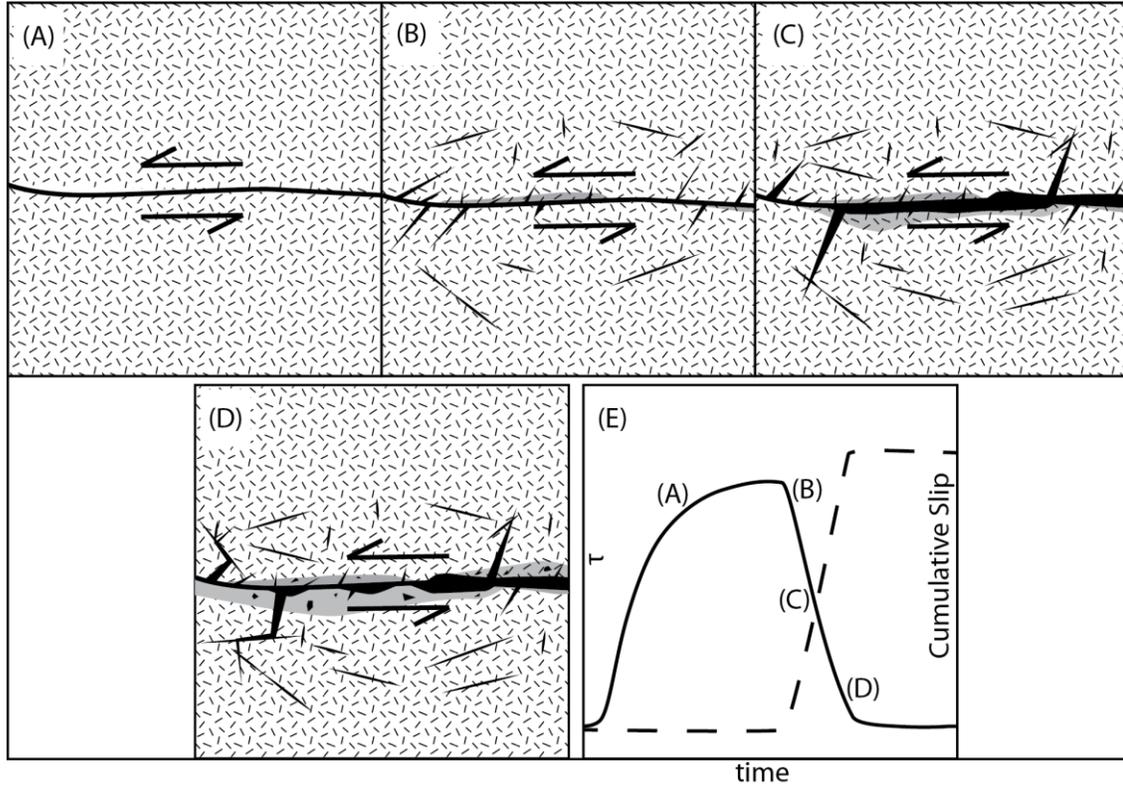
Figure 2-17: Conceptual model of pseudotachylyte evolution through the seismic cycle.

(A) starting condition during stress accumulation (E). (B) early co-seismic period,

generation of new fractures, and cataclasites. (C) mid-late co-seismic period, continued

cataclasis, and generation of frictional melt. (D) late co-seismic period, some deformation

of pseudotachylyte and cataclasite. (E) evolution of shear stress (τ) and cumulative slip

(dashed line) through the seismic cycle.

References

Allen, J.L., 2005, A multi-kilometer pseudotachylyte system as an exhumed record of
    earthquake rupture geometry at hypocentral depths (Colorado, USA):
    Tectonophysics, v. 402, p. 37–54, doi: 10.1016/j.tecto.2004.10.017.

Austrheim, H., Erambert, M., and Boundy, T.M., 1996, Garnets recording deep crustal earthquakes: Earth and Planetary Science Letters, v. 139, p. 223–238, doi: 10.1016/0012-821X(95)00232-2.

Barker, S.L., Sibson, R.H., Palin, J.M., FitzGerald, J.D., Reddy, S., Warr, L.N., and van der Pluijm, B.A., 2010, Cretaceous age, composition, and microstructure of pseudotachylyte in the Otago Schist, New Zealand: New Zealand Journal of Geology and Geophysics, v. 53, p. 15–29, doi: 10.1080/00288301003631764.

Bateman, P.C., 1992, Plutonism in the central part of the Sierra Nevada batholith, California: U.S. Geological Survey Professional Paper 1483, 186 p.

Beggan, C., and Hamilton, C.W., 2010, New image processing software for analyzing object size-frequency distributions, geometry, orientation, and spatial distribution: Computers & Geosciences, v. 36, p. 539–549, doi: 10.1016/j.cageo.2009.09.003.

Ben-Zion, Y., and Sammis, C.G., 2003, Characterization of fault zones: Pure and Applied Geophysics, v. 160, p. 677–715.

Bestmann, M., Pennacchioni, G., Frank, G., Göken, M., and de Wall, H., 2011, Pseudotachylyte in muscovite-bearing quartzite: Coseismic friction-induced melting and plastic deformation of quartz: Journal of Structural Geology, v. 33, p. 169–186, doi: 10.1016/j.jsg.2010.10.009.

Bestmann, M., Pennacchioni, G., Nielsen, S., Göken, M., and de Wall, H., 2012, Deformation and ultrafine dynamic recrystallization of quartz in pseudotachylyte-bearing brittle faults: A matter of a few seconds: Journal of Structural Geology, v. 38, p. 21–38, doi: 10.1016/j.jsg.2011.10.001.

Bjørnerud, M., and Magloughlin, J.F., 2004, Pressure-related feedback processes in the generation of pseudotachylytes: Journal of Structural Geology, v. 26, p. 2317–2323, doi: 10.1016/j.jsg.2002.08.001.

Blanpied, M.L., Lockner, D.A., and Byerlee, J.D., 1991, Fault stability inferred from granite sliding experiments at hydrothermal conditions: Geophysical Research Letters, v. 18, p. 609–612, doi: 10.1029/91GL00469.

Blanpied, M.L., Lockner, D.A., and Byerlee, J.D., 1995, Frictional slip of granite at hydrothermal conditions: Journal of Geophysical Research: Solid Earth, v. 100, p. 13045–13064, doi: 10.1029/95JB00862.

Boullier, A.-M., Ohtani, T., Fujimoto, K., Ito, H., and Dubois, M., 2001, Fluid inclusions in pseudotachylytes from the Nojima fault, Japan: Journal of Geophysical Research: Solid Earth, v. 106, p. 21965–21977, doi: 10.1029/2000JB000043.

Caine, J.S., Evans, J.P., and Forster, C.B., 1996, Fault zone architecture and permeability structure: Geology, v. 24, p. 1025–1028, doi: 10.1130/0091-7613(1996)024<1025:FZAAPS>2.3.CO;2.

Chen, J.H., and Moore, J.G., 1982, Uranium-lead isotopic ages from the Sierra Nevada Batholith, California: Journal of Geophysical Research: Solid Earth, v. 87, p. 4761–4784, doi: 10.1029/JB087iB06p04761.

Chester, F.M., and Chester, J.S., 1998, Ultracataclasite structure and friction processes of the Punchbowl fault, San Andreas system, California: Tectonophysics, v. 295, p. 199–221, doi: 10.1016/S0040-1951(98)00121-8.

Chester, F.M., Evans, J.P., and Biegel, R.L., 1993, Internal structure and weakening mechanisms of the San Andreas Fault: Journal of Geophysical Research: Solid Earth, v. 98, p. 771–786, doi: 10.1029/92JB01866.

Cowan, D.S., 1999, Do faults preserve a record of seismic slip? A field geologist's opinion: Journal of Structural Geology, v. 21, p. 995–1001, doi: 10.1016/S0191-8141(99)00046-2.

Craddock, J.P., and Magloughlin, J.F., 2005, Calcite strains, kinematic indicators, and magnetic flow fabric of a Proterozoic pseudotachylyte swarm, Minnesota River valley, USA: Tectonophysics, v. 402, p. 153–168, doi: 10.1016/j.tecto.2004.12.035.

Di Toro, G., Nielsen, S., and Pennacchioni, G., 2005, Earthquake rupture dynamics frozen in exhumed ancient faults: Nature, v. 436, p. 1009–1012, doi: 10.1038/nature03910.

Di Toro, G., Niemeijer, A., Tripoli, A., Nielsen, S., Di Felice, F., Scarlato, P., Spada, G., Alessandroni, R., Romeo, G., Di Stefano, G., Smith, S., Spagnuolo, E., and Mariano, S., 2010, From field geology to earthquake simulation: a new state-of-the-art tool to investigate rock friction during the seismic cycle (SHIVA): Rendiconti Lincei, v. 21, p. 95–114, doi: 10.1007/s12210-010-0097-x.

Di Toro, G., and Pennacchioni, G., 2005, Fault plane processes and mesoscopic structure of a strong-type seismogenic fault in tonalites (Adamello batholith, Southern Alps): Tectonophysics, v. 402, p. 55–80, doi: 10.1016/j.tecto.2004.12.036.

Di Toro, G., and Pennacchioni, G., 2004, Superheated friction-induced melts in zoned pseudotachylytes within the Adamello tonalites (Italian Southern Alps): Journal of Structural Geology, v. 26, p. 1783–1801, doi: 10.1016/j.jsg.2004.03.001.

Evans, J.P., and Chester, F.M., 1995, Fluid-rock interaction in faults of the San Andreas system: Inferences from San Gabriel fault rock geochemistry and microstructures: Journal of Geophysical Research: Solid Earth, v. 100, p. 13007–13020, doi: 10.1029/94JB02625.

Fabbri, O., A. Lin, and H. Tokushige, 2000, Coeval formation of cataclasite and pseudotachylyte in a Miocene forearc granodiorite, southern Kyushu, Japan, Journal of Structural Geology, v. 22, p. 1015–1025.

Fagereng, A., and Toy, V.G., 2011, Geology of the earthquake source: an introduction: Geological Society, London, Special Publications, v. 359, p. 1–16, doi: 10.1144/SP359.1.

Ferrill, D.A., Morris, A.P., Evans, M.A., Burkhard, M., Groshong Jr., R.H., and Onasch, C.M., 2004, Calcite twin morphology: a low-temperature deformation geothermometer: Journal of Structural Geology, v. 26, p. 1521–1529, doi: 10.1016/j.jsg.2003.11.028.

Fiebig, J., and Hoefs, J., 2002, Hydrothermal alteration of biotite and plagioclase as inferred from intragranular oxygen isotope- and cation-distribution patterns: European Journal of Mineralogy, v. 14, p. 49–60, doi: 10.1127/0935-1221/2002/0014-0049.

Fulton, P.M., and Saffer, D.M., 2009, Effect of thermal refraction on heat flow near the San Andreas Fault, Parkfield, California: Journal of Geophysical Research: Solid Earth, v. 114, doi: 10.1029/2008JB005796.

Griffith, W.A., Mitchell, T.M., Renner, J., and Di Toro, G., 2012, Coseismic damage and softening of fault rocks at seismogenic depths: Earth and Planetary Science Letters, v. 353–354, p. 219–230, doi: 10.1016/j.epsl.2012.08.013.

Griffith, W.A., Di Toro, G., Pennacchioni, G., and Pollard, D.D., 2008, Thin pseudotachylytes in faults of the Mt. Abbot quadrangle, Sierra Nevada: Physical constraints for small seismic slip events: Journal of Structural Geology, v. 30, p. 1086–1094, doi: 10.1016/j.jsg.2008.05.003.

Heilbronner, R., and Keulen, N., 2006, Grain size and grain shape analysis of fault rocks: Tectonophysics, v. 427, p. 199–216, doi: 10.1016/j.tecto.2006.05.020.

Hirose, T., and Shimamoto, T., 2003, Fractal dimension of molten surfaces as a possible parameter to infer the slip-weakening distance of faults from natural pseudotachylytes: Journal of Structural Geology, v. 25, p. 1569–1574, doi: 10.1016/S0191-8141(03)00009-9.

Hirose, T., and Shimamoto, T., 2005, Growth of molten zone as a mechanism of slip weakening of simulated faults in gabbro during frictional melting: Journal of Geophysical Research: Solid Earth, v. 110, doi: 10.1029/2004JB003207.

Imber, J., Holdsworth, R.E., Butler, C.A., and Strachan, R.A., 2001, A reappraisal of the Sibson-Scholz fault zone model: The nature of the frictional to viscous ("brittle-ductile") transition along a long-lived, crustal-scale fault, Outer Hebrides, Scotland: Tectonics, v. 20, p. 601–624, doi: 10.1029/2000TC001250.

Jacobs, J.R., Evans, J.P., and Kolesar, P.T., 2006, Energetics of chemical alteration in fault zones and its relationship to the seismic cycle, *in* Abercrombie, R., McGarr, A., Kanamori, H., and Di Toro, G. eds., Geophysical Monograph Series, American Geophysical Union, Washington, D. C., p. 181–191.

Janecke, S.U., and Evans, J.P., 1988, Feldspar-influenced rock rheologies: Geology, v. 16, p. 1064–1067, doi: 10.1130/0091-7613(1988)016<1064:FIRR>2.3.CO;2.

Jerram, D.A., and Higgins, M.D., 2007, 3D Analysis of Rock Textures: Quantifying Igneous Microstructures: Elements, v. 3, p. 239–245, doi: 10.2113/gselements.3.4.239.

Kanamori, H., and Brodsky, E.E., 2004, The physics of earthquakes: Reports on Progress in Physics, v. 67, p. 1429, doi: 10.1088/0034-4885/67/8/R03.

Kanamori, H., and Riveira, L., 2006, Energy partitioning during an earthquake, *in* Abercrombie, R., McGarr, A., and Kanamori, H. eds., Earthquakes: Radiated Energy and the Physics of Faulting, Geopysical Monograph Series 170, American Geophysical Union, Washington, D. C., p. 3–13.

Kirkpatrick, J.D., Dobson, K.J., Mark, D.F., Shipton, Z.K., Brodsky, E.E., and Stuart, F.M., 2012, The depth of pseudotachylyte formation from detailed thermochronology and constraints on coseismic stress drop variability: Journal of Geophysical Research: Solid Earth, v. 117, doi: 10.1029/2011JB008846.

Kirkpatrick, J.D., and Rowe, C.D., 2013, Disappearing ink: How pseudotachylytes are lost from the rock record: Journal of Structural Geology, v. (in press), doi: 10.1016/j.jsg.2013.03.003.

Kirkpatrick, J.D., and Shipton, Z.K., 2009, Geologic evidence for multiple slip weakening mechanisms during seismic slip in crystalline rock: Journal of Geophysical Research: Solid Earth, v. 114, doi: 10.1029/2008JB006037.

Kirkpatrick, J.D., Shipton, Z.K., Evans, J.P., Micklethwaite, S., Lim, S.J., and McKillop, P., 2008, Strike-slip fault terminations at seismogenic depths: The structure and kinematics of the Glacier Lakes fault, Sierra Nevada United States: Journal of Geophysical Research: Solid Earth, v. 113, doi: 10.1029/2007JB005311.

Kirkpatrick, J.D., Shipton, Z.K., and Persano, C., 2009, Pseudotachylytes: Rarely Generated, Rarely Preserved, or Rarely Reported?: Bulletin of the Seismological Society of America, v. 99, p. 382–388, doi: 10.1785/0120080114.

Lachenbruch, A.H., and Sass, J.H., 1980, Heat flow and energetics of the San Andreas Fault Zone: Journal of Geophysical Research: Solid Earth, v. 85, p. 6185–6222, doi: 10.1029/JB085iB11p06185.

Lavallée, Y., Mitchell, T.M., Heap, M.J., Vasseur, J., Hess, K.-U., Hirose, T., and Dingwell, D.B., 2012, Experimental generation of volcanic pseudotachylytes: Constraining rheology: Journal of Structural Geology, v. 38, p. 222–233, doi: 10.1016/j.jsg.2012.02.001.

Lin, A., 1994a, Glassy pseudotachylyte veins from the Fuyun fault zone, northwest China: Journal of Structural Geology, v. 16, p. 71–83, doi: 10.1016/0191-8141(94)90019-1.

Lin, A., 1994b, Microlite Morphology and Chemistry in Pseudotachylite, from the Fuyun Fault Zone, China: The Journal of Geology, v. 102, p. 317–329, doi: 10.2307/30070517.

Lin, A., 1999, Roundness of clasts in pseudotachylytes and cataclastic rocks as an indicator of frictional melting: Journal of Structural Geology, v. 21, p. 473–478, doi: 10.1016/S0191-8141(99)00030-9.

Lin, A., 2008, Fossil Earthquakes: the formation and preservation of pseudotachylytes: Springer, New York.

Lin, A., 2011, Seismic slip recorded by fluidized ultracataclastic veins formed in a coseismic shear zone during the 2008 Mw 7.9 Wenchuan earthquake: Geology, v. 39, p. 547–550, doi: 10.1130/G32065.1.

Lin, A., and Shimamoto, T., 1998, Selective melting processes as inferred from experimentally generated pseudotachylytes: Journal of Asian Earth Sciences, v. 16, p. 533–545, doi: 10.1016/S0743-9547(98)00040-3.

Lin, A., Yamashita, K., and Tanaka, M., 2013, Repeated seismic slips recorded in ultracataclastic veins along active faults of the Arima–Takatsuki Tectonic Line, southwest Japan: Journal of Structural Geology, v. 48, p. 3–13, doi: 10.1016/j.jsg.2013.01.005.

Lockner, D.A., and Okubo, P.G., 1983, Measurements of frictional heating in granite: Journal of Geophysical Research: Solid Earth, v. 88, p. 4313–4320, doi: 10.1029/JB088iB05p04313.

Maddock, R.H., Grocott, J., and Van Nes, M., 1987, Vesicles, amygdales and similar structures in fault-generated pseudotachylytes: Lithos, v. 20, p. 419–432, doi: 10.1016/0024-4937(87)90019-3.

Magloughlin, J.F., 1989, The nature and significance of pseudotachylite from the Nason terrane, North Cascade Mountains, Washington: Journal of Structural Geology, v. 11, p. 907–917, doi: 10.1016/0191-8141(89)90107-7.

Magloughlin, J.F., 2005, Immiscible sulfide droplets in pseudotachylyte: Evidence for high temperature (> 1200 °C) melts: Tectonophysics, v. 402, p. 81–91, doi: 10.1016/j.tecto.2004.11.011.

Magloughlin, J.F., 2011, Bubble Collapse Structure: A Microstructural Record of Fluids, Bubble Formation and Collapse, and Mineralization in Pseudotachylyte: The Journal of Geology, v. 119, p. 351–371, doi: 10.1086/659143.

Magloughlin, J.F., and Spray, J.G., 1992, Frictional melting processes and products in geological materials: introduction and discussion: Tectonophysics, v. 204, p. 197–204, doi: 10.1016/0040-1951(92)90307-R.

Marone, C., and Richardson, E., 2010, Learning to read fault-slip behavior from fault-zone structure: Geology, v. 38, p. 767–768, doi: 10.1130/focus082010.1.

McGarr, A., 1999, On relating apparent stress to the stress causing earthquake fault slip: Journal of Geophysical Research: Solid Earth, v. 104, p. 3003–3011, doi: 10.1029/1998JB900083.

McKenzie, D., and Brune, J.N., 1972, Melting on Fault Planes During Large Earthquakes: Geophysical Journal International, v. 29, p. 65–78, doi: 10.1111/j.1365-246X.1972.tb06152.x.

McNulty, B.A., 1995, Pseudotachylyte generated in the semi-brittle and brittle regimes, Bench Canyon shear zone, central Sierra Nevada: Journal of Structural Geology, v. 17, p. 1507–1521, doi: 10.1016/0191-8141(95)00052-F.

Meneghini, F., Toro, G.D., Rowe, C.D., Moore, J.C., Tsutsumi, A., and Yamaguchi, A., 2010, Record of mega-earthquakes in subduction thrusts: The black fault rocks of Pasagshak Point (Kodiak Island, Alaska): Geological Society of America Bulletin, v. 122, p. 1280–1297, doi: 10.1130/B30049.1.

Mittempergher, S., Pennacchioni, G., and Di Toro, G., 2009, The effects of fault orientation and fluid infiltration on fault rock assemblages at seismogenic depths: Journal of Structural Geology, v. 31, p. 1511–1524, doi: 10.1016/j.jsg.2009.09.003.

Mount, V.S., and Suppe, J., 1987, State of stress near the San Andreas fault: Implications for wrench tectonics: Geology, v. 15, p. 1143–1146, doi: 10.1130/0091-7613(1987)15<1143:SOSNTS>2.0.CO;2.

Mysen, B.O., and Richet, P., 2005, Silicate Glasses and Melts: Properties and Structure: Elsevier, Amsterdam.

Nielsen, S., Toro, G.D., and Griffith, W.A., 2010, Friction and roughness of a melting rock surface: Geophysical Journal International, v. 182, p. 299–310, doi: 10.1111/j.1365-246X.2010.04607.x.

Ozawa, K., and Takizawa, S., 2007, Amorphous material formed by the mechanochemical effect in natural pseudotachylyte of crushing origin: A case study of the Iida-Matsukawa Fault, Nagano Prefecture, Central Japan: Journal of Structural Geology, v. 29, p. 1855–1869, doi: 10.1016/j.jsg.2007.08.008.

Pachell, M.A., and Evans, J.P., 2002, Growth, linkage, and termination processes of a 10-km-long strike-slip fault in jointed granite: the Gemini fault zone, Sierra Nevada, California: Journal of Structural Geology, v. 24, p. 1903–1924, doi: 10.1016/S0191-8141(02)00027-5.

Pachell, M.A., Evans, J.P., and Taylor, W.L., 2003, Kilometer-scale kinking of crystalline rocks in a transpressive convergent setting, Central Sierra Nevada, California: Geological Society of America Bulletin, v. 115, p. 817–831, doi: 10.1130/0016-7606(2003)115<0817:KKOCRI>2.0.CO;2.

Parry, W.T., and Downey, L.M., 1982, Geochemistry of hydrothermal chlorite replacing igneous biotite: Clays and Clay Minerals, v. 30, p. 81–90.

Passchier, C.W., and Trouw, R.A.J., 2005, Microtectonics: Springer.

Pittarello, L., Di Toro, G., Bizzarri, A., Pennacchioni, G., Hadizadeh, J., and Cocco, M., 2008, Energy partitioning during seismic slip in pseudotachylyte-bearing faults (Gole Larghe Fault, Adamello, Italy): Earth and Planetary Science Letters, v. 269, p. 131–139, doi: 10.1016/j.epsl.2008.01.052.

Plattner, U., Markl, G., and Sherlock, S., 2003, Chemical heterogeneities of Caledonian (?) pseudotachylites in the Eidsfjord Anorthosite, north Norway: Contributions to Mineralogy and Petrology, v. 145, p. 316–338, doi: 10.1007/s00410-003-0455-0.

Rempel, A.W., and Weaver, S.L., 2008, A model for flash weakening by asperity melting during high-speed earthquake slip: Journal of Geophysical Research: Solid Earth, v. 113, p. n/a–n/a, doi: 10.1029/2008JB005649.

Rice, J.R., 2006, Heating and weakening of faults during earthquake slip: Journal of Geophysical Research, v. 111, doi: 10.1029/2005JB004006.

Rowe, C.D., Kirkpatrick, J.D., and Brodsky, E.E., 2012, Fault rock injections record paleo-earthquakes: Earth and Planetary Science Letters, v. 335–336, p. 154–166, doi: 10.1016/j.epsl.2012.04.015.

Scholz, C.H., 2002, The Mechanics of Earthquakes and Faulting: Cambridge University Press.

Schulz, S.E., and Evans, J.P., 2000, Mesoscopic structure of the Punchbowl Fault, Southern California and the geologic and geophysical structure of active strike-slip faults: Journal of Structural Geology, v. 22, p. 913–930, doi: 10.1016/S0191-8141(00)00019-5.

Segall, P., McKee, E.H., Martel, S.J., and Turrin, B.D., 1990, Late Cretaceous age of fractures in the Sierra Nevada batholith, California: Geology, v. 18, p. 1248–1251, doi: 10.1130/0091-7613(1990)018<1248:LCAOFI>2.3.CO;2.

Shaw, H.R., 1972, Viscosities of magmatic silicate liquids; an empirical method of prediction: American Journal of Science, v. 272, p. 870–893, doi: 10.2475/ajs.272.9.870.

Shipton, Z.K., Evans, J.P., Abercrombie, R.E., and Brodsky, E.E., 2006, The missing sinks: Slip localization in faults, damage zones, and the seismic energy budget, *in* Abercrombie, R., McGarr, A., Kanamori, H., and Di Toro, G. eds., Geophysical Monograph Series, American Geophysical Union, Washington, D. C., p. 217–222.

Sibson, R.H., 1975, Generation of Pseudotachylyte by Ancient Seismic Faulting: Geophysical Journal of the Royal Astronomical Society, v. 43, p. 775–794, doi: 10.1111/j.1365-246X.1975.tb06195.x.

Sibson, R.H., 1983, Continental fault structure and the shallow earthquake source: Journal of the Geological Society, v. 140, p. 741–767, doi: 10.1144/gsjgs.140.5.0741.

Sibson, R.H., and Toy, V.G., 2006, The habitat of fault-generated pseudotachylyte: Presence vs. absence of friction-melt: Geophysical Monograph Series, v. 170, p. 153–166, doi: 10.1029/170GM16.

Sipp, A., and Richet, P., 2002, Equivalence of volume, enthalpy and viscosity relaxation kinetics in glass-forming silicate liquids: Journal of Non-Crystalline Solids, v. 298, p. 202–212, doi: 10.1016/S0022-3093(02)00948-1.

Smith, S.A.F., Collettini, C., and Holdsworth, R.E., 2008, Recognizing the seismic cycle along ancient faults: CO2-induced fluidization of breccias in the footwall of a sealing low-angle normal fault: Journal of Structural Geology, v. 30, p. 1034–1046, doi: 10.1016/j.jsg.2008.04.010.

Smith, S. A. F., Toro, G.D., Kim, S., Ree, J.-H., Nielsen, S., Billi, A., and Spiess, R., 2013, Coseismic recrystallization during shallow earthquake slip: Geology, v. 41, p. 63–66, doi: 10.1130/G33588.1.

Spray, J.G., 1987, Artificial generation of pseudotachylyte using friction welding apparatus: simulation of melting on a fault plane: Journal of Structural Geology, v. 9, p. 49–60, doi: 10.1016/0191-8141(87)90043-5.

Spray, J.G., 1992, A physical basis for the frictional melting of some rock-forming minerals: Tectonophysics, v. 204, p. 205–221, doi: 10.1016/0040-1951(92)90308-S.

Spray, J.G., 1993, Viscosity determinations of some frictionally generated silicate melts: Implications for fault zone rheology at high strain rates: Journal of Geophysical Research: Solid Earth, v. 98, p. 8053–8068, doi: 10.1029/93JB00020.

Spray, J.G., 2010, Frictional Melting Processes in Planetary Materials: From Hypervelocity Impact to Earthquakes: Annual Review of Earth and Planetary Sciences, v. 38, p. 221–254, doi: 10.1146/annurev.earth.031208.100045.

Stern, T.W., Bateman, P.C., Morgan, B.A., Newell, M.F., and Peck, D.L., 1981, Isotopic U-Pb ages of zircon from the granitoids of the central Sierra Nevada, California: U.S. Dept. of the Interior, Geological Survey U.S. Geological Survey Professional Paper 1185, 17 p.

Stünitz, H., Keulen, N., Hirose, T., and Heilbronner, R., 2010, Grain size distribution and microstructures of experimentally sheared granitoid gouge at coseismic slip rates – Criteria to distinguish seismic and aseismic faults?: Journal of Structural Geology, v. 32, p. 59–69, doi: 10.1016/j.jsg.2009.08.002.

Swanson, M.T., 1992, Fault structure, wear mechanisms and rupture processes in pseudotachylyte generation: Tectonophysics, v. 204, p. 223–242, doi: 10.1016/0040-1951(92)90309-T.

Tanaka, H., Chen, W.M., Wang, C.Y., Ma, K.F., Urata, N., Mori, J., and Ando, M., 2006, Frictional heat from faulting of the 1999 Chi-Chi, Taiwan earthquake: Geophysical Research Letters, v. 33, doi: 10.1029/2006GL026673.

Toy, V.G., Ritchie, S., and Sibson, R.H., 2011, Diverse habitats of pseudotachylytes in the Alpine Fault Zone and relationships to current seismicity: Geological Society, London, Special Publications, v. 359, p. 115–133, doi: 10.1144/SP359.7.

Tullis, T.E., 1994, Predicting earthquakes and the mechanics of fault slip: Geotime, v. 39, p. 19–21.

Ujiie, K., Yamaguchi, H., Sakaguchi, A., and Toh, S., 2007, Pseudotachylytes in an ancient accretionary complex and implications for melt lubrication during subduction zone earthquakes: Journal of Structural Geology, v. 29, p. 599–613, doi: 10.1016/j.jsg.2006.10.012.

Warr, L.N., and van der Pluijm, B.A., 2005, Crystal fractionation in the friction melts of seismic faults (Alpine Fault, New Zealand): Tectonophysics, v. 402, p. 111–124, doi: 10.1016/j.tecto.2004.12.034.

Webb, S., and Knoche, R., 1996, The glass-transition, structural relaxation and shear viscosity of silicate melts: Chemical Geology, v. 128, p. 165–183, doi: 10.1016/0009-2541(95)00171-9.

Wenk, H.-R., Johnson, L.R., and Ratschbacher, L., 2000, Pseudotachylites in the Eastern Peninsular Ranges of California: Tectonophysics, v. 321, p. 253–277, doi: 10.1016/S0040-1951(00)00064-0.

Wibberley, C.A.., and Shimamoto, T., 2003, Internal structure and permeability of major strike-slip fault zones: the Median Tectonic Line in Mie Prefecture, Southwest Japan: Journal of Structural Geology, v. 25, p. 59–78, doi: 10.1016/S0191-8141(02)00014-7.

CHAPTER 3

IRIDESCENT-METALLIC HIGHLY POLISHED SLIP SURFACES: EVIDENCE

FOR ANCIENT SEISMICITY ALONG EXHUMED FAULTS

Abstract

The generation of high temperatures by frictional heating is expected at seismic slip rates (0.1-1.0 m s^{-1}) along discrete fault slip surfaces. Despite this prediction the only convincing evidence for the preservation of the rapid thermal transients expected during seismicity is tectonic pseudotachylyte (rapidly-quenched frictional melt). Here we document new evidence for ancient seismicity along the Brigham City segment of the Wasatch fault, UT, in the form of highly-polished (mirrored) slip surfaces that formed in the Paleoproterozoic Farmington Canyon Gneiss. Slip along the Wasatch fault generated patchy iridescent-metallic highly-polished slip surfaces (HPSS) in veins of acicular hematite crystal on many highly-polished and striated slip surfaces. The iridescence is interpreted to be the result of high-temperature oxidation at small (< 20 μm-wide) asperities along HPSS. The iridescent surfaces are less-than 10 μm-thick and developed at temperatures > 400 ˚C based on the transition from hematite to magnetite and experimental data. Nano-scale, tabular Fe_2O_3 crystals comprise the iridescent surfaces and are preferentially aligned parallel to the slip surface. Similar iridescent surfaces have been documented in rotary shear experiments on metallic surfaces and geologic materials at elevated temperatures (> 400 ˚C). We propose that the iridescent-metallic slip surfaces in the Wasatch fault zone are the result of seismic slip. The presence of thousands of

these surfaces in the 100's of m map distance from the surface trace of the Wasatch fault indicates that this volume of the footwall experienced many seismic slip events perhaps as aftershocks ro a main rupture on the main fault segment.

Introduction

Analyses of the total energy budget of earthquakes indicate that up to 80% of the energy released during seismicity is consumed by processes in the fault zone (Lockner and Okubo, 1983; McGarr, 1999; Di Toro et al., 2005; Sibson and Toy, 2006; Tanaka et al., 2006). Because the majority of the energy released during seismicity is consumed by dissipative processes in the fault zone it is difficult to constrain the total energy budget of earthquakes using seismologic data sets alone (Scholz, 2002; Kanamori and Riveiro, 2006). Much of this energy is thought to be converted to heat during frictional sliding (McKenzie and Brune, 1972; Sibson, 1975; Lockner and Okubo, 1983; Kanamori and Brodsky, 2004; Di Toro et al., 2005; Tanaka et al., 2006; Sibson and Toy, 2006). The only convincing evidence for the preservation of this heat is pseudotachylyte (Sibson, 1975; Spray, 1992, 2010; Sibson and Toy, 2006; Kirkpatrick and Rowe, 2013). Pseudotachylyte however, is rarely reported in the geologic record (Sibson and Toy, 2006; Kirkpatrick and Rowe, 2013). The apparent rareness of pseudotachylyte can be explained by uncommon formation during seismicity (Sibson, 1975, 2003; Spray, 1992; Lin, 2008; Kirkpatrick et al., 2009; Bjørnerud, 2010; Kirkpatrick and Rowe, 2013). If pseudotachylyte is rarely generated there must be other fault-related rock-types and deformation products that consume the frictional heat generated in fault zones and record

evidence for this deformation history (Sibson, 2003; Rice, 2006; Jacobs et al., 2006; Shipton et al., 2006; Kirkpatrick and Shipton, 2009; Siman-Tov et al., 2013; Smith et al., 2013).

To unequivocally demonstrate a seismic origin for fault-related deformation a connection must be made between the observed deformation and strain rate, temperature, and or pressure; and demonstrate that these conditions are in disequilibrium with the geologic context of the fault zone (Cowan, 1999; Marone and Richardson, 2010). Here we demonstrate that highly-polished slip surfaces in the footwall of the northern Wasatch fault, Utah (Fig. 3.1), were generated by elevated temperatures that are only reasonable explained by frictional heating during ancient seismic events. This study employs a variety of traditional and novel methods to quantify the three-dimensional topography, and composition of highly-polished slip surfaces.

Methods

Highly-polished slip surfaces were analyzed in place and in the laboratory using optical petrographic microscopy, scanning electron microscopy, x-ray diffraction (XRD), and x-ray photoelectron spectroscopy (XPS) analyses focused on microstructural, compositional, and mineralogical characterization of fault-related rocks. We also use white-light interferometery, lab-based 3D laser metrology, and a three-dimensional (3D) infrared range camera (Microsoft Kinect™) analyses to describe the micro- to meso-scale topography of fault surfaces.
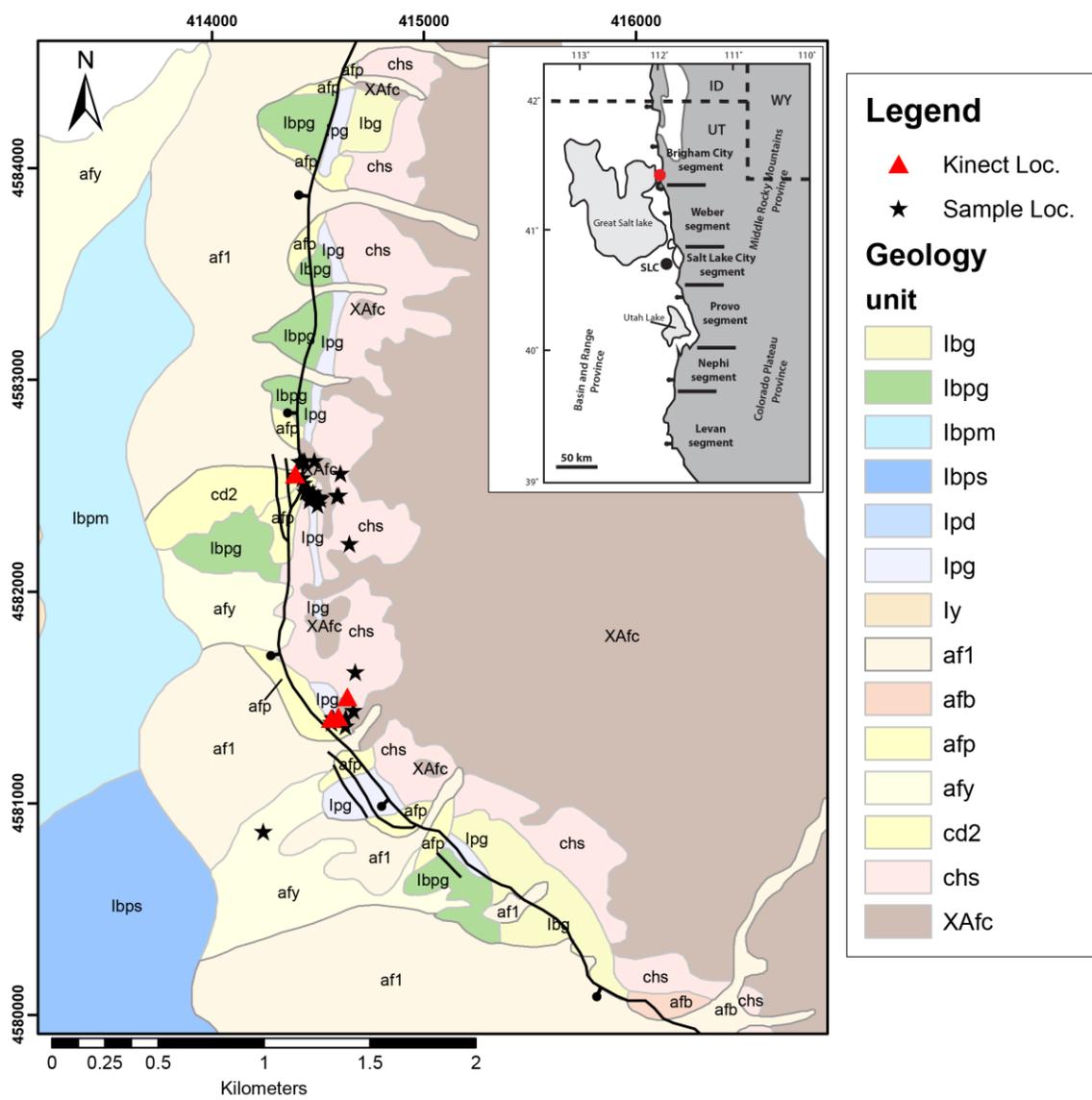
Scanning electron microscopy, back-scattered electron images (SEM-BSE) were acquired to document the micro-scale textures of HPSS at the University of Wisconsin Madison Geosciences Electron Microbeam Lab. The XRD analyses were conducted using an X Pert Pro Diffractometer system (45kV/40 MA) at Utah State University. The XPS analyses were conducted using a Kratos Axis Ultra X-Ray spectrophotometer, operating with a spot size of 15 μm and depth of investigation of approximately 10 nm, at the University of Utah NanoFab lab. Due to the very thin nature of the slip surfaces, traditional electron beam methods cannot resolve the composition of the iridescent zones and X-ray diffraction can detect mineral phases that comprise $\geq 5\%$ of the rock. We use X-ray photelectron spectroscopy (XPS) to measure the valance state of the elements that comprise the HPSS. The XPS method targets the sample with a beam of X-rays under a very high vacuum (10^{-9} torr and greater) and detects the energy of the electrons that escaped from the upper 1-10 nm of the sample. The samples examined here were examined after cleaning with a series of ultrapure solutions, and after cleaning with an Ar- ion beam for 60 seconds.

White-light interferometry analyses were conducted using a Zygo NewView optical profiler at the University of Utah NanoFab lab. The 3D laser scans and point cloud data were collected using a Laser Design Inc. bench top high-precision laser scanning system by GKS Services. Field- and lab-based 3d infrared range camera data were conducted with a Microsoft Kinect with vertical resolution ~ 1 mm (Khoshelham

and Elberink, 2012; Mankoff and Russo, 2012; Gonzalez-Jorge et al., 2013; Chapter 5), at Utah State University.

Background

Highly-polished slip surfaces (HPSS) are a common fault-related structure and are found in a variety of rock types and tectonic settings (Gilbert, 1928; Petit, 1987; Power et al., 1987; Will and Wilson, 1989; Power and Tullis, 1989; Evans and Langrock, 1994; Doblas, 1998; Candela et al., 2009, 2011b; Sagy and Brodsky, 2009; Caine et al., 2010; Siman-Tov et al., 2013; Smith et al., 2013). Despite the pervasiveness of highly-polished slip surfaces in the rock record, their characteristics and formation mechanisms have been little studied (Power and Tullis, 1989; Will and Wilson, 1989; Han et al., 2007, 2011; Sagy and Brodsky, 2009; Caine et al., 2010; Mouslopoulou et al., 2011; Rowe et al., 2012; Siman-Tov et al., 2013; Smith et al., 2013). The generation of highly-polished slip surfaces has been attributed to frictional grinding by ultrafine-grained material (Engelder, 1974, 1978; Siman-Tov et al., 2013), the development of very thin mineralized and sheared surfaces (Means, 1993; Will, 1987), melting (Friedman et al., 1974; Spray, 1989), preferred orientation of grains by rotation during slip (Power and Tullis, 1989; Caine et al., 2010), preferred alignment of phyllosilicates during slip (Will and Wilson, 1989), and dynamic recystallization (Smith et al., 2013). It is important to note that not all of the hypotheses for HPSS formation are mutually exclusive, and the formation conditions are very likely highly dependent on the deformation history, tectonic setting, protolith, and minerology of the fault zone.

Fault zone morphology and the distribution of asperities may have a controlling influence on: grain comminution and abrasion (Sagy and Brodsky, 2009; Brodsky et al., 2011), the static and dynamic coefficient of friction (Scholz, 2002), co-seismic generation of heat (O'Hara, 2005; Rice, 2006; Rempel and Weaver, 2008), earthquake nucleation (Scholz, 2002), and rupture propagation and arrest (Aki, 1984; Rubin et al., 1999; Schaff et al., 2002; Resor and Meer, 2009; Candela et al., 2011a). The morphology of faults at small-scales however, is often simplified in geologic and geophysical studies. This simplification is understandable given the impossibility of inferring the small-scale morphology of fault zones from geophysical data (Scholz, 2002; Kanamori and Brodsky, 2004; Renard et al., 2006). The meso- to microscale roughness of fault surfaces has been investigated on a variety of fault types and tectonic settings (Power et al., 1987, 1988; Power and Tullis, 1989; Stewart, 1996; Giaccio et al., 2003; Renard et al., 2006; Sagy et al., 2007; Candela et al., 2009, 2011a; Sagy and Brodsky, 2009; Brodsky et al., 2011; Candela and Renard, 2012). We expand on this work by combining descriptions of slip-surface morphology from the µm- to m-scales.

Geologic Setting

The 350 km-long Wasatch fault is the longest normal fault of the Intermountain Seismic Belt and defines the active eastern edge of the Basin and Range province (Fig. 3-1) (Schwartz and Coppersmith, 1984; Machette et al., 1991; Friedrich et al., 2003; DuRoss, 2008). The Wasatch fault consists of between 6 to 10 segments, delineated by microseismic, paleoseismic, and geologic mapping data (Fig. 3-1) (Schwartz and

Coppersmith, 1984; Machette et al., 1991; DuRoss, 2008; DuRoss et al., 2012; Personius et al., 2012). Paleoseismic studies of the Wasatch fault confirm recent (Holocene) Mw $\geq$ 7 earthquakes that are confined to single segments or jumped to adjacent segments across structurally complex segment boundaries (Machette et al., 1991; McCalpin and Nishenko, 1996; DuRoss, 2008; Personius et al., 2012). The footwall of the Wasatch fault is a thrust stack emplaced during the Sevier orogeny (Yonkee et al., 1989; DeCelles and Giles, 1996; DeCelles and Coogan, 2006). The thrust stack is composed of Proterozoic and Paleozoic sedimentary, metasedimentary, and gneissic rocks that were thrust eastward over Mesozoic sedimentary rocks (Fig. 3-2) (Yonkee et al., 1992; DeCelles and Giles, 1996; DeCelles and Coogan, 2006). The rocks at the study site may be exhumed from up to 10 km depth, based on restored cross sections for the Sevier thrust complex in the region (Yonkee et al., 1992) and from thermochronology (Fig. 3-2) (Armstrong et al., 2003, 2004; Ehlers et al., 2003; Friedrich et al., 2003).

Previous work along the southern 5 km of the Brigham City segment of the Wasatch fault documented highly-polished slip surfaces in the footwall damage zone of the fault (Evans and Langrock, 1994). These faults lie in a zone of deformed Paleoproterozoic Farmington Canyon Complex rocks that is bounded on the west by the active trace of the Wasatch Fault, and on the eastern edge by the edge of the bedrock damage zone (Evans and Langrock, 1994). The HPSS are concentrated in a region approximately 1.5 km long and 300-400 m wide in the Farmington Canyon Complex (Fig. 3-1). Fe-, chloritic, and epidote alteration associated with the faulting creates a red-

brown hue to the damage zone, and is distinct from the grey gneiss of the protolith (Fig.

3-3).
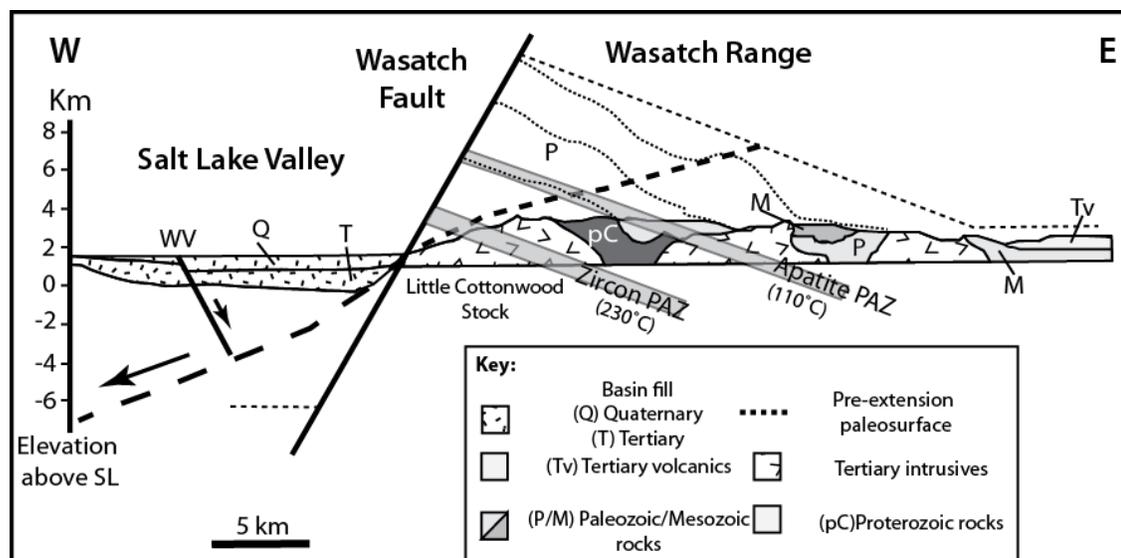
Figure 3-2: Schematic cross-section of central Wasatch fault (modified from Friedrich et

al., 2003). Apatite and zircon partial annealing zones (PAZ), and estimated pre-extension

surface illustrates the estimated 5-11 km of footwall uplift, two fault dip-angle

possibilities are illustrated here 60 ˚ (solid line) and 30˚ (dashed line) (Friedrich et al.,

2003; Armstrong et al., 2003).

Slip and the amount of uplift at the southern end of the Brigham City segment of

the Wasatch fault is loosely constrained. The Brigham City segment of the Wasatch fault

here probably dips ~ 50 to 30° with modest amounts of small magnitude earthquakes

(Smith and Bruhn, 1984; Bjarnason and Pechmann, 1989), and geologic constraints

suggests that the fault has a dip-slip displacement of 4-7 km (Zoback, 1983; Crittenden and Sorensen, 1985; Jensen and King, 1999; Armstrong et al., 2003, 2004; Ehlers et al., 2003; Friedrich et al., 2003). The active trace of the fault ruptures in M 7.0 and greater earthquakes that create large Holocene fault scarps (Personius, 1990; DuRoss et al., 2012; Personius et al., 2012).
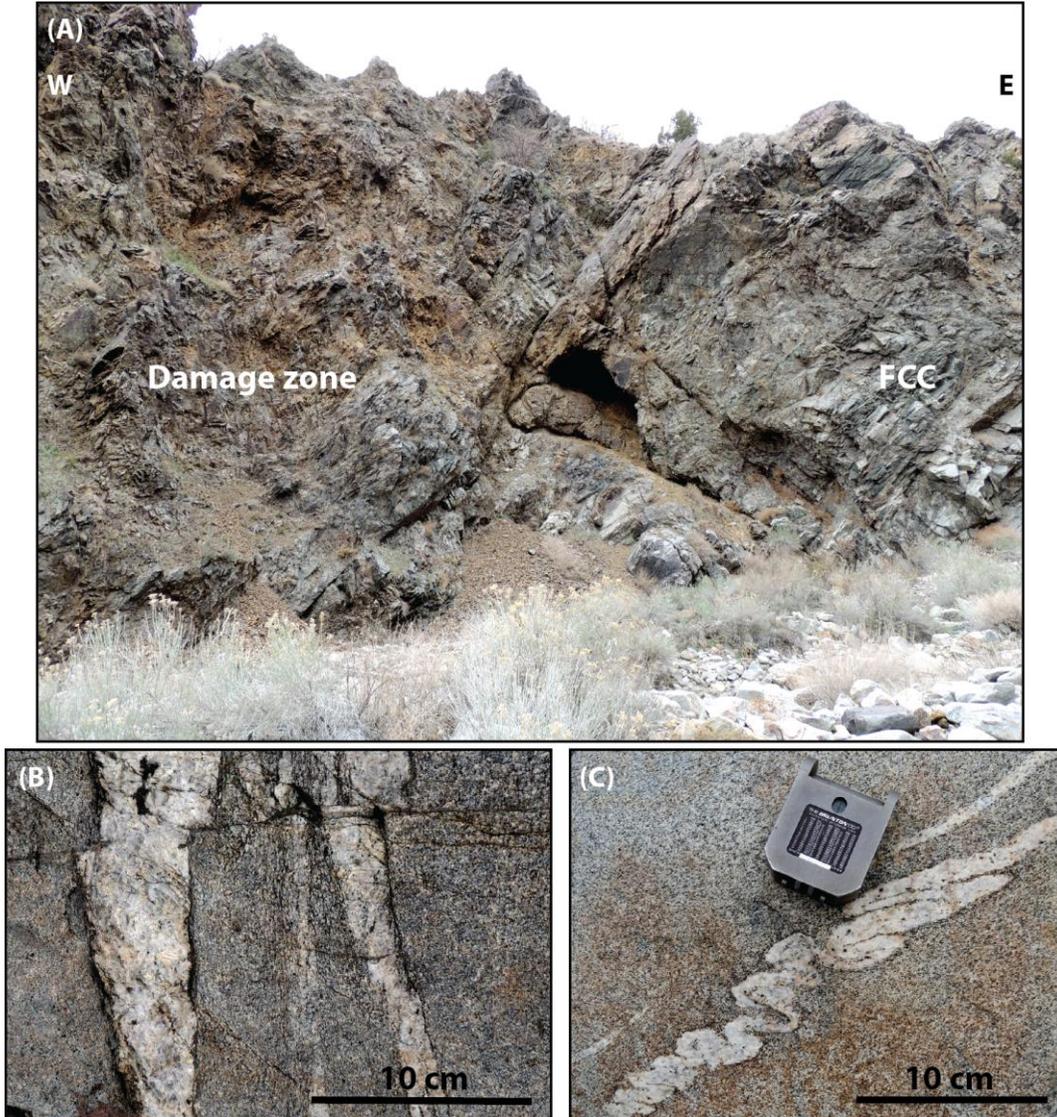
Figure 3-3: (A) Field photograph of footwall damage zone of the Brigham City segment of the Wasatch fault and transition in to Farming Canyon Complex (FCC) quartzofeldspathic gneiss. (B) Field photograph of FCC migmatitic gneiss with foliation defined by alternating bands of mafic melansomes and felsic leucosomes. Small faults crosscut the FCC in the footwall damage zone. (C) Gray FCC gneiss with ptygmatic folded quartz rich vein.

Results

Field observations

Highly-polished slip surfaces are exposed along the southern portion of the Brigham City segment in the structurally complex, footwall damage zone of the fault in the Paleoproterozoic Farmington Canyon complex (Fig. 3-1) (Personius, 1990; Yonkee et al., 1992; Evans and Langrock, 1994; Nelson et al., 2002; Armstrong et al., 2003, 2004; Ehlers et al., 2003; Mueller et al., 2011). The Farmington Canyon Complex in the study area is composed of quartz-feldspar-biotite-hornblende gneiss with a well defined mineral banding foliation defined by parallel alignment of biotite and hornblende (Fig. 3-3 B, C) (Bryant, 1988; Evans and Langrock, 1994; Nelson et al., 2002; Mueller et al., 2011).

The highly-polished slip surfaces are composed of very fine-grained deep red to purple coatings, have metallic luster with a high degree of reflectivity, and contain multiple slip indicators (slickensides) (Fig. 3-4 C) (Evans and Langrock, 1994; Yonkee et al., 1992). The metallic highly-polished slip surfaces reported by Evans and Langrock (1994) formed in the quartzofeldspathic gneiss of the Farmington Canyon Complex and are associated with numerous, < 0.25 mm to 2 cm thick, curved hematite fracture fills (Fig. 3-4; Fig. 3-5) (Evans and Langrock, 1994). The morphology of some of the hematite fracture fills suggest an injection origin, sourced from the highly polished slip surfaces (Fig. 3-6 C, D). In other areas the hematite lies in veins that cut the gneiss, appear to be precursory to the faults, and mark a mineralization event within the gneiss.
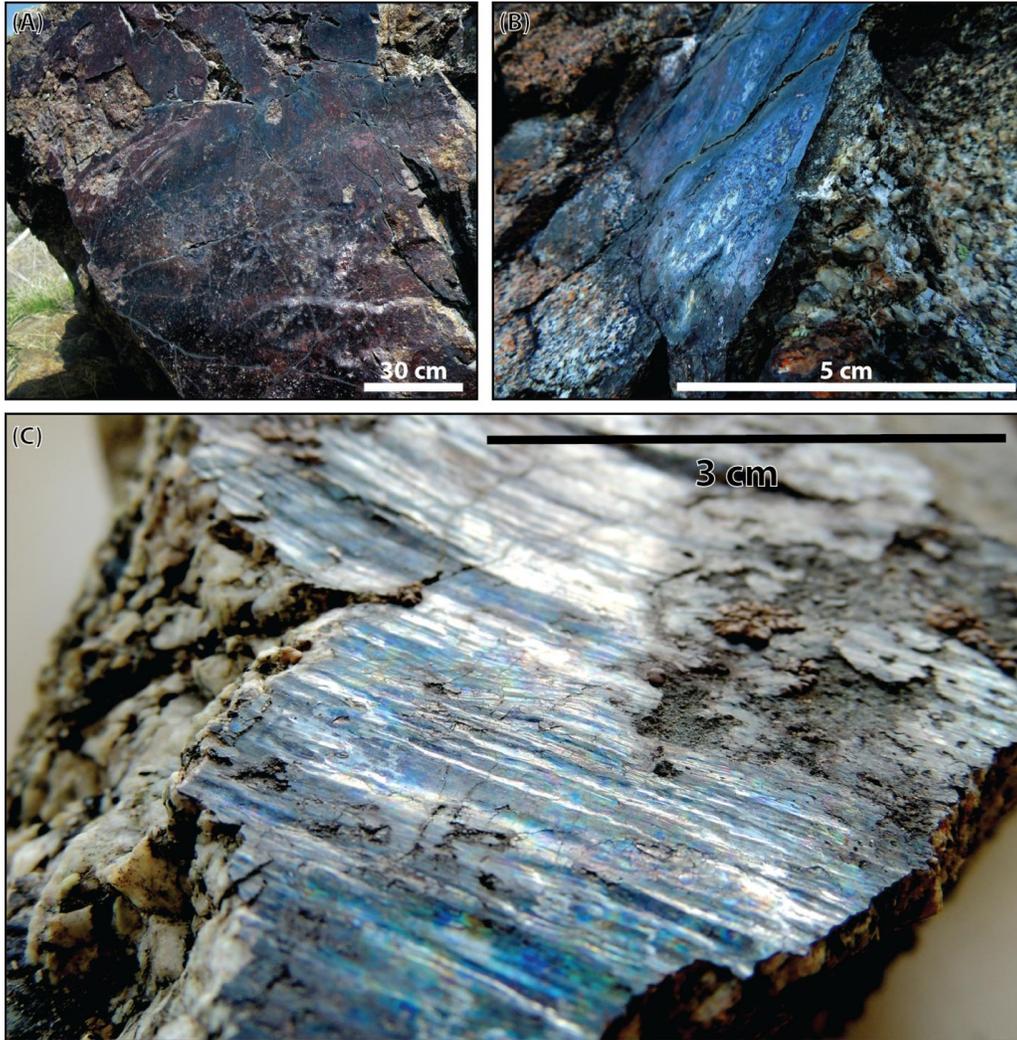
Figure 3-4: Field and hand sample photos of iridescent and metallic highly polished slip surfaces (HPSS) from the footwall damge zone of the Wasatch fault. (A) Field photograph of metallic-HPSS, slip surface contains several slickenside kinematic indicators. (B) Oblique field photo of blue-purple iridescent-metallic slip surface lacking short wave-length roughness or slickensides. (C) Oblique photo of iridescent-metallic HPSS with short wave-length slickensides.
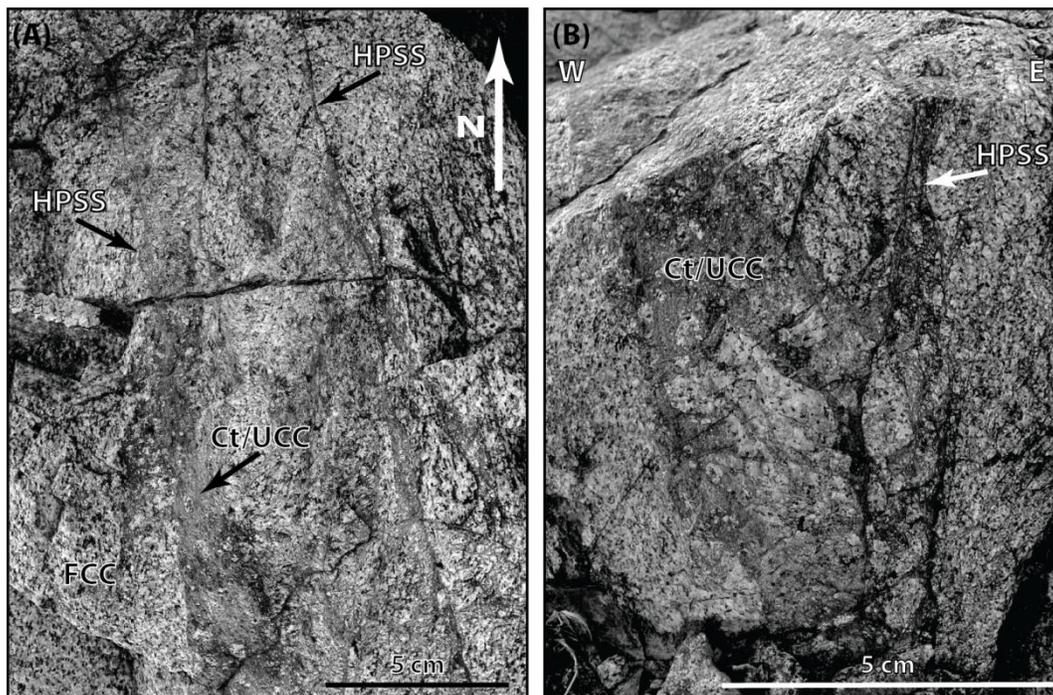
Figure 3-5: Field photographs of small fault in the footwall damage zone of the Wasatch fault in the Paleoproterozoic Farmington Canyon Complex (FCC) approximately 200 m from the main trace of the fault. A) Photograph looking down at approximately horizontal outcrop of parallel HPSS composed of hematite bounding cataclasite (Ct) and ultracataclasite (UCC). B) Photograph looking at vertical face (orthogonal to A); note the anastamosing hematite-rich HPSS bounding the fault core.
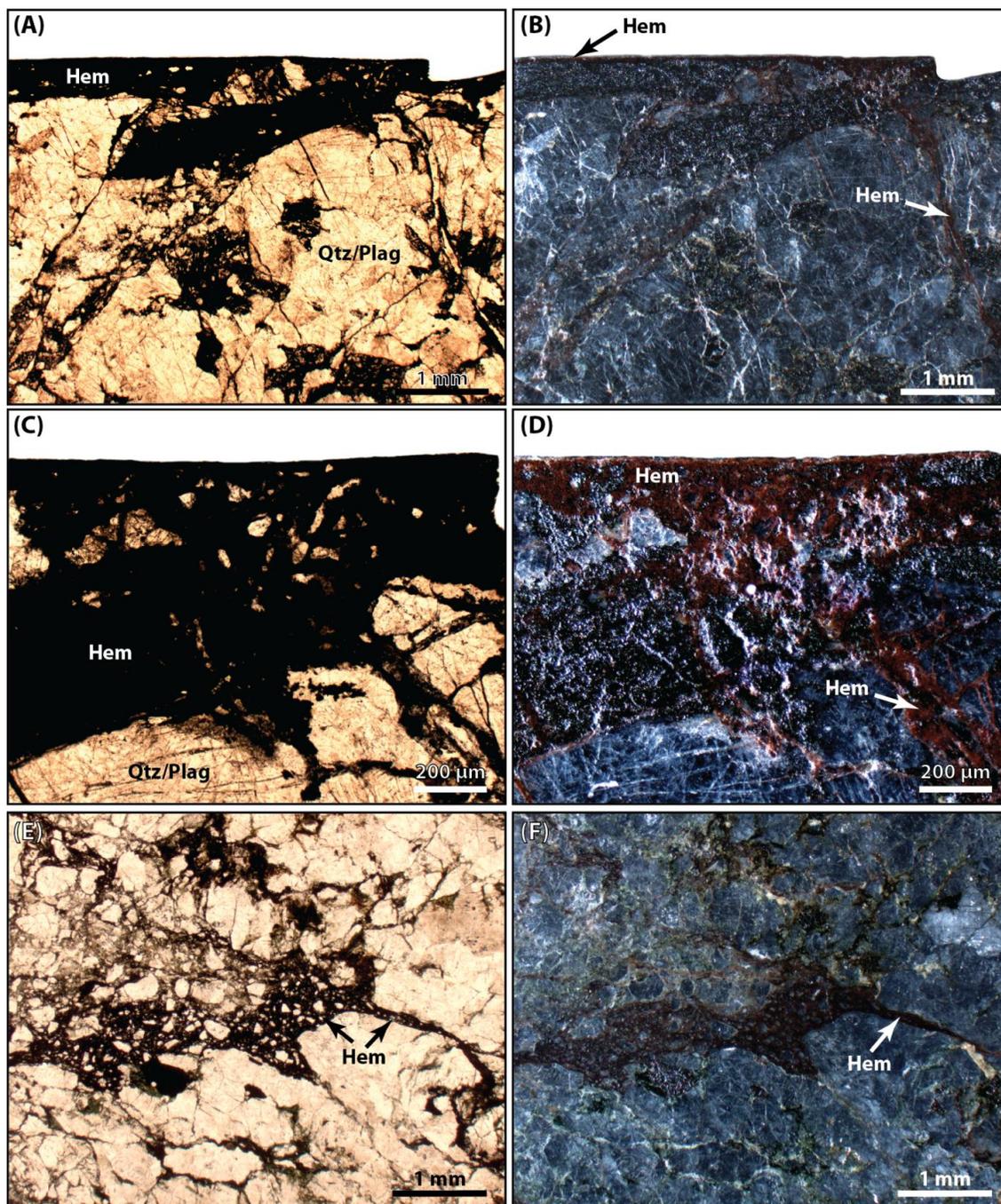
The most notable feature of the HPSS in meso- and micro-scales is the presence of rainbow iridescent zones (Fig. 3-4 B, C; Fig. 3-7). These zones of banded color < 0.5 mm to 23 mm wide range from orange, red, blue, green, to purple (Fig. 3-4 B, C; Fig. 3-7). Their shapes vary, from small elliptical spots several mm wide to zones that are distributed across the polished fault surfaces (Fig. 3-4 B, C; Fig. 3-7). The iridescent-surfaces are << 1 mm-thick.
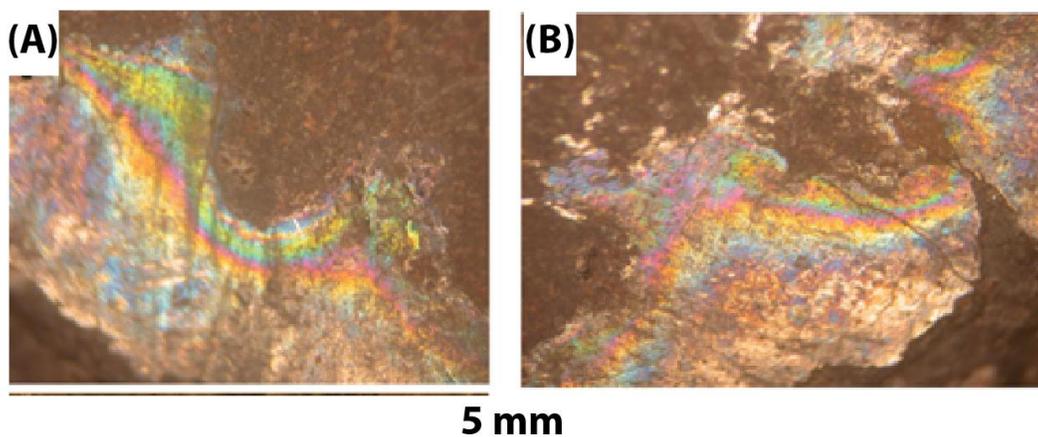
Figure 3-7: (A, B) Reflected light images of iridescent-metallic highly-polished slip surfaces. The bands of iridescence have been attributed to a very-thin layer of hematite.

X-ray diffraction analysis

Powdered samples of the iridescent-metallic highly polished slip surfaces and veins were analyzed using standard x-ray diffraction (XRD) methods. The iridescent-metallic HPSS were isolated from underlying cataclasites and injection veins by grinding the material from the surface with a Dremel tool. Small samples of the HPSS were also analyzed without removal from the underlying material and yield similar mineralogical

results (Supplemental Material). The iridescent and red (non-iridescent) fracture fill is composed of hematite, and some quartz (Fig. 3-8). The protolith is composed of quartz, albite, microcline, and minor amounts of hematite (Fig. 3-8).
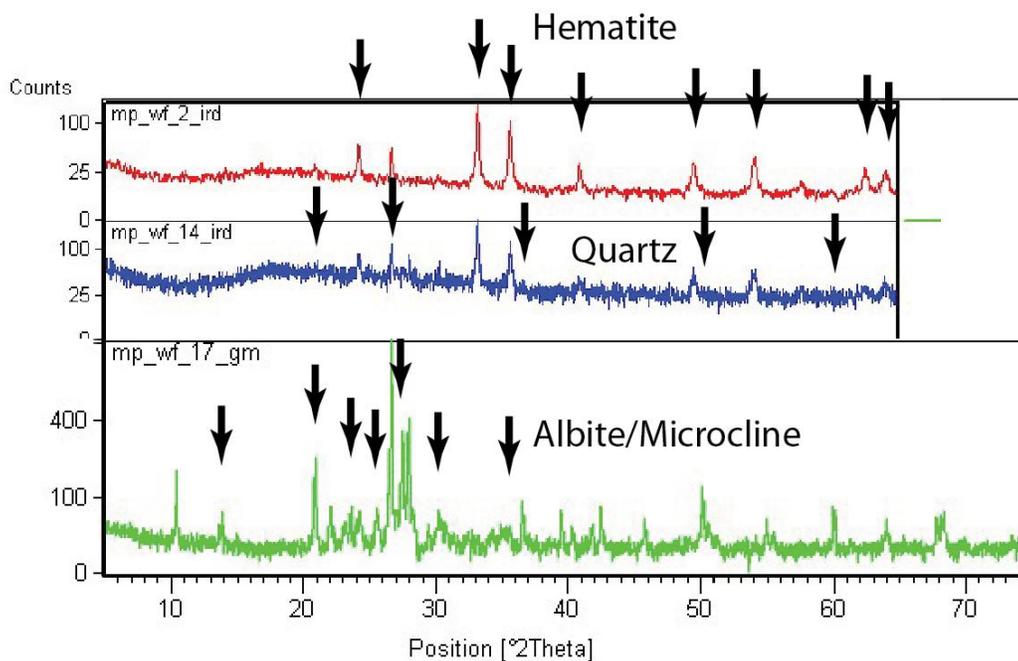
Figure 3-8: X-ray diffraction spectra of powdered material that comprises the iridescent-metallic HPSS (MP-WF-2-ird; MP-WF-14-ird) and protolith (MP-WF-17-gm). The iridescent samples are composed primarily of hematite and minor amounts of quartz, while the protolith is composed primarily of albite and microcline, with some quartz and trace amounts of biotite and chlorite (below the concentrations for detection via XRD).

X-ray Photoelectron spectroscopy results

X-ray photoelectron spectroscopy was used to characterize the composition of the HPSS. Iridencent samples are composed of cations associated with plagioclase and

biotite) (Ca, Al, Mg, Si) and high concentration of Fe and trace amounts of Ti (Fig. 3-9

A). We further split the Fe into Fe (III) and Fe (II) to estimate the relative percentages of

iron oxides that comprise the HPSS (Fig. 3-9 B). Using methods described in Biesinger et

al. (2011) the high-resolution XPS specra of the Fe peak were deconvoluted. Using peaks

from standards with know composition the percentage of Fe^{3+} from hematite (Fe_2O_3) and

magnetite (Fe_3O_4), and Fe^{2+} from magnetite (Fe_3O_4) (Fig. 3-9 B). These analyses indicate

the the iron oxide that comprises the HPSS is 69.5 % hematite and 30.5 % magnetite

(Fig. 3-9 B).

Petrography and SEM-EDS

Textural and compositional analyses at the microscale were conducted using

transmitted and reflected light thin-section petrography, and scanning electron

microscopy. These analyses were focused on fault-related textures and cataclastic

deformation associated with HPSS.

Thin section petrography

The HPSS are characterized by an opaque layer between 100 μm to 1 mm thick,

composed of hematite and sub-rounded to sub-angular quartz and feldspar clasts (Fig. 3-6

A-D). In transmitted light, quartz deformation in the protolith and in preserved clasts in

cataclasite and the HPSS material is manifested as undulose extinction, subgrains, and

grain-boundary bulging (Fig. 3-6 A, C, E). The protolith also contains plagioclase,

microcline, biotite, and chlorite. Evidence for cataclastic deformation is pervasive below

the HPSS and characterized by angular to sub-rounded quartz and feldspar clasts (Fig. 3-

6). In reflected light the HPSS are red and speckled with variable colors (Fig. 3-6 B, D,

F). Opaque veins in the groundmass below the HPSS are composed of hematite, have an

anastamosing texture, and may contain quartzofeldspathic clasts (Fig. 3-6 E, F). The

HPSS have very little relief (see discussion below) and are much more planar than

hematite veins in the protolith (Fig. 3-6).
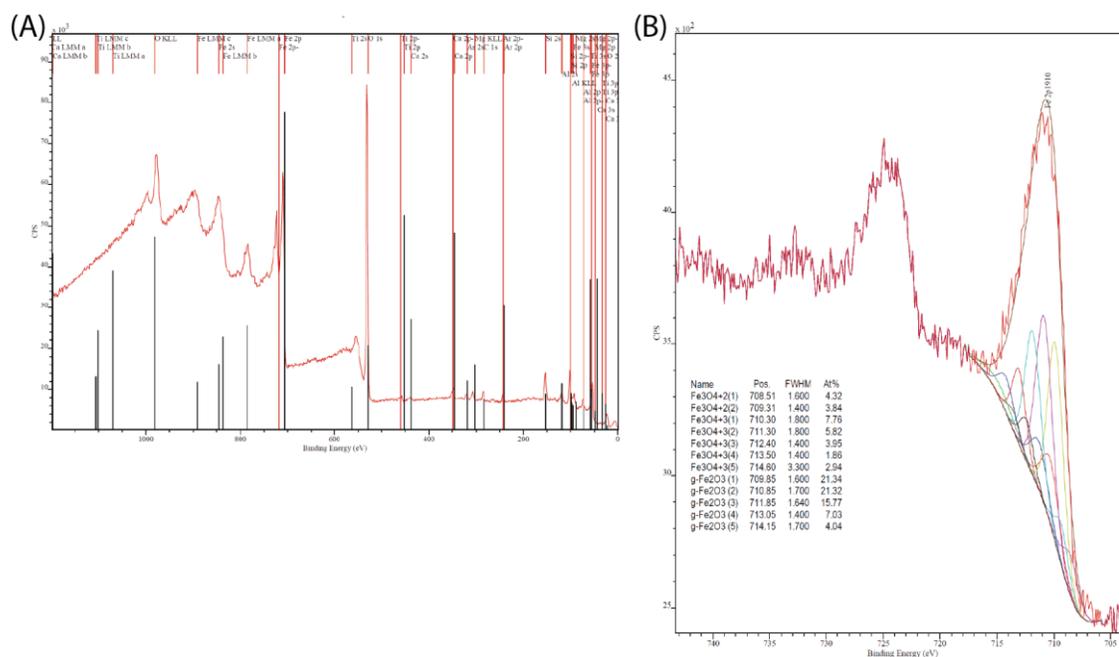
Figure 3-9: X-ray photoelectron spectroscectra of iridescent HPSS. A) Counts per second

(CPS) vs binding energy (eV) for general characterization of HPSS. The spectra are

dominated by O, Fe, Ca, Al, Si, Mg, and Ti. B) High resolution scan of Fe peak in the

XPS spectra from the HPSS used to estimate the oxidation state of Fe species in the

HPSS using methods described in Besinger et al. (2011).

Scanning Electron microscopy observations

Scanning electron microscopy (SEM) using back-scattered (BSE) and secondary electrons (SE) was carried out on samples parallel and perpendicular to the iridescent-metallic HPSS (Fig. 3-10). These analyses focused on describing the morphology, textures, and composition of the HPSS. Images parallel to the HPSS reveal multiple slip indicators on single surfaces that are nearly orthogonal to each other (Fig. 3-10 A). In cross-section, HPSS are underlain by very fine-grained (5-10 μm) tabular hematite and fine-grained quartz and feldspar grains (Fig. 3-10 C, D). The tabular hematite grains are randomly oriented, forming a framework of inter-grown hematite in most of the material that makes up the HPSS (Fig. 3-10 C, D). The hematite grains at the surface of the HPSS are oriented with the long axes parallel the margin, are typically < 5 μm-long, and have a less well defined tabular form (Fig. 3-10 C, D). The preferred orientation of the long-axis of tabular hematite grains parallel to the direction of slip suggests that grains were reoriented or recrystallized during slip (Fig. 3-10). This very-thin (< 3 μm) layer of slip-parallel hematite grains are likely to be responsible for the observed high-reflectivity and iridescence of the HPSS.

3D topography and roughness

We use three high-resolution surface metrology techniques to describe the topography of HPSS from the m- to μm-scale. The 3D point cloud data were used to construct digital elevation models of HPSS. The digital elevation models were then used

to extract 2D profiles perpendicular and parallel to the inferred direction of slip. Several methods have been used by other workers to quantify the roughness of synthetic and natural fault surfaces (Power et al., 1987, 1988; Power and Tullis, 1991; Renard et al., 2006, 2012; Sagy et al., 2007; Candela et al., 2009, 2011b; Sagy and Brodsky, 2009; Wei et al., 2010; Brodsky et al., 2011). We use root mean square (RMS) roughness (Table 3-1), to quantify the roughness of the iridescent-metallic HPSS (Power et al., 1988; Power and Tullis, 1991; Brown, 1995; Gadelmawla et al., 2002; Renard et al., 2006, 2012; Sagy et al., 2007; Candela et al., 2009, 2011b, 2012; Brodsky et al., 2011). The RMS roughness of 2D profiles is calculated from:

$$R_q = \sqrt{\frac{1}{l}\int_0^l \{y(x)\}^2 dx} \qquad (3\text{-}1)$$

where l is the total length of the profile, $y(x)$ is the height at point x above the mean surface, and x is the distance along the profile (Power et al., 1988; Power and Tullis, 1989, 1991; Gadelmawla et al., 2002). The RMS roughness is an effective tool to describe the roughness of relatively smooth manufactured surfaces and can be used to derive the Hurst exponent (H) which describes the fractal behavior of surface roughness (i.e self-similar or self-affine) (Gadelmawla et al., 2002; Wei et al., 2010; Webb et al., 2012)
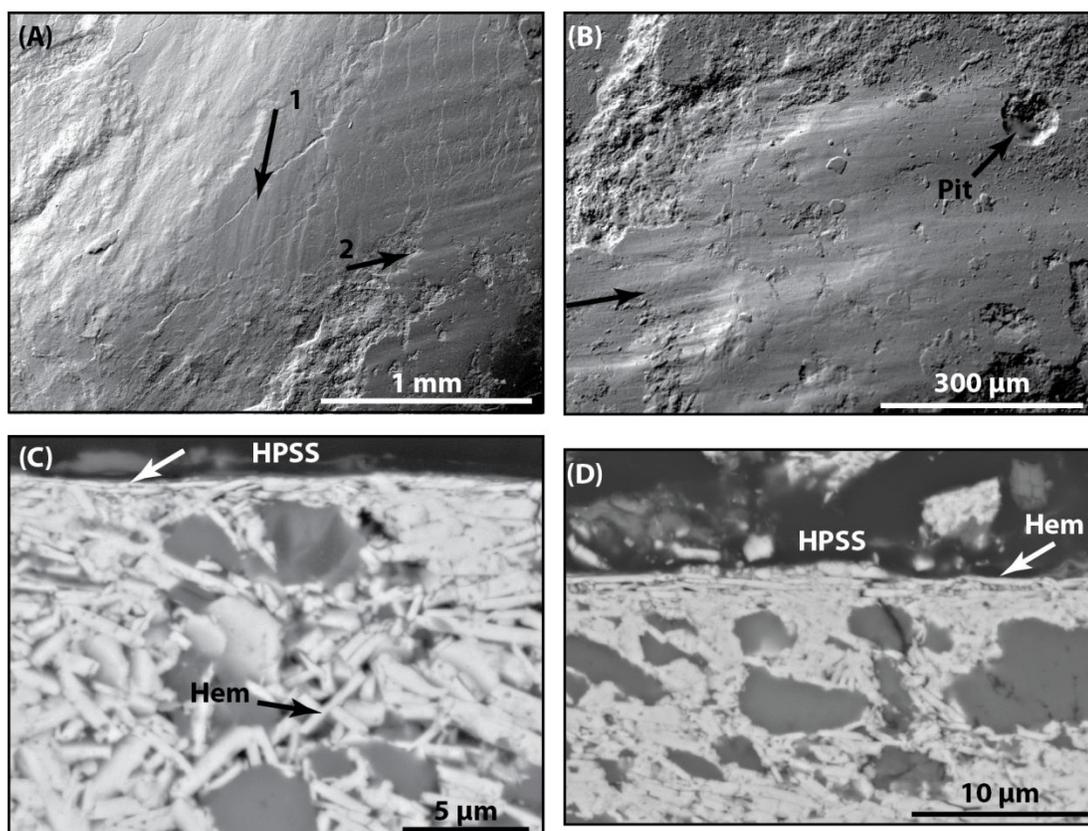
Figure 3-10: SEM-SEI and BSE images of iridescent-metallic highly-polished slip surfaces (HPSS) from the damage zone of the Wasatch fault. A) SEM-SEI image of HPSS in map view, complex surface topography and near orthogonal slip indicators (arrow 1 and 2) are clear. B) SEM-SEI image of HPSS in map view, the rough surface is striated by a single visible set of slickensides, a single circular pit is present on the surface. This pit may be analogous to similar structures observed during deformation of steel (Chen, 2010). C, D) SEM-BSE image of HPSS in cross-section, tabular hematite (Hem) grains are intergrown and randomly oriented in the fracture fill below the HPSS and Hem grains are oriented sub-parallel the the HPSS approaching the HPSS (white arrow).

$$R_q(x) \propto \Delta x^H \qquad (3\text{-}2)$$

RMS roughness, however, is limited because it is dependent on the length of the profile and reveals nothing about the roughness of surfaces at multiple wavelengths (Power et al., 1988; Power and Tullis, 1991; Brown, 1995; Candela et al., 2009).

: Table 3-1: Summary of RMS roughness data collected from HPSS parallel (RMS$_{pa}$) and perpendicular (RMS$_{pe}$). White light interferometer (WLI), laser scanner (LS), and Kinect.

	mean RMS$_{pa}$ (m)	S.D.	mean RMS$_{pa}$ Length (m)	mean RMS$_{pe}$ (m)	S.D.	mean RMS$_{pe}$ length (m)
WLI	1.40×10^{-6}	1.39×10^{-6}	4.70×10^{-4}	1.38×10^{-6}	9.09×10^{-7}	5.54×10^{-4}
LS	7.50×10^{-4}	3.85×10^{-4}	8.71×10^{-2}	2.02×10^{-3}	1.38×10^{-3}	8.94×10^{-2}
Kinect	3.16×10^{-3}	2.35×10^{-3}	4.32×10^{-1}	5.53×10^{-3}	3.02×10^{-3}	2.92×10^{-1}

The fractal behavior of signals that are self-affine remain unchanged by the transformation $\delta x \rightarrow \lambda\, \delta x$, $\delta y \rightarrow \lambda^H \delta z$, in which δx is the coordinate along the profile, δz is the roughness amplitude, and λ is the scaling factor (Meakin, 1998; Candela et al., 2009). This means that surfaces will appear rougher at finer scales of magnification (Candela et al., 2009; Power and Tullis, 1991; Renard et al., 2006; Sagy et al., 2007). The fractal behavior of most studied fault-surfaces has a strong roughness anisotropy in slip parallel and perpendicular directions and self-affinity (Power and Tullis, 1991; Schmittbuhl et al., 1993; Brown, 1995; Renard et al., 2006; Sagy et al., 2007; Candela et al., 2009, 2011b;

Brodsky et al., 2011). The following sections describe three methods used to characterize

the 3D topography of the HPSS and the results of RMS roughness analyses.

3D infrared range camera surface topography results

      The Windows Kinect™ was used as a high-accuracy (mm-scale), 3D range

camera to obtain fault topography data at the outcrop and for hand samples. The Kinect™

has been used to map 3D environments with centimeter- to millimeter-scale resolution in

indoor and outdoor environments (Khoshelham and Elberink, 2012; Mankoff and Russo,

2012; Smisek et al., 2013). High-density point cloud data were collected from multiple

HPSS in the damage zone of the Wasatch fault (Fig. 3-1, 3-11) (Supplemental Data). The

RMS roughness parallel to the inferred direction of slip varies from 6.9×10^{-4} m to 7.5×10^{-3} m and 8.1×10^{-4} m to 9.8×10^{-3} m perpendicular to slip (Table 3-1) (Supplemental Data).

Laser scan results

      Light Detection and Ranging (LiDAR) is a travel-time based 3D measurement

that is commonly used to generate point cloud data sets in the geologic sciences and fault

roughness studies (e.g. Bellian et al., 2005; Jones, 2006; Jones et al., 2009; Candela et al.,

2011; Bistacchi et al., 2011; Wilson et al., 2011). Here we employ a bench-top laser

metrology system that is similar to LiDAR to investigate the mm-scale topography of the

iridescent highly polished slip surfaces. The point cloud data sets we then used to

generate digital elevation models (DEMs) for roughness analysis (Fig. 3-12)

(Supplemental Data). Slip-parallel and slip-perpendicular profiles were extracted from

the DEMs and roughness parameters were calculated for these profiles (Fig. 3-12). The

A'

B'
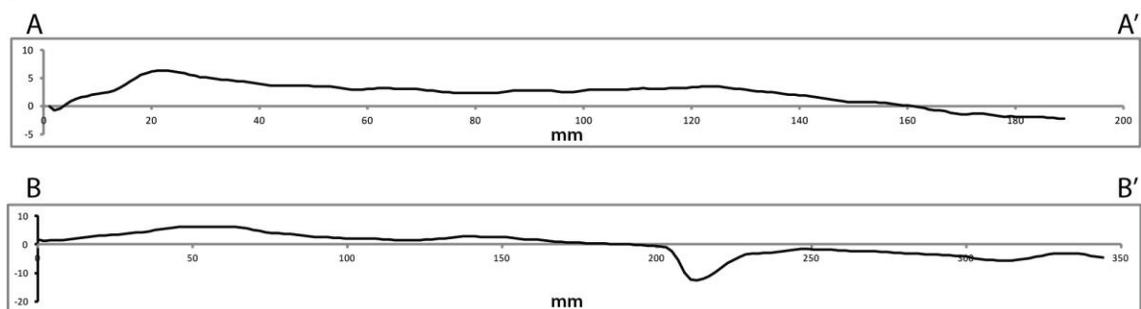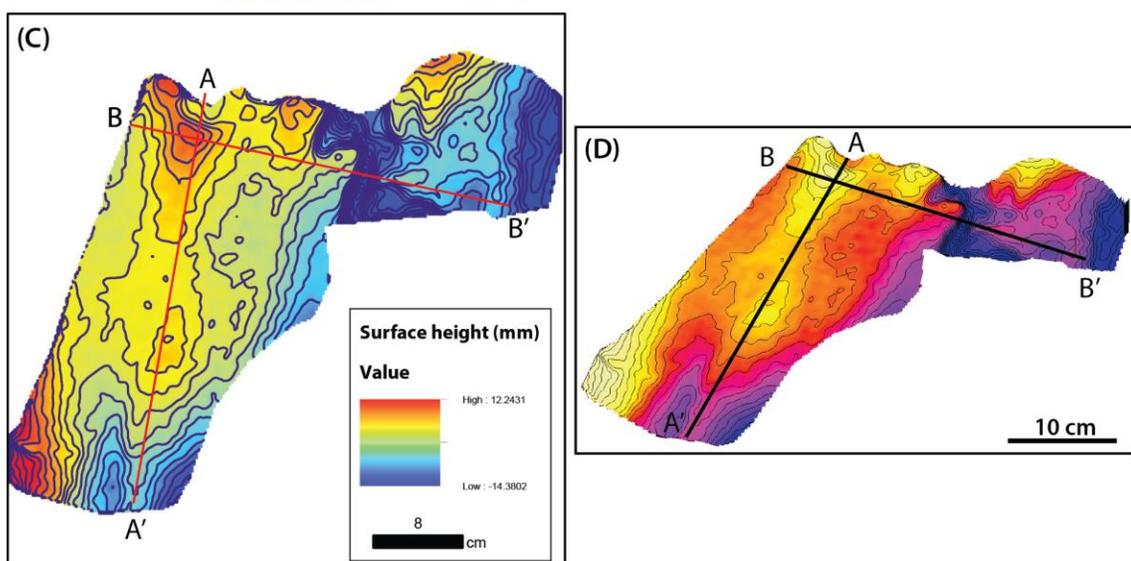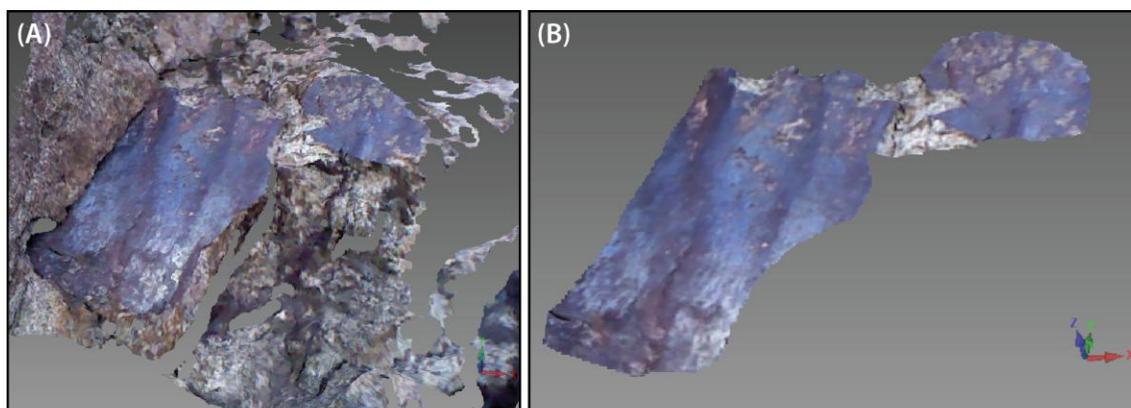
slip-parallel RMS roughness of HPSS varies from $1.3x10^{-4}$ m to $1.4x10^{-3}$ m and the slip

perpendicular RMS roughness varies from $1.1x10^{-4}$ m to $3.8x10^{-3}$ m (Table 3-1)

(Supplemental Data).

White-Light interferometry results

Understanding the 3D topography of fault surfaces at the microscale is a key

component in understanding the mechanical properties of faults, predicting weakening

and/or strengthening processes during slip, and estimating the temperature rise at seismic

slip rates (Scholz, 2002; Kanamori and Brodsky, 2004; Bjørnerud and Magloughlin,

2004; O'Hara, 2005; Rice, 2006). We use white-light interferometry (WLI) to examine

the micrometer-scale topography and roughness of the iridescent-metallic highly polished

slip surfaces (Fig. 3-13). Point cloud data collected by WLI were then used to extract 2D

profiles parallel and perpendicular to slip for roughness characterization (Fig. 3-13). The

RMS roughness of slip parallel profiles varies from $1.7x10^{-7}$ m to $5.4X10^{-6}$ m and $3.2x10^{-7}$ m to $3.2x10^{-6}$ m for slip perpendicular profiles (Table 3-1) (Supplemental Data).
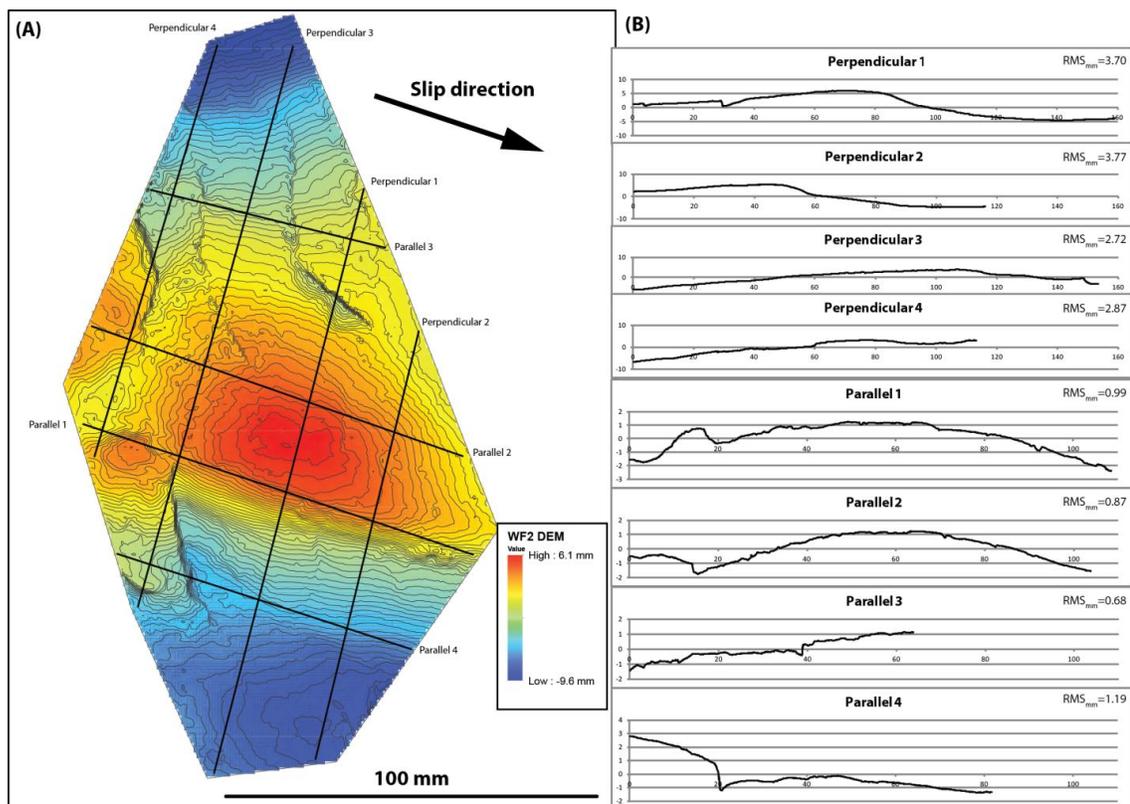
Figure 3-12: A) digital elevation model (DEM) of hand sample of iridescent-metallic

HPSS from the southern Brigham City segment of the Wasatch fault, interpolated from

point cloud data collected using a bench-top laser scanner (contour interval=0.25 mm). B)

2d profiles extracted from the DEM perpendicular and parallel to slip, RMS roughness

(mm) were calculated using equation 1.
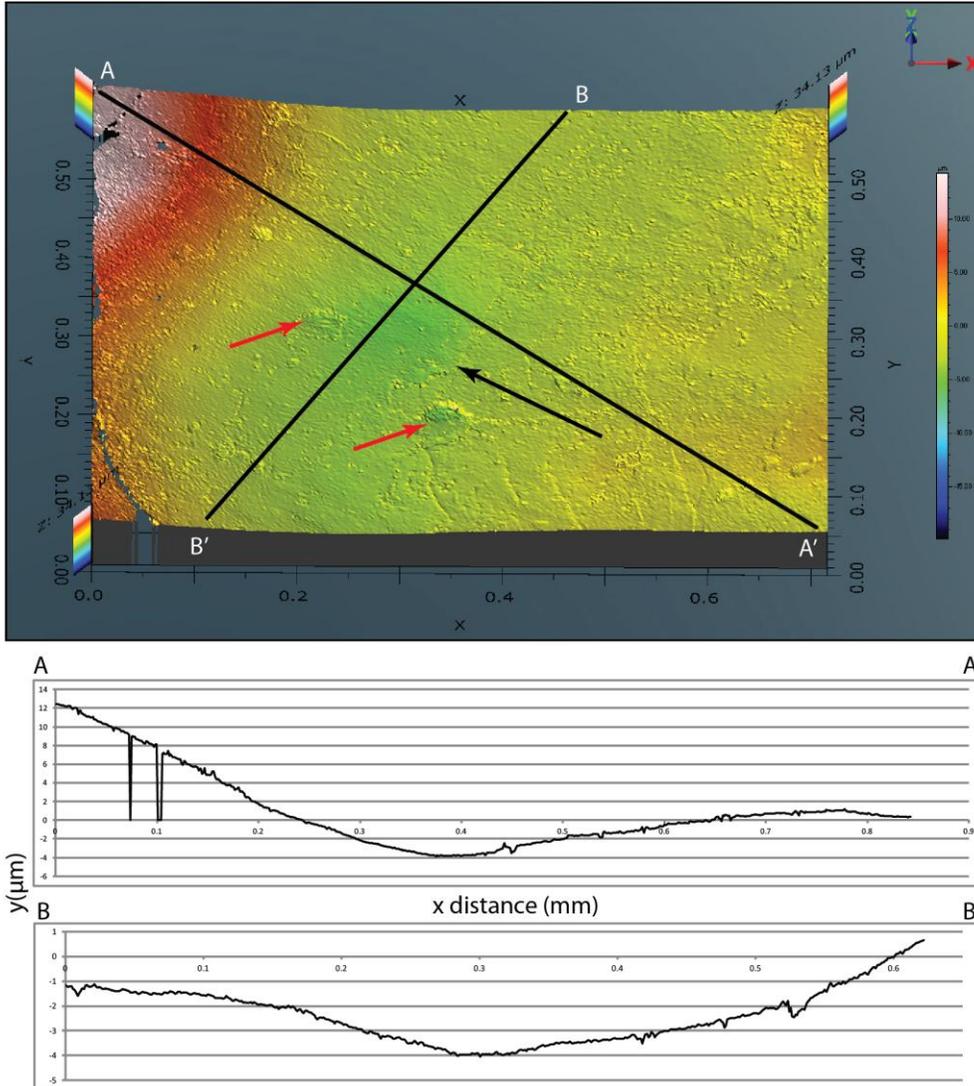
Figure 3-13: White-light interferometry digital elevation model of iridescent-metallic

HPSS and examples of slip parallel (A-A') and slip perpendicular (B-B') profiles

(vertically exaggerated). The direction of slip is inferred from the μm-scale striations

(black arrow). Erosion or possibly tool-marks are also preserved in the surface as small

(< 100 μm) diameter pits (red arrows). The small sample size (< 1mm^2) limits the

usefulness the roughness data to wave numbers less than the inverse profile length.

RMS Roughness analyses

The RMS roughness of multiple scans parallel and perpendicular to the inferred direction of slip provide overlapping results (Table 3-1). The RMS roughness of the HPSS analyses over four orders of magnitude define a power law relationship when plotted on a log-log plot (Fig. 3-14). This observation that with increased scales of observation the RMS roughness of profiles increases is expected (Power and Tullis, 1991; Schmittbuhl et al., 1993; Brown, 1995; Renard et al., 2006; Sagy et al., 2007; Candela et al., 2009, 2011b; Brodsky et al., 2011). The Hurst exponent of 1.17 for slip parallel data and 1.35 for slip perpendicular data was estimated using the best-fit line to the data (Equation 3-2) (Fig. 3-14). These values are greater than Hurst exponents that characterize self-affine surfaces ($0 \leq H \leq 1$), typical of most reported faults which apprear more rough at fine-scales (Power et al., 1988; Candela et al., 2009; Siman-Tov et al., 2013; Wei et al., 2010). The HPSS have a self-similar fractal behavior ($H > 1$), meaning they appear equally smooth at all scales of observation (Fig. 3-13) (Meakin, 1998; Candela et al., 2009).

Discussion

The compositional, textural, crystallinity, and roughness data collected in this study have been used to test the origin of highly polished slip surfaces exposed in the footwall of the Wasatch fault. The hematite-rich HPSS are unambiguously related to fault-related slip, based on the presence of kinematic indicators (slickensides), cataclastic fabrics, and the low RMS-roughness (Fig. 3-4; Fig; 3-6; Fig. 3-8; Fig. 3-14). The
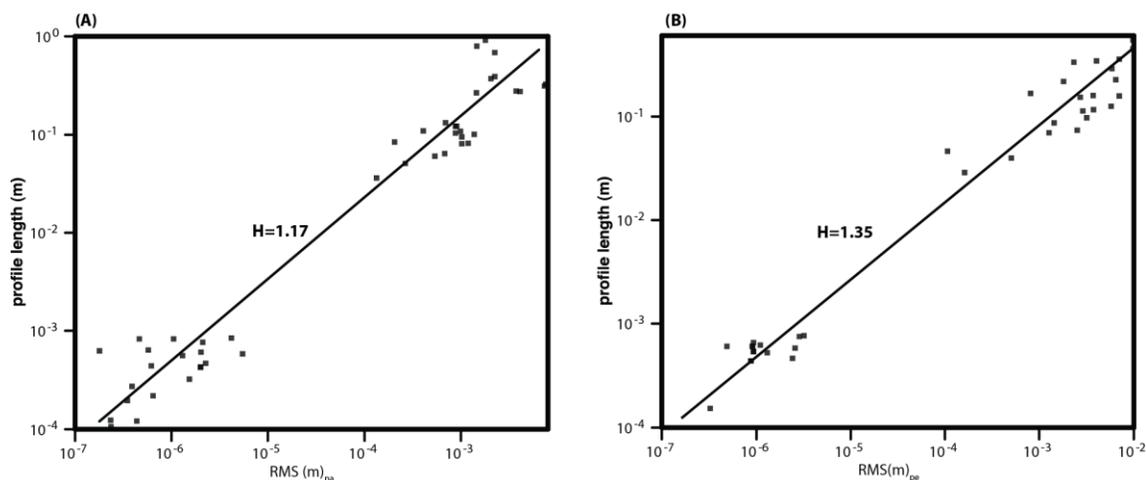
Figure 3-14: Log-log plots of RMS-roughness of individual 2D profiles as a function of profile length. 2D profiles were extracted from point cloud data sets collected over four orders of magnitude. Power law relationship defines the distribution of the RMS-roughness (equation 2) and the Hurst exponent for slip-parallel (A) and slip-perpendicular (B) profiles.

following discussion is focused on the origin of the hematite-rich HPSS and how this relates to the seismic-cycle and the dissipation of co-seismic energy.

Origin of hematite-rich HPSS

The origin of hematite along the extremely smooth and fine-grained iridescent HPSS can be explained in several ways. It is possible that HPSS formed along pre-existing hematite veins present in the Farmington Canyon Complex (Fig. 3-5; Fig. 3-6) (Evans and Langrock, 1994). This hypothesis suggests that the extent and orientation of the iridescent-metallic HPSS should be controlled by the distribution of the preexisting hematite veins, and that these veins were refined (smoothed) and material was

redistributed during slip along these planes. This hypothesis predicts that the HPSS

should contain evidence for comminution and reworking of the hematite that makes up

the HPSS. However, hematite from the HPSS is not highly comminuted or fractured

based on observation from SEM-BSE images (Fig. 3-10). Alternatively, the hematite

comprising the HPSS may be related to high-temperature oxidation and shearing of the

host-rock. The documentation of hematite (Fe_2O_3) and magnetite (Fe_3O_4) along the HPSS

suggests temperatures > 300 ˚C (Wisniewski et al., 2011). Noda et al. (2011) document

the development of hematite- and magnetite- rich surfaces at high-temperature (> 800 ˚C)

at constant slip-rates (0.01 m s^{-1}) and normal stress (1 MPa) at vairiable

temperatures.Therefore, the resulting changes in deformation and coefficient of friction

were the result of temperature controlled reactions (Noda et al., 2011). The material used

in the experiments was dolerite, composed of plagioclase (44%), clinopyroxene (28%),

hornblende (9%), and minor amounts of quartz, K-feldspar, orthopyroxene, biotite,

apatite, and opaque minerals (Noda et al., 2011). The increased hematite and magnetite

content at temperatures > 800 ˚C is attributed to the decomposition of clinopyroxene and

other mafic minerals via oxidation reactions (Noda et al., 2011). Noda et al. (2011) also

note the development of an amorphous phase with a broad XRD peak from 2θ 20-35˚;

associated with gouge produced at temperatures below 400˚C. This broad peak is

associated with amorphous hematite and rapidly quenched iron-rich ceramics (Noda et

al., 2011; Wisniewski et al., 2011). Samples deformed or annealed at higher temperatures

lack this broad peak and are composed of coarser-grained hematite similar to samples of

the iridescent-metallic HPSS (Noda et al., 2011; Wisniewski et al., 2011). Similar

mirror-like fault surfaces have been generated in laboratory rotary shear experiments at

seismic slip rates and high temperatures (Han et al., 2007, 2011). These experiments

were performed with siderite gouge at slip-rates between 1.3-2.0 m s^{-1}, the resulting

mirror-like striated surfaces have been attributed to thermal decomposition of the siderite

($FeCO_3$) and the generation of magnetite (Fe_3O_4) (Han et al., 2007). The similarity in

composition, crystallinity, and morphology of the iridescent-metallic HPSS exposed in

the footwall of the Wasatch fault suggests that similar thermal decomposition during

seismicity is responsible for the generation of these surfaces.

Experimental production of iridescence

Hematite and magnetite-coated surfaces have been generated in rotary shear

experiments at seismic slip rates and temperatures expected during seismicity using

geologic and synthetic material (Chen, 2010; Noda et al., 2011). Chen (2010) documents

the development of extremely thin (200-500 nm) iridescent-hematite films along steel

during sliding. The iron-oxide films may be the result of oxidation of very thin Fe_2O_3

surfaces at high temperatures (> 300 ˚C) (Haosheng and Jiang, 2009; Chen, 2010). In the

case of the steel examples the high-temperatures are concentrated around expanding gas-

bubbles at the contact between sliding surfaces (Haosheng and Jiang, 2009; Chen, 2010).

Similar mirror-like fault surfaces have been identified in laboratory rotary shear

experiments at seismic slip rates and high temperatures, and similar thin-films of

iridescent-Fe_2O_3 are associated with high temperature wear of steel (Han et al., 2007, 2011; Haosheng and Jiang, 2009; Chen, 2010).

HPSS topography and roughness

The cm- to μm-scale topography of the iridescent-metallic HPSS was measured using three methods (see discussion above). Point cloud data from these methods were then used to generate digital elevation models and 2D profiles were extracted from these models for roughness analyses (Fig. 3-11; Fig. 3-12; Fig. 3-13). The Hurst exponent for the iridescent-metallic HPSS is greater than those for self-affine faults described by other workers (Power and Tullis, 1991; Renard et al., 2006; Candela et al., 2009; Brodsky et al., 2011); instead the HPSS display a self-similar fractal behavior (Fig. 3-14). This self-similar fractal behavior describes the scaling properties of roughness from the cm- to μm-scales, indicating that the HPSS are equally rough at all the scales observed by the methods used here. The slip-parallel and slip-perpendicular roughness anisotropy documented by other studies is not as clear in the iridescent-metallic HPSS (Table 3-1) (Power et al., 1988; Power and Tullis, 1991; Renard et al., 2006; Sagy et al., 2007; Sagy and Brodsky, 2009; Candela et al., 2009, 2011b, 2012; Brodsky et al., 2011). This is consistent with descriptions of other HPSS that may be related to seismic-slip, where the slip perpendicular and parallel roughness are similar and fractal scaling behavior is similar (Siman-Tov et al., 2013).

In addition to the roughness analysis, SEM images indicate that single slip-surfaces preserve evidence for multiple directions at high-angles (Fig. 3-10). The

observation that a single slip surface can contain multiple slip indicators is consistent

with the conclusion from other studies that slip-surfaces accommodate deformation

through multiple earthquake cycles (Chester and Chester, 1998; Evans and Chester, 1995;

Sibson, 2003; and many others). Alternatively, the presence of multiple slip-indicators is

also consistent with a more complex slip-path during individual earthquakes in the

footwall of the Wasatch fault at this site. Because these possibilities have similar

expected deformation (i.e. overlapping slip-indicators, and cataclasis) it is difficult to

distinguish between the two hypotheses.

We interpret the observed variability in roughness, and crystallinity of the

iridescent-metallic highly polished slip surfaces to be the result of refinement

(smoothness) and development of iridescence during seismic slip (Fig. 3-15). With

increased culumative slip by descrete seismic slip events the HPSS become more planar,

which is consistent with conclusions from other studies focused on the relationship

between fault roughness and cumulative slip (Han et al., 2007; Sagy et al., 2007; Brodsky

et al., 2011; Candela et al., 2011b). The decreased roughness with slip also has

implications for the generation of heat during seismicity. With decreased RMS roughness

the contact area between opposing fault surfaces increases. This increased contact area is

expected to result in the generation of higher temperatures during flash heating at

asperities, estimated by (Archard, 1959; O'Hara, 2005):

$$\Delta T = 0.345 \frac{\mu \pi p_m}{\rho C_p} \sqrt{\frac{aV}{2k/\rho C_p}} \tag{5}$$

where the change in temperature (ΔT) is a function of the coefficient of friction (μ),

density (ρ), heat capacity (C_p), compressive yield strength (p_m), the asperity contact

radius (a), slip rate (V), and thermal conductivity (k). Using typical material properties for

geologic materials (Spray, 1992, 2010; O'Hara, 2005), asperities with contact radii > 10

μm are expected to generate temperatures between 500-1000 ˚C (O'Hara, 2005). We

therefore consider the high temperatures required for the generation of iridescent,

hematite-rich slip surfaces (> 400 ˚C) to be at seismic slip rates.

Conclusions

We document fault-related deformation linked to seismic slip along a portion of

the seismically active Wasatch fault. The features documented here require a rationale for

anomalously high temperature conditions, elevated pressure conditions, or high strain

rates (Cowan, 1999; Marone and Richardson, 2010; Boutareaud et al., 2010; Siman-Tov

et al., 2013; Smith et al., 2013). Highly-polished slip surfaces are a proposed indicator of

ancient seismicity by several workers in multiple tectonic settings and rock types (Power

and Tullis, 1991; Smith et al., 2013; Siman-Tov et al., 2013). Here we propose a link

between iridescent-metallic highly polished slip surfaces and co-seismic slip rates. The

development of very-thin, hematite-rich, and anomalously smooth surfaces in the damage

zone of the Wasatch fault are the result of slip at co-seismic rates. The very-thin (< 10

μm) and iridescent-hematite HPSS formed at temperatures between 400-1000 ˚C (Chen,

2010; Noda et al., 2011). These high temperatures and the very isolated nature of the

deformation is only reasonably explain by flash heating during ancient seismicity in the

(A)

5 cm

(B)

**Seismic Slip
(0.1-1.0 m/s)**

(C)

(D)

5 cm

(E)

300 ˚C   1000 ˚C

(F)
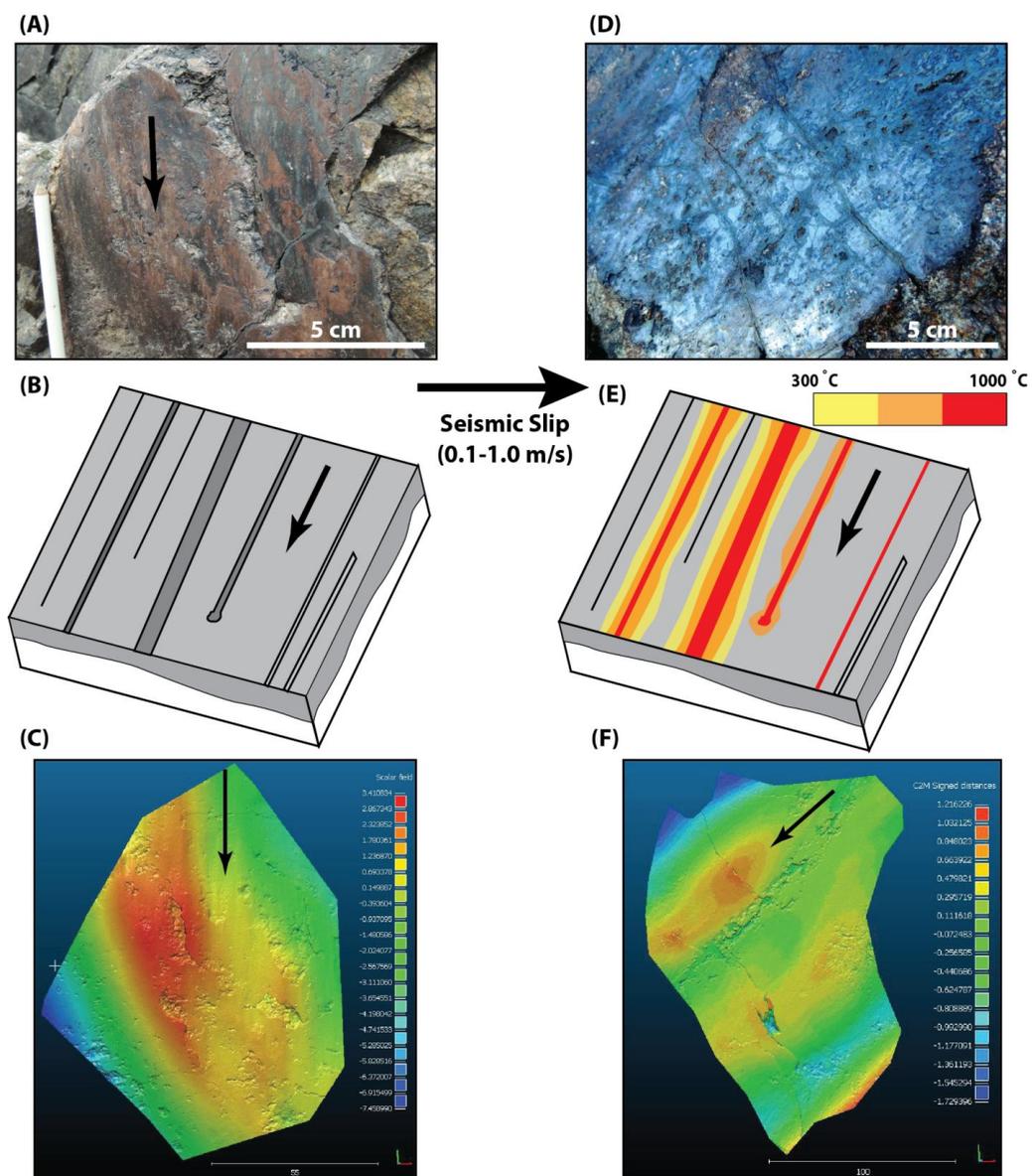
fault zone (McKenzie and Brune, 1972; Scholz, 1980; Kanamori and Brodsky, 2004; O'Hara, 2005; Rice, 2006; Rempel and Weaver, 2008). This conclusion suggests that the iridescence associated with the HPSS is a new and reliable indicator of ancient seismicity in exhumed fault zones.

The relatively wide-spread distribution (10s m) of iridescent-metallic HPSS in the damage zone of the southern end of the Brigham City segment of the Wasatch fault suggests that much of the co-seismic slip and deformation was distributed over the structurally complex damage zone (Evans and Langrock, 1994). This wide distribution of seismic slip associated with this structurally complex segment boundary is expected if mesoscopic asperities or fault zone complexity can act as an impediment for the transfer of a rupture between segments of the fault (Aki, 1984; Voisin et al., 2002; Peyrat et al., 2004). Paleoseismologic investigations of the Wasatch fault suggest that several recent earthquakes are common to multiple segments of the fault (DuRoss, 2008; DuRoss et al., 2012). An alternative hypothesis is that the distribution of iridescent-metallic HPSS reflects the distribution of aftershocks in the footwall damage zone of the Wasatch fault. The distribution of aftershocks associated with large magnitude earthquakes often defines a wide zone around the epicenter of the main slip event (Mendoza and Hartzell, 1988; Scholz, 2002).

The iridescent-metallic highly polished slip surfaces exposed in the footwall of the Brigham City Segment of the Wasatch fault represent a previously undocumented and convincing indicator of ancient seismicity. The anomalously high temperatures (> 400

˚C) required to generate the iridescent-metallic HPSS are easily explained by flash heating during seismic slip (Scholz, 1980; O'Hara, 2005; Rice, 2006; Rempel and Weaver, 2008).

References

Aki, K., 1984. Asperities, barriers, characteristic earthquakes and strong motion prediction. Journal of Geophysical Research: Solid Earth 89, 5867–5872.

Archard, J.F., 1959. The temperature of rubbing surfaces. Wear 2, 438–455.

Armstrong, P.A., Ehlers, T.A., Chapman, D.S., Farley, K.A., Kamp, P.J.J., 2003. Exhumation of the central Wasatch Mountains, Utah: 1. Patterns and timing of exhumation deduced from low-temperature thermochronology data. Journal of Geophysical Research: Solid Earth 108. doi:10.1029/2001JB001708

Armstrong, P.A., Taylor, A.R., Ehlers, T.A., 2004. Is the Wasatch fault footwall (Utah, United States) segmented over million-year time scales? Geology 32, 385. doi: 10.1130/G20421.1

Bellian, J.A., Kerans, C., Jennette, D.C., 2005. Digital Outcrop Models: Applications of Terrestrial Scanning Lidar Technology in Stratigraphic Modeling. Journal of Sedimentary Research 75, 166–176. doi: 10.2110/jsr.2005.013

Biesinger, M.C., Payne, B.P., Grosvenor, A.P., Lau, L.W.M., Gerson, A.R., Smart, R.S.C., 2011. Resolving surface chemical states in XPS analysis of first row transition metals, oxides and hydroxides: Cr, Mn, Fe, Co and Ni. Applied Surface Science 257, 2717–2730. doi: 10.1016/j.apsusc.2010.10.051

Bistacchi, A., Griffith, W.A., Smith, S.A.F., Toro, G.D., Jones, R., Nielsen, S., 2011. Fault Roughness at Seismogenic Depths from LIDAR and Photogrammetric Analysis. Pure and Applied Geophysics 168, 2345–2363. doi: 10.1007/s00024-011-0301-7

Bjarnason, I.T., Pechmann, J.C., 1989. Contemporary tectonics of the Wasatch front region, Utah, from earthquake focal mechanisms. Bulletin of the Seismologic. Society of America 79, 731–755.

Bjørnerud, M., 2010. Rethinking conditions necessary for pseudotachylyte formation: Observations from the Otago schists, South Island, New Zealand. Tectonophysics 490, 69–80. doi: 10.1016/j.tecto.2010.04.028.

Bjørnerud, M., Magloughlin, J.F., 2004. Pressure-related feedback processes in the generation of pseudotachylytes. Journal of Structural Geology 26, 2317–2323. doi: 10.1016/j.jsg.2002.08.001.

Boutareaud, S., Boullier, A.-M., Andréani, M., Calugaru, D.-G., Beck, P., Song, S.-R., Shimamoto, T., 2010. Clay clast aggregates in gouges: New textural evidence for seismic faulting. Journal of Geophysical Research 115. doi: 10.1029/2008JB006254.

Brodsky, E.E., Gilchrist, J.J., Sagy, A., Collettini, C., 2011. Faults smooth gradually as a function of slip. Earth and Planetary Science Letters 302, 185–193. doi: 10.1016/j.epsl.2010.12.010.

Brown, S.R., 1995. Simple mathematical model of a rough fracture. Journal of Geophysical Research Solid Earth 100, 5941–5952. doi: 10.1029/94JB03262

Bryant, B., 1988. Geology of the Farmington Canyon Complex, Wasatch Mountains, Utah, U.S. Geological Survey Professional paper 1476. United States Geological Survey, Reston, Va.

Caine, J.S., Bruhn, R.L., Forster, C.B., 2010. Internal structure, fault rocks, and inferences regarding deformation, fluid flow, and mineralization in the seismogenic Stillwater normal fault, Dixie Valley, Nevada. Journal of Structural Geology 32, 1576–1589. doi: 10.1016/j.jsg.2010.03.004.

Candela, T., Renard, F., 2012. Segment linkage process at the origin of slip surface roughness: Evidence from the Dixie Valley fault. Journal of Structural Geology 45, 87–100. doi: 10.1016/j.jsg.2012.06.003.

Candela, T., Renard, F., Bouchon, M., Brouste, A., Marsan, D., Schmittbuhl, J., Voisin, C., 2009. Characterization of Fault Roughness at Various Scales: Implications of Three-Dimensional High Resolution Topography Measurements. Pure and Applied Geophysics 166, 1817–1851. doi: 10.1007/s00024-009-0521-2.

Candela, T., Renard, F., Bouchon, M., Schmittbuhl, J., Brodsky, E.E., 2011a. Stress Drop during Earthquakes: Effect of Fault Roughness Scaling. Bulletin of the Seismological Society of America 101, 2369–2387. doi: 10.1785/0120100298.

Candela, T., Renard, F., Klinger, Y., Mair, K., Schmittbuhl, J., Brodsky, E.E., 2012. Roughness of fault surfaces over nine decades of length scales. Journal of Geophysical Research: Solid Earth 117. doi: 10.1029/2011JB009041.

Candela, T., Renard, F., Schmittbuhl, J., Bouchon, M., Brodsky, E.E., 2011b. Fault slip distribution and fault roughness. Geophysical Journal International 187, 959–968. doi: 10.1111/j.1365-246X.2011.05189.x.

Chen, H., 2010. Iridescent rings around cavitation erosion pits on surface of mild carbon steel. Wear 269, 602–606. doi: 10.1016/j.wear.2010.06.007.

Chester, F.M., Chester, J.S., 1998. Ultracataclasite structure and friction processes of the Punchbowl fault, San Andreas system, California. Tectonophysics 295, 199–221. doi: 10.1016/S0040-1951(98)00121-8.

Cowan, D.S., 1999. Do faults preserve a record of seismic slip? A field geologist's opinion. Journal of Structural Geology 21, 995–1001. doi: 10.1016/S0191-8141(99)00046-2.

Crittenden, M.D., Sorensen, M.L., 1985. Geologic map of the Mantua quadrangle and part of the Willard quadrangle, Box Elder,Weber, and Cache Counties, Utah. U.S. Geological Survey Miscellaneous Investigations Series I-1605.

DeCelles, P.G., Giles, K.A., 1996. Foreland basin systems. Basin Research 8, 105–123. doi: 10.1046/j.1365-2117.1996.01491.x.

DeCelles, P.G., and Coogan, J.C., 2006, Regional structure and kinematic history of the Sevier fold-and-thrust belt, central Utah: Geological Society of America Bulletin, v. 118, p. 841–864, doi: 10.1130/B25759.1.

Di Toro, G., Nielsen, S., Pennacchioni, G., 2005. Earthquake rupture dynamics frozen in exhumed ancient faults. Nature 436, 1009–1012. doi: 10.1038/nature03910.

Doblas, M., 1998. Slickenside kinematic indicators. Tectonophysics 295, 187–197. doi: 10.1016/S0040-1951(98)00120-6.

DuRoss, C.B., 2008. Holocene Vertical Displacement on the Central Segments of the Wasatch Fault Zone, Utah. Bulletin of the Seismological Society of America 98, 2918–2933. doi: 10.1785/0120080119.

DuRoss, C.B., Personius, S.F., Crone, A.J., McDonald, G.N., Briggs, R.W., Utah Geological Survey, 2012. Late Holocene earthquake history of the Brigham City segment of the Wasatch Fault zone at the Hansen Canyon, Kotter Canyon, and

Pearsons Canyon trench sites, Box Elder County, Utah, Special Study 142. Utah Geological Survey, Salt Lake City, Utah.

Ehlers, T.A., Willett, S.D., Armstrong, P.A., Chapman, D.S., 2003. Exhumation of the central Wasatch Mountains, Utah: 2. Thermokinematic model of exhumation, erosion, and thermochronometer interpretation. Journal of Geophysical Research: Solid Earth 108. doi: 10.1029/2001JB001723.

Engelder, J.T., 1974. Microscopic wear grooves on slickensides: Indicators of paleoseismicity. Journal of Geophysical Research 79, 4387–4392. doi: 10.1029/JB079i029p04387.

Engelder, T., 1978. Aspects of asperity-surface interaction and surface damage of rocks during experimental frictional sliding. Pure and Applied Geophysics 116, 705–716. doi: 10.1007/BF00876533.

Evans, J.P., Chester, F.M., 1995. Fluid-rock interaction in faults of the San Andreas system: Inferences from San Gabriel fault rock geochemistry and microstructures. Journal of Geophysical Research: Solid Earth 100, 13007–13020. doi: 10.1029/94JB02625.

Evans, J.P., Langrock, H., 1994. Structural analysis of the Brigham City-Weber segment boundary zone, Wasatch normal fault, Utah: implications for fault growth and structure. Pageoph 142, 663–685.

Friedman, M., Logan, J.M., Rigert, J.A., 1974. Glass-Indurated Quartz Gouge in Sliding-Friction Experiments on Sandstone. Geological Society of America Bulletin 85, 937–942. doi: 10.1130/0016-7606(1974)85<937:GQGISE>2.0.CO;2.

Friedrich, A.M., Wernicke, B.P., Niemi, N.A., Bennett, R.A., Davis, J.L., 2003. Comparison of geodetic and geologic data from the Wasatch region, Utah, and implications for the spectral character of Earth deformation at periods of 10 to 10 million years. Journal of Geophysical Research: Solid Earth 108. doi: 10.1029/2001JB000682.

Gadelmawla, E.S., Koura, M.M., Maksoud, T.M.A., Elewa, I.M., Soliman, H.H., 2002. Roughness parameters. Journal of Materials Processing Technology 123, 133–145. doi: 10.1016/S0924-0136(02)00060-2.

Giaccio, B., Galadini, F., Sposato, A., Messina, P., Moro, M., Zreda, M., Cittadini, A., Salvi, S., Todero, A., 2003. Image processing and roughness analysis of exposed bedrock fault planes as a tool for paleoseismological analysis: results from the

Campo Felice fault (central Apennines, Italy). Geomorphology 49, 281–301. doi: 10.1016/S0169-555X(02)00191-5.

Gilbert, G.K., 1928. Studies of Basin-range structure, U.S. Geological Survey Professional paper 153. U.S. Govt. Print. Off, Washington.

Gonzalez-Jorge, H., Riveiro, B., Vazquez-Fernandez, E., Martínez-Sánchez, J., Arias, P., 2013. Metrological evaluation of Microsoft Kinect and Asus Xtion sensors. Measurement 46, 1800–1806. doi: 10.1016/j.measurement.2013.01.011.

Han, R., Hirose, T., Shimamoto, T., Lee, Y., Ando, J. -i., 2011. Granular nanoparticles lubricate faults during seismic slip. Geology 39, 599–602. doi: 10.1130/G31842.1.

Han, R., Shimamoto, T., Ando, J., Ree, J.-H., 2007. Seismic slip record in carbonate-bearing fault zones: An insight from high-velocity friction experiments on siderite gouge. Geology 35, 1131. doi: 10.1130/G24106A.1.

Haosheng, C., Jiang, L., 2009. A ring area formed around the erosion pit on 1Cr18Ni9Ti stainless steel surface in incipient cavitation erosion. Wear 266, 884–887. doi: 10.1016/j.wear.2008.08.002.

Jacobs, J.R., Evans, J.P., Kolesar, P.T., 2006. Energetics of chemical alteration in fault zones and its relationship to the seismic cycle, in: Abercrombie, R., McGarr, A., Kanamori, H., Di Toro, G. (eds.), Geophysical Monograph Series. American Geophysical Union, Washington, D. C., pp. 181–191.

Jensen, M.E., King, J.K., 1999. Geologic map of the Brigham City 7.5-minute quadrangle. Utah Geological Survey M-173.

Jones, L.D., 2006. Monitoring landslides in hazardous terrain using terrestrial LiDAR: an example from Montserrat. Quarterly Journal of Engineering Geology and Hydrogeology 39, 371–373. doi: 10.1144/1470-9236/06-009.

Jones, R.R., Kokkalas, S., McCaffrey, K.J.W., 2009. Quantitative analysis and visualization of nonplanar fault surfaces using terrestrial laser scanning (LIDAR)—The Arkitsa fault, central Greece, as a case study. Geosphere 5, 465–482. doi: 10.1130/GES00216.1.

Kanamori, H., Brodsky, E.E., 2004. The physics of earthquakes. Reports on Progress in Physics 67, pp. 1429. doi: 10.1088/0034-4885/67/8/R03.

Kanamori, H., Riveiro, L., 2006. Energy partitioning during an earthquake, in: Abercrombie, R., McGarr, A., Kanamori, H. (Eds.), Earthquakes: Radiated Energy and the Physics of Faulting, Geopysical Monograph Series. American Geophysical Union, Washington, D. C., pp. 3–13.

Khoshelham, K., Elberink, S.O., 2012. Accuracy and Resolution of Kinect Depth Data for Indoor Mapping Applications. Sensors 12, 1437–1454. doi: 10.3390/s120201437.

Kirkpatrick, J.D., Rowe, C.D., 2013. Disappearing ink: How pseudotachylytes are lost from the rock record. Journal of Structural Geology 52, 183-198. doi: 10.1016/j.jsg.2013.03.003.

Kirkpatrick, J.D., Shipton, Z.K., 2009. Geologic evidence for multiple slip weakening mechanisms during seismic slip in crystalline rock. Journal of Geophysical Research: Solid Earth 114. doi: 10.1029/2008JB006037.

Kirkpatrick, J.D., Shipton, Z.K., Persano, C., 2009. Pseudotachylytes: Rarely Generated, Rarely Preserved, or Rarely Reported? Bulletin of the Seismological Society of America 99, 382–388. doi: 10.1785/0120080114.

Lin, A., 2008. Fossil Earthquakes: the formation and preservation of pseudotachylytes. Springer, New York. 348 pp.

Lin, A., Shimamoto, T., 1998. Selective melting processes as inferred from experimentally generated pseudotachylytes. Journal of Asian Earth Sciences16, 533–545. doi: 10.1016/S0743-9547(98)00040-3.

Lockner, D.A., Okubo, P.G., 1983. Measurements of frictional heating in granite. Journal of Geophysical Research: Solid Earth 88, 4313–4320. doi: 10.1029/JB088iB05p04313.

Machette, M.N., Personius, S.F., Nelson, A.R., Schwartz, D.P., Lund, W.R., 1991. The Wasatch fault zone, utah—segmentation and history of Holocene earthquakes. Journal of Structural Geology 13, 137–149. doi: 10.1016/0191-8141(91)90062-N.

Mankoff, K.D., Russo, T.A., 2012. The Kinect: a low-cost, high-resolution, short-range 3D camera. Earth Surf. Process. Landforms. doi: 10.1002/esp.3332.

Marone, C., Richardson, E., 2010. Learning to read fault-slip behavior from fault-zone structure. Geology 38, 767–768. doi: 10.1130/focus082010.1.

McCalpin, J.P., Nishenko, S.P., 1996. Holocene paleoseismicity, temporal clustering, and probabilities of future large (M > 7) earthquakes on the Wasatch fault zone, Utah. Journal of Geophysical Research: Solid Earth 101, 6233–6253. doi: 10.1029/95JB02851.

McGarr, A., 1999. On relating apparent stress to the stress causing earthquake fault slip. Journal of Geophysical Research: Solid Earth 104, 3003–3011. doi: 10.1029/1998JB900083.

McKenzie, D., Brune, J.N., 1972. Melting on Fault Planes During Large Earthquakes. Geophysical Journal International 29, 65–78. doi: 10.1111/j.1365-246X.1972.tb06152.x.

Meakin, P., 1998. Fractals, Scaling and Growth Far from Equilibrium. Cambridge University Press. 700 pp.

Means, W.D., 1993. Elementary geometry of deformation processes. Journal of Structural Geology 15, 343–349. doi: 10.1016/0191-8141(93)90131-S.

Mendoza, C., Hartzell, S.H., 1988. Aftershock patterns and main shock faulting. Bulletin of the Seismological Society of America 78, 1438–1449.

Mouslopoulou, V., Moraetis, D., Fassoulas, C., 2011. Identifying past earthquakes on carbonate faults: Advances and limitations of the "Rare Earth Element" method based on analysis of the Spili Fault, Crete, Greece. Earth and Planetary Science Letters 309, 45–55. doi: 10.1016/j.epsl.2011.06.015.

Mueller, P.A., Wooden, J.L., Mogk, D.W., Foster, D.A., 2011. Paleoproterozoic evolution of the Farmington zone: Implications for terrane accretion in southwestern Laurentia. Lithosphere L161.1. doi: 10.1130/L161.1.

Nelson, S.T., Harris, R.A., Dorais, M.J., Heizler, M., Constenius, K.N., Barnett, D.E., 2002. Basement complexes in the Wasatch fault, Utah, provide new limits on crustal accretion. Geology 30, 831–834. doi: 10.1130/0091-7613(2002)030<0831:BCITWF>2.0.CO;2.

Noda, H., Kanagawa, K., Hirose, T., Inoue, A., 2011. Frictional experiments of dolerite at intermediate slip rates with controlled temperature: Rate weakening or temperature weakening? Journal of Geophysical Research: Solid Earth 116. doi: 10.1029/2010JB007945.

O'Hara, K., 2005. Evaluation of asperity-scale temperature effects during seismic slip. Journal of Structural Geology 27, 1892–1898. doi: 10.1016/j.jsg.2005.04.013.

Personius, S.F., 1990. Surficial geologic Map of the Brighan City Segment and Adjacent Parts of the Weber and Collinston Segments, Wasatch Fault Zone, Box Elder and Weber Counties, Utah. I.

Personius, S.F., DuRoss, C.B., Crone, A.J., 2012. Holocene Behavior of the Brigham City Segment: Implications for Forecasting the Next Large-Magnitude Earthquake on the Wasatch Fault Zone, Utah. Bulletin of the Seismological Society of America 102, 2265–2281. doi: 10.1785/0120110214.

Petit, J.P., 1987. Criteria for the sense of movement on fault surfaces in brittle rocks. Journal of Structural Geology 9, 597–608. doi: 10.1016/0191-8141(87)90145-3.

Peyrat, S., Olsen, K.B., Madariaga, R., 2004. Which Dynamic Rupture Parameters Can Be Estimated from Strong Ground Motion and Geodetic Data? Pure and Applied Geophysics 161, 2155–2169. doi: 10.1007/s00024-004-2555-9.

Power, W.L., Tullis, T.E., 1989. The relationship between slickenside surfaces in fine-grained quartz and the seismic cycle. Journal of Structural Geology 11, 879–893.

Power, W.L., Tullis, T.E., 1991. Euclidean and fractal models for the description of rock surface roughness. Journal of Geophysical Research: Solid Earth 96, 415–424. doi: 10.1029/90JB02107.

Power, W.L., Tullis, T.E., Brown, S.R., Boitnott, G.N., Scholz, C.H., 1987. Roughness of natural fault surfaces. Geophysical Research Letters 14, 29–32. doi: 10.1029/GL014i001p00029.

Power, W.L., Tullis, T.E., Weeks, J.D., 1988. Roughness and wear during brittle faulting. Journal of Geophysical Research: Solid Earth 93, 15268–15278. doi: 10.1029/JB093iB12p15268.

Rempel, A.W., Weaver, S.L., 2008. A model for flash weakening by asperity melting during high-speed earthquake slip. Journal of Geophysical Research: Solid Earth 113. doi: 10.1029/2008JB005649.

Renard, F., Mair, K., Gundersen, O., 2012. Surface roughness evolution on experimentally simulated faults. Journal of Structural Geology 45, 101–112. doi: 10.1016/j.jsg.2012.03.009.

Renard, F., Voisin, C., Marsan, D., Schmittbuhl, J., 2006. High resolution 3D laser scanner measurements of a strike-slip fault quantify its morphological anisotropy at all scales. Geophysical Research Letters 33. doi: 10.1029/2005GL025038.

Resor, P.G., Meer, V.E., 2009. Slip heterogeneity on a corrugated fault. Earth and Planetary Science Letters 288, 483–491. doi: 10.1016/j.epsl.2009.10.010.

Rice, J.R., 2006. Heating and weakening of faults during earthquake slip. Journal of Geophysical Research 111. doi: 10.1029/2005JB004006.

Rowe, C.D., Kirkpatrick, J.D., White, J.C., Faber, C., Caine, J.S., 2012. "Gray Areas": Silica gels, amorphous silica and cryptocrystalline silica on fault surfaces. Present. 2012 Fall Meet. Agu San Francisco Calif 3-7 Dec T13E, 2654.

Rubin, A.M., Gillard, D., Got, J.-L., 1999. Streaks of microearthquakes along creeping faults. Nature 400, 635–641. doi: 10.1038/23196.

Sagy, A., Brodsky, E.E., 2009. Geometric and rheological asperities in an exposed fault zone. Journal of Geophysical Research: Solid Earth 114. doi: 10.1029/2008JB005701.

Sagy, A., Brodsky, E.E., Axen, G.J., 2007. Evolution of fault-surface roughness with slip. Geology 35, 283–286. doi: 10.1130/G23235A.1.

Schaff, D.P., Bokelmann, G.H.R., Beroza, G.C., Waldhauser, F., Ellsworth, W.L., 2002. High-resolution image of Calaveras Fault seismicity. Journal of Geophysical Research: Solid Earth 107, doi: 10.1029/2001JB000633.

Schmittbuhl, J., Gentier, S., Roux, S., 1993. Field measurements of the roughness of fault surfaces. Geophysical Research Letters 20, 639–641. doi: 10.1029/93GL00170.

Scholz, C.H., 1980. Shear heating and the state of stress on faults. Geophysical Research Letters Solid Earth 85, 6174–6184.

Scholz, C.H., 2002. The Mechanics of Earthquakes and Faulting. Cambridge University Press. 508 pp.

Schwartz, D.P., Coppersmith, K.J., 1984. Fault behavior and characteristic earthquakes: Examples from the Wasatch and San Andreas Fault Zones. Journal of Geophysical Research: Solid Earth 89, 5681–5698.

Shipton, Z.K., Evans, J.P., Abercrombie, R.E., Brodsky, E.E., 2006. The missing sinks: Slip localization in faults, damage zones, and the seismic energy budget, in: Abercrombie, R., McGarr, A., Kanamori, H., Di Toro, G. (eds.), Geophysical Monograph Series. American Geophysical Union, Washington, D. C., pp. 217–222.

Sibson, R.H., 1975. Generation of Pseudotachylyte by Ancient Seismic Faulting. Geophysical Journal of the Royal Astronomical Society 43, 775–794. doi: 10.1111/j.1365-246X.1975.tb06195.x.

Sibson, R.H., 2003. Thickness of the Seismic Slip Zone. Bulletin of the Seismological Society of America 93, 1169–1178. doi: 10.1785/0120020061.

Sibson, R.H., Toy, V.G., 2006. The habitat of fault-generated pseudotachylyte: Presence vs. absence of friction-melt. Geophysical Monograph Series 170, 153–166. doi: 10.1029/170GM16.

Siman-Tov, S., Aharonov, E., Sagy, A., Emmanuel, S., 2013. Nanograins form carbonate fault mirrors. Geology 41, 703-706. doi: 10.1130/G34087.1.

Smisek, J., Jancosek, M., Pajdla, T., 2013. 3D with Kinect, in: Fossati, A., Gall, J., Grabner, H., Ren, X., Konolige, K. (eds.), Consumer Depth Cameras for Computer Vision, Advances in Computer Vision and Pattern Recognition. Springer London, pp. 3–25.

Smith, R.B., Bruhn, R.L., 1984. Intraplate extensional tectonics of the Eastern basin-Range: Inferences on structural style from seismic reflection data, regional tectonics, and thermal-mechanical models of brittle-ductile deformation. Journal of Geophysical Research: Solid Earth 89, 5733–5762. doi: 10.1029/JB089iB07p05733.

Smith, S. A. F., Toro, G.D., Kim, S., Ree, J.-H., Nielsen, S., Billi, A., Spiess, R., 2013. Coseismic recrystallization during shallow earthquake slip. Geology 41, 63–66. doi: 10.1130/G33588.1.

Spray, J.G., 1989. Slickenside formation by surface melting during the mechanical excavation of rock. Journal of structural geology 11, 895–905.

Spray, J.G., 1992. A physical basis for the frictional melting of some rock-forming minerals. Tectonophysics 204, 205–221.

Spray, J.G., 2010. Frictional Melting Processes in Planetary Materials: From Hypervelocity Impact to Earthquakes. Annual Review of Earth and Planetary Sciences 38, 221–254. doi: 10.1146/annurev.earth.031208.100045.

Stewart, I., 1996. A rough guide to limestone fault scarps. Journal of Structural Geology 18, 1259–1264. doi: 10.1016/S0191-8141(96)00049-1.

Tanaka, H., Chen, W.M., Wang, C.Y., Ma, K.F., Urata, N., Mori, J., Ando, M., 2006. Frictional heat from faulting of the 1999 Chi-Chi, Taiwan earthquake. Geophysical Research Letters 33. doi: 10.1029/2006GL026673.

Tsutsumi, A., Shimamoto, T., 1997. High-velocity frictional properties of gabbro. Geophysical Research Letters 24, 699–702. doi: 10.1029/97GL00503.

Voisin, C., Ionescu, I., Campillo, M., 2002. Crack growth resistance and dynamic rupture arrest under slip dependent friction. Physics of the Earth and Planetary Interiors 131, 279–294. doi: 10.1016/S0031-9201(02)00054-7.

Webb, H.K., Truong, V.K., Hasan, J., Fluke, C., Crawford, R.J., Ivanova, E.P., 2012. Roughness Parameters for Standard Description of Surface Nanoarchitecture. Scanning 34, 257–263. doi: 10.1002/sca.21002.

Wei, Z., He, H., Shi, F., Gao, X., Xu, C., 2010. Topographic Characteristics of Rupture Surface Associated with the 12 May 2008 Wenchuan Earthquake. Bulletin of the Seismological Society of America 100, 2669–2680. doi: 10.1785/0120090260.

Will, T.M., 1987. Structural investigations on experimental and naturally produced slickensides (M.S. thesis). State University of New York at Albany.

Will, T.M., Wilson, C.J., 1989. Experimentally produced slickenside lineations in pyrophyllitic clay. Journal of Structural Geology 11, 657–667.

Wilson, C.E., Aydin, A., Karimi-Fard, M., Durlofsky, L.J., Amir, S., Brodsky, E.E., Kreylos, O., Kellogg, L.H., 2011. From outcrop to flow simulation: Constructing discrete fracture models from a LIDAR survey. AAPG Bulletin 95, 1883–1905. doi: 10.1306/03241108148.

Wisniewski, W., Harizanova, R., Völksch, G., Rüssel, R., 2011. Crystallization of iron containing glass-ceramics and the transformation of hematite to magnetite. CrystEngComm 11, 4025–4021.

Yonkee, W.A., Evans, J.P., DeCelles, P.G., 1992. Mesozoic Tectonics of the Northern Wasatch Range, Utah, in: Wilson, J.R. (ed.), Field Guide to Geologic Excursions in Utah and Adjacent Areas of Nevada, Idaho, and Wyoming, Utah Geological Survey Misc. Pub. 92-3, pp. 429–459.

Yonkee, W.A., Parry, W.T., Bruhn, R.L., Cashman, P.H., 1989. Thermal models of thrust faulting: Constraints from fluid-inclusion observations, Willard thrust sheet, Idaho-Utah-Wyoming thrust belt. Geological Society of America Bulletin 101, 304–313.

Zoback, M.L., 1983. Structure and Cenozoic tectonism along the Wasatch fault zone, Utah, in: Miller, D.M., Todd, V.R., Howard, K.A. (eds.), Tectonic and Stratigraphic Studies in the Eastern Great Basin, Geological Society of America Memoir 157. pp. 3–28.

CHAPTER 4

EVIDENCE FOR PALEOSEISMIC SLIP ON A CONTINENTAL LOW-ANGLE

NORMAL FAULT: TECTONIC PSEUDOTACHYLYTE FROM THE WEST

SALTON DETACHMENT FAULT, CA, USA

Abstract

The potential of continental low-angle normal faults (LANF) to nucleate large ($>$ 6.0 M_w) earthquakes at low-angles remains unclear despite much focused research. We document evidence for ancient seismicity along a continental LANF (detachment fault) that formed and slipped at low-angles and produced tectonic pseudotachylyte. These thick and laterally persistent pseudotachylyte accumulations along the West Salton detachment fault (WSDF), Salton Trough, USA, preserve convincing evidence for a frictional melt origin including: spherulitic microlites, ductile-flow structures, preservation of high temperature phases as clasts, and injection veins. Cumulative thickness of pseudotachylyte along the fault ranges from 0.1 to 1.5 m, and pseudotachylyte-cataclasite in the fault core and damage zone are exposed along ~2.6 km length of the fault. Reworked fragments of pseudotachylyte in cataclasites, and multiple generations of cataclasites provide evidence for the preservation of multiple earthquake cycles. The limited exposure ($<$ 3% of the total exposed length), and unusually large volumes of pseudotachylyte along this section of the WSDF suggest special conditions for generation of frictional melt. Prior work, documenting the low dip of the WSDF

throughout its history and abundant evidence for ancient seismicity presented here, shows that research must focus on explanations for LANF formation and slip that incorporate seismic slip. A new synthesis of pseudotachylyte along detachment faults from diverse tectonic settings provides convincing evidence that repeated ancient seismicity is common along detachment faults. These data constrain models for low-angle normal fault formation and strength. These results also have important implications for the evaluation of seismic hazards associated with active examples of LANF.

1. Introduction

The presence of low-angle normal faults (LANF) or detachment faults in highly extended terranes has led to a large body of literature describing the orientation, rock types, pressure and temperature conditions, and their deformation history (Longwell, 1945; Armstrong, 1972; Davis and Lister, 1988; John, 1987; Wernicke, 1981, 1995; Axen and Bartley, 1997; Sorel, 2000; McNulty and Farber, 2002; Cowan et al., 2003; Shirvell et al., 2009; Collettini, 2011; and many others). Detachment faults are low-angle normal faults with gentle dips, large aerial extent, large displacements ($\geq$ 5-15 km), that often exhume mid to lower continental crust in their footwalls (Davis and Lister, 1988). Debate has focused on whether low-angle normal faults formed and/or slipped at low dip angles ($<30°$) in the brittle crust against the general expectations of Andersonian fault mechanics (Anderson, 1951) that low-angle normal faults are unfavorably oriented for slip, and that seismic activity on low-angle normal faults is rare (Jackson, 1987; Jackson and White, 1989; Thatcher and Hill, 1991; Wernicke, 1995; Abers et al., 1997; Abers,

2001, 2009; Collettini and Sibson, 2001; Axen, 2004; Collettini, 2011). A growing body of research shows that low-angle normal faults have nucleated moderate to large earthquakes, localized seismicity on coeval normal faults in their hanging walls, and slipped seismically when earthquakes propagate onto them (Abers, 1991, 2001; Rietbrock et al., 1996; Axen, 1999; Sorel, 2000; Boncio et al., 2000; Collettini, 2011). Additionally, the presence of Holocene fault scarps associated with modern examples of low-angle normal faults may be related to recent seismic slip (Johnson and Loy, 1992; Caskey et al., 1996, 2004; Axen et al., 1999).

The relative paucity of seismicity associated with low-angle normal faults contrasts with compelling geologic evidence that some low-angle normal faults were active in the brittle-crust and has significant implications for fault mechanics and the evolution of highly extended terranes (e.g. Axen and Selverstone, 1994; Wernicke, 1995; Collettini and Sibson, 2001; Axen, 2004; Collettini, 2011; Selverstone et al., 2012; and many others). Models and data sets relevant to this paradox include: (1) models of low-angle normal fault formation in which the fault rotates from a moderate to low-angle during slip (Proffett, 1977; Davis, 1983; Buck, 1988; Wernicke and Axen, 1988), (2) existence of a small number of moderate-to-large magnitude earthquakes on low-angle normal faults (Abers, 1991, 2001; Wernicke, 1995; Axen, 1999; McNulty and Farber, 2002), (3) the possibility of aseismic creep along low-angle normal faults (Jackson, 1987; Doser and Smith, 1989; Hreinsdottir and Bennett, 2009; Abers, 2009; Ikari et al., 2009; Smith and Faulkner, 2010; Lecomte et al., 2012), and (4) a rationale for especially long

recurrence intervals between earthquake ruptures on low-angle normal faults, such that they exceed the historic record (Doser and Smith, 1989; Wernicke, 1992, 1995). These hypotheses and data sets have different implications for expected fault-related deformation and structural relationships: option 1 requires evidence for large magnitude rotation about a horizontal axis during progressive exhumation (Davis, 1983; Buck, 1988; Fletcher and Spelz, 2009), options 2 and 4 predict evidence for ancient seismicity (Axen, 2004; Collettini, 2011), and option 3 predicts a lack of evidence for large magnitude seismicity (Axen, 2004; Lecomte et al., 2012).

Here we present evidence for ancient seismicity, in the form of substantial cumulative thicknesses of tectonic pseudotachylyte along the West Salton detachment fault zone, CA (Fig. 4-1) (Frost and Shafiquallah, 1989; Axen and Fletcher, 1998; Kairouz, 2005; Steely, 2006; Shirvell et al., 2009; Luther, 2012; Luther and Axen, 2013). Tectonic pseudotachylyte (rapidly-quenched frictional melt) provides the most convincing evidence for ancient seismic slip along exhumed fault zones (Cowan, 1999; Sibson and Toy, 2006; Lin, 2008; Marone and Richardson, 2010; Kirkpatrick and Rowe, 2013). Tectonic pseudotachylyte along LANFs are seldom reported, and where present they have important implications for the mechanics and seismic potential of active LANFs (Collettini, 2011; Lecomte et al., 2012). We use outcrop, microstructural, and compositional analyses to describe the nature of fault-related rocks, fault-zone evolution and test the hypothesis that low-angle normal faults preserve evidence for ancient seismic slip.
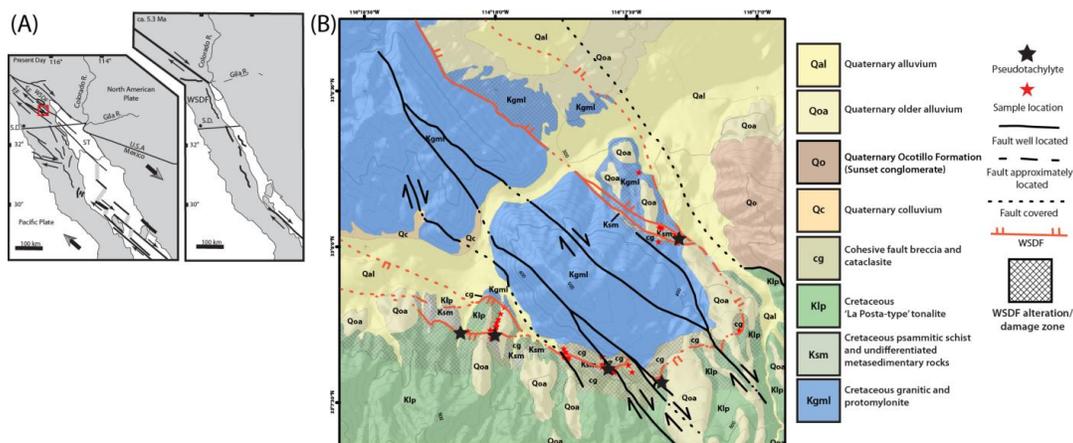
Figure 4-1. A) Regional tectonic map of the northern Gulf Extensional Province and field area (red box); and reconstruction for 5.3 Ma, restoring 350 km of dextral offset on the San Andreas Fault System (Modified from Dorsey et al., 2007). EF Elsinore fault, SAF San Andreas fault, SF San Felipe fault, ST Salton Trough, SD San Diego, WSDF West Salton detachment fault. B) Geologic map of the Yaqui Ridge area (Modified from Steely et al., 2009), > 1m thick accumulations of tectonic pseudotachylyte crop out in both the hanging wall and footwall of the WSDF in the hinge zone of the Yaqui Ridge antiform (black stars), over 2.6 km parallel to strike.

2. Methods

Detailed geologic mapping of the West Salton detachment fault at Yaqui Ridge, documents the presence of several strands of the detachment fault, and the development of thick and laterally extensive pseudotachylyte and cataclasite in the easternmost exposures of the fault zone (Schultejann, 1984; Kairouz, 2005; Steely, 2006; Janecke et al., 2008; Steely et al., 2009). We build on this work by collecting suites of oriented samples from the hanging wall and footwall of the West Salton detachment fault for

microstructural, and compositional analyses (Fig. 4-1b). Sample characterization includes optical petrographic microscopy, scanning electron microscopy, X-ray diffraction (XRD) analyses, and X-ray florescence (XRF) analyses focused on microstructural, mineralogical, and chemical characterization of the fault zone. Scanning electron microscopy, back-scattered electron images (SEM-BSE) and energy-dispersive X-ray spectroscopy (EDS) analyses were conducted using a FEI Quanta 200 equipped with an EDAX EDS system at operating voltages between 15-20 KV at Weber State University. Calcite twin thickness measurements and analyses were conducted using a three-axis universal stage and methods described by Ferrill et al. (2004). The XRD analyses were conducted using an X Pert Pro Diffractometer system (45KV/40 MA) at Utah State University. Major and trace element concentrations were determined using borate fused disk, and pressed pellet XRF analyses respectively. XRF analyses were conducted by SGS Canada.

3. Geologic Setting

The West Salton detachment fault lies along the northern half of the western margin of the Salton Trough, California, at the northern end of the Gulf Extensional Province and can be traced about 200 km-long (Fig. 4-1) (Schultejann, 1984; Frost and Shafiquallah, 1989; Axen and Fletcher, 1998; Kairouz, 2005; Shirvell et al., 2009; Steely et al., 2009; Luther 2012; Luther and Axen, 2013). The late Cenozoic Gulf Extensional Province (Gastil et al., 1975) (Fig. 4-1), is a highly oblique, transtensional, 1000-km long continental rift (Stock and Hodges, 1989; Herzig and Jacobs, 1994; Axen, 1995; Winker

and Kidwell, 1996; Martínez-Gutiérrez and Sethi, 1997; Axen and Fletcher, 1998; Dorsey and Umhoefer, 2000; Holt et al., 2000; Oskin et al., 2001; Oskin and Stock, 2003; Dorsey et al., 2007; Fletcher et al., 2007; Wong and Gans, 2008; Shirvell et al., 2009; Brothers et al., 2009; Dorsey, 2010).

The West Salton detachment fault was part of the southern San Andreas fault system from the latest Miocene to early Pleistocene, was the principal extensional structure in the western Salton Trough, and accommodated > 8-10 km of top-to-the-east normal-oblique slip and 1.1-4.25 km of exhumation (Schultejann, 1984; Frost and Shafiquallah, 1989; Axen and Fletcher, 1998; Cox et al., 2002; King et al., 2002; Matti et al., 2002, 2006; Kairouz, 2005; Steely, 2006; Dorsey et al., 2007, 2011, 2012; Shirvell et al., 2009; Steely et al., 2009). The primary low-dip angle of the WSDF is evident from syn-detachment stratigraphy in the hanging wall of the detachment, and cross-cutting relationships between the detachment and Pleistocene strata (Steely, 2006; Steely et al., 2009; Dorsey et al., 2011, 2012). The latest Miocene to early Pleistocene age of the West Salton detachment fault is constrained by provenance analysis, magnetostratigraphy, cross-cutting relationships, direct dating of fault-related rocks, and cooling ages of rocks in the footwall and hanging wall (Axen and Fletcher, 1998; Kairouz et al., 2003; Kairouz, 2005; Steely, 2006; Dorsey et al., 2007, 2011, 2012; Luther et al., 2008; Steely et al., 2009; Shirvell et al., 2009; Housen and Dorsey, 2010). The cross-cutting San Felipe fault zone folded the detachment fault and exhumed what appear to be the deepest structural levels of the West Salton detachment fault at the east tip of Yaqui Ridge (Steely et al.,

2009). This well-constrained history makes the West Salton detachment fault an excellent natural laboratory to describe the deformation associated with low-angle normal faults in the seismogenic crust.

4. Fault Zone Structure and Fault Rock Assemblage

The West Salton detachment fault zone, exposed along the NE and SW limbs of the younger Yaqui Ridge antiform (Fig. 4-1) (Steely et al., 2009), has a thick damage zone, fault core, and anastomosing principal slip surfaces (Fig.4- 2). The damage zone, up to 250 m-thick, is composed of fault breccias and highly fractured and altered protolith, but the distribution of fault-related deformation is asymmetric. Small-offset faults in the WSDF core and damage zone (i.e. Riedel shear) confirm normal-sence-offset for the main fault.

The hanging wall of the detachment, defines a thick ($\leq$ 250 m) zone of fracture and discoloration (Steely, 2006; Steely et al., 2009; Luther, 2012). The footwall damage zone is significantly thinner than the hanging wall where fractures and alteration are less pervasive, forming a thin damage zone ($\leq$ 20 m) (Fig. 4-1) (Schultejann, 1984; Steely, 2006; Steely et al., 2009; Luther, 2012). The footwall of the detachment at Yaqui Ridge is composed of foliated quartzo-feldspathic gneiss, metasedimentary rocks, and minor exposures of protomylonite (Supplemental Material) (Steely, 2006; Steely et al., 2009; Luther, 2012). The older (Mesozoic) foliation and protomylonite are related to the Mesozoic Santa Rosa shear zone that crops out in the footwall of the detachment (Schultejann, 1984; Axen and Fletcher, 1998; Steely, 2006; Steely et al., 2009). The

(A) SE / NW — Damage zone, Damage zone, WSDF, Pt, Fault core, Quartz Vein Wash, (B), (D)

(B) S / N — Damage Zone, Breccia, Fault Core, Pt, PSS, WSDF, Ct/UCC, (C), 1.0 m

(C) Pt — 5 cm

(D) S / N — 0.5 m

(E) E / W — Pt, Fault Breccia, 0.5 m
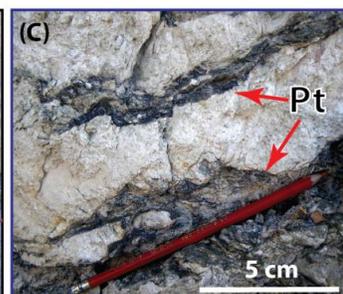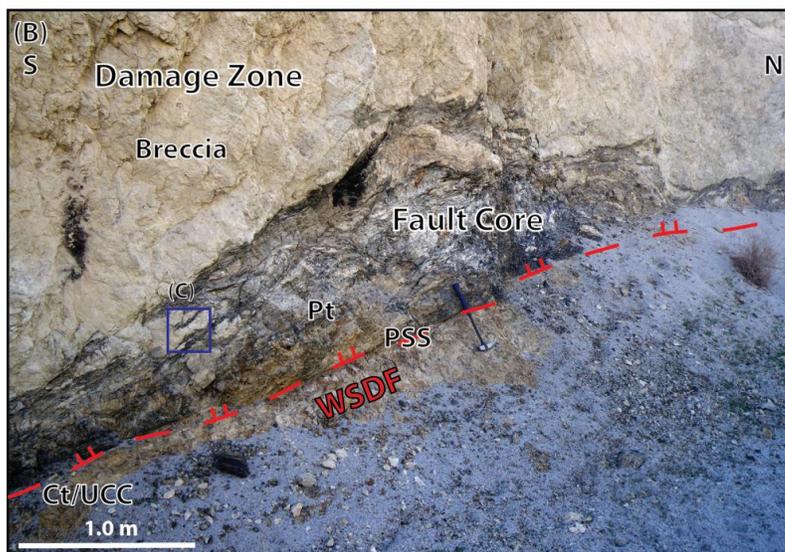
hanging wall protolith of the detachment is composed of the La Posta pluton tonalite

(Supplemental Material) (Schultejann, 1984; Steely, 2006; Steely et al., 2009; Luther,

2012). Previous studies mapped extensive chloritic fault-breccia in the hanging wall of

the detachment (Schultejann, 1984; Steely, 2006; Steely et al., 2009); however, detailed

XRD and petrographic analyses in the hanging wall and footwall of the detachment failed

to document extensive chloritization of mafic minerals (i.e. biotite and hornblende)

(Supplemental Material). Discoloration in the damage zone of the fault primarily reflects

the pervasive fracture, and saussuritized plagioclase in the granitic protolith. The fault

core is ~0.5-2 m-thick, and contains fault breccia, cataclasite, ultracataclasite, a principal

slip surface, and limited hydrothermal alteration, including late-stage cross-cutting calcite

and quartz veins, and the presence of clay minerals (Figs. 2, 3). The principal slip surface

of the WSDF is defined by a < 2 cm-thick and pervasive boundary between footwall and

hanging wall rock types (Fig. 4-2). The principal slip surface is decorated with striae that

trend dominantly to the east (Steely et al., 2009; Luther and Axen, 2013). The fault core

also contains a black fault-related rock that in outcrop exhibits injection structures in the

hanging wall and footwall of the detachment fault (Fig. 4-2).

4.1. Cataclastic rocks

Cataclasite and ultracataclasite are located in the hanging wall and footwall

portions of the damage zone and fault core of the West Salton detachment fault. These

fine-grained to very fine-grained cataclastic rocks form cm-scale lenses and layers, which

lie approximately parallel to the principal slip surface of the detachment and are typically

less than 1 m from the main detachment surface (Fig. 4-2). Cataclasite in the West Salton

detachment fault zone is composed of quartzofeldspathic, poorly sorted, monolithic and

polylithic, angular to sub-rounded, <100 μm to >1 mm, clasts supported by fine-grained,

highly comminuted silicate minerals and clay matrix (Fig. 4-3b). Ultracataclasite in the

damage zone is composed of very fine-grained and comminuted (< 5 μm) matrix, and

angular to sub-rounded and fine-grained clasts (Fig. 4-3a). Multiple generations of

cataclasite and ultracataclasite in the WSDF zone are suggestive of repeated deformation

events that might correspond to episodes of seismic slip within the fault zone (Sibson,

1986) (Fig. 4-3b).

4.2. Pseudotachylyte

The black, aphanitic rocks that occur in the hanging wall, footwall, and fault core

of the West Salton detachment fault at Yaqui Ridge are composed of up to 1.5-m thick,

layered accumulations with sharp margins and ~ 5 cm-thick injection veins that root into

the principal slip surface of the WSDF (Fig. 4-2). The layered black fault-related rock

comprises < 2- 50 mm layers of alternating black, aphanitic, friable veins, together with

quartzofeldspathic, fractured, and foliated fault breccia and cataclasite. Lens shaped and

tabular accumulations are well exposed over ~2.6 km parallel to the strike of the principal

slip surface and up to 20 m parallel to dip in the hinge zone of the Yaqui Ridge antiform

(Figs. 4-1, 4-2). The black, aphanitic veins contain variable amounts of matrix-supported

angular to rounded quartz and feldspar clasts that are typically less than 1 mm wide and

in some cases an observed reduction in grain size and change in color approaching the
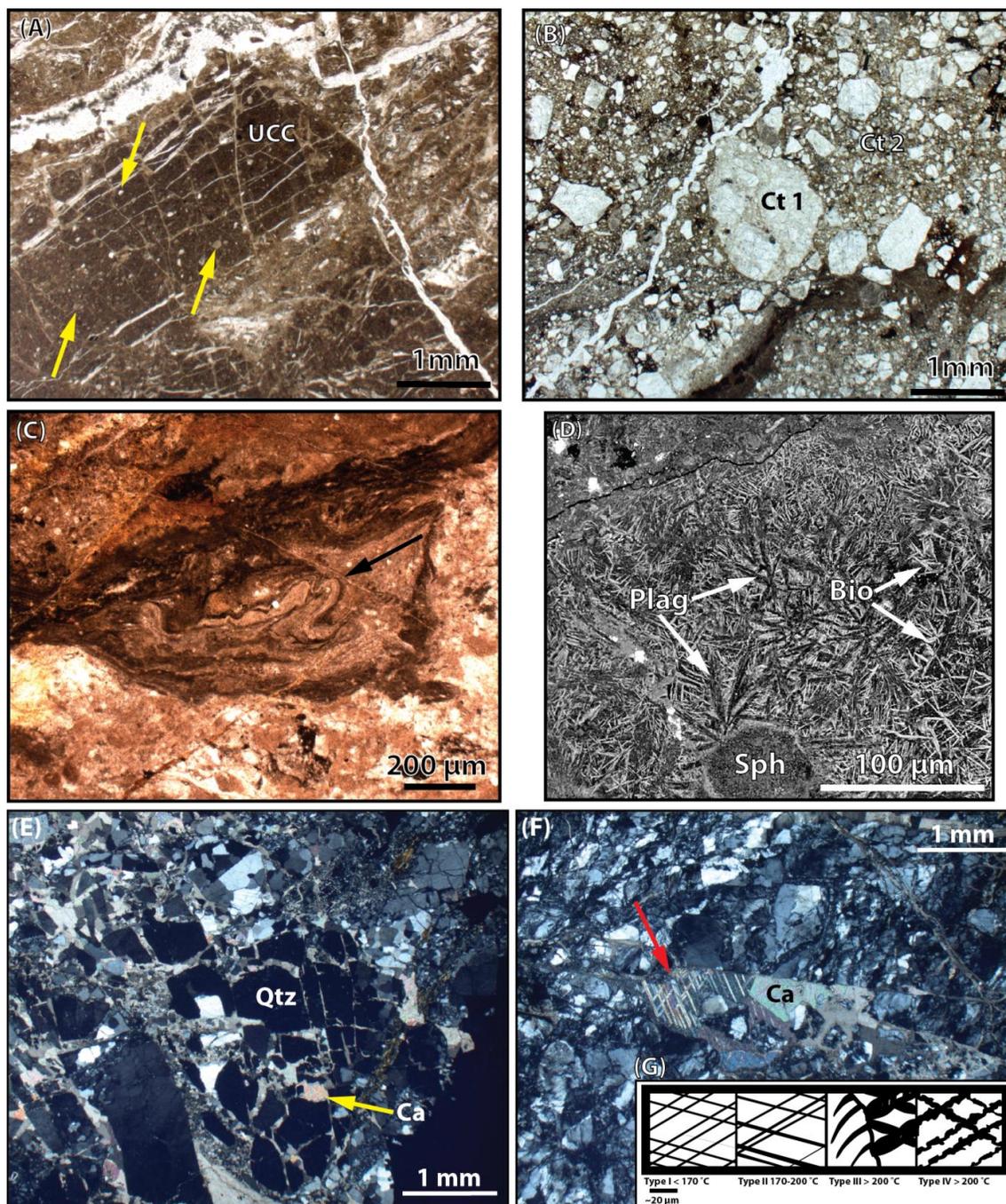
margins of veins. We interpret the change in color and reduction in grain size along the edge of some of the injection veins to represent quenched margins that formed during rapid cooling of a frictional melt.

Petrographic and SEM observations of the black fault-related rock include: 1) opaque, aphanitic (< 1 μm grain-size), anastomosing textured matrix, 2) angular to subrounded, monolithic and polylithic cataclasite composed of quartz and feldspar, 3) rounded, < 50 μm quartz and feldspar clasts with serrate margins, 4) very fine-grained (10-100 μm long) tabular, acicular and dendritic aggregates of plagioclase and biotite which typically radiate from quartz and feldspar clasts, 5) asymmetric micro-scale folds, 6) alignment of acicular biotite and plagioclase microlites parallel to vein margins, 7) a reduction in microlite grain size approaching vein margins, and 8) cross-cutting quartz and calcite filled fractures (Fig. 4-3).

4.3. Evidence for frictional melt

Numerous features of the black, aphanitic fault-related rock in the WSDF zone from the meso- to micro-scales are consistent with a frictional melt origin (Table 1) (Kairouz, 2005). The plagioclase and biotite microlites in the black matrix of the black fault-related rock is the strongest evidence for a frictional melt origin (Fig. 4-3d) (Sibson, 1975; Magloughlin and Spray, 1992; Di Toro and Pennacchioni, 2004; Kirkpatrick et al., 2009; Toy et al., 2011; Kirkpatrick and Rowe, 2013). Numerous quartz and minor plagioclase clasts in the injection veins are also convincing indicators of a frictional melt origin for the black fault-related rock (Fig. 4-3d) (Spray, 1987; Magloughlin and Spray,

Table 4-1: Summary of field and laboratory observations that are consistent with fault-related pseudotachylyte interpretation for black fault-rock (Magloughlin and Spray, 1992; Lin, 2008; Kirkpatrick et al., 2009).

Feature	Quality of evidence*	Outcrop	Optical Microscopy	SEM
Sherulites and Microlites	e.		X	X
Flow structures	v.g.	X	X	X
Quartz and Feldspar clasts	g.		X	X
Rounded/Embayed clasts	g.		X	X
Quenched margins	g.	X	X	X
Aphanitic matrix	g.	X	X	X
Injection vein morphology	g.	X	X	X
*Quality of evidence assessments: good (g.), very good (v.g.), and excellent (e.) are ranked on qualitative usefulness of a feature as an indicator of rapidly-quenched melt.				

1992; Barker et al., 2010; Nielsen et al., 2010; Toy et al., 2011; Kirkpatrick and Rowe, 2013). Experimentally produced pseudotachylyte from a quartzo-feldspathic protolith contain numerous quartz and less commonly plagioclase clasts, but lack hydrous mafic phases such as biotite and hornblende; this has been attributed to mechanical breakdown processes of weaker minerals (e.g. biotite and hornblende) which precede melting, and lower melting point of hydrous mineral phases (biotite melts at 650 °C compared with 1700 °C for quartz at 1-atm) (Spray, 1987, 1992, 2010; Nielsen et al., 2010). Additionally, similar clast compositions have been identified in pseudotachylyte from a variety of faults in numerous tectonic environments (Wenk et al., 2000; Lin, 2008;

Kirkpatrick et al., 2008; Barker et al., 2010; Toy et al., 2011). The matrices of cataclasite

and ultracataclasite from the fault zone have a distinctly different character with

numerous angular to subrounded clasts of protolith (including micas and hornblende) at

all scales of observation (Fig. 4-3a, b). Therefore, we consider the abundance of quartz

and plagioclase clasts as good evidence for a melt origin of the black fault-related rock.

Flow banding, asymmetric folds, and alignment of elongate clasts or tabular microlites in

pseudotachylyte injection veins is also an indicator of flow with a melt origin (Fig. 4-4c)

(Braathen et al., 2004; Lin, 2008; Toy et al., 2011). The presence of injection veins has

been noted in association with pseudotachylyte (Sibson, 1975; Magloughlin and Spray,

1992; Braathen et al., 2004; Kirkpatrick et al., 2009; Toy et al., 2011), but not diagnostic

of a melt origin because cataclastic deformation can also result in fluidized fault gouge

being injected into veins (Lin, 1996; Cowan et al., 2003; Rowe et al., 2005, 2012). The

presence of a black, opaque, and aphanitic flinty pseudotachylyte matrix has been noted

by many workers (Sibson, 1975; Magloughlin and Spray, 1992; Sibson and Toy, 2006;

Lin, 2008; Toy et al., 2011); however, these features are also common in fluidized fault

gouge and ultracataclasite and therefore not diagnostic of frictional melt (Lin, 2008;

Kirkpatrick et al., 2009; Toy et al., 2011). The preponderance of data that are diagnostic

of or consistent with a melt origin for the black fault-related rock indicates that

substantial production of tectonic pseudotachylyte was common during slip along the

West Salton detachment fault (Table 4-1).
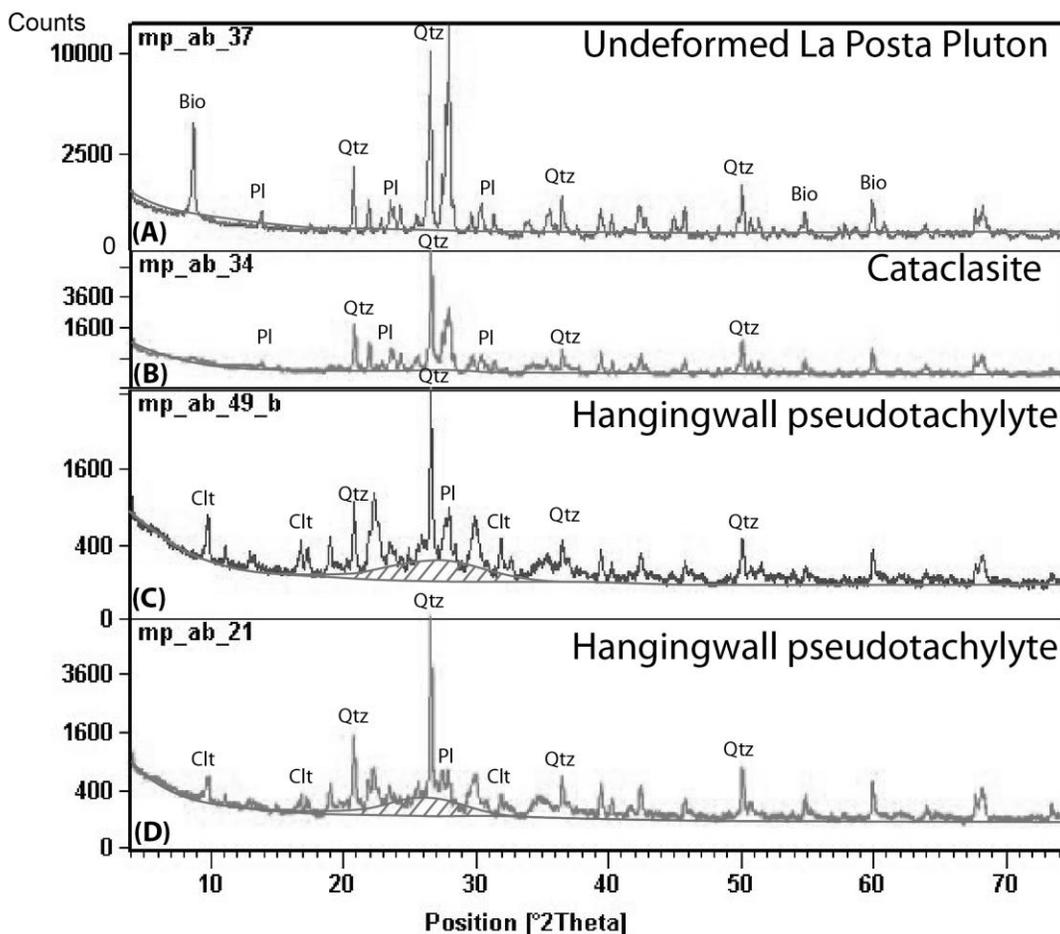
Figure 4-4. X-ray diffraction spectra of undeformed protolith (A), cataclasite in the fault

core (B), and pseudotachylyte from the fault core (C, D). Identified mineral phases

include quartz (qtz), plagioclase (Pl), biotite (Bio), and clinoptilolite (Clt).

Pseudotachylyte samples also contain a broad band with 2θ from 18-33° (hatch). This

broad band with counts above background, has been interpreted to represent preserved

glassy matrix (Lin, 1994; Lin and Shimamoto, 1998; Tsutsumi, 1999; Di Vincenzo et al.,

2004; Lin, 2008, p. 200).

4.4. Evidence for elevated pore fluid pressure and calcite twin analysis

The hanging and footwall of the West Salton detachment fault both contain evidence for elevated pore fluid pressure. Cataclastic rocks and pseudotachylyte in the fault zone are cross-cut by numerous micro-scale quartz and calcite veins (Fig. 4-3e, f). Fine- to very fine-grained and equant calcite fills a network of mode I, inter- and intra-granular fractures (Fig. 4-3e). We interpret these mode I fractures to have formed during elevated fluid pressures which exceeded the tensile strength of fractured quartz grains (30-50 MPa) (Ball and Payne, 1976). Polysynthetic ($01\bar{1}2$) mechanical twins in the

calcite fracture and vein fill have been documented to occur at differential stresses between 10-30 MPa (Passchier and Trouw, 2005). Multiple sets of thick (>10 μm) twins occur in cross-cutting veins, these thick tabular twins are likely to have formed at deformation temperatures between 150 and 300°C (Fig. 4-3f, g) (Ferrill et al., 2004; Passchier and Trouw, 2005). These temperatures are consistent with the estimated exhumation depths for the Yaqui Ridge area constrained by thermochronology (Shirvell et al., 2009).

5. Mineralogical and Geochemical Analyses

5.1. X-ray diffraction results

X-ray diffraction (XRD) analyses of tectonic pseudotachylyte identified the dominant mineral phases to be quartz, plagioclase, biotite, and clinoptilolite (zeolite) (Fig. 4-4). Additionally the pseudotachylyte spectra have a broad band from 2θ ~18° to

33° with sharp quartz and plagioclase peaks, and less pronounced biotite peaks (Fig. 4-4).

Clinoptilolite has been reported as a hydrothermal alteration product from several strike-

slip fault zones (Evans and Chester, 1995; Chester and Chester, 1998); there is not

however, convincing evidence for wide spread hydrothermal alteration associated with

the West Salton detachment fault at Yaqui Ridge; and, clinoptilolite is only observed in

association with pseudotachylyte samples from the fault zone. We interpret clinoptilolite

in the pseudotachylyte to represent devitrified glassy-matrix, analogous to devitrified

volcanic glass (Iijima, 1986; Ogihara, 2000; Kralj et al., 2009). Similarly, the broad band

has been interpreted to represent preserved or devitrified glassy, pseudotachylyte matrix

(Lin, 1994, 2008; Lin and Shimamoto, 1998; Tsutsumi, 1999; Di Vincenzo et al., 2004).

The XRD spectra from pseudotachylyte is significantly different than undeformed

granitic protolith and cataclasite from the fault zone, in that spectra from cataclasite and

protolith samples lack the broad band noted in pseudotachylyte, and have distinctly

different mineralogy (Fig. 4-4). The undeformed hangingwall protolith is composed of

plagioclase, K-feldspar, quartz, biotite, and trace hornblende, allanite, myrmekite, and

calcite below the detection limit of XRD analyses (Fig. 4-4). Cataclasite from the fault

core is made up of plagioclase, quartz, amorphous matrix, and trace allanite, hornblende,

biotite, and calcite below the detection limit of XRD analyses (Fig. 4-4).

5.2. X-ray florescence results

Samples from the hanging wall, footwall, and fault core of the West Salton

detachment fault were analyzed for major and trace element concentrations using X-ray

florescence (XRF) methods (Supplemental Material). Samples were collected across the fault zone to distinguish changes in composition as a function of position to investigate possible fluid-fault interactions at the meso-scale. Major- and trace-element variation as a function of structural position and rock type are clear in the WSDF zone (Fig. 4-5). Additionally, isocon diagrams were also produced to illustrate the relative changes in composition as a function of fault-related rock type (Fig. 4-6) (Grant, 1986, 2005).

The XRF results show that there is an enrichment in Fe_2O_3, MgO, MnO, material lost on ignition (LOI), and Rb, and a depletion in CaO, Na_2O, Al_2O_3, and Sr in the damage zone and core relative to the un-altered protolith (Fig. 4-5). Other major and trace element concentrations have no clear relationship between composition and structural position (Fig. 4-5).

Isocon plots from the West Salton detachment fault show a complex relationship between un-altered protolith and fault-related rocks (Fig. 4-6). Pseudotachylyte samples are enriched in K_2O, Zr, Ba, and Rb, and depleted in Na_2O, CaO, P_2O_5, Al_2O_3, and Sr relative to the unaltered protolith and cataclasite (Fig. 4-5a, b, d). The bulk composition of pseudotachylyte samples most closely resembles that of catacalsite (Fig. 4-6b, e). Cataclasites have a similar composition relative to the un-altered protolith with a slight depletion in Na_2O and CaO relative to the mean protolith and similar trace element concentrations (Fig. 4-6c, f). The enrichment of several major- and trace-element concentrations of pseudotachylyte relative to unaltered protolith in the West Salton detachment fault zone are similar to changes in composition reported in other studies of
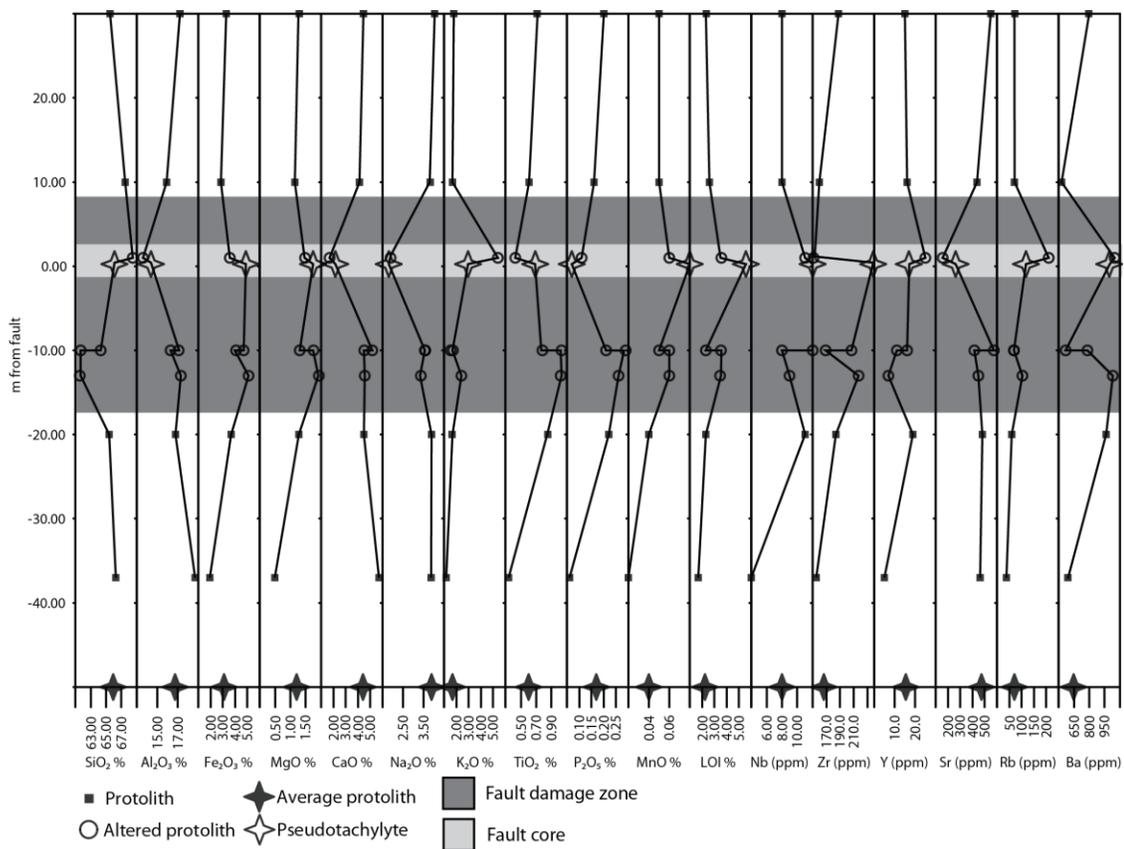
Figure 4-5. Major element concentrations across the West Salton detachment fault zone at Yaqui ridge. Y-axis is in meters from the fault zone with negative values in the footwall and positive values in the hanging wall. Major element concentrations reported in weight percent oxides (error = ± 0.01%). Trace element concentrations reported in parts per million (ppm) (error= ± 1 ppm). Detailed list of analyses can be found in Supplemental Material.

pseudotachylyte (Supplemental Material) (Sibson, 1975; Maddock, 1992; O'Hara, 1992; Lin, 1994, 2008; Wenk et al., 2000; Di Toro and Pennacchioni, 2004, 2005; Zechmeister et al., 2007; Mittempergher et al., 2009; Barker et al., 2010).

6. Discussion and Conclusions

We document convincing evidence that the black fault-related rocks in the core of the West Salton detachment fault originated as a frictional melt. The preservation of brittle deformation in the hanging wall and footwall of the West Salton detachment fault and observed deformation of calcite is consistent with deformation temperatures between 150 and 300°C (Ferrill et al., 2004; Passchier and Trouw, 2005). Assuming a geothermal gradient of 20-40°C/km these temperature estimates indicate calcite deformation between 3.75 and 15 km depth. The maximum depth estimates are greater than depths that have been calculated from thermochronologic data from the detachment fault, which suggest 1.1-4.25 km of exhumation in the footwall (Shirvell et al., 2009). These depths of exhumation are also much shallower than typical nucleation depths for large earthquakes (Lockner and Beeler, 2002; Scholz, 2010). The shallow formation depths for pseudotachylyte at Yaqui Ridge suggest that pseudotachylyte formation is not constrained to the area of rupture nucleation. Pervasive brittle-deformation in the damage zone and fault-core of the WSDF is coincident with observed changes in major and trace element concentrations as a function of structural position and the extent of detachment-related deformation is confirmed by outcrop, microstructural, and geochemical characterization of the fault zone (Fig. 4-2, 4-3, 4-5).
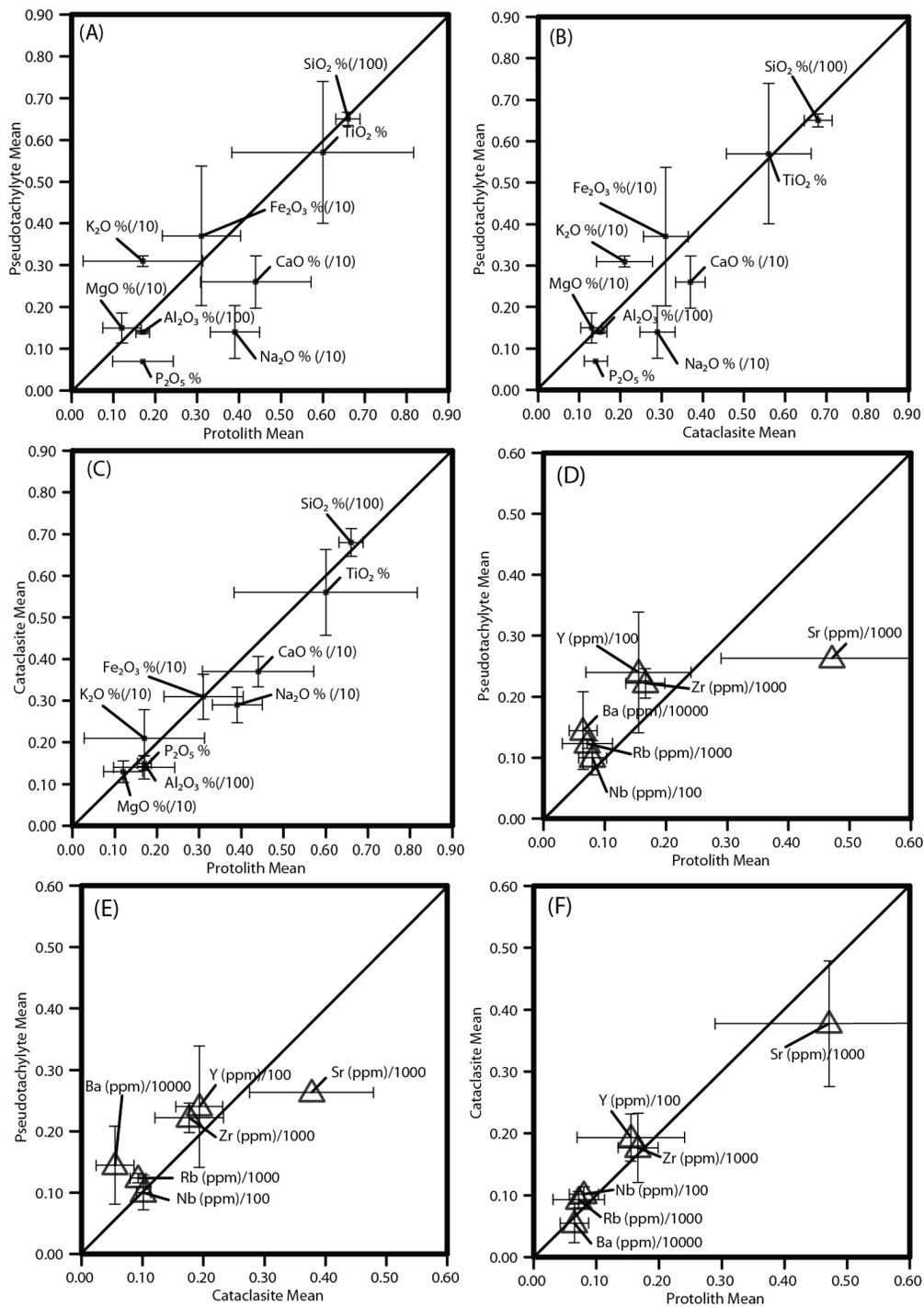
Convincing evidence for the preservation of multiple earthquake cycle in the detachment fault zone at Yaqui Ridge include: 1) layered accumulations of pseudotachylyte (Fig. 4-2), 2) multiple, cross-cutting injection veins (Supplemental material) (Fig. 4-2), 3) incorporation of pseudotachylyte clasts in cataclasites (Supplemental material), and 4) multiple-generations of cataclasites in the fault core (Figs.4- 3, 4-7). The conclusion that the WSDF fault zone preserves multiple earthquake cycles is consistent with conclusions from recent work focused on the paleostress field at Yaqui Ridge during faulting (Luther and Axen, 2013). Luther and Axen (2013) conclude that the paleostress field at Yaqui Ridge alternated from east-directed extension to south-directed thrusting as preserved by fractures in the WSDF core. This alternating stress field may be due to near total stress drop during earthquakes at Yaqui Ridge (Luther and Axen, 2013).

The thick accumulations of pseudotachylyte concentrated in the Yaqui Ridge area suggest conditions that were beneficial for pseudotachylyte generation (Barker, 2005; Sibson and Toy, 2006; Bjørnerud, 2010). The majority of reported occurrences of tectonic pseudotachylyte document thin (< 5 cm-thick) veins, associated with relatively unaltered granitic and metamorphic protoliths from fault zones composed of numerous, small-offset faults , and relatively little fluid-involvement (Di Toro and Pennacchioni, 2004; Allen, 2005; Sibson and Toy, 2006; Lin, 2008; Kirkpatrick et al., 2008, 2009; Bjørnerud, 2010; Di Toro et al., 2012). Pseudotachylyte from the West Salton detachment fault however, formed in association with a well-developed slip surface and
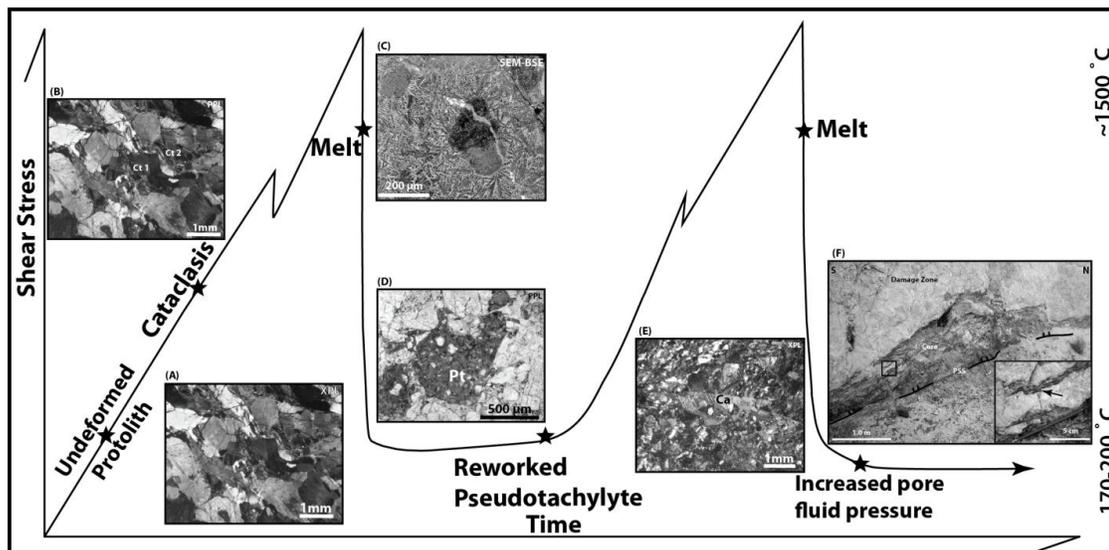
Figure 4-7. Conceptual model depicting fault-rock assemblage and history. A) undeformed La Posta pluton protolith, B) cataclasite from hanging wall of the detachment, interpreted to represent the precursor to pseudotachylyte development, possibly forming during inter- and co-seismic phases of deformation, C) SEM image of tectonic pseudotachylyte from the hanging wall of the WSDF, interpreted to form co-seismically, D) pseudotachylyte clast preserved in cataclasite in the hanging wall of the detachment, suggesting post-seismic deformation and re-working of pseudotachylyte, E) late, cross-cutting calcite filled, mode 1 fractures, suggesting fluid overpressures during portions of the fault history, F) multiple pseudotachylyte –generating earthquakes are evident from the > 1 m thick accumulations of tectonic pseudotachylyte in the hanging wall and foot wall of the detachment comprised of numerous < 5 cm thick injection veins (black arrow).

fault core that has accommodated > 8-10 km of normal-oblique slip (Axen and Fletcher, 1998; Steely, 2006; Shirvell et al., 2009; Steely et al., 2009).

The pseudotachylyte and cataclasite at Yaqui Ridge has several unusual characteristics including: 1) thick accumulations (up to 1.5 m) (Fig. 4-2), 2) presence throughout the detachment fault zone, in the hanging, footwall and fault core, 3) significant lateral extent and persistence (2.6 km) (Fig. 4-1), 4) thick, continuous, and substantial pseudotachylyte and cataclasite is limited to the hinge zone of the Yaqui Ridge antiform (Fig. 4-1) (Kairouz et al., 2003; Kairouz, 2005; Steely, 2006; Shirvell et al., 2009; Steely et al., 2009; Axen et al., 2011; Dorsey et al., 2012).

A persistent meso-scale asperity or slip-parallel corrugation at Yaqui Ridge, similar to those documented from a number of LANFs (Axen, 2004; Duebendorfer et al., 2010; Jolivet et al., 2010), may explain the large volume of pseudotachylyte at Yaqui Ridge. Fault geometry plays a primary role in controlling earthquake frequency, slip distribution, and seismic moment (Sibson, 1985; Scholz, 1985, 2002; King and Nábělek, 1985; Aydin and Du, 1995; Acharya, 1997; Carena and Suppe, 2002; Maerten et al., 2005; Marshall and Morris, 2012). Fault irregularities may give rise to more frequent earthquakes and aftershocks, and are areas of high energy release (Schwartz et al., 1990; Acharya, 1997; Carena and Suppe, 2002). Because the current antiformal geometry of the West Salton detachment fault at Yaqui Ridge is the result of contraction in a in a left-step within a dextral fault zone that post-dates slip on the detachment, it is difficult to constrain the original geometry of the fault (Steely et al., 2009). Therefore, there is no

compelling evidence for a large scale asperity or corrugation that would result in more frequent or larger magnitude seismicity, but the existence of a subtle bend in the strike of the detachment cannot be ruled out (Steely et al., 2009).

An alternative hypothesis is that the pseudotachylyte at Yaqui Ridge represents a large-scale reservoir for frictional melt generated at significant distances from their current location and injected laterally or vertically in to the present day hinge zone of the Yaqui Ridge antiform. The glassy texture of pseudotachylyte requires very-rapid (1-100 s) cooling of the melt, this cooling is often considered to take place during seismic slip (Sibson, 1975; Dixon and Dixon, 1989; Ujiie et al., 2007; Bestmann et al., 2012; Rowe et al., 2012). For pseudotachylyte to propagate laterally 500 m along the fault requires an open conduit (fracture network), and fluid flow velocities ≥ 5 m s^{-1}, this value is roughly half that of a propagating mode I fracture during rupture ($\sim$9.5 m s^{-1}), assuming typical shear wave velocities (Kanamori and Brodsky, 2004). Because the cooling time of pseudotachylyte veins is consistently greater than the fracture propagation time it is possible for pseudotachylyte to travel relatively great distances prior to cooling (Rowe et al., 2012). This hypothesis however, relies on open conduits for frictional melt to travel over great distances (100's m), and this is a difficult condition to satisfy in the subsurface. Additionally, the required large scale open fracture networks fall well outside the reported occurrences of tectonic pseudotachylyte and volume estimates for melt generation in a single slip event (McKenzie and Brune, 1972; Bjørnerud and Magloughlin, 2004; Sibson and Toy, 2006; Rowe et al., 2012; Kirkpatrick and Rowe,

2013). Based on these objections we reject the hypothesis that the pseudotachylyte migrated great distances and pooled at Yaqui Ridge.

The final and favored hypothesis is that the ambient temperature, pressure, and fluid conditions at Yaqui Ridge favored the generation and preservation of large volumes of frictional melt. The majority of pseudotachylyte is reported from granitic and metamorphic quartzofeldspathic protoliths, with relatively little fluid involvement, in association with small offset faults (Di Toro and Pennacchioni, 2004; Allen, 2005; Sibson and Toy, 2006; Lin, 2008; Kirkpatrick et al., 2008, 2009; Di Toro et al., 2012). However, pseudotachylyte has been reported from a variety of formation depths, temperature conditions, tectonic settings, and protoliths (Lin, 1994, 2008; Sibson and Toy, 2006; Kirkpatrick et al., 2009; Bjørnerud, 2010; Barker et al., 2010; Bestmann et al., 2011; Viganò et al., 2011; White, 2012). Additionally, the apparent ease of generating pseudotachylyte in rotary shear experiments suggests that the conditions for pseudotachylyte generation should be commonly satisfied in the brittle-crust (Spray, 1987; Lin and Shimamoto, 1998; Nielsen et al., 2008; Di Toro et al., 2010). The apparent rareness of pseudotachylyte may be due to a lack of preservation and identification (Kirkpatrick et al., 2009; Kirkpatrick and Rowe, 2013). We argue that the exceptionally well preserved and substantial pseudotachylyte at Yaqui Ridge suggest that conditions were especially amenable to the generation and preservation of frictional melt. The conspicuous lack of pervasive hydrothermal alteration in the damage zone and fault core at Yaqui Ridge supports this hypothesis and is consistent with previous suggestions that

pseudotachylyte is preferentially generated in "dry" conditions (Sibson, 1975; Spray, 1987, 1992; Sibson and Toy, 2006).This hypothesis is also supported by a lack of convincing pseudotachylyte reported from other well-studied localities along the fault zone where hydrothermal alteration may be more pervasive (Schultejann, 1984; Axen and Fletcher, 1998; Kairouz et al., 2003; Kairouz, 2005; Axen et al., 2011). Additionally, the footwall protoliths at Yaqui Ridge include metasedimentary rocks that may have a lower melting point contributing to the significant accumulations of pseudotachylyte (Steely et al., 2009). Despite the enigmatic nature of the large volumes of pseudotachylyte at Yaqui Ridge, the West Salton detachment fault preserves evidence for repeated seismicity in the brittle crust, with important implications for the seismic potential and mechanics of LANFs.

Ancient and active low-angle normal faults have been identified in numerous extensional settings worldwide and are thought to have formed and slipped at a low-angles in the brittle crust (Abers, 1991, 2001; Rietbrock et al., 1996; Rigo et al., 1996; Abers et al., 1997; Axen, 2004; Hreinsdottir and Bennett, 2009; Jolivet et al., 2010; Collettini, 2011). We show evidence for repeated, large magnitude earthquake nucleation or triggered earthquakes on LANFs from the West Salton detachment fault (Fig. 4-7). Evidence for periodic large magnitude earthquakes is preserved along several exhumed LANFs from highly extended regions in the form of substantial tectonic pseudotachylyte (Fig. 4-8, Table 2). Tectonic pseudotachylyte along continental LANFs has been reported from the hanging wall and footwall of faults and from a variety of formation

depths in both the brittle and ductile crust, where large earthquakes typically nucleate

(Fig. 4-8, Table 2). These results suggest that LANFs have generated large earthquakes,

and therefore models for LANF formation and activity should incorporate periodic

earthquake rupturing. The conclusion the LANF earthquakes are relatively common in

the geologic record suggests that modern examples of LANFs may pose a significant

seismic hazard in actively extending regions.

Table 4-2: Reported occurrences of melt-related pseudotachylyte from low-angle normal faults and estimated depth of formation (Modified from Collettini, 2011).

LANF	Mean dip	Pseudotachylyte formation depth	Structural position of Pseudotachylyte	References
Whipple low-angle normal fault	10-15°	Poorly constrained	Footwall	(Lister and Davis, 1989; Reynolds and Lister, 1987, 1987; Wang, 1997)
South Mountains detachment fault	10-20°	~11 km	Footwall	(Davis et al., 1986; Goodwin, 1999; Goodwin et al., 1998, 1998; Smith et al., 2012)
Chemehuevi-Sacramento detachment fault	<20°	6-10 km	Footwall	(John and Cheadle, 2010; John, 1987)
Alaşehir detachment fault	10-30°	Poorly constrained	Footwall	(Işık et al., 2003)
Otago schist (Tucker Hill)	10-30°	6-12 km	Fault core	(Barker et al., 2010; Barker, 2005; Bjørnerud, 2010)
Nordfjord-Sogn detachment fault	<30°	Seismogenic zone (~6-12 km)	Footwall	(Braathen et al., 2004)
Eidsfjord detachment fault	25-30 °	Seismogenic zone (~6-12 km)	Hanging wall	(Plattner et al., 2003; Steltenpohl et al., 2011)
Xiaoqinling detachment fault	25-50°	Poorly constrained	Footwall	(Zhang et al., 1998)
West Salton detachment fault	<30°	1.1-4.25 km (poorly constrained)	Hanging wall and footwall	(Janecke et al., 2008; Kairouz et al., 2003; Prante et al., 2011; Schultejann, 1984; Steely, 2006)
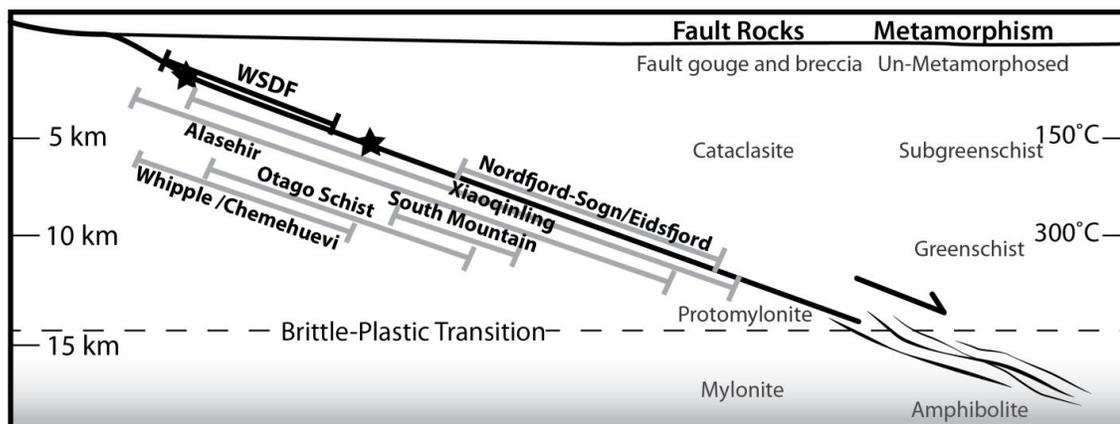
Figure 4-8. Schematic cross-section of low-angle normal fault with expected fault-related rocks and metamorphic grade (assuming geothermal gradient of 30 °C), and reported occurrences of melt related, tectonic pseudotachylyte from low-angle normal faults with structural position and estimated depth of formation (Table 4-2). Additionally, the approximate nucleation depths of two large magnitude (> Mw 6.0) earthquakes that have been interpreted to have nucleated along low-angle normal faults (black stars) (Abers et al., 1997; Abers, 2009).

7. References

Abers, G.A., 1991. Possible seismogenic shallow-dipping normal faults in the Woodlark-D'Entrecasteaux extensional province, Papua New Guinea. Geology 19, 1205–1208.

Abers, G.A., 2001. Evidence for seismogenic normal faults at shallow dips in continental rifts. Geol. Soc. Lond. Spec. Publ. 187, 305–318.

Abers, G.A., 2009. Slip on shallow-dipping normal faults. Geology 37, 767–768.

Abers, G.A., Mutter, C.Z., Fang, J., 1997. Shallow dips of normal faults during rapid extension: Earthquakes in the Woodlark-D'Entrecasteaux rift system, Papua New Guinea. J. Geophys. Res. Solid Earth 102, 15301–15317.

Acharya, H.K., 1997. Influence of fault bends on ruptures. Bull. Seism. Soc. Am. 87, 1691–1696.

Allen, J.L., 2005. A multi-kilometer pseudotachylyte system as an exhumed record of earthquake rupture geometry at hypocentral depths (Colorado, USA). Tectonophysics 402, 37–54.

Anderson, E.M., 1951. The Dynamics of Faulting. Oliver and Boyd, Edinburgh.

Armstrong, R.L., 1972. Low-angle (denudation faults), hinterland of the Sevier orogenic belt, eastern Nevada and western Utah. Geol. Soc. Am. Bull. 83, 1729–1754.

Axen, G., 1995. Extensional segmentation of the Main Gulf Escarpment, Mexico and United States. Geology 23, 515.

Axen, G.J., 1999. Low-angle normal fault earthquakes and triggering. Geophys. Res. Lett. 26, 3693–3696.

Axen, G.J., 2004. Mechanics of low-angle normal faults, in: Karner, G., Taylor, B., Driscoll, N.W., Kohlstedt, D.L. (Eds.), Rheology and Deformation in the Lithosphere at Continental Margins. Columbia University Press, New York, pp. 46–91.

Axen, G.J., Bartley, J.M., 1997. Field tests of rolling hinges: Existence, mechanical types, and implications for extensional tectonics. J. Geophys. Res. 102, 20,515–20,537.

Axen, G.J., Fletcher, J.M., 1998. Late Miocene-Pleistocene Extensional Faulting, Northern Gulf of California, Mexico and Salton Trough, California. Int. Geol. Rev. 40, 217–244.

Axen, G.J., Fletcher, J.M., Cowgill, E., Murphy, M., Kapp, P., MacMillan, I., Ramos-Velázquez, E., Aranda-Gómez, J., 1999. Range-front fault scarps of the Sierra El Mayor, Baja California: Formed above an active low-angle normal fault? Geology 27, 247–250.

Axen, G.J., Luther, A.L., Selverstone, J., Mozley, P., 2011. Layered Fault Rocks Below the West Salton Detachment Fault (WSDF), CA Record Multiple Seismogenic? Slip Events and Transfer of Material to a Fault Core. Agu Fall Meet. Abstr. -1, 2471.

Axen, G.J., Selverstone, J., 1994. Stress state and fluid-pressure level along the Whipple detachment fault, California. Geology 22, 835–838.

Aydin, A., Du, Y., 1995. Surface rupture at a fault bend: the 28 June 1992 Landers, California, earthquake. Bull. Seism. Soc. Am. 85, 111–128.

Ball, A., Payne, B.W., 1976. The tensile fracture of quartz crystals. J. Mater. Sci. 11, 731–740.

Barker, S.L., Sibson, R.H., Palin, J.M., FitzGerald, J.D., Reddy, S., Warr, L.N., van der Pluijm, B.A., 2010. Cretaceous age, composition, and microstructure of pseudotachylyte in the Otago Schist, New Zealand. New Zealand J. Geol. Geophys. 53, 15–29.

Barker, S.L.L., 2005. Pseudotachylyte-generating faults in Central Otago, New Zealand. Tectonophysics 397, 211–223.

Bestmann, M., Pennacchioni, G., Frank, G., Göken, M., de Wall, H., 2011. Pseudotachylyte in muscovite-bearing quartzite: Coseismic friction-induced melting and plastic deformation of quartz. J. Struct. Geol. 33, 169–186.

Bestmann, M., Pennacchioni, G., Nielsen, S., Göken, M., de Wall, H., 2012. Deformation and ultrafine dynamic recrystallization of quartz in pseudotachylyte-bearing brittle faults: A matter of a few seconds. J. Struct. Geol. 38, 21–38.

Bjørnerud, M., 2010. Rethinking conditions necessary for pseudotachylyte formation: Observations from the Otago schists, South Island, New Zealand. Tectonophysics 490, 69–80.

Bjørnerud, M., Magloughlin, J.F., 2004. Pressure-related feedback processes in the generation of pseudotachylytes. J. Struct. Geol. 26, 2317–2323.

Boncio, P., Brozzetti, F., Lavecchia, G., 2000. Architecture and seismotectonics of a regional low-angle normal fault zone in central Italy. Tectonics 19, 1038–1055.

Braathen, A., Osmundsen, P.T., Gabrielsen, R.H., 2004. Dynamic development of fault rocks in a crustal-scale detachment: An example from western Norway. Tectonics 23.

Brothers, D.S., Driscoll, N.W., Kent, G.M., Harding, A.J., Babcock, J.M., Baskin, R.L., 2009. Tectonic evolution of the Salton Sea inferred from seismic reflection data. Nat. Geosci. 2, 581–584.

Buck, W.R., 1988. Flexural rotation of normal faults. Tectonics 7, 959–973.

Carena, S., Suppe, J., 2002. Three-dimensional imaging of active structures using earthquake aftershocks: the Northridge thrust, California. J. Struct. Geol. 24, 887–904.

Caskey, S.J., Bell, J.W., Ramelli, A.R., Wesnousky, S.G., 2004. Historic Surface Faulting and Paleoseismicity in the Area of the 1954 Rainbow Mountain-Stillwater Earthquake Sequence, Central Nevada. Bull. Seism. Soc. Am. 94, 1255–1275.

Caskey, S.J., Wesnousky, S.G., Zhang, P., Slemmons, D.B., 1996. Surface faulting of the 1954 Fairview Peak (MS 7.2) and Dixie Valley (MS 6.8) earthquakes, central Nevada. Bull. Seism. Soc. Am. 86, 761–787.

Chester, F.M., Chester, J.S., 1998. Ultracataclasite structure and friction processes of the Punchbowl fault, San Andreas system, California. Tectonophysics 295, 199–221.

Collettini, C., 2011. The mechanical paradox of low-angle normal faults: Current understanding and open questions. Tectonophysics 510, 253–268.

Collettini, C., Sibson, R.H., 2001. Normal faults, normal friction? Geology 29, 927–930.

Cowan, D.S., 1999. Do faults preserve a record of seismic slip? A field geologist's opinion. J. Struct. Geol. 21, 995–1001.

Cowan, D.S., Cladouhos, T.T., Morgan, J.K., 2003. Structural geology and kinematic history of rocks formed along low-angle normal faults, Death Valley, California. Geol. Soc. Am. Bull. 115, 1230–1248.

Cox, B.F., Matti, J.C., King, T., Morton, D.M., 2002. Neogene strata of southern Santa Rosa Mountains, California, and their significance for tectonic evolution of western Salton Trough. Geol. Soc. Am. Abstr. Programs 34, 124.

Davis, G.A., Lister, G.S., 1988. Detachment faulting in continental extension; Perspectives from the Southwestern U.S. Cordillera. Geol. Soc. Am. Spec. Pap. 218, 133–160.

Davis, G.A., Lister, G.S., Reynolds, S.J., 1986. Structural evolution of the Whipple and South mountains shear zones, southwestern United States. Geology 14, 7–10.

Davis, G.H., 1983. Shear-zone model for the origin of metamorphic core complexes. Geology 11, 342–347.

Di Toro, G., Niemeijer, A., Tripoli, A., Nielsen, S., Di Felice, F., Scarlato, P., Spada, G., Alessandroni, R., Romeo, G., Di Stefano, G., Smith, S., Spagnuolo, E., Mariano, S., 2010. From field geology to earthquake simulation: a new state-of-the-art tool to investigate rock friction during the seismic cycle (SHIVA). Rendiconti Lincei 21, 95–114.

Di Toro, G., Pennacchioni, G., 2004. Superheated friction-induced melts in zoned pseudotachylytes within the Adamello tonalites (Italian Southern Alps). J. Struct. Geol. 26, 1783–1801.

Di Toro, G., Pennacchioni, G., 2005. Fault plane processes and mesoscopic structure of a strong-type seismogenic fault in tonalites (Adamello batholith, Southern Alps). Tectonophysics 402, 55–80.

Di Toro, G., Smith, S.A.F., Fondriest, M., Bistacchi, A., Nielsen, S., Mitchell, T.M., Mittempergher, S., Griffith, W.A., 2012. Is the fault core-damage zone model representative of seismogenic faults? Pre-existing anisotropies and fault zone complexity. Present. 2012 Fall Metting Agu San Francisco Calif 3-7 Dec T24A–01.

Di Vincenzo, G., Rocchi, S., Rossetti, F., Storti, F., 2004. 40Ar–39Ar dating of pseudotachylytes: the effect of clast-hosted extraneous argon in Cenozoic fault-generated friction melts from the West Antarctic Rift System. Earth Planet. Sci. Lett. 223, 349–364.

Dixon, J.E., Dixon, T.H., 1989. Vesicles, amygdales and similar structures in fault-generated pseudotachylites - comment. Lithos 23, 225–227.

Dorsey, R.J., 2010. Sedimentation and crustal recycling along an active oblique-rift margin: Salton Trough and northern Gulf of California. Geology 38, 443–446.

Dorsey, R.J., Axen, G.J., Peryam, T.C., Kairouz, M.E., 2012. Initiation of the Southern Elsinore Fault at ~1.2 Ma: Evidence from the Fish Creek–Vallecito Basin, southern California. Tectonics 31.

Dorsey, R.J., Fluette, A., McDougall, K., Housen, B.A., Janecke, S.U., Axen, G.J., Shirvell, C.R., 2007. Chronology of Miocene–Pliocene deposits at Split Mountain Gorge, Southern California: A record of regional tectonics and Colorado River evolution. Geology 35, 57.

Dorsey, R.J., Housen, B.A., Janecke, S.U., Fanning, C.M., Spears, A.L.F., 2011. Stratigraphic record of basin development within the San Andreas fault system:

Late Cenozoic Fish Creek-Vallecito basin, southern California. Geol. Soc. Am. Bull. 123, 771–793.

Dorsey, R.J., Umhoefer, P.J., 2000. Tectonic and eustatic controls on sequence stratigraphy of the Pliocene Loreto basin, Baja California Sur, Mexico. Geol. Soc. Am. Bull. 112, 177–199.

Doser, D.I., Smith, R.B., 1989. An assessment of source parameters of earthquakes in the cordillera of the western United States. Bull. Seism. Soc. Am. 79, 1383–1409.

Duebendorfer, E.M., Faulds, J.E., Fryxell, J.E., 2010. The South Virgin–White Hills detachment fault, southeastern Nevada and northwestern Arizona: Significance, displacement gradient, and corrugation formation. Geol. Soc. Am. Spec. Pap. 463, 275–287.

Evans, J.P., Chester, F.M., 1995. Fluid-rock interaction in faults of the San Andreas system: Inferences from San Gabriel fault rock geochemistry and microstructures. J. Geophys. Res. Solid Earth 100, 13007–13020.

Ferrill, D.A., Morris, A.P., Evans, M.A., Burkhard, M., Groshong Jr., R.H., Onasch, C.M., 2004. Calcite twin morphology: a low-temperature deformation geothermometer. J. Struct. Geol. 26, 1521–1529.

Fletcher, J.M., Grove, M., Kimbrough, D., Lovera, O., Gehrels, G.E., 2007. Ridge-trench interactions and the Neogene tectonic evolution of the Magdalena shelf and southern Gulf of California: Insights from detrital zircon U-Pb ages from the Magdalena fan and adjacent areas. Geol. Soc. Am. Bull. 119, 1313–1336.

Fletcher, J.M., Spelz, R.M., 2009. Patterns of Quaternary deformation and rupture propagation associated with an active low-angle normal fault, Laguna Salada, Mexico: Evidence of a rolling hinge? Geosphere 5, 385–407.

Frost, E.G., Shafiquallah, M., 1989. Pre-San Andreas opening of the Salton Trough as an extensional basin: K-Ar ages on regional detachment faults along the western margin of the Salton Trough. Geol. Soc. Am. Abstr. Programs 21, 81.

Gastil, R.G., Phillips, R.P., Allison, E.C., 1975. Reconnaissance geology of the State of Baja California, Memoir Geological Society of America. Geological Society of America, Boulder, Colorado.

Goodwin, L.B., 1999. Controls on pseudotachylyte formation during tectonic exhumation in the South Mountains metamorphic core complex, Arizona. Geol. Soc. Lond. Spec. Publ. 154, 325–342.

Goodwin, L.B., Reynolds, S.J., Ferranti, C., Ellzey, P., Lister, G.S., 1998. Pseudotachylytes from a metamorphic core complex, in: Fault-related Rocks-a Photographic Atlas. Princton University Press, pp. 122–123.

Grant, J.A., 1986. The isocon diagram; a simple solution to Gresens' equation for metasomatic alteration. Econ. Geol. 81, 1976–1982.

Grant, J.A., 2005. Isocon analysis: A brief review of the method and applications. Phys. Chem. Earth Parts Abc 30, 997–1004.

Herzig, C.T., Jacobs, D.C., 1994. Cenozoic volcanism and two-stage extension in the Salton trough, southern California and northern Baja California. Geology 22, 991–994.

Holt, J.W., Holt, E.W., Stock, J.M., 2000. An age constraint on Gulf of California rifting from the Santa Rosalía basin, Baja California Sur, Mexico. Geol. Soc. Am. Bull. 112, 540–549.

Housen, B.A., Dorsey, R.J., 2010. Magnetostratigraphy and Paleomagnetism of the Plio-Pleistocene Arroyo Diablo and Borrego Formations in the Borrego Badlands, western Salton Trough, CA. Agu Fall Meet. Abstr. -1, 08.

Hreinsdottir, S., Bennett, R.A., 2009. Active aseismic creep on the Alto Tiberina low-angle normal fault, Italy. Geology 37, 683–686.

Iijima, A., 1986. Occurrence of natural zeolites. Nendokagaku 26, 49–63.

Ikari, M.J., Saffer, D.M., Marone, C., 2009. Frictional and hydrologic properties of clay-rich fault gouge. J. Geophys. Res. Solid Earth 114.

Işık, V., Seyitoğlu, G., Çemen, İ., 2003. Ductile–brittle transition along the Alaşehir detachment fault and its structural relationship with the Simav detachment fault, Menderes massif, western Turkey. Tectonophysics 374, 1–18.

Jackson, J.A., 1987. Active normal faulting and crustal extension. Geol. Soc. Lond. Spec. Publ. 28, 3–17.

Jackson, J.A., White, N.J., 1989. Normal faulting in the upper continental crust: observations from regions of active extension. J. Struct. Geol. 11, 15–36.

Janecke, S.U., Steely, A.N., Evans, J.P., 2008. Seismic Slip on an Oblique Detachment Fault at Low Angles. Agu Fall Meet. Abstr. -1, 06.

John, B.E., 1987. Geometry and evolution of a mid-crustal extensional fault system: Chemehuevi Mountains, southeastern California. Geol. Soc. Lond. Spec. Publ. 28, 313–335.

John, B.E., Cheadle, M.J., 2010. Deformation and alteration associated with oceanic and continental detachment fault systems: Are they similar?, in: Rona, P.A., Devey, C.W., Dyment, J., Murton, B.J. (Eds.), Diversity of Hydrothermal Systems on Slow-spreading Ocean Ridges, AGU Monograph. pp. 175–205.

Johnson, R.A., Loy, K.L., 1992. Seismic reflection evidence for seismogenic low-angle faulting in southeastern Arizona. Geology 20, 597–600.

Jolivet, L., Labrousse, L., Agard, P., Lacombe, O., Bailly, V., Lecomte, E., Mouthereau, F., Mehl, C., 2010. Rifting and shallow-dipping detachments, clues from the Corinth Rift and the Aegean. Tectonophysics 483, 287–304.

Kairouz, M.E., 2005. Geology of the Whale Peak region of the Vallecito Mountains: Emphasis on the kinematics and timing of the west Salton detachment fault, southern California (M.S. thesis). University of California, Los Angeles.

Kairouz, M.E., Axen, G.J., Grove, M., Lovera, O., Stockli, D.F., 2003. Late Cenozoic 40Ar/39Ar ages of fault rocks formed along the West Salton detachment system, southern California. Geol. Soc. Am. Abstr. Programs 35, 629.

Kanamori, H., Brodsky, E.E., 2004. The physics of earthquakes. Reports Prog. Phys. 67, 1429.

King, G., Nábělek, J., 1985. Role of Fault Bends in the Initiation and Termination of Earthquake Rupture. Science 228, 984–987.

King, T., Cox, B.F., Matti, J.C., Powell, C.L., Osterman, L.E., Bybell, J.M., 2002. Previously unreported outcrops of Neogene Imperial Formation in southern Santa Rosa Mountains, California, and implications for tectonic uplift. Geol. Soc. Am. Abstr. Programs 34, 124.

Kirkpatrick, J.D., Rowe, C.D., 2013. Disappearing ink: How pseudotachylytes are lost from the rock record. J. Struct. Geol. (in press).

Kirkpatrick, J.D., Shipton, Z.K., Evans, J.P., Micklethwaite, S., Lim, S.J., McKillop, P., 2008. Strike-slip fault terminations at seismogenic depths: The structure and kinematics of the Glacier Lakes fault, Sierra Nevada United States. J. Geophys. Res. Solid Earth 113.

Kirkpatrick, J.D., Shipton, Z.K., Persano, C., 2009. Pseudotachylytes: Rarely Generated, Rarely Preserved, or Rarely Reported? Bull. Seism. Soc. Am. 99, 382–388.

Kralj, Polona, Rychagov, S., Kralj, Peter, 2009. Zeolites in volcanic-igneous hydrothermal systems: a case study of Pauzhetka geothermal field (Kamchatka) and Oligocene Smrekovec volcanic complex (Slovenia). Environ. Earth Sci. 59, 951–956.

Lecomte, E., Le Pourhiet, L., Lacombe, O., 2012. Mechanical basis for slip along low-angle normal faults. Geophys. Res. Lett. 39.

Lin, A., 1994. Glassy pseudotachylyte veins from the Fuyun fault zone, northwest China. J. Struct. Geol. 16, 71–83.

Lin, A., 1996. Injection veins of crushing-originated pseudotachylyte and fault gouge formed during seismic faulting. Eng. Geol. 43, 213–224.

Lin, A., 2008. Fossil Earthquakes: the formation and preservation of pseudotachylytes. Springer, New York.

Lin, A., Shimamoto, T., 1998. Selective melting processes as inferred from experimentally generated pseudotachylytes. J. Asian Earth Sci. 16, 533–545.

Lister, G.S., Davis, G.A., 1989. The origin of metamorphic core complexes and detachment faults formed during Tertiary continental extension in the northern Colorado River region, U.S.A. J. Struct. Geol. 11, 65–94.

Lockner, D.A., Beeler, N.M., 2002. Rock failure and earthquakes, in: William H.K. Lee, H.K. (Ed.), International Geophysics. Academic Press, pp. 505–537.

Longwell, C., 1945. Low-angle normal faults in the Basin and Range province. Geophys. Union Trans. 26, 107–118.

Luther, A., 2012. Deformation and Paleostress Analyses of Fault Rocks: Fault Zone Processes from the Elastic-Plastic Transition through the Brittle Crust (PhD dissertation). New Mexico Institute of Mining and Technology, Socorro, New Mexico.

Luther, A., Axen, G., 2013. Alternating extensional and shortening stress fields on the West Salton detachment fault, Southern California. Geology 41, 1047–1050.

Luther, A., Axen, G.J., Stockli, D.F., Kelley, S., Grove, M., 2008. Preliminary Apatite (U-Th)/he Thermochronology of the Eastern Santa Rosa and San Jacinto Blocks, Peninsular Ranges, Southern California. Geol. Soc. Am. Abstr. Programs 40, 444.

Maddock, R.H., 1992. Effects of lithology, cataclasis and melting on the composition of fault-generated pseudotachylytes in Lewisian gneiss, Scotland. Tectonophysics 204, 261–278.

Maerten, F., Resor, P., Pollard, D., Maerten, L., 2005. Inverting for Slip on Three-Dimensional Fault Surfaces Using Angular Dislocations. Bull. Seism. Soc. Am. 95, 1654–1665.

Magloughlin, J.F., Spray, J.G., 1992. Frictional melting processes and products in geological materials: introduction and discussion. Tectonophysics 204, 197–204.

Marone, C., Richardson, E., 2010. Learning to read fault-slip behavior from fault-zone structure. Geology 38, 767–768.

Marshall, S.T., Morris, A.C., 2012. Mechanics, slip behavior, and seismic potential of corrugated dip-slip faults. J. Geophys. Res. Solid Earth 117.

Martínez-Gutiérrez, G., Sethi, P.S., 1997. Miocene-Pleistocene sediments within the San José del Cabo Basin, Baja California Sur, Mexico. Geol. Soc. Am. Spec. Pap. 318, 141–166.

Matti, J.C., Cox, B.F., Morton, D.M., Sharp, R.V., King, T., 2002. Fault-bounded Neogene sedimentary deposits in the Santa Rosa Mountains, southern California: Crustal stretching or transpressional uplift? Geol. Soc. Am. Abstr. Programs 34, 124.

Matti, J.C., Morton, D.M., Cox, B.F., Landis, G.P., Langenheim, V.E., Premo, W.R., Kistler, R., Budahn, J.R., 2006. Fault-Bounded Late Neogene Sedimentary Deposits in the Santa Rosa Mountains, Southern CA: Constraints on the Evolution of the San Jacinto Fault. Agu Fall Meet. Abstr. -1, 0407.

McKenzie, D., Brune, J.N., 1972. Melting on Fault Planes During Large Earthquakes. Geophys. J. Int. 29, 65–78.

McNulty, B., Farber, D., 2002. Active detachment faulting above the Peruvian flat slab. Geology 30, 567–570.

Mittempergher, S., Pennacchioni, G., Di Toro, G., 2009. The effects of fault orientation and fluid infiltration on fault rock assemblages at seismogenic depths. J. Struct. Geol. 31, 1511–1524.

Nielsen, S., Di Toro, G., Hirose, T., Shimamoto, T., 2008. Frictional melt and seismic slip. J. Geophys. Res. Solid Earth 113.

Nielsen, S., Toro, G.D., Griffith, W.A., 2010. Friction and roughness of a melting rock surface. Geophys. J. Int. 182, 299–310.

O'Hara, K., 1992. Major- and trace-element constraints on the petrogenesis of a fault-related pseudotachylyte, western Blue Ridge province, North Carolina. Tectonophysics 204, 279–288.

Ogihara, S., 2000. Composition of Clinoptilolite Formed from Volcanic Glass During Burial Diagenesis. Clays Clay Miner. 48, 106–110.

Oskin, M., Stock, J., 2003. Pacific–North America plate motion and opening of the Upper Delfín basin, northern Gulf of California, Mexico. Geol. Soc. Am. Bull. 115, 1173–1190.

Oskin, M., Stock, J., Martín-Barajas, A., 2001. Rapid localization of Pacific–North America plate motion in the Gulf of California. Geology 29, 459–462.

Passchier, C.W., Trouw, R.A.J., 2005. Microtectonics. Springer.

Plattner, U., Markl, G., Sherlock, S., 2003. Chemical heterogeneities of Caledonian (?) pseudotachylites in the Eidsfjord Anorthosite, north Norway. Contrib. Miner. Pet. 145, 316–338.

Prante, M.R., Evans, J.P., Janecke, S.U., 2011. Paleoseismicity along a low-angle normal fault: Evidence from the Salton Trough, CA, USA. Present. 2011 Fall Metting Agu San Francisco Calif 5-9 Dec T41C–07.

Proffett, J.M., 1977. Cenozoic geology of the Yerington district, Nevada, and implications for the nature and origin of Basin and Range faulting. Geol. Soc. Am. Bull. 88, 247–266.

Reynolds, S.J., Lister, G.S., 1987. Structural aspects of fluid-rock interactions in detachment zones. Geology 15, 362–366.

Rietbrock, A., Tiberi, C., Scherbaum, F., Lyon-Caen, H., 1996. Seismic slip on a low angle normal fault in the Gulf of Corinth: Evidence from high-resolution cluster analysis of microearthquakes. Geophys. Res. Lett. 23, 1817–1820.

Rigo, A., Lyon-Caen, H., Armijo, R., Deschamps, A., Hatzfeld, D., Makropoulos, K., Papadimitriou, P., Kassaras, I., 1996. A microseismic study in the western part of the Gulf of Corinth (Greece): implications for large-scale normal faulting mechanisms. Geophys. J. Int. 126, 663–688.

Rowe, C.D., Kirkpatrick, J.D., Brodsky, E.E., 2012. Fault rock injections record paleo-earthquakes. Earth Planet. Sci. Lett. 335–336, 154–166.

Rowe, C.D., Moore, J.C., Meneghini, F., McKeirnan, A.W., 2005. Large-scale pseudotachylytes and fluidized cataclasites from an ancient subduction thrust fault. Geology 33, 937–940.

Scholz, C.H., 1985. The Black Mountain asperity: Seismic hazard of the southern San Francisco Peninsula, California. Geophys. Res. Lett. 12, 717–719.

Scholz, C.H., 2002. The Mechanics of Earthquakes and Faulting. Cambridge University Press.

Scholz, C.H., 2010. Large Earthquake Triggering, Clustering, and the Synchronization of Faults. Bull. Seism. Soc. Am. 100, 901–909.

Schultejann, P.A., 1984. The Yaqui Ridge antiform and detachment fault: Mid-Cenozoic extensional terrane west of the San Andreas Fault. Tectonics 3, 677–691.

Schwartz, S.Y., Orange, D.L., Anderson, R.S., 1990. Complex fault interactions in a restraining bend on the San Andreas Fault, southern Santa Cruz Mountains, California. Geophys. Res. Lett. 17, 1207–1210.

Selverstone, J., Axen, G.J., Luther, A., 2012. Fault localization controlled by fluid infiltration into mylonites: Formation and strength of low-angle normal faults in the midcrustal brittle-plastic transition. J. Geophys. Res. Solid Earth 117.

Shirvell, C.R., Stockli, D.F., Axen, G.J., Grove, M., 2009. Miocene-Pliocene exhumation along the west Salton detachment fault, southern California, from (U-Th)/He thermochronometry of apatite and zircon. Tectonics 28.

Sibson, R.H., 1975. Generation of Pseudotachylyte by Ancient Seismic Faulting. Geophys. J. R. Astron. Soc. 43, 775–794.

Sibson, R.H., 1985. Stopping of eartquakes ruptures at dilational fault jogs. Nature 316, 248–251.

Sibson, R.H., 1986. Earthquakes and Rock Deformation in Crustal Fault Zones. Annu. Rev. Earth Planet. Sci. 14, 149–175.

Sibson, R.H., Toy, V.G., 2006. The habitat of fault-generated pseudotachylyte: Presence vs. absence of friction-melt. Geophys. Monogr. Ser. 170, 153–166.

Smith, D.A., Goodwin, L.B., Feinberg, J.M., Ellis, A.P., 2012. Pseudotachylyte: Reading the Record of Paleoseismicity in Low-Angle Normal Faults. Present. 2012 Fall Metting Agu San Francisco Calif 3-7 Dec T13E–2672.

Smith, S. A. F., Faulkner, D.R., 2010. Laboratory measurements of the frictional properties of the Zuccale low-angle normal fault, Elba Island, Italy. J. Geophys. Res. Solid Earth 115.

Sorel, D., 2000. A Pleistocene and still-active detachment fault and the origin of the Corinth-Patras rift, Greece. Geology 28, 83–86.

Spray, J.G., 1987. Artificial generation of pseudotachylyte using friction welding apparatus: simulation of melting on a fault plane. J. Struct. Geol. 9, 49–60.

Spray, J.G., 1992. A physical basis for the frictional melting of some rock-forming minerals. Tectonophysics 204, 205–221.

Spray, J.G., 2010. Frictional Melting Processes in Planetary Materials: From Hypervelocity Impact to Earthquakes. Annu. Rev. Earth Planet. Sci. 38, 221–254.

Steely, A.N., 2006. The evolution from late Miocene west Salton detachment faulting to cross- cutting Pleistocene oblique strike-slip faults in the SW Salton Trough, southern California (M.S. thesis). Utah State University, Logan, UT.

Steely, A.N., Janecke, S.U., Dorsey, R.J., Axen, G.J., 2009. Early Pleistocene initiation of the San Felipe fault zone, SW Salton Trough, during reorganization of the San Andreas fault system. Geol. Soc. Am. Bull. 121, 663–687.

Steltenpohl, M.G., Moecher, D., Andresen, A., Ball, J., Mager, S., Hames, W.E., 2011. The Eidsfjord shear zone, Lofoten–Vesterålen, north Norway: An Early Devonian, paleoseismogenic low-angle normal fault. J. Struct. Geol. 33, 1023–1043.

Stock, J.M., Hodges, K.V., 1989. Pre-Pliocene Extension around the Gulf of California and the transfer of Baja California to the Pacific Plate. Tectonics 8, 99–115.

Thatcher, W., Hill, D.P., 1991. Fault orientations in extensional and conjugate strike-slip environments and their implications. Geology 19, 1116–1120.

Toy, V.G., Ritchie, S., Sibson, R.H., 2011. Diverse habitats of pseudotachylytes in the Alpine Fault Zone and relationships to current seismicity. Geol. Soc. Lond. Spec. Publ. 359, 115–133.

Tsutsumi, A., 1999. Size distribution of clasts in experimentally produced pseudotachylytes. J. Struct. Geol. 21, 305–312.

Ujiie, K., Yamaguchi, H., Sakaguchi, A., Toh, S., 2007. Pseudotachylytes in an ancient accretionary complex and implications for melt lubrication during subduction zone earthquakes. J. Struct. Geol. 29, 599–613.

Viganò, A., Tumiati, S., Recchia, S., Martin, S., Marelli, M., Rigon, R., 2011. Carbonate pseudotachylytes: evidence for seismic faulting along carbonate faults. Terra Nova 23, 187–194.

Wang, C., 1997. A microstructural study on pseudotachylytes and microbreccias from the Whipple low-angle normal fault. Geol. Soc. Am. Abstr. Programs 29, 72–73.

Wenk, H.-R., Johnson, L.R., Ratschbacher, L., 2000. Pseudotachylites in the Eastern Peninsular Ranges of California. Tectonophysics 321, 253–277.

Wernicke, B., 1981. Low-angle normal faults in the Basin and Range Province: Nappe tectonics in an extending orogen. Nature 291, 645–648.

Wernicke, B., 1992. Cenozoic extensional tectonics of the U.S. Cordillera, in: Burchfiel, B., Lipman, P.W., Zoback, M.L. (Eds.), The Cordilleran Orogen: Conterminous U.S., The Geology of North America. Geological Society of America, Boulder, Colorado, pp. 553–582.

Wernicke, B., 1995. Low-angle normal faults and seismicity: A review. J. Geophys. Res. Solid Earth 100, 20159–20174.

Wernicke, B., Axen, G.J., 1988. On the role of isostasy in the evolution of normal fault systems. Geology 16, 848–851.

White, J.C., 2012. Paradoxical pseudotachylyte – Fault melt outside the seismogenic zone. J. Struct. Geol. 38, 11–20.

Winker, C.D., Kidwell, S.M., 1996. Stratigraphy of a marine rift basin: Neogene of the western Salton Trough, California, in: Abbott, P.L., Cooper, J.D. (Eds.), Field Conference Guidebook and Volume for the Annual Convention, San Diego, California, May 1996. American Association of Petroleum Geologists, Pacific Section, pp. 295–336.

Wong, M.S., Gans, P.B., 2008. Geologic, structural, and thermochronologic constraints on the tectonic evolution of the Sierra Mazatán core complex, Sonora, Mexico: New insights into metamorphic core complex formation. Tectonics 27.

Zechmeister, M.S., Ferré, E.C., Cosca, M.A., Geissman, J.W., 2007. Slow and fast deformation in the Dora Maira Massif, Italian Alps: Pseudotachylytes and inferences on exhumation history. J. Struct. Geol. 29, 1114–1130.

Zhang, J., Liu, S., Zheng, Y., Chen, J., Shi, Q., Yu, X., Xue, L., 1998. Raman spectral analysis and genetic mechanism of pseudotachylyte in Xiaoqinling detachment fault. Sci. China Ser. Earth Sci. 41, 242–247.

CHAPTER 5

USE OF A 3D CAMERA IN MESOSCALE GEOLOGIC INVESTIGATIONS: A

CASE STUDY USING THE WINDOWS KINECT[TM]

Abstract

Accurate and rapid three-dimensional analyses and characterization of geologic and paleontologic features is critical for a range of geologic studies. Many studies have employed terrestrial Light detection and Ranging (LiDAR) to characterize geologic features at high precision (< 1 cm-scale). Geologic features are also studied in three-dimensions at the microscale using a variety of surface metrology techniques with very high precision (μm-Å) depending on the method used. Many of these methods however, require significant funding, are time consuming, or technically, logistically, and analytically challenging to obtain. Infrared-range cameras are employed in a variety of commercial applications and are capable of making detailed three-dimensional measurements ($\leq$ 1 mm resolution). Here we use an inexpensive and user-friendly infrared range camera developed for use as an active gaming device (Windows Kinect[TM]) to demonstrate its utility as a light-weight and inexpensive tool for characterizing geologic features in three dimensions. We discuss the advantages and limitations of this new method for use in the earth sciences with data sets of highly-polished and striated fault surfaces, liquefied Quaternary sediments, and Paleoproterozoic shatter cones.

Introduction

Three-dimensional analysis of mesoscale deformational and sedimentary structures, trace and body fossils, grain roughness in river beds, and stratigraphic relationships in paleoseismology investigations are commonly needed to quantify geologic relationships (McCalpin, 1996; Rockwell and Ben-Zion, 2007; Bates et al., 2008; Gunga et al., 2008; Heritage and Milan, 2009; Hecht, 2009; Platt et al., 2010; Pearce et al., 2011; Hohenthal et al., 2011; Wang et al., 2011; Stoinski, 2011). These measurements are often time consuming, challenging to set up, and can be expensive to obtain and process. Many studies have employed ground-based Light Detection and Ranging (LiDAR) and terrestrial laser scanning (TLS) to characterize landforms, structures and fracture networks, and sedimentary structures in three-dimensions (Bellian et al., 2005; Sagy et al., 2007; Buckley et al., 2008; McCaffrey et al., 2008; Armesto et al., 2009; Buckley et al., 2010; Enge et al., 2010; Brodsky et al., 2011; Pearce et al., 2011; Nelson et al., 2011; Candela and Renard, 2012; Jessop et al., 2012). Terrestrial LiDAR has greatly improved the speed, accuracy, and capabilities of studies collecting 3d data, and has become a standard tool in a variety of geologic studies. Similarly, a variety of surface metrology technologies can be used to characterize the microscale topography of geologic materials (Power et al., 1987; Power and Tullis, 1991; Luettge et al., 1999; Fischer and Gaupp, 2004; Renard et al., 2006; Liittge and Arvidson, 2008; Candela et al., 2009, 2011; Croizé et al., 2010; Hadizadeh et al., 2012; Di Toro et al., 2012; Renard et al., 2012; Siman-Tov et al., 2013). Because these laboratory based

surface metrology tools are limited to small-area samples (< 10 cm x 10 cm) their utility is reduced. Here we present the use of a high-resolution (± 1 mm-75 mm depth resolution depending on the distance to the detector), portable, and low-cost 3D camera that is capable of capturing data from large areas (10s m^2).

The Microsoft Kinect™ sensor, was developed for rapid human-pose recognition utilizes triangulation of a project infrared array and electronic speckle pattern interferometry to produce 3D images, and has recently been proposed for use in the geological sciences (Mankoff and Russo, 2012; Khoshelham and Elberink, 2012; Gonzalez-Jorge et al., 2013; Smisek et al., 2013). We present several examples of geologic applications for the use of the Kinect™ and similar infrared range cameras. The portability, low cost, high resolution, and versatility of infrared range cameras provide an additional tool to investigate geologic features and processes in three dimensions.

Methods

The Microsoft Kinect™ consists of a laser-based pattern projector that uses a wave length of 830 nm, an RGB digital camera, an infrared (IR) camera, accelerometer, microphone array, and tilt motor (Menna et al., 2011; Mankoff and Russo, 2012; Gonzalez-Jorge et al., 2013). The IR projector emits a pattern of dots onto the target; this pattern is recorded by the IR camera and referenced to a calibrated pattern for depth calculations using methods described in Zalevsky et al. (2007), Garcia et al. (2008), and Menna et al. (2011). The point-cloud data can then be combined with the RGB image and a 3D image with true color can be generated (Khoshelham and Elberink, 2012).

Measurment error from ≤ 1 to 75 mm depends on the distance from the sensor to the sample, with the greatest precision when the sensor is approximately 1 m from the sample (Menna et al., 2011; Mankoff and Russo, 2012; Khoshelham and Elberink, 2012; Gonzalez-Jorge et al., 2013).

Public and proprietary software packages are available for capturing and manipulating 3D point cloud data from the Kinect™ (Mankoff and Russo, 2012; Gonzalez-Jorge et al., 2013). For this study we use several software packages which use the Microsoft Kinect™, OpenNI, and SensorKinect software development packages to capture and edit 3D point cloud and RGB data (KScan3D 1.0 and Kinect Fusion). We use the original calibration of the Kinect^{TM} provided by Microsoft, Inc., for the measurements obtained during this study; however, several other calibration methods have been developed by other workers (Herrera et al., 2011; Smisek et al., 2013).

Limitations

Because the resolution, precision, and x-y dimensions of the point cloud data are dependent on the distance of the device from the surface being measured care must be taken to collect data from a consistent distance (Mankoff and Russo, 2012; Khoshelham and Elberink, 2012; Smisek et al., 2013; Gonzalez-Jorge et al., 2013). The optimum resolution and precision of the instrument is satisfied when the detector is approximately 1 m from the sample (Mankoff and Russo, 2012; Gonzalez-Jorge et al., 2013). This relatively short distance limits the use of this technique to studies where features are easily assessable. Because the Kinect™ method is dependent on a static pattern that is

referenced to a known pattern projected onto a planar surface (Zalevsky et al., 2007; Menna et al., 2011), the precision and resolution can vary considerable within a single image depending on the variability in topography (Menna et al., 2011; Khoshelham and Elberink, 2012; Gonzalez-Jorge et al., 2013; Smisek et al., 2013). The method is also limited to measurements that are in direct line of sight of the detector. These limitations are easily mitigated by capturing overlapping images that can be combined in to single models of the object being studied. For practical purposes and measurement calibration we recommend adding 'targets' of known size. These targets allow for easy alignment of multiple images and provide additional length scales to measurements.

The final and most challenging limitation of the method is that the infrared detector cannot distinguish the return signal well when there are other sources of infrared radiation in the environment. For example the detector will not collect data in bright sunlight (Mankoff and Russo, 2012) when outcrops are warmed by sunlight. This difficulty can be overcome by conducting field studies when direct sunlight is not shinning on the outcrop (or specimen) of interest, or in the early morning.

Example data sets

We present three different applications of the methodology to test the limits of the technique and to illustrate the utility to structural geology, sedimentology, geomorphology and impact geology. The geologic features range from hand samples to outcrops over tens of meters long and include unusually smooth as well as rough and

complex interpenetrating surfaces. Examples from the literature expand the possible applications of the method for future studies.

Fault Highly Polished Slip Surfaces

Numerous studies have examined the meso- to microscale topography and roughness of large, exposed, fault-slip surfaces using a variety of methods including ground-based LiDAR and surface metrology techniques (Power et al., 1987; Power and Tullis, 1992; Renard et al., 2006; Sagy et al., 2007; Sagy and Brodsky, 2009; Jones et al., 2009; Candela et al., 2009, 2011; Bistacchi et al., 2011; Brodsky et al., 2011; Candela and Renard, 2012; Niemeijer et al., 2012; Siman-Tov et al., 2013). Understanding the micro- to mesoscale topography of fault slip-surfaces has important implications for determining the slip processes and the evolution of fault-related rocks, earthquake triggering, and constraining the energy budget of seismicity (Power et al., 1987; O'Hara, 2005; Sagy et al., 2007; Sagy and Brodsky, 2009; Candela et al., 2011; Niemeijer et al., 2012; Marshall and Morris, 2012). We use the Kinect™ to examine micro- to mesoscale topography of fault slip surfaces along the Wasatch fault (Fig. 5-1). We use point cloud data and RGB images from the Kinect™ to generate detailed 3d maps of numerous fault slip-surfaces and obtain an average roughness and curvature.

Wasatch Fault slip surfaces

The 350-km-long Wasatch fault is the longest normal fault of the Intermountain Seismic Belt. The Wasatch fault consists of 10 segments, and defines part of the eastern
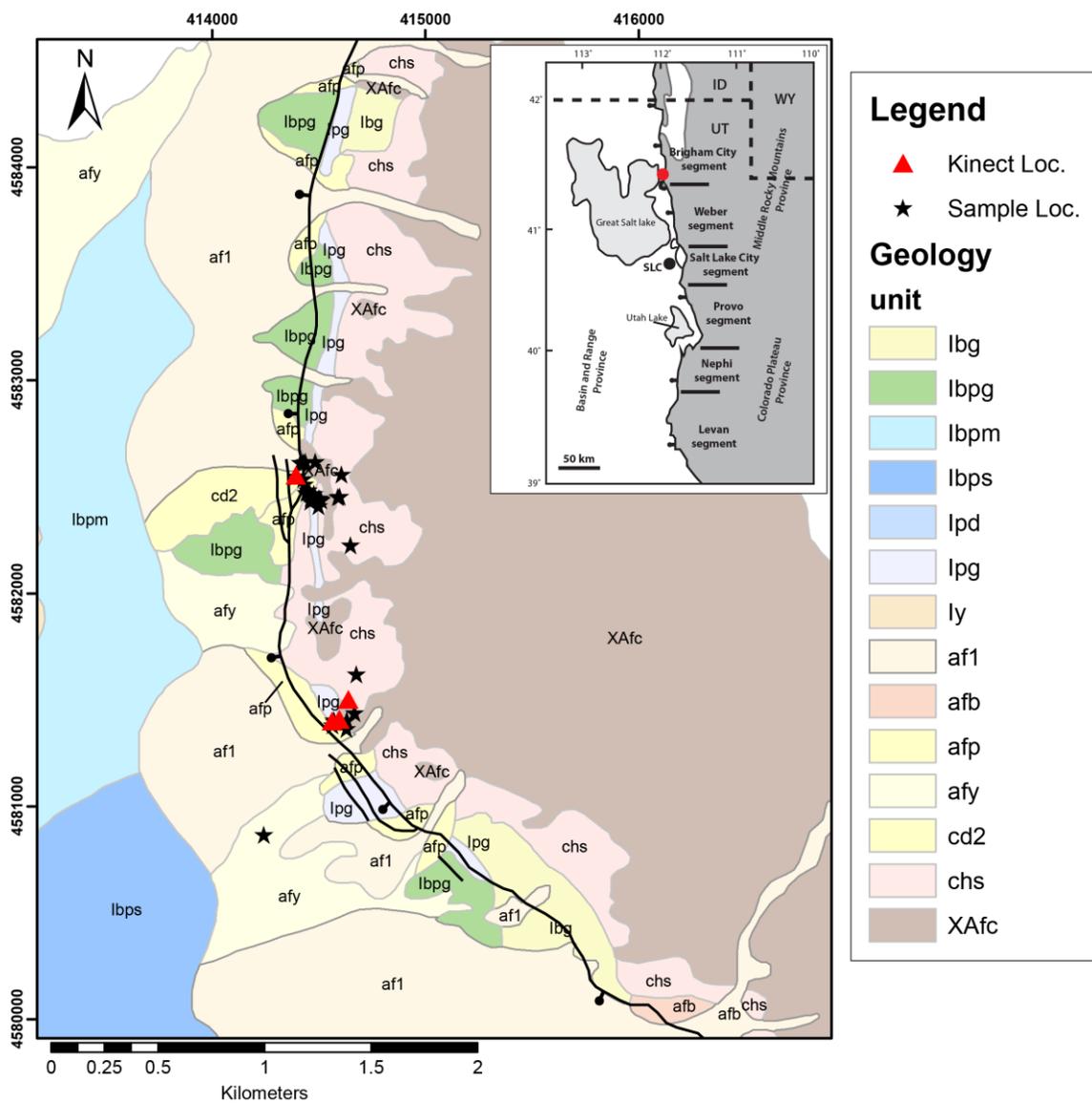
edge of the Basin and Range province (Schwartz and Coppersmith, 1984; Machette et al., 1991; Friedrich et al., 2003; Armstrong et al., 2004; DuRoss, 2008). Segments have been delineated based on microseismic, paleoseismic, and geologic mapping data (Schwartz and Coppersmith, 1984; Machette et al., 1991; DuRoss, 2008; DuRoss et al., 2012). Individual rupture events are sometimes limited to a single segment and boundaries between segments can be barriers to lateral propagation of earthquake ruptures (Machette et al., 1991; DuRoss, 2008). The Wasatch fault may have begun to slip as early as 17 Ma, with between 4-11 km of exhumation in portions of the footwall (Parry and Bruhn, 1987), and an average exhumation rate of 0.5 to 0.7 mm/yr (Friedrich et al., 2003).

Previous work along the Brigham City segment of the Wasatch fault has documented the presence of highly polished and striated slip surfaces associated with the footwall damage zone of the Wasatch fault (Fig. 5-2) (Evans and Langrock, 1994; Jensen and King, 1999). Based on data collected by Evans and Langrock (1994) and Prante et al. (in prep), and data presented here, these highly polished slip surfaces are composed of hematite and quatrzofeldspathic fault gouge, are composed of very fine grained hematite (< 1-10 µm), have metallic luster, contain multiple slip indicators (slickensides), and are the result of seismic slip (Chapter 3). The metallic highly polished slip surfaces reported by Evans and Langrock (1994) formed in the quartzo-feldspathic gneiss of the Farmington Canyon Complex and are associated with numerous, < 1 mm to 1 cm thick, curved hematite veins (Fig. 5-2B) (Evans and Langrock, 1994; Chapter 3). It has been postulated that these
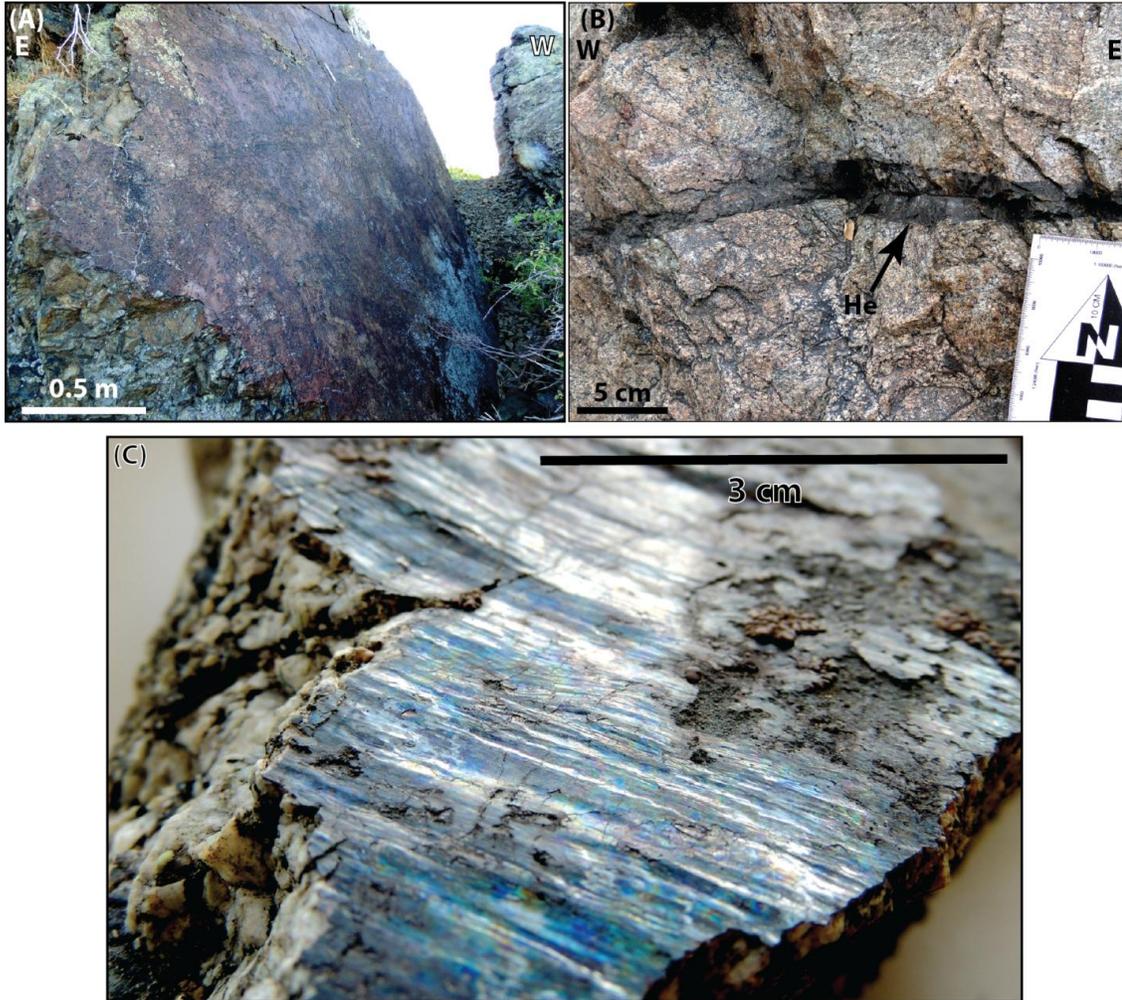
Figure 5-2: Photographs of field localities and hand samples of fault surfaces from the Wastach fault zone. A) Large (10s m^2) exposure of very planer fault surface. B) Curved hematite (He) rich vein in the footwall damage zone of the Wasatch fault. C) Photograph of hematite rich and slip surfaces with iridescent-metallic luster.

hematite veins acted as pre-existing planes of weakness during subsequent earthquakes and resulted in the formation of the iridescent highly-polished slip surfaces (Evans and Langrock, 1994; Chapter 3).

Micro- to Mesoscale topography of fault Slip Surfaces

Seven highly-polished slip surfaces that between 0.5 m^2 to 3 m^2 were analyzed using the Kinect^{TM} and digital elevation models were generated from these point cloud data (Fig. 5-3). Several slip-parallel and slip-perpendicular scans were then extracted from the DEMs for roughness analyses. These 2D profiles were used to describe the roughness of fault surfaces parallel and perpendicular to slip at a mm-scale resolution (Renard et al., 2006; Sagy et al., 2007; Candela et al., 2009; Brodsky et al., 2011; and many others).

Shatter Cones

Shatter cones are distinctive penetrative deformation structures associated with impact structures that point upward and inward toward the site of the impact (Sagy et al., 2002; Wieland et al., 2006; French and Koeberl, 2010). Shatter cones are excellent evidence for shock-related, local deformation and form at multiple scales in regions that have experience shock deformation (French and Koeberl, 2010). Shatter cones are the only convincing evidence for ancient impact related deformation in the field (French and Koeberl, 2010); however, there has not been a systematic morphologic description of shatter cones that can be used to distinguish impact-related shatter cones from similar non-impact structures, such as cone-in-cone structures found in
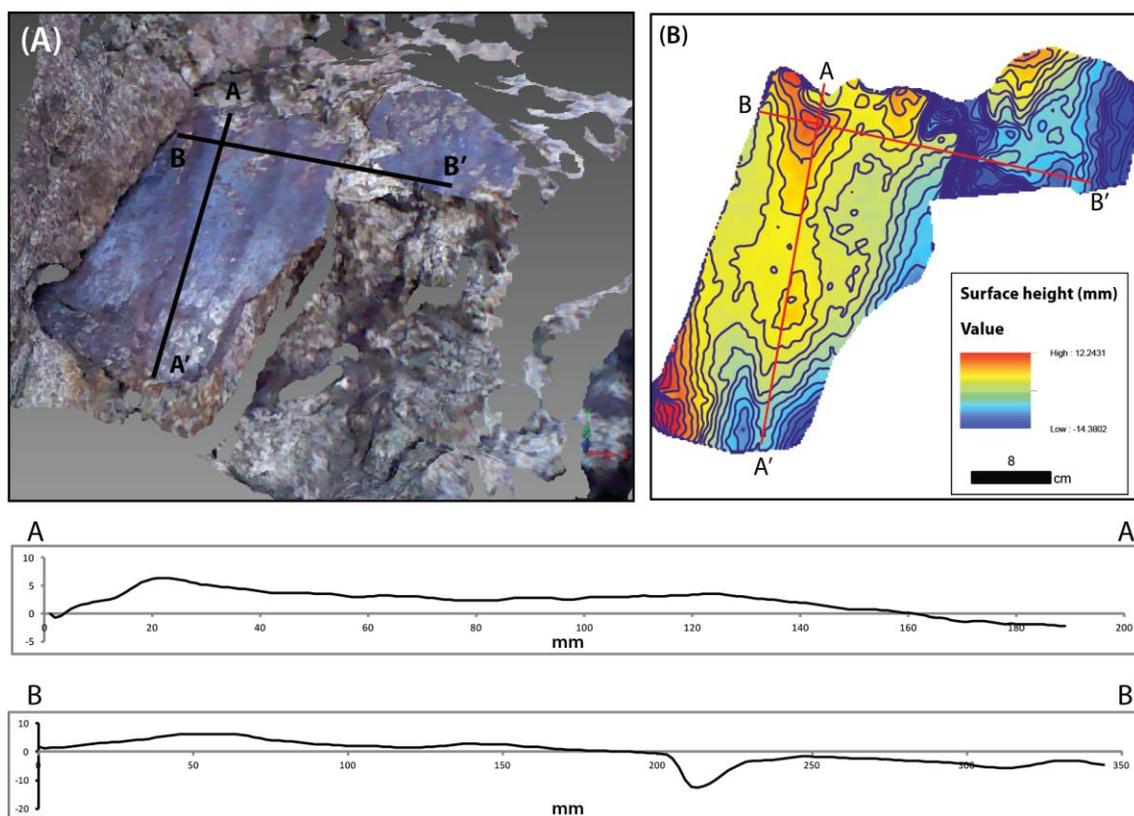
Figure 5-3: A) Point cloud data combined with RGB image of fault surface from Wasatch fault. Note areas with poor data return and large regions that are not of interest (fault zone). B) digital elevation model (DEM) generated from sub-sample of scan in (A) (contour interval = 1 mm). Profiles A-A' and B-B' were extracted from the DEM in the slip perpendicular and slip parallel directions.

sedimentary rocks (Fairbridge and Rampino, 2003). Several studies have used detailed scaling relationships of shatter cones from the meso- to micro-scale to describe the formation mechanisms of shatter cones during impact deformation (Sagy et al., 2002; Wieland et al., 2006; Salameh et al., 2008).

The potential use of detailed measurements from the m- to mm-scale and a lack of a good quantitative description of shatter cone morphology make shatter cones an ideal target for study using the Kinect[TM] (Fig. 5-4). The 3D data collected by the Kinect[TM] could be used in a variety of applications including describing the scaling relationships of shatter cones, length to width ratios, average cone volume, average cone spacing, cone orientation, and roughness of fractures (Fig. 5-4).
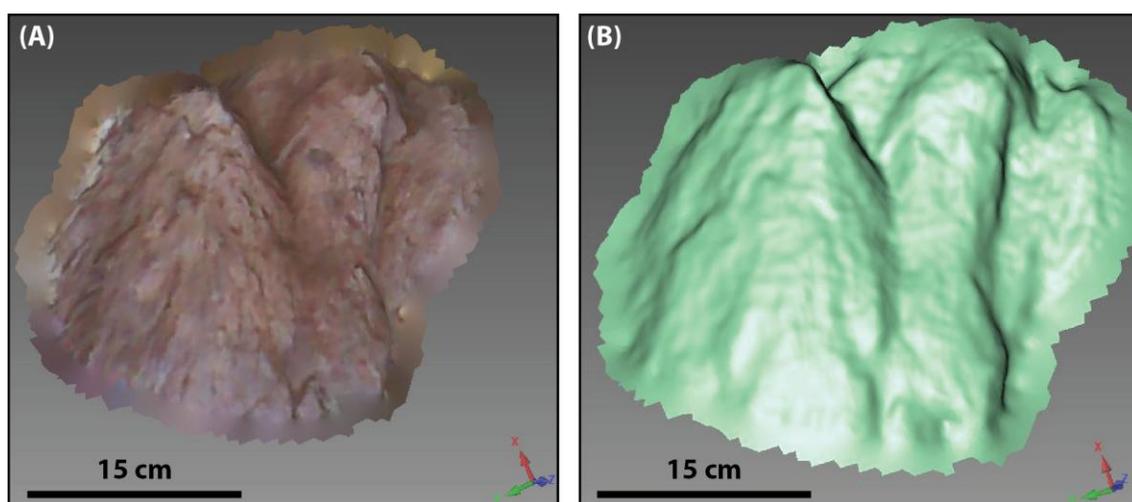
Figure 5-4: Point cloud and RGB data of shatter cone from Beaverhead impact structure (Collected by Susanne U. Janecke).

Geomorphic and sedimentologic structures

The technology can be used to rapidly acquire data from excavated or natural exposures of sedimentological and structural features for geomorphic and neotectonic analyses. We used the Kinect[TM] to depict a set of structures and sedimentary units that were liquefied during paleoearthquakes on the adjacent East Cache fault located in north-

central Utah (McCalpin, 1994; Oaks et al., 1999, 2005; Janecke et al., 2013). The exceptional ~100 m x 10 m exposure of syn-tectonic sediments and faults was partially exposed in a gravel quarry and was excavated, logged and interpreted as part of an ongoing research project focused on the paleo-seismology of the East Cache fault (Fig. 5-5). Having reliably referenced 3D data allows for a more complete description of the deformation, fault and fold orientation, clast shape and size analysis, clast orientation analysis, and descriptions of sedimentary structures (Fig. 5-5). These descriptions can then be used to construct more informed models for the origin of complex structures like the ones observed associated with the East Cache fault.

Paleontology

Three dimensional characterization is used in a variety of applications in paleontology and paleobiology (Bates et al., 2008, 2009; Hecht, 2009; Platt et al., 2010). Three dimensional characterization of articulated dinosaur specimens has been used as an integral step in estimating the mass of individual specimens (Gunga et al., 2008; Bates et al., 2009; Stoinski, 2011). Similarly terrestrial LiDAR has also been employed to characterized dinosaur trackways (Bates et al., 2008). We propose that the Kinect™ represents a reasonable low-cost replacement for LiDAR in such applications.
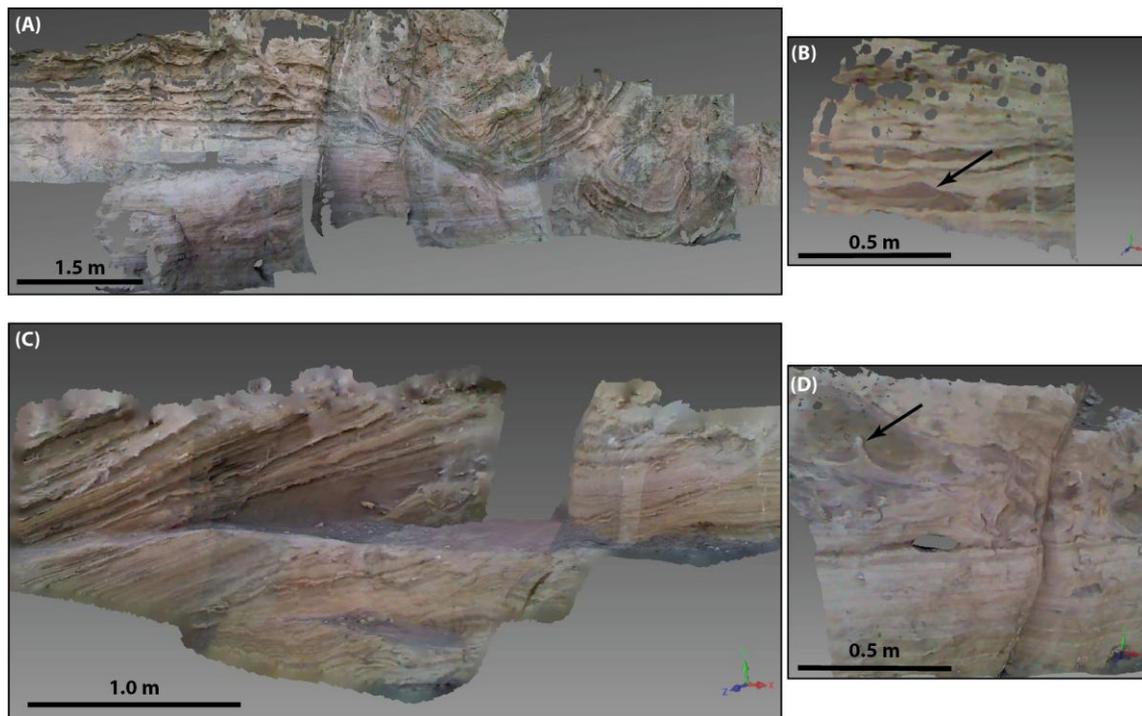
Figure 5-5: 3D models generated from point cloud data collect with the Kinect[TM] in deformed deltaic sand of Lake Bonneville in the the hanging wall of the East Cache fault. (A) Image of composite 3D mesh of outcrop with numerous cross-cutting sedimentary structures and several faults 10's of meters west of the East Cache fault. The composite was generated from > 20 overlapping scans. (B) Symmetric ripples (arrow) in poorly consolidated deltaic sands. (C) Planer cross-bedding. (D) Planer-laminated fine-grained sands and flame structure (arrow).

Geoscience education

The application of 3D data sets and interactive tools in geosciences education are now possible with terrestrial LiDAR and similar tools (McCaffrey et al., 2005, 2008). However, as has been discussed previously the use of terrestrial LiDAR systems is often

difficult and not cost effective (McCaffrey et al., 2005; Buckley et al., 2008; Mankoff and Russo, 2012). The low-cost, ease of use, and integration of RGB imagery makes the Kinect™ an ideal tool for generating 3D models for education and demonstration purposes. Because the Kinect™ was originally designed for rapid human-pose detection (Zalevsky et al., 2007; Henry et al., 2012; Khoshelham and Elberink, 2012), it can also be used as an interface tool for students to manipulate data (Cheong et al., 2012; Richards-Rissetto et al., 2012).

Discussion and Conclusions

We demonstrate the usefulness of the Windows Kinect™ in collecting high-resolution and low-cost metrology tool for the earth sciences. This tool is easily implemented and allows for the collection of high-quality 3D data sets and can be applied to a variety of geosciences applications including: structural geology (Renard et al., 2006; Candela et al., 2009; Pearce et al., 2011), geomorphology (Bellian et al., 2005; Armesto et al., 2009; Brodu and Lague, 2012), flow modeling (McCaffrey et al., 2005; Nelson et al., 2011), paleontology (Bates et al., 2008, 2009; Stoinski, 2011), sedimentary geology (Bellian et al., 2005), geosciences education (McCaffrey et al., 2008), glaciology, and many additional analyses that would benefit from accurate 3D characterization.

References

Armesto, J., Ordóñez, C., Alejano, L., and Arias, P., 2009, Terrestrial laser scanning used to determine the geometry of a granite boulder for stability analysis purposes: Geomorphology, v. 106, no. 3–4, p. 271–277, doi: 10.1016/j.geomorph.2008.11.005.

Armstrong, P.A., Taylor, A.R., and Ehlers, T.A., 2004, Is the Wasatch fault footwall (Utah, United States) segmented over million-year time scales?: Geology, v. 32, p. 385, doi: 10.1130/G20421.1.

Bates, K.T., Manning, P.L., Hodgetts, D., and Sellers, W.I., 2009, Estimating mass properties of dinosaurs using laser imaging and 3D computer modelling: PloS one, v. 4, no. 2, p. e4532, doi: 10.1371/journal.pone.0004532.

Bates, K.T., Rarity, F., Manning, P.L., Hodgetts, D., Vila, B., Oms, O., Galobart, À., and Gawthorpe, R.L., 2008, High-resolution LiDAR and photogrammetric survey of the Fumanya dinosaur tracksites (Catalonia): Implications for the conservation and interpretation of geological heritage sites: Journal of the Geological Society, v. 165, no. 1, p. 115–127, doi: 10.1144/0016-76492007-033.

Bellian, J.A., Kerans, C., and Jennette, D.C., 2005, Digital outcrop models: applications of terrestrial scanning lidar technology in stratigraphic modeling: Journal of Sedimentary Research, v. 75, no. 2, p. 166–176, doi: 10.2110/jsr.2005.013.

Bistacchi, A., Griffith, W.A., Smith, S.A.F., Toro, G.D., Jones, R., and Nielsen, S., 2011, Fault roughness at seismogenic depths from LIDAR and photogrammetric Analysis: Pure and Applied Geophysics, v. 168, no. 12, p. 2345–2363, doi: 10.1007/s00024-011-0301-7.

Brodsky, E.E., Gilchrist, J.J., Sagy, A., and Collettini, C., 2011, Faults smooth gradually as a function of slip: Earth and Planetary Science Letters, v. 302, no. 1–2, p. 185–193, doi: 10.1016/j.epsl.2010.12.010.

Brodu, N., and Lague, D., 2012, 3D terrestrial lidar data classification of complex natural scenes using a multi-scale dimensionality criterion: Applications in geomorphology: ISPRS Journal of Photogrammetry and Remote Sensing, v. 68, p. 121–134, doi: 10.1016/j.isprsjprs.2012.01.006.

Buckley, S.J., Enge, H.D., Carlsson, C., and Howell, J.A., 2010, Terrestrial laser scanning for use in virtual outcrop geology: The Photogrammetric Record, v. 25, no. 131, p. 225–239, doi: 10.1111/j.1477-9730.2010.00585.x.

Buckley, S.J., Howell, J.A., Enge, H.D., and Kurz, T.H., 2008, Terrestrial laser scanning in geology: data acquisition, processing and accuracy considerations: Journal of the Geological Society, v. 165, no. 3, p. 625–638, doi: 10.1144/0016-76492007-100.

Candela, T., and Renard, F., 2012, Segment linkage process at the origin of slip surface roughness: Evidence from the Dixie Valley fault: Journal of Structural Geology, v. 45, p. 87–100, doi: 10.1016/j.jsg.2012.06.003.

Candela, T., Renard, F., Bouchon, M., Brouste, A., Marsan, D., Schmittbuhl, J., and Voisin, C., 2009, Characterization of fault roughness at various scales: Implications of three-dimensional high resolution topography measurements: Pure and Applied Geophysics, v. 166, no. 10-11, p. 1817–1851, doi: 10.1007/s00024-009-0521-2.

Candela, T., Renard, F., Schmittbuhl, J., Bouchon, M., and Brodsky, E.E., 2011, Fault slip distribution and fault roughness: Geophysical Journal International, v. 187, no. 2, p. 959–968, doi: 10.1111/j.1365-246X.2011.05189.x.

Cheong, S.N., Yap, W.J., Logeswaran, R., and Chai, I., 2012, Design and development of kinect-based Technology-Enhanced Teaching Classroom, *in* Park, J.J. Jong H., Jeong, Y.-S., Park, S.O., and Chen, H.-C., eds., Embedded and Multimedia Computing Technology and Service, Lecture Notes in Electrical Engineering 181, Springer Netherlands, p. 179–186.

Croizé, D., Renard, F., Bjørlykke, K., and Dysthe, D.K., 2010, Experimental calcite dissolution under stress: Evolution of grain contact microstructure during pressure solution creep: Journal of Geophysical Research: Solid Earth, v. 115, no. B9, doi: 10.1029/2010JB000869.

DeCelles, P.G., and Giles, K.A., 1996, Foreland basin systems: Basin Research, v. 8, no. 2, p. 105–123, doi: 10.1046/j.1365-2117.1996.01491.x.

Di Toro, G., Mittempergher, S., Ferri, F., Mitchell, T.M., and Pennacchioni, G., 2012, The contribution of structural geology, experimental rock deformation and numerical modelling to an improved understanding of the seismic cycle: Preface to the Special Volume "Physico-chemical processes in seismic faults:" Journal of Structural Geology, v. 38, p. 3–10, doi: 10.1016/j.jsg.2012.01.025.

DuRoss, C.B., 2008, Holocene vertical displacement on the Central Segments of the Wasatch Fault Zone, Utah: Bulletin of the Seismological Society of America, v. 98, no. 6, p. 2918–2933, doi: 10.1785/0120080119.

DuRoss, C.B., Personius, S.F., Crone, A.J., McDonald, G.N., Briggs, R.W., and Utah Geological Survey, 2012, Late Holocene earthquake history of the Brigham City segment of the Wasatch Fault zone at the Hansen Canyon, Kotter Canyon, and Pearsons Canyon trench sites, Box Elder County, Utah: Utah Geological Survey, Salt Lake City, Utah.

Enge, H.D., Howell, J.A., and Buckley, S.J., 2010, The geometry and internal architecture of stream mouth bars in the Panther Tongue and the Ferron Sandstone Members, Utah, U.S.A.: Journal of Sedimentary Research, v. 80, no. 11, p. 1018–1031, doi: 10.2110/jsr.2010.088.

Evans, J.P., and Langrock, H., 1994, Structural analysis of the Brigham City-Weber segment boundary zone, Wasatch normal fault, Utah: implications for fault growth and structure: Pageoph, v. 142, p. 663–685.

Fairbridge, L., and Rampino, M., 2003, Diagenetic Structures, *in* Middleton, G.V. ed., Encyclopedia of Sediments and Sedimentary Rocks, Kluwer Academic Publishers, p. 219–225.

Fischer, C., and Gaupp, R., 2004, Multi-scale rock surface area quantification—a systematic method to evaluate the reactive surface area of rocks: Chemie der Erde - Geochemistry, v. 64, no. 3, p. 241–256, doi: 10.1016/j.chemer.2003.12.002.

French, B.., and Koeberl, C., 2010, The convincing identification of terrestrial meteorite impact structures: What works, what doesn't, and why: Earth-Science Reviews, v. 98, p. 123–170, doi: 10.1016/j.earscirev.2009.10.009.

Friedrich, A.M., Wernicke, B.P., Niemi, N.A., Bennett, R.A., and Davis, J.L., 2003, Comparison of geodetic and geologic data from the Wasatch region, Utah, and implications for the spectral character of Earth deformation at periods of 10 to 10 million years: Journal of Geophysical Research: Solid Earth, v. 108, no. B4, doi: 10.1029/2001JB000682.

Garcia, J., Zalevsky, Z., Garcia-Martinez, P., Ferreira, C., Teicher, M., and Beiderman, Y., 2008, Three-dimensional mapping and range measurement by means of projected speckle patterns: Applied Optics, v. 47, p. 3032–3040, doi: 10.1364/AO.47.003032.

Gonzalez-Jorge, H., Riveiro, B., Vazquez-Fernandez, E., Martínez-Sánchez, J., and Arias, P., 2013, Metrological evaluation of Microsoft Kinect and Asus Xtion sensors: Measurement, v. 46, no. 6, p. 1800–1806, doi: 10.1016/j.measurement.2013.01.011.

Gunga, H.-C., Suthau, T., Bellmann, A., Stoinski, S., Friedrich, A., Trippel, T., Kirsch, K., and Hellwich, O., 2008, A new body mass estimation of Brachiosaurus brancai Janensch, 1914 mounted and exhibited at the Museum of Natural History (Berlin, Germany): Fossil Record, v. 11, no. 1, p. 33–38, doi: 10.1002/mmng.200700011.

Hadizadeh, J., Mittempergher, S., Gratier, J.-P., Renard, F., Di Toro, G., Richard, J., and Babaie, H.A., 2012, A microstructural study of fault rocks from the SAFOD: Implications for the deformation mechanisms and strength of the creeping segment of the San Andreas Fault: Journal of Structural Geology, v. 42, p. 246–260, doi: 10.1016/j.jsg.2012.04.011.

Hecht, J., 2009, Lasers in Paleontology: Optics and Photonics News, v. 20, no. 10, p. 28–35, doi: 10.1364/OPN.20.10.000028.

Henry, P., Krainin, M., Herbst, E., Ren, X., and Fox, D., 2012, RGB-D mapping: Using Kinect-style depth cameras for dense 3D modeling of indoor environments: The International Journal of Robotics Research, v. 31, no. 5, p. 647–663, doi: 10.1177/0278364911434148.

Heritage, G.L., and Milan, D.J., 2009, Terrestrial Laser Scanning of grain roughness in a gravel-bed river: Geomorphology, v. 113, no. 1–2, p. 4–11, doi: 10.1016/j.geomorph.2009.03.021.

Herrera, D., Kannala, J., and Heikkilä, J., 2011, Accurate and practical calibration of a depth and color camera pair, *in* Real, P., Diaz-Pernil, D., Molina-Abril, H., Berciano, A., and Kropatsch, W. eds., Computer Analysis of Images and Patterns, Lecture Notes in Computer Science 6855, Springer, Berlin Heidelberg, p. 437–445.

Hohenthal, J., Alho, P., Hyyppä, J., and Hyyppä, H., 2011, Laser scanning applications in fluvial studies: Progress in Physical Geography, v. 35, no. 6, p. 782–809, doi: 10.1177/0309133311414605.

Janecke, S.U., Oaks, R.Q., Knight, A.J., Nutt, D., and Rittenour, T.M., 2013, Large liquefaction features and evidence for earthquakes induced by Lake Bonneville in

Cache Valley: A Progress Report: Geological Society of America Abstract with Programs, v. 45, p. 711.

Jensen, M.E., and King, J.K., 1999, Geologic map of the Brigham City 7.5-minute quadrangle: Utah Geological Survey.

Jessop, D.E., Kelfoun, K., Labazuy, P., Mangeney, A., Roche, O., Tillier, J.-L., Trouillet, M., and Thibault, G., 2012, LiDAR derived morphology of the 1993 Lascar pyroclastic flow deposits, and implication for flow dynamics and rheology: Journal of Volcanology and Geothermal Research, v. 245–246, p. 81–97, doi: 10.1016/j.jvolgeores.2012.06.030.

Jones, R.R., Kokkalas, S., and McCaffrey, K.J.W., 2009, Quantitative analysis and visualization of nonplanar fault surfaces using terrestrial laser scanning (LIDAR)—The Arkitsa fault, central Greece, as a case study: Geosphere, v. 5, no. 6, p. 465–482, doi: 10.1130/GES00216.1.

Khoshelham, K., and Elberink, S.O., 2012, Accuracy and resolution of kinect depth data for indoor mapping applications: Sensors, v. 12, no. 12, p. 1437–1454, doi: 10.3390/s120201437.

Liittge, A., and Arvidson, R.S., 2008, The mineral-water interface, *in* Brantley, S.L., Kubicki, J.D., and White, A.F. eds., Kinetics of Water-Rock Interaction, Springer New York, p. 73–107.

Luettge, A., Bolton, E.W., and Lasaga, A.C., 1999, An interferometric study of the dissolution kinetics of anorthite; the role of reactive surface area: American Journal of Science, v. 299, no. 7-9, p. 652–678, doi: 10.2475/ajs.299.7-9.652.

Machette, M.N., Personius, S.F., Nelson, A.R., Schwartz, D.P., and Lund, W.R., 1991, The Wasatch fault zone, utah—segmentation and history of Holocene earthquakes: Journal of Structural Geology, v. 13, no. 2, p. 137–149, doi: 10.1016/0191-8141(91)90062-N.

Mankoff, K.D., and Russo, T.A., 2012, The Kinect: a low-cost, high-resolution, short-range 3D camera: Earth Surface Processes and Landforms, doi: 10.1002/esp.3332.

Marshall, S.T., and Morris, A.C., 2012, Mechanics, slip behavior, and seismic potential of corrugated dip-slip faults: Journal of Geophysical Research: Solid Earth, v. 117, no. B3, doi: 10.1029/2011JB008642.

McCaffrey, K.J.W., Feely, M., Hennessy, R., and Thompson, J., 2008, Visualization of folding in marble outcrops, Connemara, western Ireland: An application of virtual

outcrop technology: Geosphere, v. 4, no. 3, p. 588–599, doi: 10.1130/GES00147.1.

McCaffrey, K.J.W., Jones, R.R., Holdsworth, R.E., Wilson, R.W., Clegg, P., Imber, J., Holliman, N., and Trinks, I., 2005, Unlocking the spatial dimension: Digital technologies and the future of geoscience fieldwork: Journal of the Geological Society, v. 162, no. 6, p. 927–938, doi: 10.1144/0016-764905-017.

McCalpin, J.P., 1994, Neotectonic deformation along the East Cache fault zone, Cache County, Utah: Utah Geological Survey Special Study 83, 83 p.

McCalpin, J., 1996, Paleoseismology: Academic Press.

Menna, F., Remondino, F., Battisti, R., and Nocerino, E., 2011, Geometric investigation of a gaming active device: , p. 80850G–80850G, doi: 10.1117/12.890070.

Nelson, C.E., Jerram, D.A., Hobbs, R.W., Terrington, R., and Kessler, H., 2011, Reconstructing flood basalt lava flows in three dimensions using terrestrial laser scanning: Geosphere, v. 7, no. 1, p. 87–96, doi: 10.1130/GES00582.1.

Niemeijer, A., Di Toro, G., Griffith, W.A., Bistacchi, A., Smith, S.A.F., and Nielsen, S., 2012, Inferring earthquake physics and chemistry using an integrated field and laboratory approach: Journal of Structural Geology, v. 39, p. 2–36, doi: 10.1016/j.jsg.2012.02.018.

O'Hara, K., 2005, Evaluation of asperity-scale temperature effects during seismic slip: Journal of Structural Geology, v. 27, no. 10, p. 1892–1898, doi: 10.1016/j.jsg.2005.04.013.

Oaks, R.Q., Janecke, S.U., Langenheim, V.E., and Kruger, J.M., 2005, Insights into geometry and evolution of extensional basins along the Wasatch fault and East and West Cache fault zones, Utah and Idaho, USA: Geological Society of America Abstract with Programs, v. 37, p. 497.

Oaks, R.Q., Smith, K.A., Janecke, S.U., Perkins, M.E., and Nash, W.P., 1999, Stratigraphy and tectonics of Tertiary strata of southern Cache Valley, north-central Utah, *in* Spangler, L.E. and Allen, C.J. eds., Geology of northern Utah and vicinity, Utah Geological Association Publication 27, p. 71–110.

Parry, W.T., and Bruhn, R.L., 1987, Fluid inclusion evidence for minimum 11 km vertical offset on the Wasatch fault, Utah: Geology, v. 15, no. 1, p. 67–70, doi: 10.1130/0091-7613(1987)15<67:FIEFMK>2.0.CO;2.

Pearce, M.A., Jones, R.R., Smith, S.A.F., and McCaffrey, K.J.W., 2011, Quantification of fold curvature and fracturing using terrestrial laser scanning: AAPG Bulletin, v. 95, no. 5, p. 771–794, doi: 10.1306/11051010026.

Personius, S.F., 1990, Surficial geologic Map of the Brighan City Segment and Adjacent Parts of the Weber and Collinston Segments, Wasatch Fault Zone, Box Elder and Weber Counties, Utah: United States Geological Survey I.

Platt, B.F., Hasiotis, S.T., and Hirmas, D.R., 2010, Use of low-cost multistripe laser triangulation (MLT) scanning technology for three-dimensional, quantitative paleoichnological and neoichnological studies: Journal of Sedimentary Research, v. 80, no. 7, p. 590–610, doi: 10.2110/jsr.2010.059.

Power, W.L., and Tullis, T.E., 1991, Euclidean and fractal models for the description of rock surface roughness: Journal of Geophysical Research: Solid Earth, v. 96, no. B1, p. 415–424, doi: 10.1029/90JB02107.

Power, W.L., and Tullis, T.E., 1992, The contact between opposing fault surfaces at Dixie Valley, Nevada, and implications for fault mechanics: Journal of Geophysical Research: Solid Earth, v. 97, no. B11, p. 15425–15435, doi: 10.1029/92JB01059.

Power, W.L., Tullis, T.E., Brown, S.R., Boitnott, G.N., and Scholz, C.H., 1987, Roughness of natural fault surfaces: Geophysical Research Letters, v. 14, no. 1, p. 29–32, doi: 10.1029/GL014i001p00029.

Renard, F., Mair, K., and Gundersen, O., 2012, Surface roughness evolution on experimentally simulated faults: Journal of Structural Geology, v. 45, p. 101–112, doi: 10.1016/j.jsg.2012.03.009.

Renard, F., Voisin, C., Marsan, D., and Schmittbuhl, J., 2006, High resolution 3D laser scanner measurements of a strike-slip fault quantify its morphological anisotropy at all scales: Geophysical Research Letters, v. 33, no. 4, p. n/a–n/a, doi: 10.1029/2005GL025038.

Richards-Rissetto, H., Remondino, F., Agugiaro, G., Robertsson, J., von Schwerin, J., and Girardi, G., 2012, Kinect and 3D GIS in archaeology, *in* 2012 18th International Conference on Virtual Systems and Multimedia (VSMM), p. 331–337.

Rockwell, T.K., and Ben-Zion, Y., 2007, High localization of primary slip zones in large earthquakes from paleoseismic trenches: Observations and implications for earthquake physics: Journal of Geophysical Research: Solid Earth, v. 112, no. B10, doi: 10.1029/2006JB004764.

Sagy, A., and Brodsky, E.E., 2009, Geometric and rheological asperities in an exposed fault zone: Journal of Geophysical Research: Solid Earth, v. 114, no. B2, doi: 10.1029/2008JB005701.

Sagy, A., Brodsky, E.E., and Axen, G.J., 2007, Evolution of fault-surface roughness with slip: Geology, v. 35, no. 3, p. 283–286, doi: 10.1130/G23235A.1.

Sagy, A., Reches, Z., and Fineberg, J., 2002, Dynamic fracture by large extraterrestrial impacts as the origin of shatter cones: Nature, v. 418, p. 310–313, doi: 10.1038/nature00903.

Salameh, E., Khoury, H., Reimold, W.U., and Schneider, W., 2008, The first large meteorite impact structure discovered in the Middle East: Jebel Waqf as Suwwan, Jordan: Meteoritics & Planetary Science, v. 43, no. 10, p. 1681–1690.

Schwartz, D.P., and Coppersmith, K.J., 1984, Fault behavior and characteristic earthquakes: Examples from the Wasatch and San Andreas Fault Zones: Journal of Geophysical Research: Solid Earth, v. 89, no. B7, p. 5681–5698, doi: 10.1029/JB089iB07p05681.

Siman-Tov, S., Aharonov, E., Sagy, A., and Emmanuel, S., 2013, Nanograins form carbonate fault mirrors: Geology,, doi: 10.1130/G34087.1.

Smisek, J., Jancosek, M., and Pajdla, T., 2013, 3D with Kinect, *in* Fossati, A., Gall, J., Grabner, H., Ren, X., and Konolige, K. eds., Consumer Depth Cameras for Computer Vision, Advances in Computer Vision and Pattern Recognition, Springer London, p. 3–25.

Stoinski, S., 2011, From a Skeleton to a 3D Dinosaur, *in* Elewa, A.M.T. ed., Computational Paleontology, Springer Berlin Heidelberg, p. 147–164.

Wang, C.-K., Wu, F.-C., Huang, G.-H., and Lee, C.-Y., 2011, Mesoscale terrestrial laser scanning of fluvial gravel surfaces: IEEE Geoscience and Remote Sensing Letters, v. 8, no. 6, p. 1075–1079, doi: 10.1109/LGRS.2011.2156758.

Wieland, F., Reimold, W.U., and Gibson, R.L., 2006, New observations on shatter cones in the Vredefort impact structure, South Africa, and evaluation of current

hypotheses for shatter cone formation: Meteoritics & Planetary Science, v. 41, no. 11, p. 1737–1759.

Zalevsky, Z., Shpunt, A., Maizels, A., and Garcia, J., 2007, Method and system for object reconstruction: Patent Number WO/2007/043036.

CHAPTER 6

CONCLUSIONS

Constraining the total energy budget of earthquakes is of great importance to the earth science community (Scholz, 2002; Kanamori and Brodsky, 2004; Kanamori and Riveiro, 2006; Jacobs et al., 2006; Fagereng and Toy, 2011). Theoretical and experimental studies suggest that the majority of the energy released during earthquakes is consumed by processes in the fault zone (McGarr, 1999; Kanamori and Brodsky, 2004; Di Toro et al., 2005; Kanamori and Riveiro, 2006; Jacobs et al., 2006; Shipton et al., 2006; Tanaka et al., 2006). This energy may be consumed by fracture formation, refinement of slip surfaces, grain-size reduction, generation of frictional heat, overcoming gravity, and/or driving chemical changes (Kanamori and Brodsky, 2004; Di Toro et al., 2005; Kanamori and Riveiro, 2006; Jacobs et al., 2006). Fault zones preserve abundant evidence for the consumption of this energy in the form of brittle-deformation; however, it is difficult to draw a convincing link between this deformation and strain-rate (Sibson, 1975; Cowan, 1999; Marone and Richardson, 2010; Fagereng and Toy, 2011).

This dissertation summarizes three studies that examine deformation that resulted from the energy consumed by fault-zone processes during the earthquake cycle. This deformation includes the development of pseudotachylyte, highly-polished slip surfaces, and hydrothermal alteration products in fault zones with varied tectonic settings, depth of formation, fluid-rock interactions, and protolith compositions. We also present an

innovative tool for collecting high-resolution three-dimmensional point cloud data sets from mm- to m-scales in the earth sciences and geoscience education.

The only unequivocal evidence for ancient seismicity in the geologic record is fault-related tectonic pseudotachylyte (Cowan, 1999; Marone and Richardson, 2010; Tullis, 1994). Pseudotachylytes have been reported from a variety of tectonic environments, depths, and rock types (Sibson, 1975; Magloughlin, 1989, 2011; Magloughlin and Spray, 1992; Cowan, 1999; Wenk et al., 2000; Boullier et al., 2001; Plattner et al., 2003; Allen, 2005; Di Toro et al., 2005; Sibson and Toy, 2006; Lin, 2008; Kirkpatrick and Shipton, 2009; Bestmann et al., 2011; and many others). Despite the abundance of research focused on understanding the formation and preservation conditions of frictional melt and many studies focused on fault zones in general, pseudotachylyte is somewhat rarely reported (e.g. Sibson and Toy, 2006; Kirkpatrick et al., 2009; Kirkpatrick and Rowe, 2013). The apparent rareness of pseudotachylyte in the geologic record suggests that other processes consume 80-90% of the energy released during seismicity (Cowan, 1999; Scholz, 2002; Kanamori and Riveiro, 2006; Shipton et al., 2006; Jacobs et al., 2006).

In Chapter 2 of this work we examine outcrop to micro-scale features of pseudotachylyte, cataclastic rock, and products of hydrothermal alteration from the central Sierra Nevada, CA. This work concludes that the conditions of pseudotachylyte formation are broader than previously concluded based on the presence of hydrothermal alteration in association with pseudotachylyte (Sibson, 1975; Sibson and Toy, 2006;

Kirkpatrick et al., 2009). Additionally, the documentation of coeval or cyclic pseudotachylyte and hydrothermal alteration suggests that hydrothermal alteration is one of the processes that consumes the energy released during seismicity (Kanamori and Brodsky, 2004; Kanamori and Riveiro, 2006; Shipton et al., 2006; Tanaka et al., 2006). The coeval hydrothermal alteration records temperatures between 10-210 ˚C above the ambient temperature conditions during faulting (Kirkpatrick et al., 2012; Chapter 2). The elevated temperature conditions in the fault zone helps to constrain the total energy budget of earthquakes, and also helps to explain the lack of anomalous heat flow associated with large faults (e.g. Fulton and Saffer, 2009).

We also present a detailed analysis and a new deformation product that is diagnostic of seismic slip in the form of iridescent-metallic, Fe-rich, highly polished slip surfaces (Chapter 3; Prante et al., in prep). The connection between the low RMS-roughness, iridescence, and hematite development associated with the HPSS and high-temperatures (400-800 ˚C) is most lilely to be the result of ancient seismicity and heat generation at asperity contacts (McKenzie and Brune, 1972; Scholz, 1980, 2002; Spray, 1987; O'Hara, 2005; Han et al., 2007, 2011; Noda et al., 2011). The conclusion that some HPSS are the result of co-seismic deformation is consistent with several recent experimental and natural fault HPSS (Han et al., 2007, 2011; Noda et al., 2011; Smith et al., 2013; Siman-Tov et al., 2013).

We also present textural, compositional, and microstructural analyses of tectonic pseudotachylyte from a low-angle normal fault (Chapter 4; Prante et al., in review). This

work contributes to the debate regarding the mechanics and seismic potential of low-angle normal faults (Detachment faults) (Wernicke, 1995; Axen, 2004; Abers, 2009). The documentation of pseudotachylyte along the West Salton detachment fault, CA, provides unequivocal evidence for ancient seismicity along a low-angle normal fault when it was at a low-angle. Additionally, we provide a synthesis of additional examples of pseudotachylyte from other low-angle normal fault (Table 6-1). This synthesis concludes that seismicity is a common feature of low-angle normal fault evolution and has significant implications for the mechanics of low-angle normal faults (e.g. Wernicke, 1995; Axen, 2004; Cowan et al., 2003; Haines and van der Pluijm, 2012).

We also present (Chapter 5; Prante et al., in prep) a new method for collecting and analyzing 3D point cloud data in the geological sciences (Mankoff and Russo, 2012). We demonstrate the advantages and limitations for the use of 3D infrared range cameras in collecting high-resolution (mm-scale) point cloud data in field and laboratory in the geological sciences. We present several examples of geologic data sets collected with the low-cost and high-resolution method (Chapter 5).

The work presented in the preceding chapters shows that the enormous amounts of energy released during seismicity is consumed by a variety of processes in the brittle crust (Kanamori and Brodsky, 2004; Kanamori and Riveiro, 2006; Sibson and Toy, 2006; Shipton et al., 2006; Chapter 2, 3). The documentation of coeval pseudotachylyte generation and hydrothermal alteration along the Glacier Lakes and Granite Pass faults suggests that some of the frictional heat generated during seismicity is consumed by

hydrothermal alteration (Chapter 2; Prante et al., in prep). We also show that some

highly-polished slip surfaces are the result of ancient seismicity by linking iridescent

textures and HPSS composition to the generation of frictional heat (Chapter 3; Prante et

al., in prep). Through better understanding fault-related deformation along the West

Salton detachment fault, we conclude that some low-angle normal faults are seismically

active during portions of their evolution (Chapter 4; Prante et al., in review). This has

important implications for the mechanics of low-angle normal fault formation and the

seismic potential of active low-angle normal faults. Finally, we present the Windows

Kinect^{TM} as a low-cost and high-resolution tool for the geosciences and present several

example data sets and applications.

Table 6-1: Reported occurrences of melt-related pseudotachylyte from low-angle normal

faults and estimated depth of formation (Modified from Collettini, 2011).

LANF	Mean dip	Pseudotachylyte formation depth	Structural position of Pseudotachylyte	References
Whipple low-angle normal fault	10-15°	Poorly constrained	Footwall	(Reynolds and Lister, 1987; Lister and Davis, 1989; Wang, 1997)
South Mountains detachment fault	10-20°	~11 km	Footwall	(Davis et al., 1986; Goodwin et al., 1998, 1998; Goodwin, 1999; Smith et al., 2012)
Chemehuevi-Sacramento detachment fault	<20°	6-10 km	Footwall	(John and Cheadle, 2010; John, 1987)
Alaşehir detachment fault	10-30°	Poorly constrained	Footwall	(Işık et al., 2003)
Otago schist (Tucker Hill)	10-30°	6-12 km	Fault core	(Barker, 2005; Barker et al., 2010; Bjørnerud, 2010)
Nordfjord-Sogn detachment fault	<30°	Seismogenic zone (~6-12 km)	Footwall	(Braathen et al., 2004)
Eidsfjord detachment fault	25-30 °	Seismogenic zone (~6-12 km)	Hanging wall	(Plattner et al., 2003; Steltenpohl et al., 2011)
Xiaoqinling detachment fault	25-50°	Poorly constrained	Footwall	(Zhang et al., 1998)
West Salton detachment fault	<30°	1.1-4.25 km (poorly constrained)	Hanging wall and footwall	(Schultejann, 1984; Kairouz et al., 2003; Steely, 2006; Janecke et al., 2008; Prante et al., 2011)

References

Abers, G.A., 2009, Slip on shallow-dipping normal faults: Geology, v. 37, p. 767–768, doi: 10.1130/focus082009.1.

Allen, J.L., 2005, A multi-kilometer pseudotachylyte system as an exhumed record of earthquake rupture geometry at hypocentral depths (Colorado, USA): Tectonophysics, v. 402, p. 37–54, doi: 10.1016/j.tecto.2004.10.017.

Axen, G.J., 2004, Mechanics of low-angle normal faults, *in* Karner, G., Taylor, B., Driscoll, N.W., and Kohlstedt, D.L. eds., Rheology and deformation in the lithosphere at continental margins, New York, Columbia University Press, p. 46–91.

Bestmann, M., Pennacchioni, G., Frank, G., Göken, M., and de Wall, H., 2011, Pseudotachylyte in muscovite-bearing quartzite: Coseismic friction-induced melting and plastic deformation of quartz: Journal of Structural Geology, v. 33, p. 169–186, doi: 10.1016/j.jsg.2010.10.009.

Boullier, A.-M., Ohtani, T., Fujimoto, K., Ito, H., and Dubois, M., 2001, Fluid inclusions in pseudotachylytes from the Nojima fault, Japan: Journal of Geophysical Research: Solid Earth, v. 106, p. 21965–21977, doi: 10.1029/2000JB000043.

Chester, F.M., Evans, J.P., and Biegel, R.L., 1993, Internal structure and weakening mechanisms of the San Andreas Fault: Journal of Geophysical Research: Solid Earth, v. 98, p. 771–786, doi: 10.1029/92JB01866.

Cowan, D.S., 1999, Do faults preserve a record of seismic slip? A field geologist's opinion: Journal of Structural Geology, v. 21, p. 995–1001, doi: 10.1016/S0191-8141(99)00046-2.

Cowan, D.S., Cladouhos, T.T., and Morgan, J.K., 2003, Structural geology and kinematic history of rocks formed along low-angle normal faults, Death Valley, California: Geological Society of America Bulletin, v. 115, p. 1230–1248, doi: 10.1130/B25245.1.

Di Toro, G., Nielsen, S., and Pennacchioni, G., 2005, Earthquake rupture dynamics frozen in exhumed ancient faults: Nature, v. 436, p. 1009–1012, doi: 10.1038/nature03910.

Fagereng, A., and Toy, V.G., 2011, Geology of the earthquake source: an introduction: Geological Society, London, Special Publications, v. 359, p. 1–16, doi: 10.1144/SP359.1.

Fulton, P.M., and Saffer, D.M., 2009, Effect of thermal refraction on heat flow near the San Andreas Fault, Parkfield, California: Journal of Geophysical Research: Solid Earth, v. 114, doi: 10.1029/2008JB005796.

Haines, S.H., and van der Pluijm, B.A., 2012, Patterns of mineral transformations in clay gouge, with examples from low-angle normal fault rocks in the western USA: Journal of Structural Geology, v. 43, p. 2–32, doi: 10.1016/j.jsg.2012.05.004.

Han, R., Hirose, T., Shimamoto, T., Lee, Y., and Ando, J. -i., 2011, Granular nanoparticles lubricate faults during seismic slip: Geology, v. 39, p. 599–602, doi: 10.1130/G31842.1.

Han, R., Shimamoto, T., Ando, J., and Ree, J.-H., 2007, Seismic slip record in carbonate-bearing fault zones: An insight from high-velocity friction experiments on siderite gouge: Geology, v. 35, p. 1131, doi: 10.1130/G24106A.1.

Jacobs, J.R., Evans, J.P., and Kolesar, P.T., 2006, Energetics of chemical alteration in fault zones and its relationship to the seismic cycle, *in* Abercrombie, R., McGarr, A., Kanamori, H., and Di Toro, G. eds., Geophysical Monograph Series, Washington, D. C., American Geophysical Union, p. 181–191.

Kanamori, H., and Brodsky, E.E., 2004, The physics of earthquakes: Reports on Progress in Physics, v. 67, p. 1429, doi: 10.1088/0034-4885/67/8/R03.

Kanamori, H., and Riveira, L., 2006, Energy partitioning during an earthquake, *in* Abercrombie, R., McGarr, A., and Kanamori, H. eds., Earthquakes: Radiated Energy and the Physics of Faulting, Geopysical Monograph Series 170, Washington, D. C., American Geophysical Union, p. 3–13.

Kirkpatrick, J.D., Dobson, K.J., Mark, D.F., Shipton, Z.K., Brodsky, E.E., and Stuart, F.M., 2012, The depth of pseudotachylyte formation from detailed thermochronology and constraints on coseismic stress drop variability: Journal of Geophysical Research: Solid Earth, v. 117, doi: 10.1029/2011JB008846.

Kirkpatrick, J.D., and Rowe, C.D., 2013, Disappearing ink: How pseudotachylytes are lost from the rock record: Journal of Structural Geology, v. (in press), doi: 10.1016/j.jsg.2013.03.003.

Kirkpatrick, J.D., and Shipton, Z.K., 2009, Geologic evidence for multiple slip weakening mechanisms during seismic slip in crystalline rock: Journal of Geophysical Research: Solid Earth, v. 114, doi: 10.1029/2008JB006037.

Kirkpatrick, J.D., Shipton, Z.K., and Persano, C., 2009, Pseudotachylytes: Rarely Generated, Rarely Preserved, or Rarely Reported?: Bulletin of the Seismological Society of America, v. 99, p. 382–388, doi: 10.1785/0120080114.

Lachenbruch, A.H., and Sass, J.H., 1980, Heat flow and energetics of the San Andreas Fault Zone: Journal of Geophysical Research: Solid Earth, v. 85, p. 6185–6222, doi: 10.1029/JB085iB11p06185.

Lin, A., 2008, Fossil Earthquakes: the formation and preservation of pseudotachylytes: New York, Springer, 348 p.

Magloughlin, J.F., 2011, Bubble Collapse Structure: A Microstructural Record of Fluids, Bubble Formation and Collapse, and Mineralization in Pseudotachylyte: The Journal of Geology, v. 119, p. 351–371, doi: 10.1086/659143.

Magloughlin, J.F., 1989, The nature and significance of pseudotachylite from the Nason terrane, North Cascade Mountains, Washington: Journal of Structural Geology, v. 11, p. 907–917, doi: 10.1016/0191-8141(89)90107-7.

Magloughlin, J.F., and Spray, J.G., 1992, Frictional melting processes and products in geological materials: introduction and discussion: Tectonophysics, v. 204, p. 197–204, doi: 10.1016/0040-1951(92)90307-R.

Mankoff, K.D., and Russo, T.A., 2012, The Kinect: a low-cost, high-resolution, short-range 3D camera: Earth Surface Processes and Landforms,, p. n/a–n/a, doi: 10.1002/esp.3332.

Marone, C., and Richardson, E., 2010, Learning to read fault-slip behavior from fault-zone structure: Geology, v. 38, p. 767–768, doi: 10.1130/focus082010.1.

McGarr, A., 1999, On relating apparent stress to the stress causing earthquake fault slip: Journal of Geophysical Research: Solid Earth, v. 104, p. 3003–3011, doi: 10.1029/1998JB900083.

McKenzie, D., and Brune, J.N., 1972, Melting on Fault Planes During Large Earthquakes: Geophysical Journal International, v. 29, p. 65–78, doi: 10.1111/j.1365-246X.1972.tb06152.x.

Mount, V.S., and Suppe, J., 1987, State of stress near the San Andreas fault: Implications for wrench tectonics: Geology, v. 15, p. 1143–1146, doi: 10.1130/0091-7613(1987)15<1143:SOSNTS>2.0.CO;2.

Noda, H., Kanagawa, K., Hirose, T., and Inoue, A., 2011, Frictional experiments of dolerite at intermediate slip rates with controlled temperature: Rate weakening or temperature weakening?: Journal of Geophysical Research: Solid Earth, v. 116, doi: 10.1029/2010JB007945.

O'Hara, K., 2005, Evaluation of asperity-scale temperature effects during seismic slip: Journal of Structural Geology, v. 27, p. 1892–1898, doi: 10.1016/j.jsg.2005.04.013.

Plattner, U., Markl, G., and Sherlock, S., 2003, Chemical heterogeneities of Caledonian (?) pseudotachylites in the Eidsfjord Anorthosite, north Norway: Contributions to Mineralogy and Petrology, v. 145, p. 316–338, doi: 10.1007/s00410-003-0455-0.

Scholz, C.H., 1980, Shear heating and the state of stress on faults: Journal of Geophysical Research: Solid Earth, v. 85, p. 6174–6184, doi: 10.1029/JB085iB11p06174.

Scholz, C.H., 2002, The Mechanics of Earthquakes and Faulting: Cambridge University Press, 508 p.

Shipton, Z.K., Evans, J.P., Abercrombie, R.E., and Brodsky, E.E., 2006, The missing sinks: Slip localization in faults, damage zones, and the seismic energy budget, *in* Abercrombie, R., McGarr, A., Kanamori, H., and Di Toro, G. eds., Geophysical Monograph Series, Washington, D. C., American Geophysical Union, p. 217–222.

Sibson, R.H., 1975, Generation of Pseudotachylyte by Ancient Seismic Faulting: Geophysical Journal of the Royal Astronomical Society, v. 43, p. 775–794, doi: 10.1111/j.1365-246X.1975.tb06195.x.

Sibson, R.H., and Toy, V.G., 2006, The habitat of fault-generated pseudotachylyte: Presence vs. absence of friction-melt: Geophysical Monograph Series, v. 170, p. 153–166, doi: 10.1029/170GM16.

Siman-Tov, S., Aharonov, E., Sagy, A., and Emmanuel, S., 2013, Nanograins form carbonate fault mirrors: Geology,, doi: 10.1130/G34087.1.

Smith, S. A. F., Toro, G.D., Kim, S., Ree, J.-H., Nielsen, S., Billi, A., and Spiess, R., 2013, Coseismic recrystallization during shallow earthquake slip: Geology, v. 41, p. 63–66, doi: 10.1130/G33588.1.

Spray, J.G., 1987, Artificial generation of pseudotachylyte using friction welding apparatus: simulation of melting on a fault plane: Journal of Structural Geology, v. 9, p. 49–60, doi: 10.1016/0191-8141(87)90043-5.

Tanaka, H., Chen, W.M., Wang, C.Y., Ma, K.F., Urata, N., Mori, J., and Ando, M., 2006, Frictional heat from faulting of the 1999 Chi-Chi, Taiwan earthquake: Geophysical Research Letters, v. 33, doi: 10.1029/2006GL026673.

Tullis, T.E., 1994, Predicting earthquakes and the mechanics of fault slip: Geotime, v. 39, p. 19–21.

Wenk, H.-R., Johnson, L.R., and Ratschbacher, L., 2000, Pseudotachylites in the Eastern Peninsular Ranges of California: Tectonophysics, v. 321, p. 253–277, doi: 10.1016/S0040-1951(00)00064-0.

Wernicke, B., 1995, Low-angle normal faults and seismicity: A review: Journal of Geophysical Research: Solid Earth, v. 100, p. 20159–20174, doi: 10.1029/95JB01911.

VITA

Mitchell R. Prante
December 2013
Geologist
Shell E&P Co.

EDUCATION:

PhD in Geology, Department of Geology, Utah State University (2013)

Advisor: Dr. James Evans

MS in Geology, Department of Geology, Northern Arizona University (2009)

Advisor: Dr. Ernest Duebendorfer

BS in Geological Science, Department of Earth Science, University of California at Santa

Barbara (2007)

Advisor: Dr. Bruce Tiffney

EXPERIENCE:

Graduate Assistant, Utah State University Geology Department (7/2010 – 8/2013)

Course Instructor, Utah State University Geology Department (6/2012)

GeoScience Intern, Shell E&P New Ventures and Business Development (6/2010 –

8/2010 and 5/2011 – 7/2011)

Geologic Consultant, San Diego Natural History Museum (7/2009 – 12/2009)

Graduate Teaching Assistant, Northern Arizona University Department of Geology

(8/2007 – 12/2009)

Geologic Consultant, Davis-Namson Consulting Geologists (6/2008 – 7/2008)

USGS/NAGT Intern, USGS Menlo Park geo-hazards team (4/2007)

Research Assistant, UCSB Department of Earth Science (9/2005 – 5/2007)

MEMBERSHIPS & POSITIONS HELD:

American Association of Petroleum Geologists (2010 – present, student chapter president

2011 – 2013)

Geological Society of America (2006 – present)

Society of Success and Leadership (2004 – present)

HONORS, AWARDS & GRANTS:

Stonegate/Paris Hills Agricom Award (2012)

GSA Student Research Grant (2011)

AAPG Imperial Barrel Award Global Competition Finalist, Rocky Mountain Section

(2011, team manager)

Southern California Earthquake Center: Earthquake Petrology: Defomrational processes

near the Brittle-Plastic Transition (2011 proposal author)

GSA ExxonMobil Bighorn Basin Field Award (2009)

GSA Student Research Grant (2008)

Tom and Rose Bedwell Earth Physics Award (2008)

Four Corners Geological Society Thesis Grant (2008)

UCSB Earth Sciences Outstanding Academic Achievement (2007)

PUBLICATIONS:

Prante, M.R., and Evans, J.P., 2013, Pseudotachylyte and Fluid Alteration at seismogenic depths (Glacier Lakes And Granite Pass Faults, Central Sierra Nevada USA): Pure and Applied Geophysics, In Review

Prante, M.R., Evans, J.P., Janecke, S.U., Steely, A. 2013, Evidence for paleoseismic slip on a continental low-angle normal fault: Tectonic pseudotachylyte from the West Salton detachment fault, CA, USA: Earth ans Planetary Science Letters, In Press, DOI: http://dx.doi.org/10.1016.j.epsl.2013.10.048

Prante, M.R., Evans, J.P., Janecke, S.U., 2013, Use of a 3D Infrared-Range Camera in Mesoscale Geologic Investigations: A Case Study Using the Windows Kinect: Geological Society of America *Abstracts with Programs.* Vol. 45, No. 7, p.146.

Prante, M.R., Evans, J.P., Janecke, S.U., 2013, Evidence for Ancient Seismicity Along Exhumed Faults: Iridescent-Metallic Slip Surfaces: Geological Society of America *Abstracts with Programs.* Vol. 45, No. 7, p.679.

Prante, M.R., Evans, J.P., Janecke, S.U., 2011, Paleoseismicity along a low-angle normal fault: Evidence from the Salton Trough, CA, USA: Abstract T41C-07 presented at 2011 Fall Meeting, AGU, San Francisco, Ca.

Duebendorfer, E.M., Bonamici, C.E., Portis, D., Prante, M.R., 2010, Redefining the early history of the Mojave-Yavapai Collision: pre-collision reifting and post-collision gravitational collapse: GSA Abstracts and Programs, v. 42, p. 413.

Prante, M.R., and Duebendorfer, E.M., 2009, Paleoproterozoic deformation and metamorphism in the central and southern Peacock Mountains, NW Arizona: Implications for the location of the Mojave-Yavapai boundary zone: GSA Abstracts and Programs, v. 41, no. 6, p. 37.